Simulation and Experimental Studies on Renewable Energy-Based Building Cooling Systems

Doctoral Thesis

By

Gaurav Singh

(2017MEZ0026)

Department of Mechanical Engineering

Submitted

in the partial fulfillment of the requirements of the degree

of

Doctor of Philosophy

to the

Indian Institute of Technology Ropar

Rupnagar 140001, India

November 2022

INDIAN INSTITUTE OF TECHNOLOGY ROPAR, PUNJAB, INDIA

CANDIDATE'S DECLARATION

I hereby certify that the work presented in this thesis, titled "**Simulation and Experimental Studies on Renewable Energy-Based Building Cooling Systems**" in partial fulfillment of the requirements for the award of the degree of Doctor of Philosophy and submitted to Department of Mechanical Engineering, IIT Ropar, is an authentic record of my own work carried out during the period January 2018 to November 2022 under the supervision of Dr. Ranjan Das.

The content presented in this thesis has not been submitted elsewhere for the award of any degree.

Gaurav Singh

(Mr. Gaurav Singh)

Date: 31/03/, 2023

This is to certify that the above statement made by the candidate is correct to the best of my knowledge. The Ph.D. Viva-Voce examination of Mr. Gaurav Singh, Research Scholar, has been held on 31/03/2023

Ranjan Das

(Dr. Ranjan Das)

Date: 31/03/, 2023

ACKNOWLEDGEMENTS

My first and foremost words of gratitude shall go to my parents who are the ones behind every achievement of my life, let alone my doctoral programme's research work. It is their unremitting support and encouragement that has made possible for me to shatter clouds of negativity and despair in my mind and move forward to overcome every obstacle that showed up in my life.

My appreciation and thanks for the completion of this study is directed to my supervisor Dr. Ranjan Das for his years of patience and careful guidance of this research. It was because of his insightful suggestions that I was able to refine my every single work to the level that is required for publishing in the academic community. Further, I would also extend my thanks to my Ph.D. doctoral committee members Prof. Navin kumar, Dr. Rakesh K. Maurya, Dr. Devranjan Samanta and Dr. S.C. Martha for evaluating and providing useful suggestions in my work. Further, I extend my thanks to Chhabra Engineers and Instrument, Ambala for helping me out to fabricate the setup. I am very thankful to my thesis proposal seminar expert Prof. Prabal Talukdar and synopsis seminar expert Prof. Santanu Bandyopadhyay for providing useful comments related to my work. I would like to acknowledge department of science and technology (DST) for providing funding support under the project no "TMD/CERI/BEE/2016/021" and IIT Ropar for providing required facilities.

Finally, I would express my thankfulness to my colleagues: Mr. Rohtash Goswami, Mr. Adityabir Singh. Mr. Abhishek Kumar, and Mr. Sunirmit Verma. The humorous discussions that I had with them at regular intervals in the lab, along with the brief, relaxing strolls to the canteen to pause the boredom of the day's routine were quite useful to retain my work's momentum going. Eventually, I thank God for helping me in getting me through all the difficulties.

(Gaurav Singh)

ABSTRACT

Continuous increase in the usage of refrigeration and air-conditioning systems, rapid depletion of conventional sources of fossil fuels, and environmental concerns, necessitate the research focus towards development of efficient technologies. This work is aimed at the assessment of various building cooling systems for addressing the environmental concerns related to global warming, air quality and waste management. Here, various configurations of air-conditioning systems have been studied via simulation and experimental investigations. Based on the research gaps identified in the literature survey, the present work has been executed in the following steps.

The first study assesses the possibility of integrating a "triple-hybrid" single-stage vapor absorption (VA) system for building air-conditioning using EnergyPlus simulations. The modifications required for making the absorption system energy efficient with respect to the conventional (compression-based) system are proposed. This analysis reveals the necessity of triple hybridization of the absorption system towards fulfilling its thermal energy requirement. Results show the possibility of annual electricity savings of around 18.5 % and 29.8 %, depending on the climatic condition. Furthermore, performance enhancement aspects through desiccant material-based via dedicated outdoor air system (DOAS) and multi-staging methods are investigated. In desiccant-coupled systems, the role of indirect evaporative cooling arrangement (IEC), sensible heat recovery wheel (SHRW) and cooling coil in the supply air path are mainly assessed. Results show that a double-staging system can save up to 36.4 % of annual electrical energy compared to a compression-based system. However, with single-staging, the saving is nearly 19.5 %. Further, in a double-stage absorption system, the amount of required thermal capacity at the generator side is lesser compared to the catered cooling load, that gives the coefficient of performance (COP) greater than one. However, in the single-stage absorption system, the required thermal energy is always more than the cooling load (i.e., refrigeration effect). But, the needed heat source temperature is high (approximately 150 ºC) in double-staged absorption systems that limits the usage of the multiple-staging systems under general working conditions.

In the second study, the suitability of the triple-hybrid absorption system is checked with the proven energy-efficient radiant cooling system (RCS). In this context, three configurations of RCS are compared: RCS and DOAS coupled with the compression-based system, RCS coupled with absorption system and DOAS, and absorption-assisted RCS associated with desiccant and IEC-assisted DOAS. The simulation results reveal around 13 % of energy savings by the last configuration against the first one. This study demonstrates the possibility of coupling an absorption-based system with only RCS. However, the absorption-based system cannot be coupled to the DOAS, and compression chiller is necessary in such a situation.

In the third study, to make the building cooling space fully independent of electrical energy, an analysis is performed to examine the electric grid independency potential of absorption and compression-based air-conditioning systems under different climatic conditions. Here, solar photovoltaic (PV) and solar collector systems have been installed for electricity generation and thermal energy generation, respectively. In the case of compression-based air-conditioning, the maximum area of the roof can be occupied with solar PVs, whereas, with absorption-based systems, half of the roof area is used for solar collector installation. In the case of absorption-based air-conditioning configuration, although more energy savings can be obtained compared to the compression-based system, still, this system cannot attain the target of grid independency. However, the compression-based air-conditioning system (in particular, the compression-based radiant system) effectively shows the achievement of grid independency criteria. It is revealed that 98 %, 100 %, and 74 % of the grid independency target can be attained by this configuration under composite, hot-dry, and warm-humid climates, respectively.

In the fourth study, for different climatic conditions, a desiccant-assisted improved strategy of air-conditioning systems termed as variable refrigerant flow (VRF) is examined with respect to the conventional variable air volume (VAV) and VRF designs. In the proposed design, an IEC is used in the path of desiccant process air. For this purpose, an EnergyPlus simulation model is developed for a large scale office building. A loop of flat-plate solar collector with auxiliary heating element is used for the desiccant regeneration. Simulation results revealed that, for warm-humid climate,

electrical energy saving potential of the proposed solar energy-assisted VRF system is around 23.9 % and 9.5 % higher than the conventional all-air VAV and VRF systems, respectively. The same savings percentage under composite climate are determined as 13.8 % and 9.4 %. For the hot-dry climate, these values are 17.5 % and 11.6 % against conventional all-air VAV and VRF systems, respectively.

In the fifth study, specific outcomes of the simulation studies are used for fabricating an experimental test bench. For this purpose, a small-scale triple-hybrid-based absorption chiller (1.1 Ton or 3.85 kW capacity) is designed and fabricated. Solar thermal, waste biomass-based electricity, and biomass-based waste heat sources are used to drive the entire absorption system. Waste biomass is fed to a biomass gasifier that generates clean syngas and it is used in the electricity generator. Cold water obtained from the absorption chiller is supplied to the test chamber for air-conditioning purpose. The absorption chiller performance is assessed under different lithium bromide (LiBr)-water concentrations (54% and 58 %) and generator temperatures (60 ºC, 70 ºC, and 80 ºC). Experimental study reveals the possibility of coupling solar and biomass-based resources with an absorption-based air-conditioning system. Experimental data are further used for generating new empirical correlations. The response surface method is used to create the correlations with the coefficient of determination of 0.991 and 0.993 for evaporator load and temperature, respectively. The overall heat transfer coefficients estimated for each of the components of the absorption chiller are determined. Interestingly, the developed test bench can supply surplus energy savings. The absorption chiller can lower the room air temperature from 37 ºC to 27.5 ºC with 58 % concentration and 80 ºC generator temperature. The associated harmful emissions are found to be considerably lesser compared to the conventional modes of air-cooling.

LIST OF PUBLICATIONS

Journals

[J1] Singh, G., and Das, R., 2019. Energy saving potential of a combined solar and natural gas-assisted vapor absorption building cooling system. Journal of Solar Energy Engineering, Transactions of the ASME 141 (1), pp. 011016 (14 Pages).

[J2] Singh, G., and Das, R., 2019. A novel design of triple-hybrid absorption radiant building cooling system with desiccant dehumidification. Journal of Energy Resources Technology, Transactions of the ASME 141 (7), pp. 072002 (13 Pages).

[J3] Singh, G., and Das, R., 2020. Comparative assessment of different air-conditioning systems for nearly/net zero-energy buildings. International Journal of Energy Research, 44 (5), pp. 3526-3546.

[J4] Singh, G., and Das, R., 2021. Experimental study of a combined biomass and solar energy-based fully grid-independent air-conditioning system. Clean Technologies and Environmental Policy, 23(6), pp.1889-1912.

[J5] Singh, G., and Das, R., 2021. Experimental study on a new small-scale absorption system: response surface and inverse analyses. Journal of Energy Resources Technology, Transactions of the ASME 143(9), pp. 092103 (12 Pages).

[J6] Singh, G., and Das, R., 2022. Performance analysis of evaporation and heat wheel-based building air conditioning systems. Journal of Energy Resources Technology, Transactions of the ASME 145 (3), pp. 032101 (9 Pages).

[J7] Singh, G., and Das, R., 2022. A novel variable refrigerant flow system with solar regeneration-based desiccant-assisted ventilation. Solar Energy, 238, pp. 84-104.

Conference Proceedings

[C1] Singh, G., and Das, R., Performance analysis of solar and natural gas based building cooling system, International Conference on Sustainable Energy and Environmental Challenges (SEEC-2018), 31 December 2017-03 January 2018, IISc Bangalore, India.

[C2] Singh, G., and Das, R., Performance analysis of desiccant aided building cooling system, (Poster presentation), International Workshop on Sustainable Energy, Power and Propulsion (ISEPP-2018) 18 March -22 March, 2018, NIT Kurukshetra, India.

[C3] Singh, G., and Das, R., Energy saving potential of an air-conditioning system with desiccant and solar assisted ventilation, International Conference on Recent Innovations and Developments in Mechanical Engineering (IC-RIDME-2018), NIT Meghalaya, Shillong, India, 8 November-10 November, 2018. [Published in Advances in Mechanical Engineering under Lecture Notes in Mechanical Engineering, Springer, pp. 1351-1359, 2020].

[C4] Singh, G., and Das, R., Assessment of desiccant assisted compression and absorption based air-conditioning systems for hot-dry and composite climates, 2nd International Conference on New Frontiers in Engineering, Science and Technology (NFEST-2019), February 18-22, 2019. NIT Kurukshetra. [Published in Journal of Physics, Conference Series, 1240, 012087 (8 Pages), 2019].

[C5] Singh, G., and Das, R., Assessment of evaporative cooling and heat wheel assisted air-conditioning system for composite climate, International Mechanical Engineering Congress (IMEC-2019), NIT Tiruchirappalli, Tamil Nadu, India, 29 November– 01 December, 2019.

[C6] Singh, G., and Das, R., Energy saving assessment of triple-hybrid vapor absorption building cooling system under hot-dry climate, ASME Power Conference, Virtual (Online), 20 July-22 July, 2021.

[C7] Singh, G., and Das, R., Comparative performance assessment of multi-stage absorption air-conditioning under warm-humid climate, ASTFE Thermal and Fluids Engineering Conference (TFEC 2022), Partially

online (virtual) and in person at University of Nevada, Las Vegas, NV, USA, 15 May-18 May, 2022.

[C8] Singh, G., and Das, R., Performance assessment of solar and desiccant aided building air-conditioning system. 8th International Symposium on Hydrogen Energy, Renewable Energy and Materials (HEREM 2022), Online (virtual), 14 October -15, October 2022.

[C9] Singh, G., and Das, R., Comparative assessment of various dual-phase cycles used for space-cooling. Paper will be presented in 8th Thermal and Fluids Engineering Conference (TFEC 2023), Partially online (virtual) and in person at University of Maryland, College Park, MD, USA, March 26-29, 2023.

TABLE OF CONTENTS

Contents

LIST OF FIGURES

LIST OF TABLES

NOMENCLATURE

A	Area of solar collector, m^2
A_{bare}	Area of bare pipe, m^2
A_e ,A_a ,A_c , and A_g	Area of heat exchanger of evaporator, absorber, condenser and generator, respectively. m^2
A_{fin}	Area of fins, m^2
c	Concentration of solution, %
$c_{p,w}$	Specific heat of water, kJ/(kg·K)
c_{ss} and c_{ws}	Solution concentration of strong and weak solution, respectively
d_{pipe}	Diameter of the heat exchanger pipe, m
f_{pl}	Part load factor
f_{size}	Sizing factor
$h_{a,coil,in}$ and $h_{a,i,coil}$	Enthalpy of air at coil inlet, kJ/kg
$h_{a,coil,out}$ and $h_{a,o,coil}$	Enthalpy of air at coil outlet, kJ /kg
$h_{ref,in,2}$ and$h_{ref,out,2}$	Enthalpy of refrigerant at inlet and outlet of VRF indoor unit, respectively. kJ/kg
$h_{Ref,c,in}$ and $h_{Ref,c,out}$	Enthalpy of refrigerant at condenser inlet and outlet, respectively. kJ /kg
$h_{Ref,in}$ and $h_{Ref,out}$	Enthalpy of refrigerant at inlet and outlet of evaporator, respectively. kJ/kg
$h_{ws,in}$	Enthalpy of weak solution at inlet, kJ/kg
$h_{ss,out}$	Enthalpy of strong solution at outlet, kJ/kg
$h_{hw,in}$ and $h_{hw,out}$	Enthalpy of hot water at inlet and outlet, respectively. kJ/kg
I	Incident solar radiation (W/m^2)
K1, K2, K3,,	Number of independent quantities
L_{coil}	Length of the coil, m
$\dot{m}_a$	Mass flow rate of air, kg/s
$\dot{m}_{hw}$	Mass flow rate of hot water, kg/s
$\dot{m}_{Ref}$	Mass flow rate of refrigerant, kg/s

$\dot{m}_{Ref,des}$	Designed mass flow rate of refrigerant, kg/s
$\dot{m}_{ref,IU,2}$	Mass flow rate of refrigerant through indoor unit, kg/s
$\dot{m}_{we}$ and $\dot{m}_{wg}$	Mass flow rate of water through evaporator and generator, respectively. kg/s
$\dot{m}_{ws}$ and $\dot{m}_{ss}$	Mass flow rate of weak and strong solutions, respectively. kg/s
$\dot{m}_{tw}$	Mass flow rate of water through cooling tower, kg/s
$M_{sol,g}$	Total mass of the LiBr salt solution in generator, kg
ΔP	Pressure difference, Pa
q	Heat gained by collector fluid, W
q_{source}	Internal heat source, W
$Q_{a,inside}$	Absorber heat transfer rate, kW
Q_b	Boiler capacity, kWh
Q_{BT}	Thermal power of the biomass based resources, kW
Q_c	Chiller cooling capacity, kWh
$Q_{c,Ref}$	Heat transfer through condenser, kW
Q_{coil}	Cooling load across the cooling coil, kWh
$Q_{coil,DOAS,VCC}$	DOAS cooling coil designed cooling load, kWh
Q_{des}	Designed cooling power for radiant system, kW
Q_e	Evaporator cooling capacity, kWh
Q_E	Evaporator capacity, kW
$Q_{e,max}$	Evaporator maximum/designed cooling capacity, kWh
Q_f	Fan energy consumption, kWh
Q_g	Heat supplied to the generator, kWh
Q_G	Generator capacity, kW
Q_{Gas}	Heating energy of gas, kWh
Q_{hw}	Heat transfer through hot water, kW
$Q_{Iu,2}$	Capacity of indoor unit, W
Q_s	Heat supplied by the solar collectors, kWh
Q_{ST}	Thermal power by the solar collector, kW
Q_t	Total heat supplied to the generator, kWh

Q_{tw}	Heat transfer through cooling tower, kW
$Q_{Total,2}$	Total cooling capacity of VRF system, W
$Q_{w,h}$	Energy consumption of water heater, kWh
ROI	Return on investment, years
t	Time, s
T_{CW}	Temperature of chilled water, ˚C
T_{RCW}	Temperature of returning chilled water, ˚C
$T_{a,coil,i}$ and $T_{a,i,coil}$	Temperature of air inlet from cooling coil, ˚C
$T_{a,coil,o}$ and $T_{a,o,coil}$	Temperature of air outlet from cooling coil, ˚C
$T_{cw,in}$ and $T_{cw,out}$	Temperature of chilled water at evaporator inlet and outlet, respectively. ˚C
$T_{Ref,s}$	Temperature of refrigerant steam, ˚C
T_G and T_g	Generator temperature, ˚C
$T_{g,i}$	Water temperature at generator inlet, ˚C
$T_{g,o}$	Water temperature at generator outlet, ˚C
$T_{hw,in}$ and $T_{hw,out}$	Hot water inlet and outlet temperature, respectively ˚C
T_o	Water outlet temperature to the heater, ˚C
T_i	Water inlet temperature to the heater, ˚C
$T_{R,a}$	Room air temperature, ˚C
$T_{w,i}$	Water inlet temperature to the evaporator, ˚C
$T_{we,i}$	Water inlet temperature from the evaporator, ˚C
$T_{we,o}$	Water outlet temperature from the evaporator, ˚C
$T_{wg,i}$	Water inlet temperature from the generator, ˚C
$T_{wg,o}$	Water outlet temperature from the generator, ˚C
$T_{wh,i}$ and $T_{wh,o}$	Water inlet and outlet temperature from the heater, respectively ˚C
$T_{sol,in}$	Solution temperature at inlet, ˚C
$T_{w,si}$	Water temperature at solar collector inlet, ˚C

T_{∞}	Surrounding air temperature, ˚C
ΔT_c	Temperature change in water across chiller, ˚C
ΔT_e	Temperature change in water across evaporator, ˚C
ΔT_b	Temperature change in water across boiler, ˚C
ΔT_R	Temperature change in water across radiant tubing, ˚C
$(\Delta T_{lm})_e$, $(\Delta T_{lm})_a$, $(\Delta T_{lm})_c$, $(\Delta T_{lm})_g$	Logarithmic mean temperature difference for evaporator, absorber, condenser and generator, respectively.
U	Overall heat transfer coefficient, W/(m^2·K)
U_e, U_a, U_c, and U_g	Overall heat transfer coefficient of evaportaor, absorber, condenser, and generator, respectively. W/(m^2·K)
$\dot{V}_a$	Air volume flow rate, m^3/s
$\dot{V}_{a,IEC}$	Air volume flow rate through IEC, m^3/s
$\dot{V}_{a,IEC,des}$	Designed air volume flow rate through IEC, m^3/s
$\dot{V}_{a,DOAS,VCC}$	Air volume flow rate through DOAS cooling coil, m^3/s
$\dot{V}_c$	Water volume flow rate through chiller, m^3/s
$\dot{V}_e$	Water volume flow rate through condenser, m^3/s
$\dot{V}_{Gas}$	Volume flow rate of gaseous fuel, m^3/s
$\dot{V}_R$	Water flow rate through radiant tubing, m^3/s
V_t	Volume of water tank, m^3
V_g	Volume of the generator tank, m^3
w_p	Pump energy consumption, kWh
$w_{p,IEC}$	IEC Pump energy consumption, kWh
$w_{p,IEC,des}$	Designed IEC Pump energy consumption, kWh
w_f	Fan energy consumption, kWh
$w_{f,IEC}$	IEC Fan energy consumption, kWh
$w_{f,IEC,des}$	Designed IEC Fan energy consumption, kWh
$W_{compressor,2}$	Power of VRF compressor unit, W

$W_{controller,2}$	Power of VRF controller unit, W
$W_{f,2}$	Power of VRF fan unit, W
$W_{IU,2}$ and $W_{OU,2}$	Power of VRF indoor and outdoor unit, respectively. W
$W_{VRF,2}$	Power of VRF unit, W
X,Y,F, and *W*	Conduction transfer functions
X1, X2,.. Xn	Controlling/driving variables
Z	Independent parameters

Greek symbols

η	Efficiency of solar collector
η_f	Efficiency of fan
$\eta_{w,h}$	Efficiency of water heater
ρ_a	Density of air, kg/m^3
ρ_w	Density of water, kg/m^3
ρ_{ws}	Density of weak solution, kg/m^3
$\rho_{Ref,vapor}$	Density of refrigerant vapor at generator exit, kg/m^3
$\omega_{a,coil,i}$ and $\omega_{a,i,coil}$	Specific humidity of air at cooling coil inlet, kg/kg of dry air
$\omega_{a,coil,o}$ and $\omega_{a,o,coil}$	Specific humidity of air at cooling coil outlet, kg/kg of dry air
ϕ and ø	Uncertainty
ξ and ψ	Absolute uncertainty
λ	Circulation ratio

Abbreviations

AEC	Annual electric consumption
AHU	Air handling unit
BBD	Box Behnken design
CFC	Chlorofluorocarbon
CFM	Cubic feet per minute

COP	Coefficient of performance
CTF	Conduction transfer function
DBT	Dry bulb temperature
DOAS	Dedicated outdoor air system
DOE	Department of energy
ECBC	Energy conservation building code
EER	Energy efficiency rating
EES	Engineering equation solver
FCU	Fan coil unit
GHG	Greenhouse gas
GUI	Graphical user interface
HFC	Hydro fluorocarbon
HVAC	Heating ventilation and air-conditioning
IEC	Indirect evaporative cooler
kWh	Kilowatt hour
Kg	Kilogram
LHV	Lower heating value
LiBr	Lithium bromide salt
LiCl	Lithium chloride
MWh	Megawatt hour
NPV	Net present value
NREL	National renewable energy laboratory
PCM	Phase change material
PLR	Part load ratio
PPD	Percentage of person dissatisfied
PMV	Predicted mean vote
PTAC	Packaged terminal air conditioner
PTSC	Parabolic trough solar collector
PV	Photovoltaic
RCS	Radiant cooling system
SF	Scaling factor
SHGC	Sensible heat gain coefficient

SHRW	Sensible heat recovery wheel
TPC	Total power consumption
VA	Vapor absorption
VAC	Vapor absorption chiller
VACS	Vapor absorption cooling system
VAV	Variable air volume
VC	Vapor compression
VCC	Vapor compression chiller
VCS	Vapor compression system
VLT	Visible light transmittance
VRF	Variable refrigerant flow
WWR	Window to wall ratio

CHAPTER 1

*INTRODUCTION

This chapter summarizes the origin, need for air-conditioning, and outlines some of the commonly available air-conditioning techniques in the market, basic working principles behind these machines along with various other aspects. The requirement for air-conditioning kept changing over time because this development was needed to improve the system's performance. The content presented in this chapter shall help the reader to understand the practical application and working of air-conditioning systems. It will also lay the basis of understanding needed to grasp and enjoy the discussions embedded in further chapters.

1.1. Background

Achieving a comfortable indoor environment has always been one of the key interests of human beings. In ancient times, people used various architectural techniques such as high thermal mass, shading, vents, etc. to maintain a cool and soothing indoor environment. Till date, these techniques are still being used in the buildings as far as possible, but to a limited extent. After industrial revolution, artificial/mechanical cooling techniques took place in the market to obtain cooling response. Urbanization has also increased the use of air-conditioning machines to maintain a comfortable building environment. In urban areas, due to lack of space, buildings are losing their natural ability to be built as climate–responsive. A climate-responsive building will require a tremendous amount of construction material to gain adequate thermal inertia, but the limited availability of construction material is causing the construction of the building envelope with low thermal inertia.

Today, the requirement of air conditioning has become an essential entity to fulfill human's basic necessities at working place as well as at home. This thing has increased the energy demand and the same continues to grow. Survey reveals that in the buildings

* Content presented in this chapter can be found in the publication C9.

sector, around 40-50% of electrical energy is consumed by the air-conditioning systems only and the remaining is ascribed to other components like lightning, electrical appliances and others [Zhou et al. 2018, and Perez Lombard et al. 2008]. The major electricity generation in developed and developing countries is based on thermal power generation, in which coal, diesel, and gas are used as the fuel. In countries like India, the maximum portion of electrical energy is getting generated by coal-based plants [Buragohain et al. 2010]. Due to this, there is a very high demand for coal and this is causing rapid depletion of coal-based resources. Other consequences are greenhouse gas (GHG) emissions, smoke, and small particulate pollutions, which are some of the noticeable concerns. Further, global warming is also an important issue associated with air-conditioners, because of refrigerants and thermal energy rejection by condensers. All of these things together are creating an unhealthy environment and posing severe problems for the earth [Raghuvanshi et al. 2006, and Lubis et al. 2016]. Thus, it can be said that extensive use of mechanical air-conditioners has impacted the consumption/depletion of natural resources. So, there is a need for raising steps towards sustainable development. This is a core area where researchers have begun to recognize the importance of developing improved technology, modified design aspects, and enhanced energy performance of air-conditioners. Earlier, evaporative cooling was one of the preferable options for cooling purposes, although in some parts of the globe still, this cooling methodology is in use. Evaporative cooling requires a significant amount of water to cool the room air [Yang et al. 2019 and Misra and Ghosh 2018]. In locations where humidity levels are pretty high and water scarcity is also there, using an evaporative cooler is not a good option. Additionally, the evaporative cooler's response is not the same in all climatic conditions. So, the attention has shifted towards mechanical compressor-based air-conditioning systems.

Conventionally, most of the mechanical air-conditioning systems use a compressor to perform the cooling function in buildings. This compressor is the primary energy consumer of the air conditioner. In the market, various kinds of commonly air-conditioning systems are available that work on different operating cycles. Some of these operating cycles are discussed next.

1.2. Types of refrigeration cycles

The term refrigeration is the process of maintaining a temperature in any space or product below the ambient temperature [Arora 2000]. In this process, the heat energy

is rejected from the low-temperature source to the high-temperature source by using a certain amount of outsourced energy. Refrigeration is generally used to preserve the food and to provide comfort cooling to humans through air-conditioning. Other refrigeration applications can be found in chemical industries, transportation, pharmacy and others. Here, some of the commonly used cycles for the air-conditioning purpose are listed below [C9]:

- Mechanical compression refrigeration cycle
- Vapor absorption refrigeration cycle
- Vapor adsorption refrigeration cycle
- Ejector refrigeration cycle
- Vortex tube refrigeration cycle
- Thermoelectric refrigeration cycle
- Thermionic refrigeration cycle
- Evaporative cooling cycle

1.2.1. Mechanical compression refrigeration cycle

A mechanical compression refrigeration cycle is also known as vapor compression (VC) cycle. In this cycle, a compressor is used as the main working component. The basic components of the VC cycle are evaporator, compressor, condenser and expansion device [Arora 2000]. This is a closed loop cycle. Figure 1.1 shows the arrangement of working elements in the basic VC cycle and the direction of the refrigerant flow through these components. In this cycle, an evaporator is a heat exchanger that exchanges heat energy between the space air and refrigerant flowing inside the pipes/tubes. The compressor is the main part of the VC cycle which compresses the vapor refrigerant coming from the evaporator to high pressure and temperature equal to the condensing temperature. Next, the high pressure and enhanced temperature refrigerant stream passes through the condenser of the VC cycle. A condenser is also a heat exchanger that liberates the heat energy of refrigerant to the ambient and condenses the refrigerant vapor into liquid form. Next, this liquid refrigerant passes through an expansion device: capillary tube and by throttling process, where the pressure of this liquid refrigerant gets reduced. Then refrigerant flows through evaporator and cycle continues. The refrigeration/cooling effect is observed at the evaporator side of the VC refrigeration cycle. These refrigeration cycles are used

for low temperature as well as ultra-low temperature applications like medical purposes, food preservations and others. Earlier, the refrigerants used in the VC cycles were Chlorofluorocarbons (CFCs) and hydro fluorocarbon (HFCs), but due to high ozone-depleting potential of these refrigerants, they had been put obsolete [Dalkilic et al. 2010]. Now, various environment-friendly refrigerants have been developed like R134a, R290, R600, R717, R124, and many more that can address the above-discussed issues [Emani et al. 2018]. The compressor used in the VC cycle may be centrifugal type, screw type, or reciprocating type. The compressor type depends on the size of the refrigeration plant and the type of refrigerant used.

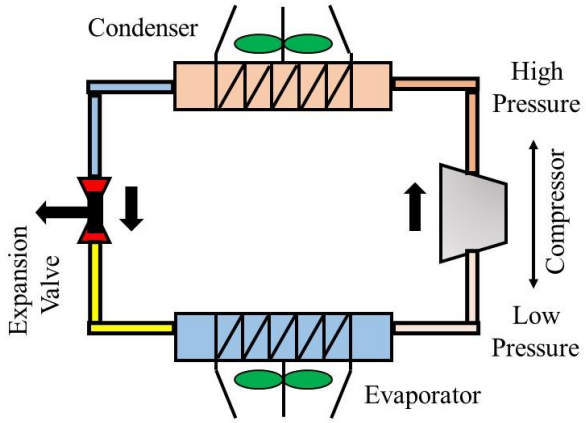

Figure 1.1: Layout of vapor compression cycle

1.2.2. Vapor absorption refrigeration cycle

The working principle of the vapor absorption (VA) refrigeration cycle is similar to the VC cycle. In this cycle, the compressor of VC cycle is replaced with the assembly of the pump, absorber, generator, separate expansion valve and heat exchanger for performance improvement [Whitman et al. 2012]. The schematic layout of the VA cycle is shown in Figure 1.2. In the VA cycle a working pair of absorbent and refrigerant is used. Some examples of commonly used absorbent-refrigerant pairs are Lithium bromide (LiBr)-water and Ammonia-water [Ashassi-Sorkhabi et al. 2018]. In the LiBr-water pair, the water is used as the refrigerant; while in ammonia-water pair, ammonia is used as the refrigerant. The selection of the type of working pair depends on the relevant application purpose of the system i.e., either in refrigeration or air-conditioning. The operation of the VA cycle under both working pairs is similar, but additional components like a rectifier and analyzer are required for the ammonia-water pair. VA cycle operating with LiBr-water for air-conditioning applications uses water

as the refrigerant and the cooling effect is produced by evaporating the refrigerant under vacuum conditions in the evaporator. In this system, the mixture of absorbent-refrigerant is sent towards the generator from the absorber by using a solution circulation pump. Here, a high-temperature heat source: hot water, exhaust, steam, and flue gas etc. is supplied to the generator and due to this, the mixture boils and the refrigerant vapor comes out at saturated state. This vapor goes into the condenser and condenses into liquid refrigerant. This liquid refrigerant reaches into the evaporator via an expansion device. After this, the refrigerant boils in the evaporator by thermal energy transfer from the surrounding fluid and solution mixture in the absorber attracts these vapors and the cycle continues [Whitman et al. 2012].

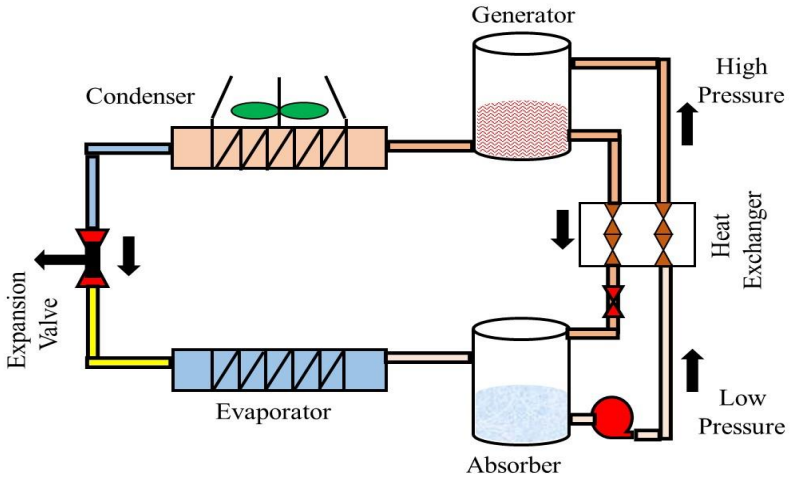

Figure 1.2: Vapor absorption cycle

1.2.3. Vapor adsorption refrigeration cycle

This cycle is similar to the absorption cycle. The only difference is that the process of absorption of refrigerant vapor coming through evaporator is different. In the adsorption cycle, this vapor is adsorbed over a solid surface in place of the liquid as in absorption. A pair of adsorbent (silica gel, zeolite, and activated carbon etc.) and adsorbate i.e., refrigerant (water, ammonia and methanol etc.) is selected. Adsorption system consists of an adsorbent bed in which process of refrigerant adsorption and desorption take place. Working layout of an adsorption cycle is shown in Figure 1.3. Low grade thermal energy in form of either solar or waste heat, waste heat and of other similar nature, is utilized in the adsorbent bed to continue the operation. The process of adsorption and desorption of bed is little complex because sequential heating and cooling is required for adsorbent material. This cycle with single bed gives intermittent

operation, hence double bed configuration is preferred for making system continuous in cooling operation. Additional information related to cooling performance, characteristics, properties of adsorbent/refrigerant mixture can be found in some of these literature [Wang et al. 2014 and Choudhary et al. 2013].

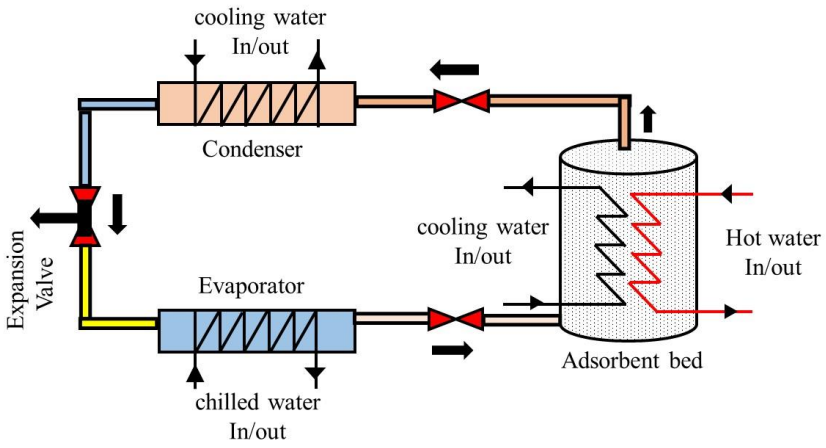

Figure 1.3: Vapor adsorption cycle

1.2.4. Ejector refrigeration cycle

In this cycle, the compression process is attained by an ejector mechanism. The process of compression in a conventional VC cycle is replaced by the ejector in the ejector refrigeration cycle. The working principle of this cycle is shown in Figure 1.4.

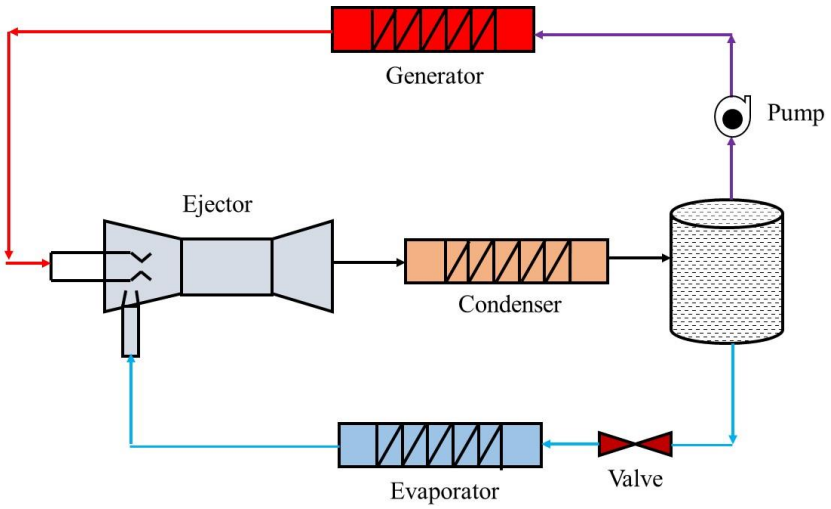

Figure 1.4: Ejector refrigeration cycle

Here also, some low grade thermal energy is used to generate high pressure vapors from the refrigerant and sent towards the nozzle (i.e., primary flow) of the ejector. Thereafter this vapor creates low pressure conditions and attracts refrigerant vapor from the secondary flow passage. Then combined high pressure and high temperature refrigerant

vapor is sent towards the condenser side of the cycle. The liquid refrigerant coming from the condenser flows into two distributed lines, one in evaporator side and another in generator/boiler side and cycle continues. The performance characteristics of the ejector system depends on the design configuration of ejector. Additional details can be found in some the published studies [Besagni et al. 2016, and Abdulateef et al. 2009].

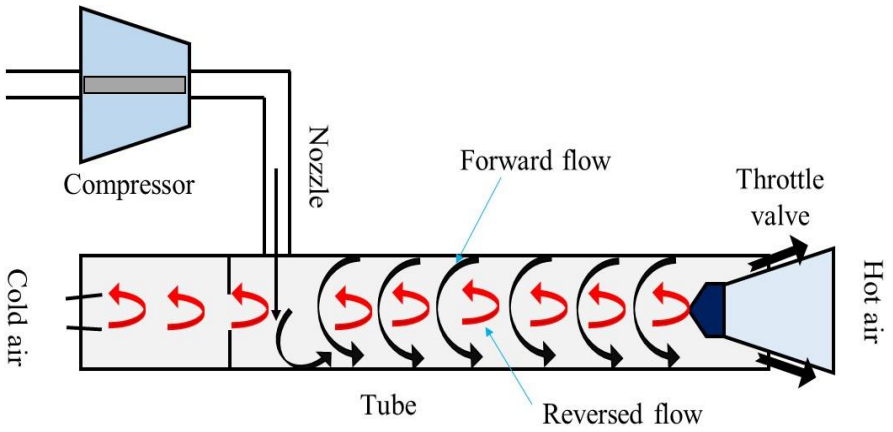

Figure 1.5: Vortex refrigeration cycle

1.2.5. Vortex tube refrigeration cycle

In this type of refrigeration system, both cooling and heating effects are obtained simultaneously. A part called vortex tube is used as the main working component in this cycle. This tube consists of nozzle, diaphragm, valve, hot air and cold air side. The cycle comprises of a compressor, nozzle, and pipe arrangement. A typical layout of the vortex tube refrigeration is shown in Figure 1.5. Here, one end of the nozzle is fixed in tangential direction to tube/pipe's inner surface and the other end is connected to a compressor. Likewise, a throttle valve is connected to one end of the tube and other end is kept open. As the compressed air expands through nozzle, swirl motion is created inside the tube. This compressed air moves as free vortex towards the throttle valve side. As this swirl motioned compressed air reaches the throttle, a stagnation point is formed, where all kinetic energy of the air gets converted into potential energy, and flow takes place in the reverse direction. As a result, reversed vortex flow gets rotated and comes in contact with the coming forward vortex flow. This reversed vortex flow is at the center/core of the pipe whereas, forwards flow is at the periphery of the tube. During this, heat transfer takes place between the core motion fluid and the peripheral fluid. Therefore, this core stream gets cooler and peripheral stream gets heated. In this way, at one end (i.e., throttle valve side) heated air comes out and at the other end, cool

air comes out. By controlling the valve opening, the mass flow rate and temperature of the cool air can be varied. The advantage of using this system is that there is no refrigerant leakage problem because air is used as a refrigerant. The application of this system is limited to a small cooling capacity that can be used for spot cooling. The coefficient of performance (COP) of this system is also very low. Additional detail of the design aspects and performance parameters can be found in some of the published articles [Ahlborn and Gordon 2000, and Yilmaz et al. 2009].

1.2.6. Thermoelectric refrigeration cycle

No refrigerant is used in this type of refrigeration. This cycle works on the principle of the Peltier effect. This cycle relies on the properties of thermocouples when electric current flows through them. When a certain amount of current is given to the thermocouple, then one end will be hot and the other will be cool [Goldsmid 2010]. This cool node is placed in the area where refrigeration is needed, and it will extract the heat energy from that place. This cycle cannot be used for large-scale cooling applications due to its complex installation arrangement, low cooling capacity, poor COP and cost aspects. It is preferably used where hard to access cooling load is needed, for instance, in some electronic systems. Working of this cycle is shown in Figure 1.6.

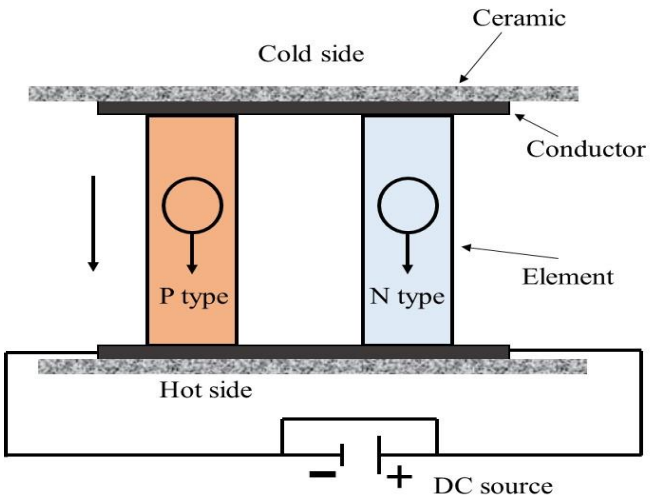

Figure 1.6: Thermoelectric refrigeration

1.2.7. Thermionic refrigeration cycle

Thermionic refrigeration cycle is a type of solid state cooling process similar to thermoelectric refrigeration cycle. Working of this cycle is shown in Figure 1.7. As, in thermoelectric cooling, the flow of electrons take place through a physical contact

between semiconductors, in contrast, thermionic cooling uses flow of electrons between two electrodes which are separated by a very small gap (around 1 μm). In thermionic devices, the flow of electrons follow ballistic electron transport mechanism, i.e., electrons will not collide with any obstacle while moving between electrodes. Basically, thermionic refrigeration is the process of thermionic emission, in which the electron discharges from the free surface as there is an increase in the electron energy to overcome the electrostatic forces. Typically, there is exchange of electrons between two surfaces. Applying a potential differential induces a current that transports high energy electrons from cathode to anode. This electron transportation results in cooling of cathode and heating of anode. In this system, fewer frictional losses will occur because there are no moving and rotating parts. The main disadvantage of using this system is that it generally requires a comparatively high heat source temperature.

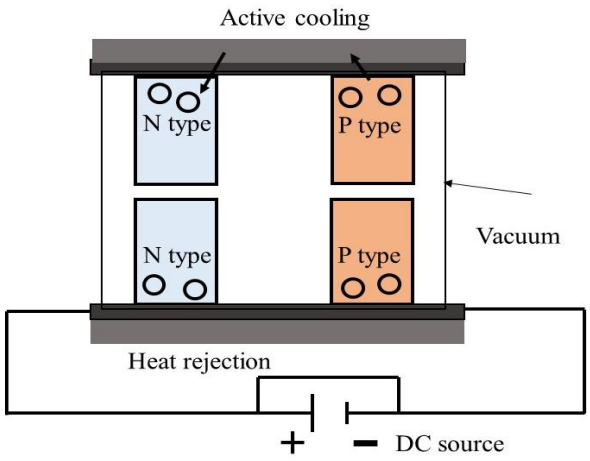

Figure 1.7: Thermionic refrigeration cycle

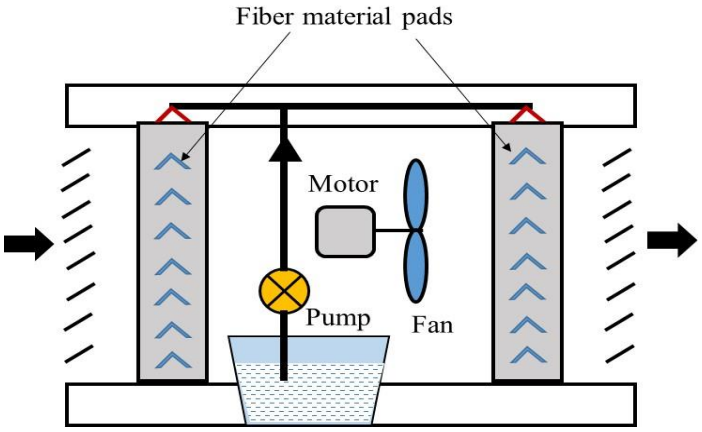

Figure 1.8: Evaporative cooling unit

1.2.8. Evaporative cooling cycle

The evaporative coolers are also known as swamp coolers. In this system, water is used as the heat transport medium from the atmospheric air. The hot air falls over the cooled water pads and absorbs hot air heat. Water then evaporates and cool-air enters the room space. This is the simplest way of cooling the hot air and providing fresh air to the indoor space [Wu et al. 2014]. However, it adds humidity to the air, which may lose thermal comfort in some areas like warm-humid regions. But in high humidity conditions and looking at the water scarcity scenario, these systems are not beneficial for large-scale cooling applications. Working of this cycle is shown in Figure 1.8.

1.3. Classifications of air-conditioning systems

The categorization of the air-conditioning systems depends on various factors such as the size of the space, utility of the building, amount of heat generation, location and many more. There are multiple types of air-conditioning systems for different applications as per the requirement. It is observed that most of the cooling systems in the building air-conditioning are based on the VC cycle, i.e., compressor will be the key component to run these categorized systems. The compressor is used in different ways as per the design specifications. These compression-driven systems possess some advantages like quick response time, easy installation, low maintenance, reliable operation, accessible transportation, easily moldable according to the requirement etc. Thus, the classification in this section is focused on compression-based systems. However, this categorization can also be suitable for systems other than compression-driven systems. In general, for residential and commercial applications, it is observed that air-conditioning systems can be classified as:

- Window unit systems
- Split unit systems
- Packaged system
- Chiller based system

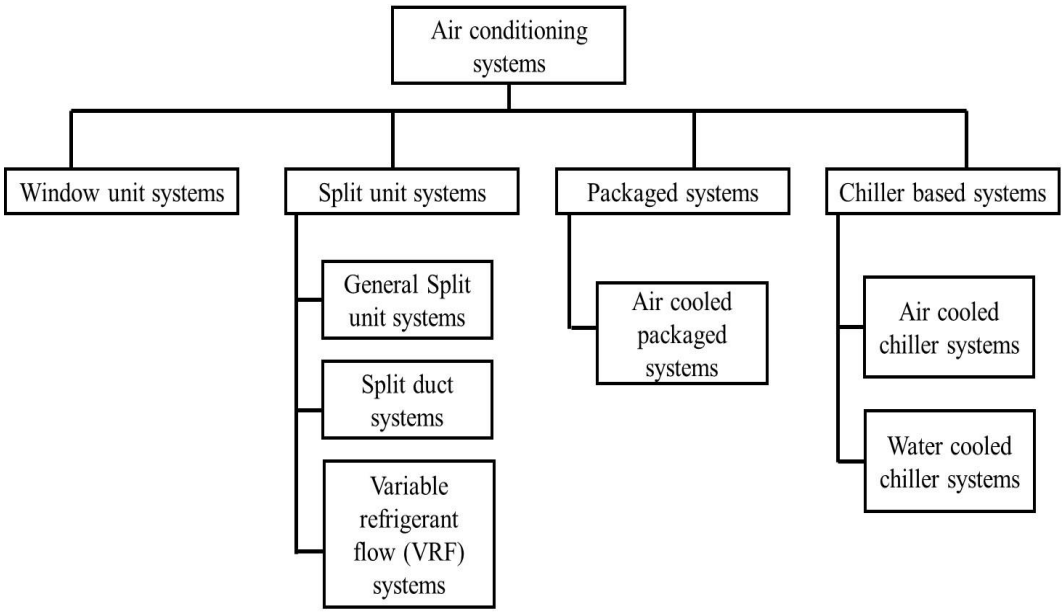

Figure 1.9: Classification of air-conditioning system

These main types of air-conditioning systems can be further divided into other subsystems also. This categorization can be seen in Figure 1.9. These sub-divisions depend upon the system's capacity and design, space availability, medium of heat transportation, etc. These systems and subsystems are discussed below.

1.3.1 Window unit system

This is the most common type of air-conditioning system used for residential and also some commercial applications. In a window-type air conditioner, all the components, evaporator, compressor, condenser, and expansion, are installed in a single unit [Whitman et al. 2012]. Controls are also provided within this unit only. They do not require any significant modification for installation. A damper is provided for the provision of fresh air intake with the recirculated air of room space. The usual capacity of these systems is up to 2-3 Tons. The layout diagram of window unit is shown in Figure 1.10. In this type of system, a common motor is used for the condenser fan motor and evaporator side blower. This type of system can be used at places where proper provision of condenser heat rejection is adjacent to the conditioned area.

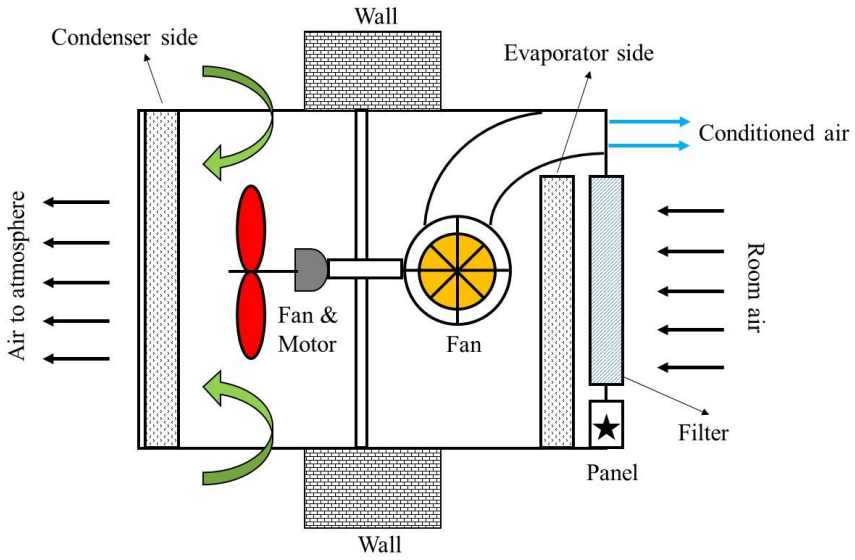

Figure 1.10: Layout of window air conditioner

1.3.2. Split unit system

Two separate units exist in this type of system. The indoor unit consists of evaporator cooling coil, fan arrangements and control panels, while in the outdoor unit, compressor, condenser, expansion device and other accessories are installed [Whitman et al. 2012]. This type of system is suitable in places where window unit installation is not possible, or space for heat rejection is not nearby. The outdoor unit is placed outside of the building space, and the indoor unit is installed inside the room space. This type of system mostly recirculates the room air for cooling purpose. These systems are preferable for the cooling load ranging around 3-5 Tons. The typical layout of a split system is shown in Figure 1.11.

1.3.2.1. General split system

This type of split system is used either in a single room or multiple rooms. Layout of general split system is shown in Figure 1.11a. The indoor unit is installed at a suitable height inside the room, and the outdoor unit is placed a little far away so that condensing heat can be removed. In this system, no additional ductwork is required. Only an indoor unit is sufficient to supply and distribute the cool and dehumidified air. In this type of system, each indoor unit of a different room consists of blower and coil arrangement.

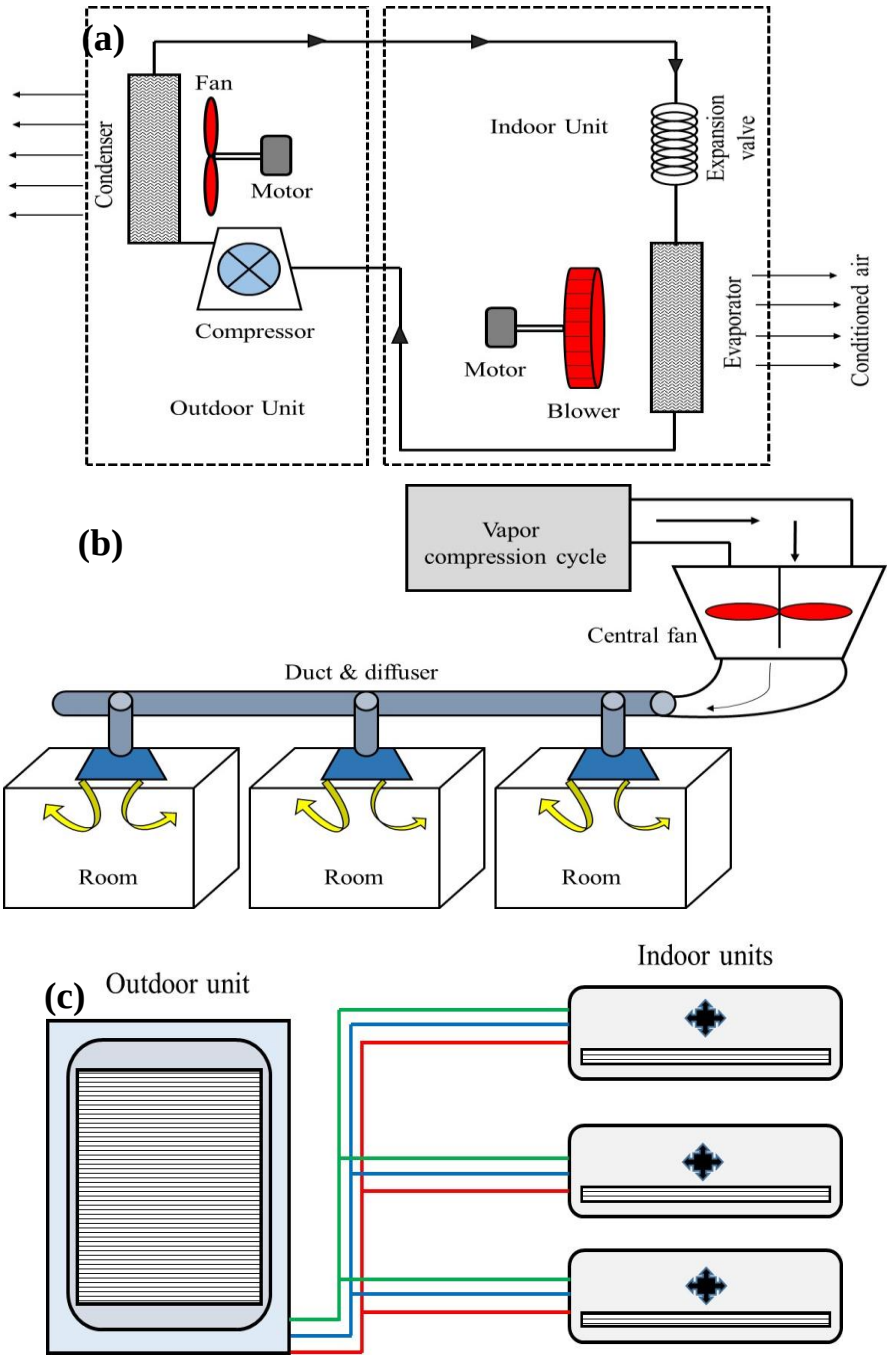

Figure 1.11: Layout diagram of split unit system (a) general split system, (b) split duct system, and (c) variable refrigerant flow

1.3.2.2. Split duct system

This system is similar to a general split system; but here, instead of having an indoor blowing unit directly to the room, a central fan coil unit (FCU) supplies air to various rooms through diffusers and ducting. A dedicated control system is required for each indoor unit. It can also be conceived as a central air-conditioning system. In this type of system, control of air flow is only provision for controlling the thermal comfort

conditions inside the room. Layout of split duct system is shown in Figure 1.11b. Here, air to be cooled comes in direct contact with evaporator surface.

1.3.2.3. Variable refrigerant flow (VRF) system

VRF systems are generally used for medium to large-scale applications. This system is also known as a ductless multi-split system. Layout of VRF system is shown in Figure 1.11c. This is also a type of split air-conditioning system in which a single outdoor unit supplies refrigerant to multiple evaporator units [Goetzlet 2007 and, Aynur et al. 2010]. This system has the ability to control the flow of refrigerant through each of the indoor evaporator units by some control mechanisms. Thus this system enables the use of multi-evaporator with different capacities and can maintain individual thermal comfort zone irrespective of ambient. This system also provides distributed control of the indoor unit. Further discussion about the VRF system can be found in the relevant literature [Lin et al. 2015, and Zhang et al. 2019].

1.3.3. Packaged system

A packaged air-conditioning system contains all its components into a single unit. Evaporator, compressor, condenser and expansion units are assembled into a single metal box [Alabdulkarem et al. 2015]. This box is placed outside the house or office. Special duct work is required to connect outdoor assembly and indoor system, and this ductwork supplies cool air inside the space.

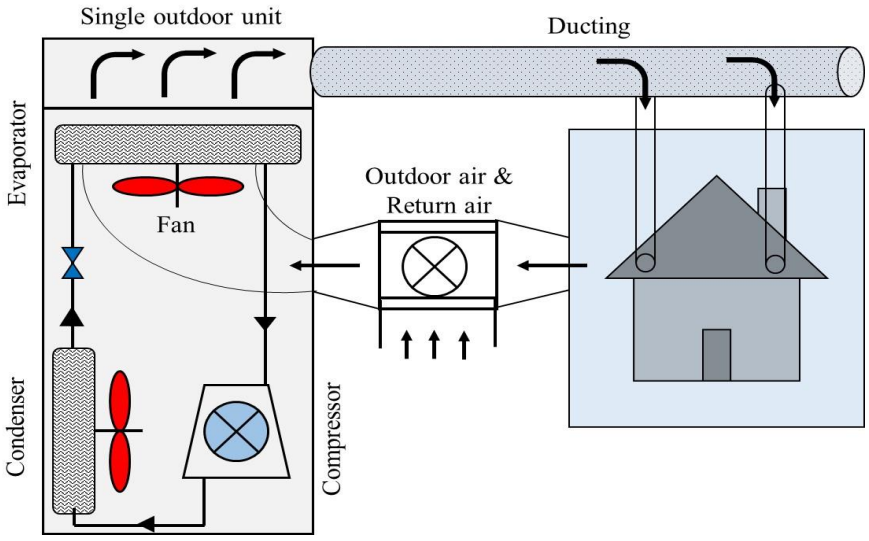

Figure 1.12: Layout of air-cooled packaged system

1.3.3.1.Air-cooled packaged system

Layout of air-cooled packaged system is shown in Figure 1.12. The cooling effect of the packaged air-conditioning units can be around between 10-20 Tons [Arora 2000]. In air-cooled packaged system, the condenser unit is cooled by the ambient air. In the packaged systems, a centrifugal blower is used for handling large volume flow rate of air. These air-cooled packaged systems are more commonly used than water-cooled packaged systems. This type is generally used for low-scale cooling applications. However, a condenser can be water cooled in the packaged system but such system is not available in the market. Because of the cooling range for which these systems are generally designed, the cost of the system will become higher in the case of water cooled condenser design.

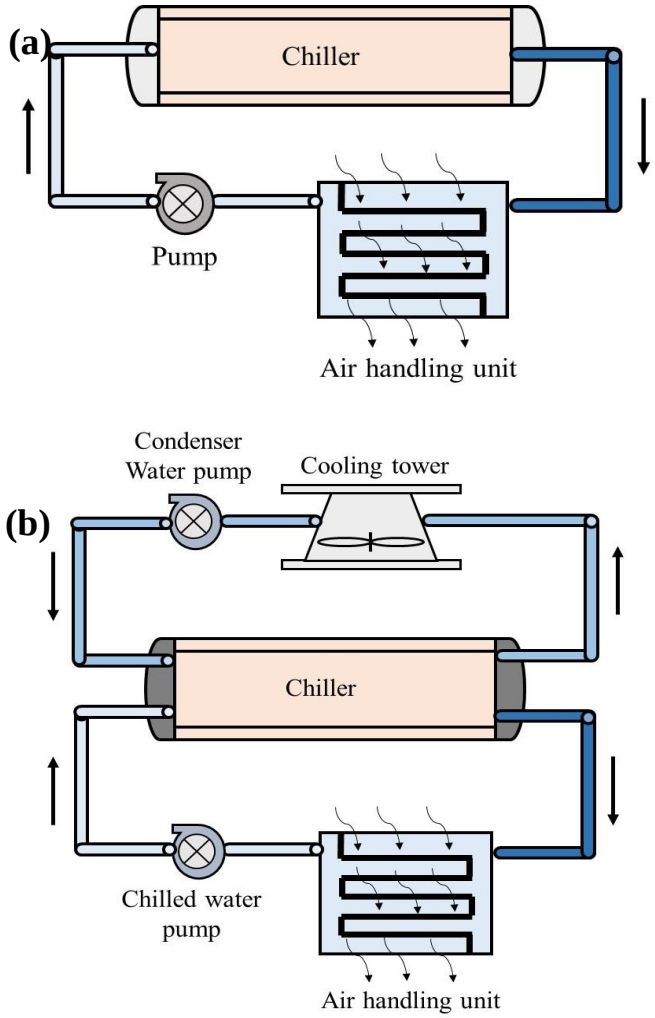

Figure 1.13: Chiller based system (a) air-cooled chiller system, (b) water-cooled chiller system

1.3.4. Chiller based system

Chiller-based systems are used for large-scale applications such as office buildings, theaters, hospitals, shopping mall, etc. In a chiller-based system, a central chiller generally working either on VC cycle, or VA cycle is used to cool the water and this water is transported to the cooling coil of air handling unit (AHU). A large fan arrangement is also there to supply cool and dehumidified air into the space through ducts and diffusers. Here, process water is used as the heat transport medium that cools the air to be supplied into the indoor space.

1.3.4.1. Air-cooled chiller system

An air-cooled chiller consists of compressor, evaporator, expansion device, blower fan and controls in a packaged unit. This unit supplies chilled water to the AHU located at various floors or locations. Hot air from the space is drawn back to AHU through return vanes. Air-cooled systems are used where heat discharge and optimum functioning are not important factors. The maintenance of air-cooled system is easier than that of the water-cooled system. The layout of the air-cooled chiller system is shown in Figure 1.13a. Additional discussion on this kind of system can be found in published studies available elsewhere [Yu et al. 2011 and Yu et al. 2013].

1.3.4.2.Water-cooled chiller system

In this type of system, condenser heat is rejected/discharged to the cooling water coming from the cooling tower. Major components of this system are chiller, chilled water circulation pumps, condenser water pumps, cooling towers and controls. The layout of the water-cooled chiller system is shown in Figure 1.13b. These systems are used for relatively large scale cooling applications. Further discussion can be studied in other articles [Jia et al. 2021 and Yu et al. 2014]. The COP of the water cooled chiller system is better than the air-cooled chiller system [Yu et al. 2014]. Although, the requirement of additional components in water-cooled systems may rise the initial capital cost of the plant. The use of either air or water cooled chiller system is dependent on thermal load, size of the building, utility of building and allied aspects.

1.4. Historical perspective and improvements in air-conditioning system

The first air-conditioning system was invented at the beginning of the 19th century, but at that time, these systems were quite large. Later in the mid-century, air-conditioning

systems became compact and also cheaper. These systems, which typically used VC cycle for operation, were using CFC based refrigerants and these refrigerants had very high potential of ozone layer depletion. Later in 1987, a protocol was signed to obsolete the use of this CFC-based refrigerant for the protection of ozone layer [Bohringer 2003]. After this, various environment-friendly refrigerants like: R134A, R22, etc. were developed which had low/nil ozone depletion potential. To date, multiple developments/modifications have been done in air-conditioning systems to improve the energy performance, cooling performance, reliability, reducing size, etc. The compressor is the main energy-consuming component in air-conditioning units as compared to other components like: fan motor, circuit, etc. Earlier, these air-conditioning systems used to consume significant amount of electrical energy, but now the energy efficiency rating (EER) of these systems has increased. Now, in the market, inverter-based air-conditioning systems are available that consume much lesser power than earlier air-conditioning systems [Nezhad et al. 2021]. In these inverter-based systems, the speed of the compressor is adjusted according to the flow of refrigerant, whereas in earlier non inverter designs, the compressor used to start and stop repeatedly, due to which energy consumption was quite high.

Various researchers have introduced many modifications in the direction of technological advancement. In this context, hybridization, cascading, coupling of accessories, design improvements are some of the terminologies that have been introduced to improve the system's performance. The extended application of VC cycle has been achieved via coupling of radiant cooling system, desiccant cooling system, etc. In the radiant cooling system, a loop of water circulation tubing circuit is applied to the building envelope such as: wall, floor, and roof. High conducting material pipings or panels are embedded either in building structure or false ceiling structure. A VC cycle system supplies chilled water in this piping loop and cooling effect is experienced via radiation and convection effects. Studies reported that radiant cooling system performs better than conventional air-conditioning system designs [Hu et al. 2012, and Hu et al. 2022]. Further, introducing desiccant material with VC cycle is also an effective way to improve performance. Desiccant is a material like: silica gel, zeolite, etc. which controls the humidity of air by the process of chemical dehumidification. In chemical dehumidification process, the vapor particles of the air are adsorbed on the desiccant material surface and released heat is added to the air. Consequently, this raises

the temperature of air. The addition of desiccant typically reduces the latent load of the air-conditioning system that consequently reduces energy consumption. Further, over time with the improvement phase of the VC system, the role of indirect and direct evaporative cooling, and heat recovery devices is also investigated.

As the trend of air-conditioning started with time, various issues came into the scenario, like global warming, disposal of refrigerants, condenser heat rejection, reduced air quality and many more. These issues forced development of some alternatives to the VC-driven air-conditioning systems. So, in market, inclusion of the absorption system took place. Although VA refrigeration cycle was invented long time ago, but usage of such VA systems for air-conditioning was not so popular. The advantages of VA systems in terms of low grade thermal energy based operation and usage of environment-friendly refrigerants attracted attention to these systems for air-conditioning applications [Srikhirin et al. 2001]. Earlier, single-stage absorption systems came into the picture, but due to the poor performance of this system, multi-stage absorption systems came into the scenario. Over time various modifications in the design of components, refrigerant-absorbent pair, and other aspects continue to be developed and discovered. As discussed earlier, the most suitable pair of refrigerant-absorbent used for the air-conditioning purpose is LiBr-water, where water works as a refrigerant. One of the major issues of using LiBr-water as a working pair is the crystallization of LiBr salt. Crystallization occurs when salt settles down under high concentration and very low-temperature conditions. This crystallization can block the pipe circuit of VA system, which eventually affects the working of the system. The experts have provided various guidelines for avoiding crystallization [Sun et al. 2012]. Apart from commonly used air-conditioning technologies like VC and VA, there are other air-conditioning methodologies/techniques such as: adsorption cooling, M-cycle, combined cooling and power cycle, also exist, but these have not yet gained market popularity.

1.5. Motivation and outline of research work

As stated above, mostly air-conditioning systems are grid-dependent and eventually causing rapid depletion of natural resources like coal, diesel, and petroleum reserves. Apart from this, global warming is an additional key concern of using these present air-conditioning systems. Significant amount of condenser heat in the urban areas is getting added to the sink i.e., atmosphere, that is causing rise in atmospheric temperature.

Alternative of this can be, renewable energy-based air-conditioning systems. Various forms of renewable energy are present like solar, biomass, geothermal, which are cleaner source of energy. On various parts of the globe, plenty of solar energy and resources of biomass are available that may be integrated with various air-conditioning techniques like VC and VA based systems. So, one of the reasons to conduct this study is to investigate the performance of commonly available and modified (i.e. assisted by desiccant, hybridization etc.) air-conditioning methods by integrating with renewable energy-based resources.

Integrating solar energy into the air-conditioning system is possible either in thermal or solar photovoltaic (PV) form. The direct integration of solar energy with the VC system is possible through the PV system. Still, economic issues/aspects and life cycle assessment can be the primary concern here. However, integrating solar thermal energy is possible with modified air-conditioning systems in various forms, such as regenerating desiccant, etc. [Khan et al. 2017]. One of the exciting motives of this work is to investigate the performance of solar thermal energy-assisted desiccant-based VC and VA systems, where the methods/techniques used for the cooling of process air (i.e., use of cooling coils, sensible heat recovery devices, evaporative cooler) after passing through desiccant is not systematically explored so that one can understand the overall scenario in the previous work. Additionally, the performance of air-conditioning systems with these methods/techniques is attributed to climatic conditions.

Further, today, in various industries where a huge amount of waste heat is available, there absorption systems are playing a significant role [Li et al. 2019]. The application of such systems for the condition where waste heat is not available but solar energy is present, like district office buildings, schools, and hospitals, there VA systems can play a prominent role. It is generally observed that the intermittency issue related to solar energy can affect the working of VA systems, so in such cases, auxiliary heating can be used. But, this area is not so clear because it may or may not be feasible to couple auxiliary heating energy supply all the time under all climatic conditions. This becomes another motivating aspect for this thesis work to explore the utility of the VA system according to the building type, locations, and type of auxiliary heating. Additionally, there are various other factors like collector area, heat source temperature and various heat input sources whose influence on the system performance is unclear. The comparative performance of VC and VA-based air-conditioning systems in terms of

electricity consumption, chiller performance, energy savings, solar fractions and various other parameters for the same building type, climate and other boundary conditions is also not available. In addition, an investigation of integrating a hybrid VA system with the radiant cooling methodology and comparison with conventional radiant cooling design is not done yet. Even if there are energy savings in a particular air-conditioning system, that system may or may not be feasible to attain the target of grid independency status. This investigation is also not done so far attributed to different climates and systems. Further, in this thesis, combined power and cooling generating system is explored using the solar and biomass based resources. That provides a fully renewable energy-based (solar and biomass) grid-independent air-conditioning systems is done to put a step toward sustainable development.

The relevant objectives have been investigated through simulation and experimental analyses on small and medium-scale office buildings. A simulation tool, namely EnergyPlus, has been used for modeling and assessing different considered air-conditioning configurations. All investigations are attributed to different climatic conditions such as: warm-humid, composite and hot-dry. The details of this simulation tool will be discussed in the later part of this thesis.

CHAPTER 2

LITERATURE REVIEW

The previous chapter demonstrated various kinds of air-conditioning techniques, configurations/classifications that are commonly used in the market and the associated concerns with them. It was highlighted that various environmental issues such as global warming, natural resources depletion and others are associated with the available air cooling techniques. The incorporation of renewable energy based resources in the field of air-conditioning technology can play an important role in addressing these issues. Although many researchers have introduced the addition of various forms of renewable energy in different ways, there is still ample opportunity to explore this area. Keeping this in mind, this work mainly focuses on analyzing the available renewable energy based air-conditioning systems and developing an improved/modified renewable energy-based air-conditioning system using solar and biomass-based energy resources. The literature review for the present work has been categorized into various sections. The first section discusses different commonly available air-conditioning technologies, modifications incorporated, ways of using renewable energy and allied aspects. The second section includes the literature related to the absorption-based cooling technologies, suggested modifications, and performance enhancement techniques employed. Finally, the last section concludes with some important observations, and research gaps identified which are useful for the present work.

2.1 Commonly available air-conditioning techniques incorporating renewable energy resources

Till date, considerable number of technologies have emanated in the field of building air-conditioning. Currently, maximum portion of the air-conditioning segment is based on high grade energy driven compressor-based systems. Such systems work on the VC cycle in which a compressor is used as the main working entity. Apart from this, VA-based systems are also playing a significant role in air-conditioning field. Many improvements in the compression driven air-conditioning technology have been made

by introducing the concept of variable air volume (VAV), VRF, hybridization, decoupling strategies, integration of components, and integration of solar energy in the form of PV and thermal. In the past, several studies have been reported towards improvement in energy performance and thermal comfort improvement of conventional compression driven and absorption-based systems. This task is attained by integrating the compression driven chillers with other improved systems such as: radiant cooling system, desiccant-based system, evaporative system. Not only this, significant amount of work has also been done ahead in this area of the radiant cooling system, desiccant cooling, hybridization etc. Here, some of the kinds of literature explaining the integration/hybridization, concept/methodology, limitations, drawbacks, additional improvements, novel directions etc. and various other aspects of the compression based technology are discussed below. Focus is on renewable energy and waste heat based cooling systems.

Yadav (1995) studied the performance of a solar-assisted hybrid compression and liquid desiccant based air-conditioning system of 1 kW room load. A set of flat-plate solar collectors in combination with condenser heat at 60 ºC temperature was used to regenerate the desiccant material. This combined system partially converted the latent load into the sensible load. In this study, LiBr salt was used as the liquid desiccant and R-11 refrigerant was used for compression cycle. Results of the thermodynamic model revealed that at 40% latent load conditions, the hybrid system saved around 53% of electrical energy savings. This saving proportion increased as the latent load fraction was increased. Finally, the author concluded that the proposed hybrid system was more suitable for warm-humid climatic conditions.

Sun (1997) investigated solar energy-powered combined ejector and compression driven air-conditioning and refrigeration system. The working fluids used in the combined proposed cycle were water and HFC-134a. In this cycle, the evaporator of the ejector sub-cycle was used as the condenser for the compression cycle. The cooling capacity of the combined cycle was 5 kW. Results of this study showed 50% more COP of the proposed system than the conventional compression driven systems. This environment-friendly system could also save more than 50% of energy. They presented this system as cost-efficient, low maintenance, and with less or zero ozone layer depletion potential.

Dai et al. (2001) established a hybrid air-conditioning system that included VC, desiccant and evaporative cooler arrangements for the humid climate. They explored various aspects of incorporating liquid desiccant material with a VC system and reported improved hybrid system performance. They proposed the usage of solar energy to regenerate the desiccant material. Evaporative cooling was used to cool the dehumidified process air of desiccant. The sensible load of the space was catered by compression system and latent load was handled by the desiccant. Experimental results of this study revealed 42.9% of less energy consumption and 2% more COP of the proposed hybrid system compared to the conventional compression cycle design. This hybrid system reported around 20-30% more cooling capacity than the conventional system. Further, the reduced temperature at the condenser exit was also highlighted in the proposed system.

Farayedhi et al. (2002) experimentally investigated the hybrid liquid desiccant-based compression air conditioning system for Saudi Arabia. Calcium chloride solution was used as the desiccant material in the packed bed dehumidifier and solar energy was used for regeneration. A VC chiller of 5-ton capacity along with heat recovery unit was used. Condenser heat with regeneration air was used for the desiccant regeneration. Three different strategies were used to regenerate the desiccant: direct desiccant heating, heating of air and heating of both desiccant and air. Results of this study reported the highest COP of the system of 1.615 with heating of air methodology. The overall COP of the system was comparatively higher than the conventional VC system-based air conditioning system.

Ghaddar et al. (2003) modeled a liquid desiccant-assisted compression-based air-conditioning system for 40 kW and 10.5 kW cooling applications in a restaurant and house, respectively, in Beirut. The design configuration in this study utilized the packed beds of counterflow between the air stream and solution for dehumidification and regeneration purposes. This study revealed an optimized airflow ratio in the regenerator to dehumidifier as 0.3-0.4. The obtained COP of the system for restaurant and house was 0.41 and 0.45, respectively. Solar fraction was investigated for different collector area. The different collector areas were 28.72 m^2, 57.44 $m^{2,}$ and 86.16 m^2. For these

collector area, the solar fractions were 0.25, 0.47, and 0.68, respectively for house and 0.19, 0.38 and 0.54, respectively for restaurant.

Yong et al. (2006) experimentally investigated the performance of a hybrid desiccant dehumidification-based compression-driven air-conditioning system for a very high-humid climate in Hong Kong. In this study, a desiccant-based heat exchanger was coupled with the evaporator and condenser section of the air-conditioner. An additional indirect evaporative cooler (IEC) was also connected with this system. Where condensing heat and the auxiliary heater were used for regeneration of desiccant. This supplemental heating value was converted equivalent to the solar energy/waste heat source energy. They highlighted that the desiccant process air flow rate and regeneration temperature greatly influenced the system performance. The system could attain a maximum performance of 0.5 based on primary energy input i.e., the equivalence of electrical energy input to that of the thermal energy input.

Jia et al. (2006) experimentally examined the effect of operating parameters on the performance of hybrid desiccant and refrigerant R-22 compression-based air-conditioning system. A solid desiccant wheel with lithium chloride material was integrated in parallel with the compression system's evaporator and condenser. A mathematical model was also developed and validated against the experimental results. It was found that the sensible heat factor of the evaporator increased significantly, and about 75% of the evaporator was operating at dry state. The proposed system reported around 37.5% of energy savings against the conventional system at the thermal comfort condition of 30 ºC and 55% relative humidity.

Eltawil and Samuel (2007) investigated the solar PV-operated VC system for potato storage under different operating conditions. Cold storage of 2.53 m^3 was constructed for experimental evaluation. The system contained a drier cum filter besides the other essential components. The energy consumption of the system was around 0.125-0.205 kWh. The actual obtained COP of the system was around 3.44. The average daily solar PV energy output and energy consumption by load were 5.65 and 4.115 kWh, respectively. It was finally concluded that solar PV panels could be used to run the whole system efficiently almost throughout the year.

Yutong and Hongxing (2008) performed a steady and transient simulation study on the solar liquid desiccant-based central air-conditioning system for Hong Kong. They optimized the collector length requirement for adequate regeneration of the desiccant. A conventional AHU was used in the system configuration with a solar-desiccant-based ventilation unit. Results of this study revealed that the use of the proposed system could provide 25-50% energy savings compared to conventional design. These energy savings would rise with an increase in the latent load portion. It was highlighted that higher regenerator temperatures could reduce the required collector length.

Li et al. (2010) performed a simulation study using the EnergyPlus to assess the energy performance of desiccant dehumidification coupled with a compression-driven air cooling system for Hong Kong. The economic aspects of the proposed system were also compared with the conventional design. The initial cooling capacity of the conventional system was 28 kW, and after an additional desiccant dehumidification unit, this capacity reduced up to 19 kW. The installed collector area for the flat plate solar collector was around 30 m^2. The improvement in the COP of the proposed system over the conventional design was about 1.3. Simulation results revealed that the proposed system was providing a saving of 6760 kWh electricity annually. An economic analysis of the system reported a payback period of 7 years.

La et al. (2011) experimentally and theoretically investigated the performance of a solar-based two-stage desiccant and VC driven air-conditioning system under different climates such as, temperate, humid and extreme humid. The simulation study was done by using the TRNSYS for an office building. An array of flat-plate collectors of 90 m^2 was used for desiccant system of 10 kW cooling capacity and compression system of 20 kW. A cooling tower arrangement was used in this study with the desiccant process air cooling. Results of this showed the hybrid system to be capable of handling 33% of the total cooling load with COP of 0.85 for humid climate. As a result, the electric energy consumption was reduced by 34% compared to conventional design. They also reported the feasibility of the proposed system for other climates, with energy savings of 31% and 22% for temperate and extreme humid climates, respectively.

Alili et al. (2012) introduced a novel hybrid solar PV and thermal collector system coupled with desiccant cooling and compression cycle. A “TRNSYS” simulation study

was performed for the warm-humid climatic conditions for 17.5 kW cooling capacity. A heat recovery wheel along with the compression cooling coil was installed in the path of process air passing through desiccant wheel. Solar thermal energy was used to run the desiccant cycle, whereas generated electricity was used for compression cycle. The overall performance of the proposed system was compared with conventional design and solar collector-assisted VA cycle. The average cooling COP of the proposed system, conventional system and absorption system was 0.68, 0.34 and 0.29, respectively. Overall results of this study reported that the proposed system was more effective than the standalone conventional compression system towards ensuring proper thermal comfort inside the building.

Hurdogan et al. (2012) investigated the utilization of solar energy in a desiccant-based solar air-conditioning system for Adana, Turkey. A set of desiccant wheel, heat exchangers, fan, and the evaporative cooler was used to simulate the solar energy for the refrigeration unit. A "FORTRAN" model was developed to assess solar energy performance and comparing it with experimental data acquired during the period of 1986 to 2006. The results obtained from the model and experiments were compared and found to be in suitable similarity. Results of this study depicted that utilization of solar energy in the proposed system increase the system COP between 50% and 120%.

Dang et al. (2012) performed a simulation study of a hybrid ejector and compression-driven air-conditioning system using solar energy for the climate of Tokyo, Japan. This hybrid system could operate for both cooling and heating applications. The working fluid used for the ejector cycle was R1234ZE, and R410A for compression cycle. The cooling capacity of the hybrid system was 2 kW with 80 ºC heat source temperature. Results of this study reported 50% of annual energy savings by the hybrid system in heating mode and 20% of annual energy savings in cooling mode against the conventional cooling system.

Mohammad et al. (2013) performed a survey to investigate the performance of different configurations of desiccant-assisted compression-based systems. They covered various system characteristics, performance indexes, and available hybrid cooling technique configurations. They discussed the principle of liquid desiccant regeneration and dehumidification process. They also elaborated that at high latent load conditions,

almost 60% of energy savings can be attained by using a hybrid system against the traditional air-conditioning system. They analyzed various configurations of hybrid cooling systems for cooling and heating applications using different desiccant materials. The study highlighted the usage of solar energy, waste heat and other low grade thermal energy to provide efficient cooling. It was reported that the most efficient utilization of such system can be ensured under warm-humid climatic conditions.

Mohan et al. (2015) investigated the performance of a hybrid liquid desiccant-compression assisted air-conditioning system under varying room temperature and humidity conditions. A liquid desiccant system was coupled to improve the dehumidification of air. In this setup, one column of the liquid desiccant was placed after the evaporator and another column was placed after the condenser unit of VC system of 0.8-ton capacity. Cool air, after passing through the evaporator was sent through a dehumidifier and was dehumidified before entering the room. On the other side, condenser waste heat was supplied to regenerate the desiccant. Experimental results revealed that, an increase in the room air reduced the dehumidification and regeneration process. 2 g/kg of moisture was removed from the process air by the proposed prototype.

Jani et al. (2015) investigated the suitability of a hybrid solid desiccant and VC based air-conditioning system having capacity of 1.8 kW under a warm-humid climate. “TRNSYS” simulations were performed from the month of March to September on a test chamber of 9 m^2 area. Occupancy of 5 persons generated 1.371 kW of sensible cooling load and 0.391 kW of latent load. A heat recovery wheel was used in the path of process air to exchange the heat between the cool return air and dehumidified hot air from the desiccant. An auxiliary heater was used for the desiccant regeneration in this work. They suggested that solar energy and waste heat can also be used as per availability. The results of this highlighted the suitability of the proposed system and alternative to the conventional system under the studied climate. Further, this work also observed that the system performance was greatly influenced by ambient temperature, humidity ratio and regeneration temperature.

Jani et al. (2016) experimentally investigated the performance of hybrid solid desiccant and compression-based air-conditioning systems for hot and humid climatic conditions.

They analyzed the system performance with varying outdoor conditions during the cooling demand season prevailing from March to October. A test room of 27 m^3 with a total cooling load of 1.75 kW was considered for the experimental study. To regenerate the desiccant material, they suggested the utilization of free sources of energy such as solar, and waste thermal energy to replace the auxiliary heating energy. A cooling coil was used in the path of process air to cool the dehumidified air coming from the desiccant. The humidity reduction through desiccant was from 18.5 g/kg of dry air to 7.10 g/kg of dry air that significantly reduced the latent load in the building. It was finally concluded that the system performance could be highly sensitive to ambient conditions.

Huang et al. (2016) investigated the running probability of an air-conditioning system equipped with a standalone solar PV system under variable outdoor temperature and radiation conditions of subtropical climate. Six different sizes of air-conditioner and PV configurations were made and tested. A battery arrangement was installed to address any intermittency issues. The cooling load power was varied in the range of 200 W - 650 W and installed PV power was varied from 430 W - 1380 W. Test results showed that the operating probability of the system was more than 0.98 under the condition of more than 600 W/m^2 solar radiation, with ratio of maximum power generation to load power greater than 1.71. The average run time fraction was around 1.0 under the condition of daily total solar radiation of more than 13 MJ/m^2 per day.

Goldsworthy (2017) performed a detailed simulation study to assess the feasibility of a small off-grid solar PV based air-conditioning system for different building thermal designs. “TRNSYS” simulations were performed for different Australian climates. They study highlighted that building’s thermal design aspect influences the size of solar PV required to fulfil the air-conditioner’s electricity requirement. The simulation model was composed of a VC cycle, solar PV and battery storage modules. Results of this study reported that, by using a certain combination of building thermal design and ambient, 100% comfort can be obtained by PV assisted air-conditioning system.

Khan et al. (2017) studied an alternative methodology of dehumidification by using desiccant material coupled with the radiant cooling system. The performance of desiccant-assisted DOAS was investigated with different solar collector areas under the

warm-humid climate. “EnergyPlus” simulations were done for a medium office building with 5000m^2 of total floor area and the solar collector area varied from 500m^2 to 1000m^2. The regeneration temperature for the desiccant material was considered as 60 ºC and the required hot water temperature from the solar collector loop was 80 ºC. An auxiliary water heater was also coupled with the solar collector loop for addressing any solar intermittency. They assessed the system performance of the proposed desiccant DOAS coupled with an IEC against the conventional cooling coil-assisted DOAS for radiant cooling system. Simulation results revealed that by varying solar collector area, energy saving varies from 7.4% to 28.6%. They highlighted that for the studied air-conditioning system, 700 m^2 collector area gave optimum results for economical cooling.

Ali et al. (2018) investigated the performance of five solar desiccant-based air-conditioning systems at the global and system level scale by using equation-based object orientation modeling. They included a wide range of climate data such as arid/semi-arid (Karachi, Pakistan), dry summer tropical (Adelaide, Australia), and mesothermal (Sao Paulo, Brazil and Shanghai, China) to continental conditions (Vienna, Austria). Solar energy was used to regenerate the desiccant material. The five configurations of air-conditioning were ventilation cycle, recirculation and ventilated recirculation cycle, dunkle, and ventilated dunkle cycle. In the dunkle cycle, an additional heat exchanger (heat recovery wheel) was used with the desiccant wheel. The simulation study was done in the “DYMOLA/Modelica” environment. Using the simulation outcomes, the authors suggested the ventilated dunkle cycle to be suitable for the climate of Vienna, Sao Paulo, and Adelaide with COP of 0.36, 0.84 and 0.93, respectively. Further, the use of ventilated cycle was found suitable for Karachi and Shanghai with COP of 2.32, 2.90, respectively.

Fong et al. (2019) discussed the stratum air distribution in a building to facilitate high-temperature cooling. They evaluated the potential of using this strategy with solar-driven compression-based air-conditioning system. Different combinations of various air conditioning techniques such as absorption, adsorption, compression and desiccant were coupled and analyzed using TRNSYS. Solar energy was used to run the absorption, adsorption and desiccant units. They explored the dynamic behavior of all the considered systems throughout the year. The total generated cooling load was 29

kW in an office building of 14m × 14m × 3.6 m. Simulation results reported 29%-59% of energy savings by the proposed stratum ventilation strategy against the conventionally used mixed ventilation strategy.

Kim et al. (2019) investigated the performance of a desiccant-assisted compression-based air-conditioning system using the EnergyPlus simulation tool for the Korean climate. This climate was warm-humid in the summer season and cold-dry in winter. An energy recovery device was coupled with the desiccant system using the condenser heat of the compression system. The total gross area of the considered building was 21796 m^2. The summer and winter set point temperatures were 25 ºC and 22 ºC, respectively. Different air circulation strategies i.e. recirculating and bypassing air were examined with the system. Results reported that the appropriate winter ventilation strategy that included indoor humidity control of 30% and constant energy recovery showed 23% heating energy savings. The summer ventilation strategy, including an energy recovery ventilation, hybrid desiccant system, and fixed enthalpy economizer control, saved 22.5% of cooling energy.

Song and Sobhani (2020) assessed the unsteady performance of solar desiccant cooling systems assisted by phase change material (PCM) and Maisotsenko cooler under hot-humid climate. Solar PV and thermal collector loop was installed to work as a heat source for the regeneration, whereas, PCM was used to supply heat energy during the night hours. The simulations were done in a small office building having 174 m^2 of floor area in Bandar Abbas, Iran. The maximum cooling load of the building during August was 18.7 kW and maximum regeneration energy was 45.06 kW. The maximum obtained COP of the combined system was 0.404. The solar loop's maximum energy and exergy efficiency was around 5.4% and 19.7%, respectively. It was also highlighted that the usage of PCM aids in maintaining uniform temperature of PV modules, thereby improving the system's performance.

Liu et al. (2020) evaluated the performance of solar-powered hybrid two-stage rotary desiccant and compression driven air-conditioning systems for low latitude isolated islands. "MATLAB" tool was used to analyze various performance parameters of the combined system involving dehumidification capacity, cooling capacity and other performance coefficients. They also optimized the requirement of solar PV area and

solar collector area based on the metrological parameters. Results of this study showed that for each 10 ºC rise in regeneration temperature, dehumidification and cooling capacities increase by 0.9 g/kg -2.7 g/kg and 0.4 kW – 1.9 kW, respectively. It was also highlighted that the total installed area of solar PV and collector systems increase when moisture of surrounding air and condensation temperature increase.

Chen and Norford (2020) presented a thermodynamic and simulation model using the EnergyPlus tool for different configurations of a DOAS coupled with a compression-based system. In this DOAS, different arrangements of various components such as the desiccant wheel, heat wheel, enthalpy recovery wheel and membrane based were studied. Renewable energy-assisted system were also coupled to improve the system performance. In this study, desiccant and membrane-based DOAS systems were the advanced cases, whereas other component-assisted systems were the base case. Based on industry standards, a low-energy office building prototype was constructed for evaluation purposes in Boston. Results of this study reported that the proposed membrane-based cooling systems achieved higher energy efficiencies than the baseline chiller system and its variations in most examined climates. Further, the proposed desiccant cooling system outperformed the baseline chiller system and its variations in energy efficiency in most examined climates, especially hot and humid conditions.

Varvagiannis et al. (2021) analyzed the performance of a novel refrigerant–paraffin PCM based water heat exchanger that replaced the evaporator of a conventional compression chiller. For this purpose, they built a semi-dynamic lumped model using the TRNSYS software and annually evaluated the system performance for the single zone reference building for Greek. A solar PV system with electrical storage was used to drive the compression chiller. It was found that the COP of the compression chiller drops drastically during the charging of PCM. At the full charge condition, the COP was 2.2. It was concluded that the addition of thermal storage enhanced the system performance and improved the solar fraction obtained.

Gao et al. (2021) performed a systematic review study on the integration of desiccant units in different configurations with compression-driven air-conditioning systems to improve the system performance. They divided their study into the following sections by discussing overviews, integration approaches of desiccant, configuration

improvements, and design-control optimization study of desiccant-assisted cooling system. Integration of various types of solar collectors, biomass, and natural gas with the desiccant unit was also discussed. They highlighted different outcomes of their study, such as solar collector was the most widely used and economical way to integrate with desiccant assisted compression based air-conditioning system. Most of the design and control optimization were simulation-based, so experimental evaluation for optimization is critical. Finally they recommended integrating desiccant technology with a compression-driven system to improve the system performance.

Elhelw et al. (2022) proposed a new hybrid solar-driven compression-based air-conditioning system design. Three different cases of solar integration with compression system was investigated: the first was a conventional design, the second was a conventional design with the addition of an evacuated tube solar collector along with a compressor for refrigerant compression, and the third was conventional design with the addition of evacuated tube solar collector-heat exchanger along with compressor for refrigerant compression. They first theoretically investigated the considered cases and then experimentally evaluated the best suitable case. Third system was found to be best performer compared to the other two. Experimental results showed an improvement in COP by 20.3% in the proposed case against the conventional case with refrigerant R-290. Further, for the proposed case, the compressor power was reduced by 8.2%, and the increase in cooling capacity was 10.1% in comparison with the conventional one.

Ibrahim and Ahmed (2022) theoretically investigated a hybrid liquid desiccant-based compression-driven air-conditioning system. In this system, the dehumidifier was internally cooled, and the regenerator was adiabatic. Waste condenser heat and outsourced solar energy was used to regenerate the desiccant material. A falling film model was applied to the desiccant-compression unit. They investigated the effect of an internally cooled dehumidifier on the air temperature and humidity ratio. Along with this, the effect of different air mass flow rates on effectiveness of dehumidifier and regenerator was also evaluated. Simulation results revealed a decrease in COP of the conventional system by 47.2%, whereas an increase in COP of the proposed hybrid system by 49.8% when there was a rise in condenser temperature. The effectiveness of the dehumidifier and regenerator dropped with the increase in air flow rate.

Wang et al. (2022) compared the solid-liquid desiccant assisted system and conventional air-conditioning system using the EnergyPlus tool in different climatic conditions. The developed building model had 7836 m^2 of total floor area with 30% window-to-wall ratio. Results of this depicted the better performance of both the solid and liquid desiccant-based systems in all climates than the conventional air-conditioning system. Further, it was highlighted that solid desiccant had better temperature control, and the liquid desiccant system had better humidity control. In a hot and humid climate, 45% relative humidity could be reached and stably maintained by liquid desiccant-based system in summer when the relative humidity set point was 50%. While in the case of a building controlled by a split air conditioner system and solid desiccant air conditioner system, indoor air relative humidity could reach 65% in summer.

After discussing some of the VC-based configurations of renewable energy-assisted air-conditioning system, next, VA, adsorption and ejector systems are discussed, which are also most commonly-used techniques of air-conditioning. These systems are also known as thermal energy driven systems in which low grade thermal energy obtained from various resources like waste heat, solar energy and other sources may be utilized. These types of systems are those in which renewable energy can be integrated effectively. Some of the modifications/improvements and strategies concerning the domain of renewable energy-based absorption, adsorption and ejector systems are now discussed below.

Muneer and Uppal (1985) developed a detailed numerical model of a commercially available LiBr- water based absorption chiller having the capacity of 2 Tons. The study was performed for arid location by using the summer season meteorological data, solar insolation and humidity levels. The developed numerical model calculated hourly thermal load, cooling water temperature and required generator temperature, and chiller's COP. The simulation program was run for a wide range of collector area, storage volume to area ratios and two types of solar collector, depending on collector efficiency. The final outcome of this study reported the optimum ratio of hot water storage to collector area. The obtained optimum ratio of storage volume/collector area from the simulation results was found as 0.045. It was also established that the system was able to run at full load at considerably low generator temperature of around 70 ºC

-80 ºC. Thus, finally they established a huge potential of solar-based absorption chiller for arid climatic conditions.

Tsilingiris (1993) proposed a flexible theoretical model of a VA system for evaluating the operational behavior and performance prediction of small residential applications under local weather conditions. A set of flat-plate solar collector and storage tank was used for providing the heat energy. Using this model, design optimization and economic assessment can be done for many other locations also. Results of this study showed that maximum load of the system was met when storage tank water temperature was around 80 ºC. The economic analysis of this study revealed that payback period for this system was considerably long and further improvements were required for reducing this.

Horuz (1998) presented a comparative analysis between LiBr-water and ammonia-water based absorption systems. This study presented a comparison in terms of COP, cooling capacity and operating pressures. Study also explored the associated limitations and barriers to the absorption systems, like crystallization, operating conditions of using water as either refrigerant or absorbent. Author also highlighted the use of either waste heat or solar energy for operating the absorption chiller. Use of LiBr water based system was found limited to the air-conditioning application, whereas ammonia water-based system could be used for very low temperature process work. It was shown that for the same performance ammonia water based system involves more complexity than LiBr-water-based system. Results of this study revealed that LiBr-water absorption system yield better COP than ammonia water based system, but its application is limited by the crystallization of LiBr salt. The intensification in the generator temperature increased the COP of both the systems.

Romero et al. (2001) developed a mathematical model to predict the performance of a single stage absorption system for heating and cooling application. They investigated the model with two types of mixture, LiBr-water and ternary hydroxide mixture of sodium, caesium and potassium. Use of mixture in the absorption system allowed lower risks of crystallization for heat pump applications. It was revealed that at higher condenser and absorber temperatures of 50 ºC, hydroxide mixture-based absorption system show better performance than LiBr-water-based system. Results of this study

also indicated that the COP and other operating conditions were almost same for both mixtures.

Kececiler et al. (2000) performed an experimental study on a developed lab scale absorption chiller fed by geothermal energy in hot spring of Sivas, Turkey. In that particular location, a lot of geothermal energy resources was available whose temperature was more than 50 ºC with volume flow rate of around 500 liters/s. It was revealed that the COP of the system increases with generator temperature as well as evaporator temperature. Further, COP of the system also increased with decrease in condenser and absorber temperatures. Experimental results revealed that hot water mass flow rate of 12.5 kg/s at 60 ºC temperature was enough for 225.7 kW cooling effect. It was recommend that the usage of geothermal energy for refrigeration purpose is an economically feasible option.

Li and Sumathy (2001) experimentally investigated the performance of a modified solar absorption chiller by integrating it with a partitioned hot water storage tank. This modification was done by creating two separate storage volume into a single drum. The first partition of the storage tank occupied one fourth of the total tank volume. They made a comparison of the proposed system with the conventional single whole tank mode system. A loop of flat-plate collector (38 m^2 collector area) was coupled to drive a 4.7 kW of absorption chiller having storage tank volume of 2.75 m^3. This study revealed that, using the modified tank, cooling effect could be realized 2 hours earlier than the conventional design. Experimental results also revealed that solar COP of the proposed system was 15% higher than the conventional design and the chiller was also capable to deliver cooling effect even in cloudy days.

Misra et al. (2003) demonstrated an exergy-based simplified thermo-economic analysis to optimize a waste heat steam driven single-effect LiBr-water-based absorption air-conditioning system. In this study, the average cost approach was used to optimize the system thermo-economically. Using the exergo-economic cost equations, economic costs of all the internal flows and products of the systems were calculated. This study identified the effects of design variables on the system cost and also defined the values of these design variables to make system cost effective. Results of this study showed

that at the optimal design point, reduction in cost of exergy reduction was about 11.5% and reduction in cost of exergy loss was about 5.5%.

De Lucas et al. (2004) investigated the performance of a novel absorbent alternative to the LiBr salt for the absorption system. This novel absorbent consisted of LiBr and potassium formate in the mass ratio of 2:1. For comparing the system performance with conventional system, a simulation model was developed using the empirical data. Addition of potassium formate showed lower crystallization temperature, vapor pressure and viscosity. This addition also reduced heat involved in the refrigerant absorption and desorption, thus lesser heat energy was required at the generator side i.e., low grade thermal energy in form of solar energy could be utilized. Experimental results also revealed that with the new alternative absorbent, no crystallization occurred at the temperature of around 14 ºC, and generator temperature required for regeneration of refrigerant was around 55 ºC. The system possessed COP of 0.85 with alternative absorbent whereas, with only LiBr salt condition the COP was 0.75.

Pridasawas and Lundqvist (2004) performed an exergy analysis on solar based ejector refrigeration system to optimize the operating conditions. They calculated the associated irreversibility in each component of the ejector cycle. A tool Engineering equation solver (EES) was used for the modeling purpose for the cooling capacity of 5 kW and butane was used as the refrigerant for this study. They assumed 70% ejector efficiency with the evaporation temperature of 10 ºC. The obtained thermal efficiency of the solar collector system was 41.01%, with overall system efficiency of 11.24%.

Assilzadeh et al. (2005) carried out an optimization study to show the possibility of using evacuated tube solar collector with single-stage absorption air-conditioning system. Using "TRNSYS" software, they computed the system performance for Malaysia and other similar tropical climates. Results of this study presented that, during high sunshine time, the system would be able to run at its full capacity. Further, in order to ensure continuous operation of this system, a storage tank of 0.8 m^3 was needed. The optimization results of this study showed that for 1 ton of refrigeration effect the required solar collector area was 35 m^2 with 20º slope.

Vega et al. (2006) studied the performance of an absorption chiller assembly which was consisting plat-type heat exchangers in the generator, condenser, and solution heat exchanger. A vacuum tube solar collector was used to supply thermal energy. This particular heat exchanger was liquid to liquid type. Various heat transfer characteristics and correlations were taken from other previously done studies. To compare the system with other machines, the obtained results were used to predict a more realistic seasonal performance coefficient. Simulation results revealed that as the outside temperature increased, the COP of the system decreased. The obtained COP was 0.8 at 20 ºC ambient temperature and 0.75 at 30 ºC ambient temperature. At part load conditions, the overall heat transfer coefficient for the generator was obtained as 790 W/m^2. The chiller response with respect to different mass flow rates and temperatures were also presented in their study.

Ma et al. (2006) investigated the performance of a hybrid adsorption and compression driven air-conditioning system in Shanghai, China. A loop of 150 m^2 solar collector was used to run the adsorption chiller of 10 kW. Along with this a liquid desiccant system was coupled to handle the latent load. Condenser heat of the compression system was used to regenerate the desiccant material. The total cooling load of the building was around 60 kW. The results of this study reported that, at 30% latent load conditions, the proposed system was capable to perform 44.5% better than the conventional cooling design. This improvement could attain up to 73.8% at a 42% latent load condition. It was also highlighted that, if the system had run entirely on solar energy, the cost would have been very higher.

Liao and Radermacher (2007) proposed temperature-based strategies to control or avoid the crystallization problem in air-cooled LiBr-water-based absorption chiller. A simulation model was developed using the EES and validated against the experimental data obtained from the 63 kW water-cooled absorption chiller installed on the roof of university of Maryland, USA that was fed by waste heat of micro turbine exhaust. They suggested six causes of crystallization: high ambient temperature, low ambient temperature at full load, air leakage in system, excess amount of heat input in generator, unsuccessful dilution during shut down, and very low set point of chilled water temperature. The proposed temperature control strategies were very effective to avoid crystallization, these are to increase the chilled water temperature and reduce the heat

energy input temperature to the generator. They also projected the utilization of the proposed strategy in a combined cooling, heating and power-based application with considerable amount of improvement in economics of the plant.

Pongtornkulpanich et al. (2008) performed an experimental study on a fully operational solar driven single-effect LiBr-water-based absorption chiller of 10 kW capacity. This setup was designed and installed at the school of renewable energy in Thailand. A loop of evacuated tube solar collector with 72 m^2 area was coupled to the chiller and an auxiliary gas fired facility was also installed for ensuring its continuous operation. The supplied hot water at 70 - 95 ºC was coming from 400 liters storage tank. Experimental results revealed that this technology was much more environment friendly than other conventional systems. Further, results showed that 81% of required thermal energy was fulfilled by solar collector and the remaining 19% from gas fired system.

Kim and Ferreira (2009) theoretically presented that half-effect absorption chiller could work efficiently in the extreme hot and dry climatic conditions. The considered system was working with dilute LiBr salt concentration as compared to the commercially available chiller. A loop of flat-plate solar collector was used to supply hot water at 90 ºC to the chiller. They modeled both direct and indirect air-cooled absorption chillers by combining the proper components of the model and boundary conditions in matrix. The model was solved by using algebraic equation solver. Simulation results revealed that, direct and indirect cooled chillers were providing water at 5.7 ºC and 7.8 ºC with COP of 0.38 and 0.36, respectively. As compared to the commercial chiller, risk of crystallization was also very less under 100 ºC of hot water temperature condition. Finally, they concluded the direct air-cooled chiller to perform better.

Guo and Shen (2009) investigated the performance of a solar-driven ejector refrigeration cycle by using R134a refrigerant for an office building in Shanghai. This study used the lumped method with a dynamic model to predict the system performance. The designed cooling capacity was 6 kW with 8 ºC evaporator temperature. A set of vacuum tube solar collectors of 15m^2 with an auxiliary heater was employed in this study. Results of this study revealed that both COP and cooling capacity of the system first increases and then decrease with increasing the generating temperature. The maximum COP of around 0.72 was obtained at the generator

temperature of 87 ºC. For a typical office hour schedule, the average COP was 0.48, and the average solar fraction was 0.82. Further, it was also highlighted that the ejector refrigeration system could save around 75% of electrical energy savings compared to the conventional air-conditioning system.

Ma et al. (2010) designed a novel ejector-driven air-conditioning system of 5 kW capacity and experimentally evaluated the various performance parameter. Water as a refrigerant was used in this cycle for air-conditioning applications with solar energy-based regeneration. A spindle was added as a new feature for tuning the ejector. This spindle could control the nozzle's flow area and throat, changing the area ratio. They investigated the performance by changing the area ratio. Results revealed the effect of various spindle positions on the cooling capacity and COP of the system. As the spindle moved towards the nozzle side i.e. with the decreased primary flow, the cooling capacity decreased. The maximum cooling capacity of the system was obtained at the generator temperature of 92.8 ºC, and the maximum COP was found at the 90 ºC boiling temperature.

Kundu et al. (2010) analytically investigated the thermal performance of different profiles of absorber plate for a flat-plate solar collector coupled with a single-stage absorption system having 1 ton capacity. They analyzed absorption system performance by varying the shape and collector fluid inlet temperature. Various profiles: rectangular, concave, convex, trapezoidal, triangular were considered. In this study, they tried to obtain optimum fluid inlet temperature corresponding to the minimum collector volume. Simulation results revealed that for all the considered profiles, the COP value increases with increasing the inlet fluid temperature and with increase in fluid temperature, the plate volume first decreases and then increases. Finally, it was concluded that the absorption chiller's performance significantly depends on the fluid inlet temperature to the collector as compared to the shape of the profile. In this study, one of the considered concave parabolic shapes gave a minimum plate volume.

Gonzalez gil et al. (2011) experimentally investigated the performance of a solar-assisted direct air-cooled single-stage absorption air-conditioning system. In this study, a novel kind of absorber termed as adiabatic absorber was installed in the actual prototype which was using flat-fan sheets inside it. In the chiller, both condenser and

absorber were directly air-cooled. A special feature of this chiller was that, this chiller could work as both single and double-stage absorption chiller, depending upon the heat input source availability. A set of 48 m^2 flat-plate solar collector was coupled with the single-stage absorption system. This experimental study was performed during the summer in Madrid, Spain and was validated against the available literature data. Results of this work showed the efficient working of system with capacity of 2 kW to 3.8 kW. The obtained chilled water temperature was ranging between 14 ºC – 16 ºC and the lowest temperature attained was 12.8 ºC. The working prototype worked at about 85% of nominal capacity with COP of 0.6. Also, no sign of crystallization were observed during its 100 hours of working operation.

Paurine et al. (2012) developed a novel thermo-gravity-based mechanism for pumping the solution between absorber and generator in a typical absorption system. In this study, they have introduced a novel manner of converting thermal energy into mechanical energy for lifting the solution. Two kinds of float valves were used in their experimental setup. Results of this study revealed that, for 2.34 kW of refrigeration effect, the required thermal energy at the generator was around 3.26 kW only, representing its very high operating COP as compared to the other design. The highest obtained COP for this system was determined to be 0.72 and the required generator temperature for the suggested design was found to vary between 75 ºC-85 ºC.

Cabrera et al. (2013) performed a comprehensive survey on various types of solar collector systems coupled with absorption-based air-conditioning system. They presented a survey of new collector potential for double-staged absorption system. Extensive research study explored that, for single-stage absorption systems, evacuated tube collector performed better, and it is followed by parabolic trough type designs. For double-stage absorption chillers, parabolic trough collectors were found to be more efficient as compared to other collectors. These collectors offer lower thermal losses with high working efficiency compared to other available designs, like flat-plate and evacuated tube collector based systems. It was also highlighted that the parabolic trough collectors offered higher solar fraction values followed by evacuated tube and flat plate collectors in case of single-stage absorption system, whereas in case of double-stage absorption system, similar solar fractions were observed with parabolic trough, evacuated tube and flat-plate collectors. They reported a generalized design criteria for

selecting the area of solar collector as: 0 - 3 m^2/kW for single-stage absorption and 0 - 2 m^2/kW for double-stage absorption chiller.

Prasartkaew (2014) experimentally investigated the performed of a renovated LiBr-water based single-stage absorption chiller for Thailand. They replaced the working fluid and controller circuit of an out of order commercial chiller having capacity of 2 Tons. They discussed the experimental procedure and route of analyzing the chiller performance by using waste heat and renewable-based heat sources under the three generator temperature ranges: 80 ºC, 85 ºC and 90 ºC. The selected concentration of LiBr salt solution was at 59 %. Experimental results revealed the average cooling capacities for these three temperature points as 4.2 kW, 5.1 kW and 5.3 kW, respectively, and the chiller ran at 50 %, 72 % and 75% of nominal capacity at the selected generator temperatures, respectively. They proposed that, in order to obtain high COP, system should operate at 85 ºC of hot water temperature.

Ketfi et al. (2015) investigated the performance of a 70 kW LiBr-water-based single-effect absorption system using "MATLAB" simulation tool. A set of 225 m^2 flat-plate and 175 m^2 evacuated tube collectors were installed for supplying heat energy. They assessed the performance of the chiller by varying the heat exchanger efficiency, condenser, absorber and generator temperatures. Simulation results revealed that for the considered refrigeration effect, around 90 kW of thermal energy was required. Further, this study concluded other points such as, COP of the system increased with increase in generator temperature, COP of the system decreased with increasing condenser and absorber temperatures, with rise in evaporator temperature the COP of the system improved, and higher heat exchanger effectiveness provided higher COPs. Simulation results pointed out that, the COP of the system reached up to 0.77 at 92 ºC of generator temperature.

Ugla et al. (2016) performed a techno-economic analysis on different solar energy-based air-conditioning systems for Kobhar city of Saudi Arabia. They compared three different kinds of air-conditioning systems: conventional compression driven system, solar-assisted single-stage absorption system and solar PV-based compression system. They adopted two economic strategies: payback period and net present value (NPV) for the analysis. In all three considered systems, the nominal capacity (1500 kW) of the

chiller was kept same and solar energy was used for addressing the peak load during day time operation. The results of this study in terms of payback period and NPV showed that, solar absorption system was best suited with solar energy compared to the other two designs over a wide range of electricity rates. The estimated payback period for absorption system was 18.5 years whereas, for PV-based compression system it was 23.9 years.

Martinez et al. (2016) presented a reliable and validated model of a 17.6 kW absorption chiller for estimating various performance parameters by using some of the input parameters. This simulation model was developed by using the EES tool. A loop of solar collector was coupled to drive the absorption chiller. They proposed the correlations between dependent variables like: output temperatures of generator, evaporator, condenser, absorber and independent variables like: inlet temperatures of generator and other components with overall heat transfer coefficients. They validated the estimated correlations against the available experimental data. The simulation results revealed a deviation of 0.75 ºC between experimental and simulation temperature data in the generator, and 0.35 ºC deviation for the evaporator. This simulation model could also be used for obtaining the data for any absorption chiller by using some specified input parameters.

For residential buildings, Chen et al. (2017) performed an experimental and simulation study on a small-scale air-cooled absorption system fed by evacuated tube solar collector. They evaluated the annual performance of the developed system under steady-state conditions. Using “TRNSYS” simulation tool they developed the model for predicting the performance. The absorption system was having a capacity of 6 kW and 40 m^2 collector area along with 500 liters storage tank. Results of this study revealed the performance of chiller under different operating conditions. Results also showed that COP of the system reduces by increasing the ambient temperature, while the same enhances when chilled water outlet temperature increases. Inlet hot water temperature was having enormous effect on cooling capacity of the system, and the same increased by 65.52% when generator inlet temperature was increased by 20 ºC.

Sokhansefat et al. (2017) performed a transient simulation and parametric study of an absorption system of capacity 5 Ton in Tehran. Using the TRNSYS simulation tool

they developed a model for all the coupled components in solar air cooling loop such as: solar collector, tank, boiler, chiller, cooling tower, heat exchangers, AHU and pumps and presented the performance of system. Finally they gave the optimized design criteria for solar air-conditioning system including: 55 m^2 solar collector area, 1000 liter of tank, boiler temperature at 77 ºC, slope 33º and solar collector water mass flow rate of 1000 kg/h.

Porumb et al. (2017) presented a mathematical model of a single-stage solar absorption chiller by using various libraries of EES tool. They validated the proposed model against the available literatures in terms of COP and the calculated error was within -5.4% to 5.6%. In this study, they investigated the influence of various parameters on COP of the system and on crystallization conditions. They illustrated that risk of crystallization was more when hot water temperature was beyond 95 ºC and cooling water was below 20 ºC. They also established the influence of various parameters on degassing zone of the absorption chiller.

Shaarawi and Ugla (2017) performed an unsteady-state analysis of a solar-powered hybrid storage-based absorption system of 5 kW capacity for ensuring 24 hours continuous operation in Saudi Arabia. This hybrid storage was included for storing cold water and refrigerant. An additional heat storage tank was also used for addressing the crystallization issue. The components generator, absorber and condenser were running during day time only. With the help of EES tool, they developed model and graphs for evaluating the performance of the proposed system. They validated the developed model against the available literature. Results of this study delineated that, under a constant cooling load, the COP of the system is better under winter, whereas, the collector area requirement and refrigerant storage tank size are smaller in summer.

Chen et al. (2018) developed a novel air-cooled absorption chiller in which adiabatic flash evaporator and adiabatic absorber were there. In this design, a secondary outside chilled water loop was eliminated and direct refrigerant water was used in indoor air handling of the test chamber. This design also eliminated use of separate chilled water circulation pump. A non-focusing solar collector loop with heater of 40 kW was used for supplying heating energy. They performed three sets of experiments on the developed setup at different operating conditions. This novel design was capable in

improving system COP and performance with reduced size and material requirement. Results of this study showcased the attainment of chilled refrigerant water at 8.6 ºC along with maintained room temperature of 26.6 ºC, when the outdoor temperature was 35 ºC. The cooling capacity and COP of the developed system was 5.3 kW and 0.72, respectively under low ambient temperature conditions, and the same were evaluated as 4.6 kW and 0.65, respectively under high ambient temperature conditions.

Aman et al. (2018) analyzed the performance of bubble pump-driven LiBr- water and LiCl- water-based absorption air-conditioning system. In this study, they incorporated bubble pump into solar collector and absorption chiller for making it fully grid-independent in operation. They developed a theoretical model of bubble pump-driven absorption system and also compared the performance with both types of solutions as mentioned earlier. They also highlighted a few drawbacks of bubble pump driven absorption chiller like: crystallization issue, low pressure and low efficiency. Results revealed that COP of system with both the solutions was increasing with escalation of heat energy input. Simulation results revealed highest cooling effect of 49 W and COP of 0.56 with LiCl-water case, and highest cooling effect of 34 W and COP of 0.46 with LiBr-water.

Li et al. (2018) proposed and analyzed the performance of a new working pair of $CaCl_2$-LiBr-$LiNO_3$/H_2O for an absorption system driven by glass tube solar collector system. They experimentally analyzed the performance of the novel refrigerant-absorbent pair over the conventional LiBr-water pair. The novel pair was capable in raising the crystallization temperature. Results of this study revealed that crystallization temperature of the proposed solution was 25.3 ºC which was very less compared to the conventional one which was around 30-40 ºC for 65% concentration condition. Further, the required generator temperature for 7 ºC refrigeration temperature was found as 80.3 ºC which was 7.7 ºC lower than that of LiBr-water case. Results also showed 0.04 higher COP with the proposed working pair with respect to LiBr-water pair.

Over the last few decades, several kinds of performance enhancement techniques have been employed in conventional design of absorption system. These techniques are mainly based on multi-staging and incorporation of additional heat sources besides/along with solar thermal energy, thereby making the system hybrid in nature.

Multi-staged absorption systems make efficient use of high temperature heat sources compared to the single-stage ones. Further, in case of either deficiency of solar radiation or unavailability of sufficient amount of any particular heat resource, then auxiliary heat input method can be considered for ensuring uninterrupted running of the system. These auxiliary methods can either be based on electricity, natural gas, waste heat or any other suitable source. Additionally, various design related aspects are also considered for improving the absorption system performance. Some of the related literature published in this context are discussed below.

Arun et al. (2001) compared the performance of waste heat-driven LiBr-water-based double-effect parallel flow absorption system against the series flow system. They considered the condition of equilibrium temperature and salt concentration in the low pressure generator, which was not considered in the earlier studies. In the parallel flow absorption chiller, solution was sent simultaneously into both high and low pressure generators after the low pressure heat exchanger. But, in the series flow system, solution first went inside high pressure generator and then it reached the low pressure generator. Theoretical results revealed that for both parallel and series flow absorption systems, COP of the system increased with increase in evaporator temperature, heat exchanger effectiveness and energy input to the generator. The COP for the parallel flow case was found higher than that of the series flow chiller. The sensitivity analysis was also done, that portrayed that the COP is more sensitive to the evaporator temperature than absorber and condenser temperatures.

Yoon et al. (2003) experimentally examined a double-stage absorption system of 125 Tons capacity based on waste heat utilization. In this study, they did not use any outside waste heat for running the system, whereas only the waste exhaust heat from the burner of high temperature generator itself was used for preheating the solution that was going to low pressure generator. The temperature of the waste exhaust was around 200 ºC that was sufficient to preheat the solution. They reported the experimental results against the conventional design. They also proposed a methodology for reducing the time for starting the system. Experimental results displayed that, utilization of waste heat reduces the energy consumption in high temperature generator by 2.8% and 5.1% under the cooling and heating modes, respectively. A higher COP of the proposed design was

also demonstrated than that of the conventional design. Finally, the proposed design was concluded to be efficient and energy efficient than the conventional design.

In order to show efficient utilization of auxiliary energy source and less dependency on solar energy, Liu and Wang (2004) designed and theoretically analyzed a novel type of solar and gas driven double-effect absorption system of 10 kW capacity for Shanghai, China. Conventional energy and natural gas were used to feed high pressure generator, and the generated high temperature vapor along with solar thermal energy in form of hot water at 90 ºC was used at the low temperature generator. Apart from providing cooling, the developed novel system was also capable in delivering hot water during winter seasons. Simulation results indicated that with 13.5 m^2 flat-plate collector, the value of solar fraction for the cooling mode is 30.5% whereas, throughout the year solar fraction reached up to 41.4%, thereby establishing competitiveness of the proposed absorption system with the compression system. Further, economic analysis showed the system to be economically attractive as well as feasible.

Izquierdo et al. (2005) performed an exergy analysis on the double stage LiBr-water-based absorption system. A flat plate solar collector and residual waste heat were used to run the absorption chiller. In this work, ambient air and water were alternatively used as cooling fluids without crystallization up to 50 °C condensation–absorption temperatures. Results of this study stated that up to 50 ºC condensation temperature, double stage absorption chiller could run without crystallization. Irreversibility generated by the dual stage thermal compressor reported an increment with the absorption temperature up to 45 °C. The maximum value corresponding to this was around 1.35 kJ/kg.K. The double-stage absorption system showed 22% less exergetic efficiency than the single-stage absorption system.

Masson et al. (2006) proposed a performance predictive model using the TRNSYS tool for solar energy-driven double-stage absorption chiller for an intelligent workplace of 650 m^2 floor area. A chiller of 16.17 kW capacity with 30-40 m^2 of evacuated tube solar collector with storage tank of 0.6 m^3 was used for modeling purposes. A gas-fired auxiliary heating arrangement was used to address any system deficiency. The temperature of the hot working fluid was fixed at 163 ºC. Results of this study reported the feasibility of the proposed system for cooling applications with defined

configurations. Further, it was highlighted that around 20-30% heat loss from the system could also be cost-efficient. This system's life cycle assessment cost was 27,844$ to 20,527$ for energy price inflation rates from 2% to 5%.

Tierney (2007) assessed the potential of a new chiller and collector combination to reduce the demand for auxiliary gas firing. The proposed system with a double effect absorption chiller was simulated for a typical day of demand of 50 kW in July in Algiers. Different types of collectors, such as flat plate and trough collector with either single or double effect absorption chiller were examined. Simulation results revealed that potential savings were significant; 39% for a combination of single-effect chiller and trough collector; 32% for double-effect chiller and flat-plate collector; 86% for double-effect chiller and trough collector, compared to conventional double-effect chillers. For a location in Oslo, the obtained solar fraction for the double effect chiller with a trough collector was around 67%.

Using FORTRAN simulations, Gomri and Hakimi (2008) presented a second law analysis of waste heat-driven LiBr-water-based double-effect absorption system of 300 kW capacity. In this study, they performed exergy analysis to estimate exergy loss for each component installed within the chiller. This analysis discovered important information about the system's total irreversibility concerning different components. A set of computationally efficient formulae of thermodynamic properties of LiBr-water solution was used for the modeling purpose. Simulations depicted the absorber to have the largest amount of exergy destruction followed by high pressure generator and heat exchangers. Results were also plotted for COP and exergy efficiency, which showed that, increasing the temperature of low pressure generator beyond a certain value does not significantly improve the COP and the exergy efficiency. They concluded the presented results to be useful for thermo-economic analysis of the absorption system.

For production of chilled water, Gomari (2010) theoretically investigated the potential of single, double and triple-effect LiBr-water absorption chillers, each of 300 kW capacity. They carried out energy and exergy analyses of all three systems. In this study, using the thermodynamic properties of the working fluid, COP, exergetic efficiency and ratio of mass flow rate of vapor refrigerant to heat energy supplied were calculated. Solar energy was used as the driving source for the absorption system. Results showed

that for each condenser and evaporator temperature, there was an optimum generator temperature at which the COP and the exergetic efficiency become maximum. The maximum COP values obtained for single-stage chiller was in the range of 0.73-0.79, for double-stage it was 1.22-1.42 and for triple-stage system it varied between 1.62-1.90. It was also shown that the triple-effect absorption system generated more refrigerant vapor as compared to the double and single staged absorption systems, thereby making efficient utilization of high temperature waste heat.

Agyenim et al. (2010) experimentally tested the performance of LiBr-water absorption chiller coupled with cold storage tank in Cardriff University, UK. The test bench comprised of a 4.5 kW absorption chiller, 12 m^2 vacuum tube solar collector, 1000 liters cold storage tank and a 6 kW FCU. They estimated the system's actual performance by measuring the solar radiation, temperatures of ambient, inlet and outlet of different nodes, mass flow rates, and electricity consumption by each component. Experimental results disclosed the overall electrical COP as 3.64 and the chiller COP as 0.58. Further, it was estimated that 180 liters -250 liters of cold storage tank will be required for each kW of chilled water produced. Results of this study proved the integration of cold storage with absorption system to be feasible.

Fong et al. (2011) formulated a solar hybrid system using adsorption cycle, chilled ceiling and desiccant cooling for subtropical city. Using "TRNSYS" simulation tool, the annual performance aspects in terms of solar fraction, COP, and energy consumption of the system were evaluated for two office buildings and each having 196 m^2 area. A loop of 100 m^2 evacuated tube solar collector was installed to supply heat energy at 80 ^oC. Three different types of ceiling cooling techniques: chilled panels, passive chilled beams, and active chilled beams were used. Adsorption chiller was coupled with the ceiling cooling system for catering sensible load whereas, desiccant was used for latent load handling. Simulation results revealed around 47.3% of annual energy savings compared to the conventional system. Further, it was also delineated that use of passive chilled beam with the adsorption system was more energy efficient than the other two.

By using the central composite design technique, Hang et al. (2011) developed a methodology to optimize the solar-assisted double effect absorption air-conditioning

system with limited budget constraints. They explored a relationship between the solar fraction and system factors obtained through a physical model developed in the TRNSYS tool for a small office building in West Lafayette, IN, USA. The identified nominal capacity of the chiller was 23 kW with 4 m^3 of storage tank volume. The results of this study showed excellent agreement between the developed optimized model and the TRNSYS model. The agreement correction factor for the regression model was 98.8%.

Xie et al. (2012) presented an experimental investigation of a novel reformed waste heat-driven double effect LiBr-water driven absorption chiller. The system was evaluated under the sub-steady state condition, which was, augmenting absorption pressure in the absorber and decreasing temperature in the generator of the novel chiller. This system was based on the principle of pressure difference i.e. the larger the pressure difference causes a significant driving force for absorption. Results of this study reported a 1.5 times improvement in COP of the proposed system compared to conventional design when absorbed vapor pressure increases within 1.2 kPa–2.2 kPa.

Gomari (2013) performed a simulation study on the solar and natural gas fired LiBr-water single-effect absorption system of 10 kW capacity. This study proposed the suitability of natural gas as an alternative option to the renewable energy. Natural gas was used in the path of solar collector loop to provide auxiliary heating energy to hot water in case of any solar energy deficiency. Simulation results disclosed a COP of 0.82 with maximum exergy efficiency of 30% at 5 ºC evaporator temperature, 28 ºC -36 ºC condenser temperature and 54 ºC -83 ºC generator temperature. This study also highlighted that for a particular condenser temperature, there was an optimum generator temperature at which collector area requirement was minimum. It was emphasized that the use of natural gas in place of other electrical energy-based auxiliary sources could be cost effective and feasible option. Further, use of natural gas for this chiller was very small and CO_2 emission was also insignificant in this design.

For subtropical regions, Li et al. (2014) developed a parametric model of solar-assisted air-cooled double-effect absorption chiller to analyze the performance with collector temperature. This study was reported as the preliminary investigation of the air-cooled double-effect absorption chiller. The considered system in this study was containing set

of compound parabolic trough collector of 27 m^2 aperture area and tilted with horizontal at 20º. The required cooling demand was 20 kW. In this study, performance of the system was estimated against the different collector inlet temperatures. Simulation results revealed suitable working range of inlet collector temperature was 110-130 ºC. It was highlighted that inlet collector temperature should be less than 148 ºC to avoid the crystallization. Results also reported that influence of effectiveness of heat exchangers was nearly identical on the system performance.

Avanessian and Ameri (2014) performed energy and exergy analyses of the water-cooled LiBr-water-based single-effect, double-effect and direct fired double-effect absorption system using the EES tool. Natural gas fired boiler was used as the heating energy supply medium for generator of the absorption system. In this analysis firstly, they probed the effect of considering the chemical exergy of LiBr-water solution based on the second law of thermodynamics. Then, the effect of varying the operating and environmental conditions on energetic and exergetic performance was investigated. Results of this study indicated that there is no effect on second law efficiency and total irreversibility associated with chemical exergy of LiBr-water solution. Energy utilization factor was found to increase with generator and evaporator temperatures whereas, it was found to be decreasing with intensification of ambient air temperature and humidity. They also highlighted the single-stage system to be uneconomical, while the double-stage absorption system showed good payback period of around 3-4 years. Also, CO_2 emission of single-stage system was around 1.5 – 2 times higher than that of the double-stage absorption system.

Colorado and Rivera (2015) reported a comparative simulation study from first and second law of thermodynamics for conventional compression system, compression-absorption single-stage and compression-absorption double-stage cooling systems. Compression-absorption double-stage cooling mode was proposed for the first time in this work and was operated by waste heat. Working fluids, CO_2 and R134a were used in the compression cycle and LiBr-water was used for the absorption cycle. In this cascade design, the evaporator of the absorption cycle was used as the condenser of compression cycle. The considered refrigeration effect was 50 kW. Results reported that for both working fluids, around 45% lesser energy consumption was possible in case of cascade refrigeration cycle as compared to that of the conventional cycle.

Further, the COP of the double-stage absorption system was higher than the single-stage system. It was also shown that the double-stage absorption system required around 39.5% lesser heating energy than that of the single-stage absorption system.

Basu and Ganguli (2015) presented a conceptual design of a 3.5 kW absorption system for Kolkata, India. In this study, the proposed design used the solar thermal resource based on flat-plate collectors and solar PV-based electricity. Solar PV was used for supplying electrical energy to pumps and auxiliary heater in the hot water storage tank. Results reported that, 40 modules of PM-150 with 12 flat-plate collectors (each of 2m × 9.8m) were adequate for satisfactory operation. Further, the combined system was capable to provide 17.4 kWh of surplus energy savings per day. In this study, authors also performed economic analysis for both the combined system and observed the payback period to be less than 4 years.

Kaynakli et al. (2015) performed exergy and energy analyses on a double-stage series flow LiBr-water-based absorption system of 100 kW capacity. They investigated the system performance with different heat sources, such as hot water, hot air and steam obtained from solar and geothermal resources. Also, they conducted a parametric study to investigate the effect of operating parameters on the system performance. Simulation results reported a highest exergy destruction of 7.3 kW with hot air, 6.7 kW with steam and 6.5 with hot water. It was also outlined that the highest exergy destruction occurred at highest temperature of heat source and condenser. Finally they recommended the use of hot water against other considered sources, at sufficient temperature for the double-stage absorption chiller.

Li et al. (2016) developed a thermodynamic model of a novel hybrid solar absorption-subcooled compression-based solar air-conditioning system for large scale buildings in subtropical climate. Here, the subcooler part of the absorption system was coupled with condenser of the compression chiller. They examined the performance of the hybrid system at different cooling capacities and volume of storage tank. “FORTRAN”-based simulation results revealed that, COP and energy saving fraction initially increased and then gradually decreased with intensification in the rated cooling capacity. The observed capacity of the absorption chiller was 40 kW-60 kW, while for compressor chiller it was 412 kW-422 kW. Highest COP of the hybrid system observed was

determined as 4.74. It was also showed that, the system performance firstly increased and subsequently decreased with drop in the storage tank volume. For the proposed design, the optimal dimension of storage tank was 1.2 m^3. The performance of the hybrid system increased with the rise in heat exchanger effectiveness.

Using the EES tool, Majdi (2016) developed a simulation model to assess the performance of solar-based combined ejector single-effect absorption cooling system operating at steady-state condition. In this work, an attempt was made to improve the performance (i.e., the refrigeration effect) of the system by utilizing the kinetic energy of ejector. The ejector was installed between condenser and generator of the conventional design, in which two inlets were there: in the first, vapor comes from the generator and in the second, vapor comes from the evaporator. Afterwards, both streams are mixed. The proposed system was evaluated via entrainment ratio, operating temperature, thermal load and allied aspects. As compared to the basic cycle, simulation results showed higher values of COP for the modified cycle, with nearly 60 % rise in COP. Further, the modified cycle had more thermal load compared to the basic cycle. The modified system was also capable to run even under high condenser temperature condition.

Su and Zhang (2017) proposed a 260 kW capacity hybrid compression-absorption air-cooling system coupled with liquid desiccant-based dehumidification. This system introduced independent humidity and temperature control strategy. The heat energy from the condenser of the absorption chiller was recovered for the desiccant regeneration, and LiCl was used as the desiccant material. Apart from this, another low temperature heat source, such as solar waste heat could also be utilized. Use of desiccant material enhanced the evaporator temperature of the absorption chiller and subsequently improved the system performance. In order to increase the temperature and pressure of vapor, compressor was used to compress the refrigerant vapor coming from the generator of the absorption system. Simulation results reported 34.97% of energy efficiency of the proposed system against the conventional absorption cycle. The generator temperature of the proposed system was reduced from 100 ºC to 60 ºC due to coupling of compressor. Further, it was highlighted that the performance of the proposed system was greatly influenced by ambient conditions.

Alobaid et al. (2017) conducted a review study on the solar absorption cooling technologies. They extended their study for the solar thermal and PV-based absorption cooling systems. Various kinds of theoretical and experimental studies were considered for understanding the performance of absorption systems operated with different types of PV-thermal collectors. In this study, they highlighted that around 50% of primary energy savings can be ensured by solar absorption system as compared to the compression driven system, and 10%-35% electrical efficiency of solar PV-thermal was achieved. This review showed the average COP range for absorption system as 0.1-0.91, whereas thermal collector efficiency was found in the range of 0.06-0.64. They also investigated and suggested the collector area requirement for different types of collector per kW of cooling effect.

Xu and Wang (2017) evaluated the performance of a compound parabolic collector driven single- stage, double-stage and variable-effect absorption chiller to find out the better option between these. They performed a simulation study using "TRNSYS" simulation tool for Miami weather conditions to obtain 50 kW cooling effect. The model of the novel variable-effect absorption chiller was first developed in "MATLAB" and then built in "TRNSYS". Various performance parameters such as, collector area, cut-off temperature, tank volume were investigated by changing the controlling parameters. Simulation results revealed the combination of the compound parabolic collector and variable-effect absorption chiller to perform better compared to other designs. However, the variable-effect absorption chiller had higher solar cooling fraction, higher solar efficiency and lower auxiliary heat input than other designs. Further, it was also highlighted that the variable-effect and double-effect chiller result in better economic feasibility than the single- stage system.

Mohammadi et al. (2019) proposed a novel hybrid dual evaporator-based absorption system to improve the performance of the existing absorption system design. The design was introduced with ammonia-water-based system for low temperature applications using waste heat/solar thermal energy. They theoretically assessed thermodynamic, economic and environmental aspects of the proposed system. For increasing the absorber pressure, in this design, two compressors were used between the evaporator and the absorber. Results of this study demonstrated that coupling of compressors improved the COP of the system and also showed better economic

performance. For producing cooling effect of around 743 kW, the COP of the dual temperature system was 1.35 whereas, the conventional system was having a COP of 0.404. Further, they highlighted that implementation of compressor should be done carefully, otherwise associated costs might overweigh the COP improvement. For this, they employed the compressor with pressure ratio of 2.5 and reported the COP improvement from 0.404 to 0.624 whereas, the cooling production cost was increased from $0.211/ton-hour to $0.228/ton-hour.

Bi et al. (2020) theoretically investigated the performance of an independently-developed parabolic trough solar collector coupled with an absorption system and three-phase accumulator for an office building in Beijing, China. This study provided theoretical guidance for practical application of solar air-conditioning system. In this system configuration, a double-effect absorption chiller of 60 kW capacity and water storage were parallel-connected with solar collector loop. The considered building floor area was 600 m^2 and cooling load was estimated using the "DeST" software. The results of this study revealed capability of the solar air-conditioning system with three-phase accumulator to provide sustainable and stable cooling for a considerable duration. The energy storage efficiency of three-phase accumulator was obtained as 0.66 with energy storage density of 443.2 kWh/m^3. Authors also performed economic analysis of the proposed system design and reported economically acceptable payback period of six years.

Alhamid et al. (2020) examined the control strategy of a test facility of solar and natural gas-fired single/double effect absorption air conditioning system at the University of Indonesia, Depok, Indonesia. The nominal cooling capacity of the absorption system was 239 kW. Additionally, 181 m^2 of evacuated tube solar collectors were installed to supply hot water for the absorption chiller in case of single effect operation and direct gas-fired boiler for double effect absorption system operation. The net heat provided from the solar collector and gas burners were 93.3 kW and 113.2 kW. Two control strategies were used: internal control, such as solution flow rate, gas flow rate according to cooling capacity and external control such as hot, chilled, and cooling water flow rate as per the cooling load. Results of this study revealed the thermal and electrical COP of 0.9-1.1 and 4.5-5.5, respectively. The test results established the viability of the applied control strategy for the optimum and safe operation of the system.

Jalili et al. (2022) investigated the effect of type of fuel on thermo-economic performance of single and double-effect absorption systems by using life cycle cost assessment in six countries Phoenix (USA), Tarcoola (Australia), Ahwaz (Iran), Kota Bharu (Malaysia), Paya Lebar (Singapore) and Seville (Spain). Various kinds of input fuel resources such as solar, natural gas, and waste heat were considered in this study. Results of this study reported that the components of the double-effect absorption system had higher exergy efficiency than the components of the single-effect system. When chillers were integrated with the solar collectors and auxiliary heater, 70 and 50% of the required heat was supplied through solar energy for single and double-effect systems, respectively, in Phoenix (USA). Further, Malaysia's lowest LCC was observed among the considered countries in this work.

In addition to the above-mentioned, performance improvement in the solar absorption air-conditioning system has also been done by employing other heat transfer components, like desiccant material, heat recovery wheel, indirect and direct evaporative cooling arrangements, radiant cooling system, biomass-based resources, and many more. Various literatures reported that integration of these components with absorption system can be technically and economically feasible. In this context, Fong et al. (2011) proposed a solar hybrid cooling methodology and analyzed its application potential in hot-humid climate for catering high cooling demand. The hybrid design was having radiant cooling system driven by absorption chiller and desiccant-based dehumidification unit. “TRNSYS” was used for the building and system modeling. The cooling capacity of the system was 26 kW. The simulation results found that the energy saving by the proposed hybrid system was 36.5% compared to the conventional central air-conditioning system. The average solar fraction obtained with passive radiant cooling system was around 0.51 with COP of 0.867. The solar collector system used in this study was not much efficient, and due to this, the auxiliary heating consumption was around 64% of the total energy consumption.

Yin et al. (2012) experimentally investigated the performance of a mini solar absorption cooling system with radiant cooling system and compared this with FCU-based system for Shanghai, China. In this study, cooling and dehumidification of air was done independently by coupling an independent supply air system in the room. The

independent supply air system was installed to supply fresh and dehumidified air. The capacity of the taken LiBr-water chiller was 8 kW with inlet hot water temperature ranging between 70 ºC-95 ºC. Experimental results revealed that for the continuous 9 hours of operation, cooling capacity attained by the system was 4.6 kW with COP of 0.31. The electrical energy saving attained by the proposed design was 43.5%. Further, the integration of radiation cooling system increased the indoor thermal environment up to class A levels.

Prasartkaew and Kumar (2013) performed an experimental analysis on the hybrid solar and biomass-based single-stage absorption cooling system under steady state conditions for Bangkok, Thailand. The test bench included 50 m^2 of flat-plate collector, 400 liters of water storage tank and 7 kW capacity absorption chiller. Here, biomass gasifier was used in place of electrical auxiliary heating required to address solar intermittency. A mathematical model was also developed to analysis the performance parameters against variation in operating parameters, and comparison with experimental results showed well performance. Results demonstrated that the system was operating about 75% of its nominal capacity with overall COP of 0.11. It was also highlighted that biomass-based auxiliary heat input outperformed other auxiliary heat resources.

Fong and Lee (2014) proposed the advancement of solar absorption cooling system through better integration ammonia-water refrigeration cycle components. In this study, three integration strategies were developed for analysis: absorption cooling, absorption system-integrated desiccant cooling and absorption system- integrated desiccant cooling along with radiant cooling system. In the second and third configurations, an independent desiccant unit was coupled for the dehumidification purpose. The simulation study was done by using “TRNSYS” tool. Results for annual operation revealed that the first, the second and the third configurations were able to save 7.6%, 16.2% and 25.5%, respectively of energy consumption compared to the LiBr-water-based absorption system, and 38.6%, 44.3% and 50.6% respectively of energy savings were attained against the compression driven system.

Zhai et al. (2015) designed and installed a mini type solar absorption cooling system at Shanghai Jiao Tong University, China. The developed system was consisting of 96m^2

solar collector array, 8 kW absorption chiller and 3 m^3 of tank. A test chamber of 50m^2 was constructed for experimental evaluations. Here, chilled water from the absorption chiller was sent either towards FCU or radiant cooling panels installed inside the test chamber. Experimental results showed average cooling output from the system as 3-5 kW along with chiller COP as 0.2-0.3. The maintained zone air temperature after the cooling period of 2 hours was lowered from 32 ºC to 23-24 ºC. The predicted mean vote (PMV) and the predicted percentage of dissatisfaction (PPD) was around 0.22 and 5.89 %, respectively. The attained solar collecting efficiency was around 0.46. Further, results demonstrated that the cooling output of the radiant cooling-based system was 23.5% higher than fan coil-based unit. The cooling output of FCU and radiant cooling system was 3.62 kW and 4.47 kW, respectively.

Su et al. (2017) proposed a novel solar powered absorption cooling system coupled with liquid desiccant for two product delivery, one cooling and second water. This work proposed the delivery of fresh water recovered from the desiccant material. A mathematical model was developed using the "ASPEN PLUS" software, and simulations were done for warm climate conditions. Exergy, energy and economic analyses were performed to evaluate the technical feasibility of this proposed system. Simulation results revealed 25.64% of energy savings by the proposed design against the reference conventional absorption system. Further, exergy efficiency of the system was found to be 2.97% higher than the reference design. Additionally, an improved economic performance was observed with the proposed design.

Xie et al. (2017) investigated the suitability of hybrid solar and biomass absorption cooling system for different regions of China, India and America using "TRNSYS" simulation tool. In this study, four modes of operations were considered. In all modes, solar energy was used. But in the first mode, biomass auxiliary heating was used after storage tank, in second, biomass auxiliary heating was used within storage tank, in third biomass auxiliary heating was used before storage tank, and fourth, combined biomass auxiliary heating and solar energy were simultaneously added. Simulation results revealed that third mode was better than the other modes. This third mode also had better capacity to use solar energy and consume lesser biomass energy. The second mode was stated to be useful for locations where solar energy was not sufficient, but

plenty of biomass was available. Simulation results for all of the considered cities depicted the optimal solar fraction to lie between 17-32%.

Panja and Ganguly (2019) proposed a novel solar biomass hybrid absorption refrigeration system for cold storage application in India. In this work, biomass-based furnace was used in parallel with an evacuated tube solar collector system for providing hot water to the absorption system. Simulation results revealed that for generator temperature ranging between 110-125 ºC, the exergetic efficiency was obtained between 30-35% and COP was within 0.75-0.8. Economic analysis demonstrated the return on investment of around 2.6 years.

Li et al. (2019) analyzed the performance of a combined cooling heating and power system involving an internal combustion engine, variable-effect absorption chiller, and desiccant-based dehumidification unit for supplying cooling and power in Singapore. The absorption chiller and desiccant heat exchanger were operated with exhaust of biomass gasifier-based engine. They investigated the system performance under different feed stock of biomass. Results showed the final efficiency of wood chips to be two times higher than that of redwood pellets and 2.6 times higher than that of sewage sludge. Further, redwood required lowest oxygen and feedstock for power generation.

Ali et al. (2022) presented a detailed experimental analysis of a solid desiccant-assisted gas fires absorption-based air-conditioning system. A chilled water cooling coil was coupled at the process air side of the desiccant wheel arrangement. In the reference case, a heat recovery wheel was connected between the return air path and process supply air path for comparison purposes. The chiller had a cooling capacity of around 15 kW with a nominal COP of 0.67. The chilled water temperature supplied to the coil was about 10 – 12 ºC. An auxiliary heating arrangement was installed to regenerate the desiccant. Results reported 2 kW more cooling capacity of the proposed desiccant integrated with absorption system design than the conventional desiccant cooling system. The COP of the proposed system was 50-55% higher than the conventional reference case.

Hu et al. (2022) developed a mathematical model for assessing the exergy and energy analysis for the desiccant-assisted absorption air conditioning system with a cooling capacity of 10 kW. In this study, the waste heat from the condenser was utilized to regenerate the liquid desiccant material. They analyzed the exergy values for the absorption chiller at different regeneration temperatures. Results of this study reported 40% increase in exergy efficiency by utilizing the waste heat. Compared to the conventional absorption system design, the air cooling exergy efficiency was increased from 6-14%. The proposed system's performance analysis indicated that the desiccant regeneration temperature should be 38 °C to yield 14% air cooling exergy efficiency.

After discussing about various research studies on the available renewable energy-assisted air-conditioning methodologies, modifications, operations and other aspects available in literature, subsequent chapters will contain the investigation of identified research gaps. These gaps are listed below.

2.2 Objectives

Based on the literature review conducted on a wide variety of air-conditioning configurations, some of the following research gaps have been identified. The present thesis is aimed at fulfilling the following objectives,

I. First objective of this thesis is to assess a comparative analysis of VA and VC systems for office building under different climates, generator temperature and quantitative analysis of energy consumption.
II. Along with this, an investigation of coupling desiccant and evaporative cooling arrangement with VC and VA is also done. For the third objective, the aim is to perform a comparative study for the multi-stage absorption system against the single-stage and conventional system.
III. Next, the objective is to investigate the performance analysis of VA-based radiant cooling system (Integration of desiccant, evaporative cooling arrangement).
IV. In fourth objective, an investigation of the performance of VA systems for grid independency assessment against different configurations has been done.
V. In fifth objective, an experimental analysis of hybrid absorption air-conditioning system and empirical correlation generation has been performed.

CHAPTER 3

*PERFORMANCE ASSESSMENT OF COMPRESSION AND ABSORPTION-BASED SYSTEMS

This complete chapter is divided into six chapters. These chapters deal with the investigation of different configurations of renewable energy-assisted VC and VA driven air-conditioning systems. Before this, there is a discussion about the simulation tool EnergyPlus used in this thesis work and details of various climatic conditions.

In the first chapter, a comparative assessment between the VC and hybrid VA-based air-conditioning system has been done using the simulation tool. This study includes solar and natural gas-based heat input resources for the VA system, and auxiliary heating is available to address intermittency issues. Due to this, the considered VA system is triple-hybrid in nature. All the considered systems are subjected to different climatic conditions. Various performance parameters have been assessed via simulation outcomes. The system performance and energy saving potential vary according to the heat source temperature and solar collector area variation.

Second chapter theoretically investigates the performance of VC system coupled with the desiccant-assisted unit. In this chapter, a separate desiccant-assisted ventilation unit is provided and it operates simultaneously with a parallel VC system in a small-scale office building. Then, an IEC arrangement is provided in the path of the desiccant unit to reduce the effect of chemical dehumidification. A comparative analysis among these three different configurations (VC only, VC - desiccant, and VC – desiccant –IEC) have been done to analyze the energy-saving potential of the best suitable configuration.

The third chapter is an extended application of the second chapter outcome. In this chapter, the desiccant and IEC unit integration is checked with a VA-based air-conditioning system. This chapter compares the desiccant-IEC assisted VC and VA based systems under different climatic conditions. Simulation outcomes show the energy-saving aspects of the best case.

* Content presented in this chapter can be found in the publications J1, J6, C1, C2, C3, C4, C5, C6, C7, and C8.

Fourth chapter extends the analysis of the first subchapter toward the hot and dry climate with obtained different optimized collector area addition with VA system. Under the hot-dry climate, the behavior of the system is analyzed. Simulation results revealed that the system response against varying the collector area is different by changing the climatic conditions. This chapter suggests the feasibility of a system that is fully renewable dependent or fully grid independent.

Fifth chapter investigates the performance of desiccant assisted DOAS based unit coupled with two different methodologies for process air cooling: IEC and heat wheel based cooling. Simulations are done for the composite climatic conditions. Solar collector system supplies hot water for the desiccant regeneration. Although heat wheel based system utilizes return air for the desiccant regeneration. Results of this study reported the better performance of heat wheel assisted system in comparison with IEC based system.

Chapter six examines the performance of a double-stage absorption system under the warm-humid climatic condition. This chapter compares various performance outcomes of double-stage system with single-stage and compression based system. A loop of solar collector and biomass fired boiler are used for the working of single-stage and double-stage system, respectively. Simulation outcomes show superior performance of double stage absorption system than other considered systems.

3.1: Performance analysis of solar and biomass-driven hybrid-absorption-based building cooling system for different climate

3.1.1. EnergyPlus simulation tool and climatic details

EnergyPlus simulation tool is a complete package of building energy simulation program used by various researchers and engineers to model the energy consumption of heating, cooling, ventilation, lighting, etc. First release of EnergyPlus was in 2001 by the United States department of energy (DOE) with the collaboration of the national renewable energy laboratory (NREL), Berkeley lab and Oak ridge [EnergyPlus 2017]. This EnergyPlus is an open-source software provided by the U.S. department of energy. The basic roots of the EnergyPlus are clubbed with BLAST and DOE-2 programs. For more than 20 years, U.S. department of energy held the development of these two building energy simulation tools. These two programs differ in the method of load calculation. DOE-2 practices room weighting factor methodology and BLAST

practices a heat balance strategy [Crawley et al. 2001]. Each program contains a number of subroutines working simultaneously to simulate the heat and mass transfer from the building. Then in 1996, an initiative took place to develop a tool that comprises features and capabilities of both the software into a single, and EnergyPlus came into the picture.

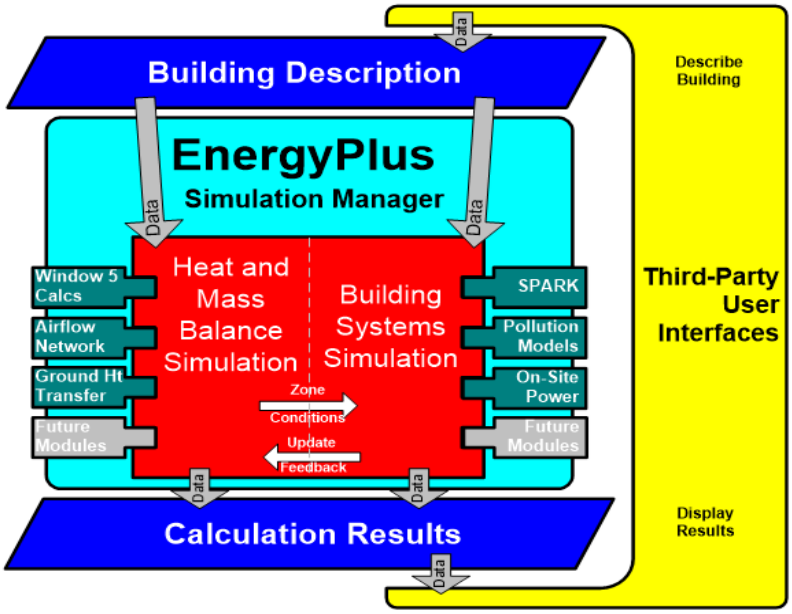

Figure 3.1.1: Structure of EnergyPlus

EnergyPlus is primarily a simulation tool that is more flexible and robust than BLAST and DOE-2 tool. This simulation tool does not contain any graphic user interface (GUI). The overall structure of EnergyPlus simulation tool is shown in Figure 3.1.1. A set of various input templates such as chiller, pump, cooling coil, fan, pipes, utility demand and supply side nodes, connection nodes etc. are provided in the library of EnergyPlus input file. Additionally, parameters related to the building load generation, such as people/occupancy density, lightning density, electric equipment density etc., are inserted according to reference/user requirements. Although no direct GUI is provided with EnergyPlus, an additional input tool will be required for building geometry generation. This thesis uses Google Sketch-up software to generate the building geometry. All the information related to the building orientation, floor layout, shading, envelope (such as wall, roof, floor and window), dimensioning details, multi-story building surface matching, etc. various aspects can be incorporated as per user requirements. A raw file/model of the building is saved into EnergyPlus support format (IDF File). Then in this EnergyPlus-supported building model, further additions

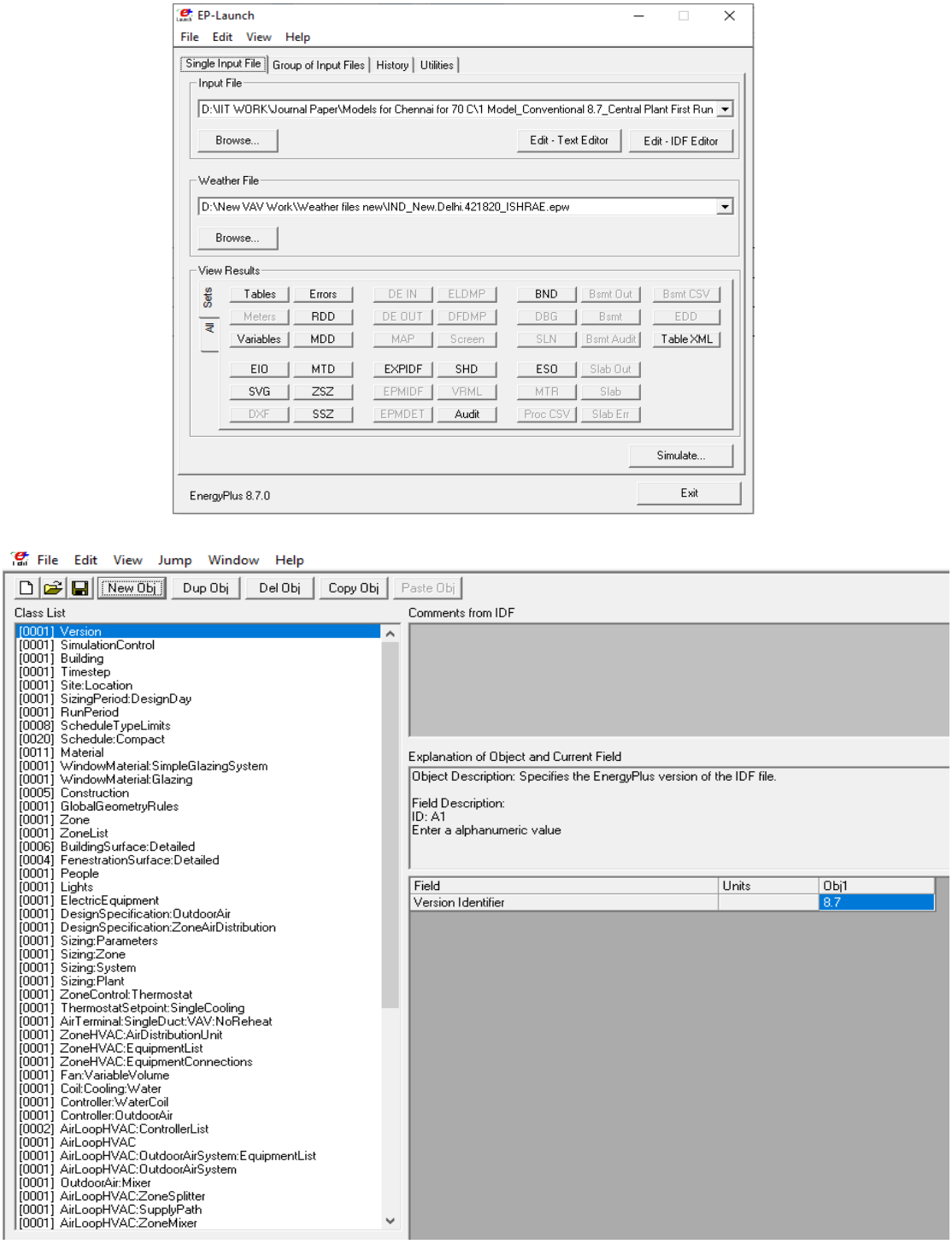

Figure 3.1.2: EnergyPlus launch file, expandable file and output file

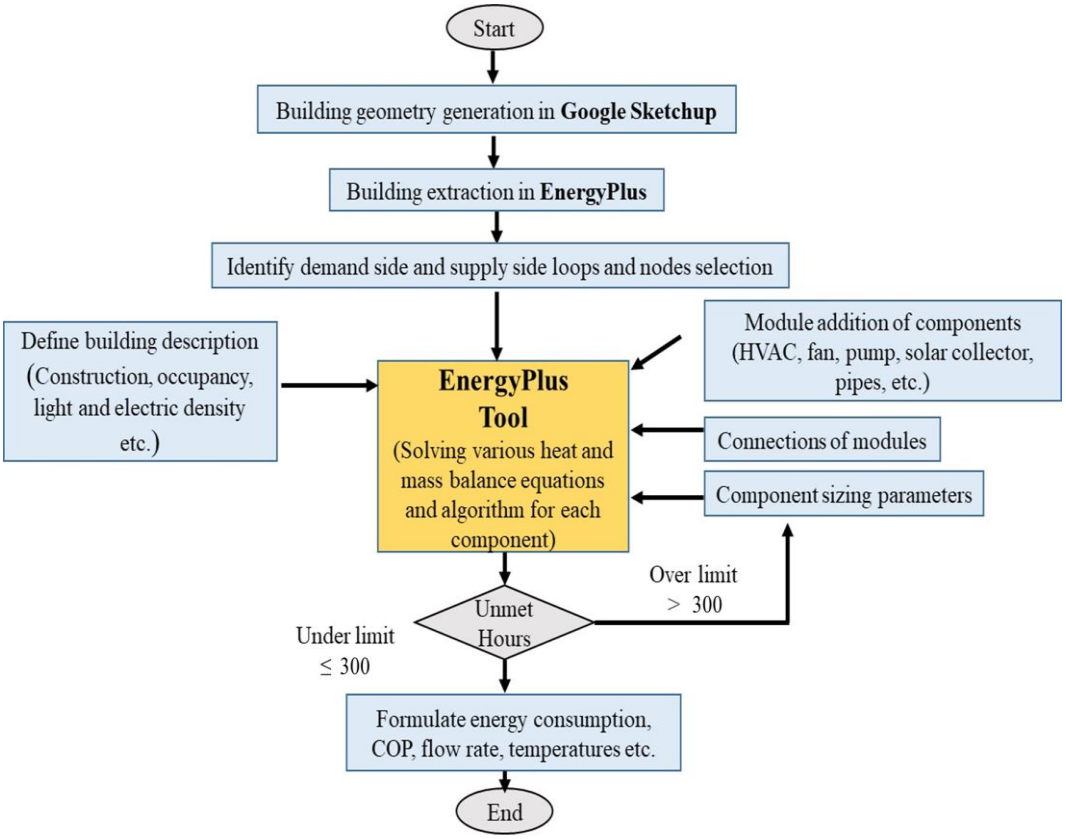

Figure 3.1.3: Flow chart of EnergyPlus modeling

are made for installing any HVAC or other components/systems. Users can create a model by using their knowledge of assembling/structure of building heating ventilation and air-conditioning (HVAC) systems. The user connects various components required for HVAC in a loop and simulates a particular weather file. An image of the EnergyPlus launch file and input expandable file are shown in Figure 3.1.2. In the present thesis, the EnergyPlus 8.7 version has been used to simulate all the considered research objectives. EnergyPlus solves various kinds of heat and mass balance equations in its engine and provides outcomes in HTML, Excel etc. formats; these equations will be discussed later.

Figure 3.1.3 shows the flow chart of the simulation model methodology adopted in the present research work. One of the significant criteria for evaluating the building model either this is correct or not, is done based on unmet hours. Unmet hours mean how many hours the system cannot maintain specified thermal comfort conditions for a particular time. In the present work, such a system has been running throughout the year, so under the annual operation condition, the unmet hours obtained from the simulation file should not be more than 300. If the unmet hours exceed the limit, then revision in the

building modeling is required. EnergyPlus provides flexibility to assess the hourly, monthly, and daily variation in the output parameters of the model.

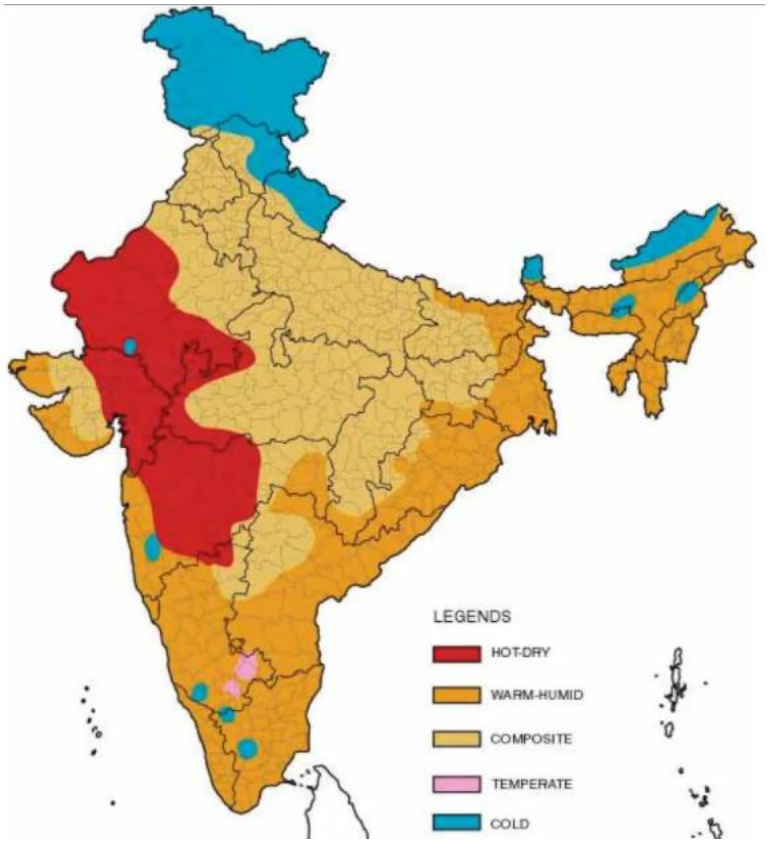

Figure 3.1.4: Different climates in India

The broad classification of the weather conditions can be done into five types: warm-humid, composite, hot-dry, temperate and cold. These classifications are based on temperature and humidity distribution throughout the season and year. There is some particular temperature and humidity range for identifying/classifying any region subjected to that particular climate. Warm and humid climatic conditions are where the annual dry bulb temperature ranges between 30-45 ºC in summer and 10-22 ºC in winter and humidity between 0.015 g/kg of dry air - 0.095 g/kg of dry air. These ranges of dry bulb temperature and humidity for hot and dry climate are 35-40 °C, for composite weather, these are 25-35 °C and for the temperate climate, this is 20-25 °C and for cold climate these parameters are 5-20 °C . A map of India studied in this thesis work is shown in Figure 3.1.4. From this Figure 3.1.4 it can be observed that the significant area covered on land falls under warm-humid and composite climate, followed by hot-dry and cold. There is significantly fewer regions of temperate climate.

3.1.2. Setup description and building model

The novelty of this work is decided based on the literature survey, where earlier studies did not consider the concept of triple-hybridization for addressing the intermittency issue related to solar energy for the continuous operation of the system. Additionally, previous literature did not report the individual component energy performance in the actual dynamic and different ambient conditions. This study has been done keeping all these gaps in mind. This work aims to analyze the quantification of energy consumed by different components, energy savings, and heat energy delivered to the generator of a single-effect vapor absorption cooling system (VACS) fitted in a small office building. Energy from collective solar, natural gas, and an additional heater is provided to the generator side of the absorption system. A reference small office building (Figure 3.1.5) is modeled in the EnergyPlus simulation tool as per the Indian constructional requirements with two unlike modes of operation, Mode 1 and Mode 2 (Figure 3.1.5 b & c). In Mode 1, a VC-based system is used, whereas in Mode 2, triple-hybrid VACS is installed for building air-cooling to satisfy the same level of space comfort,. In Mode 2, different sub-cases are considered to evaluate the needed collector area for which the system becomes comparable to Mode 1 in terms of total electricity consumption.

The present office building involves a single floor layout of a total roof area of 1000 m^2 as shown in Figure 3.1.5a. Monthly-averaged outdoor site data values for each month in terms of air dry bulb temperature (DBT), direct solar radiation I (W/m^2) and air humidity ratio (kg/kg of dry air), for diverse climatic zones are shown in Table 3.1.1. A validation study in terms of overall heat transfer coefficient (U values), visible light transmittance (VLT), sensible heat gain coefficient (SHGC), ventilation in cubic feet per minute (CFM) value, and other parameters calculated using the simulations are observed to be at par with the recommendations of national renewable energy laboratory (NREL) [Deru et al. 2011] and energy conservation building code (ECBC) [Khan et al. 2009]. Results are revealed in Table 3.1.2. Working hours for the office are assumed from 9:00 am to 6:00 pm.

The system components and templates used in EnergyPlus are well-validated experimentally and computationally with other building simulation tools [EnergyPlus 2017]. However, this study also surveys the operation of our conventional system against a reference office building available in the EnergyPlus documents [EnergyPlus 2017]. For this investigation, we have scaled down the present model of 1000 m^2 as per

the available reference model including a total floor area of 500 m^2 [EnergyPlus 2017]. Other data values are adjusted in terms of occupancy, lights, electric equipment requirement, operating schedules, construction, and COP. The cooling system results found for the modified reference building [EnergyPlus 2017] are comparable with those corresponding to the present scaled-down building as shown in Table 3.1.3.

Table 3.1.1: Site outdoor parameters for both climatic zones [Chennai data 2017 & New Delhi data 2017]

	Warm and humid climate zone			Composite climatic zone		
Month	Air *DBT*, T_∞ (^oC)	Humidity ratio (kg/kg of dry air)	Solar radiation, I_{solar} (W/m^2)	Air *DBT*, T_∞ (^oC)	Humidity ratio (kg/kg of dry air)	Solar radiation, I_{solar} (W/m^2)
January	27.3	0.0144	305.6	17.8	0.0075	372.9
February	28.9	0.0141	370.2	19.7	0.0081	368.2
March	31.2	0.0199	253.4	25.8	0.0087	529.4
April	32.0	0.0187	260.0	33.2	0.0079	685.6
May	34.5	0.0192	341.2	35.1	0.0142	474.5
June	33.6	0.0183	347.4	35.7	0.0169	472.6
July	32.5	0.0198	277.0	33.8	0.0184	361.6
August	31.9	0.0180	331.0	31.8	0.0193	261.2
September	31.3	0.0184	279.3	32.1	0.0169	325.6
October	30.1	0.0197	198.0	29.2	0.0130	381.3
November	27.7	0.0174	190.6	24.6	0.0075	532.0
December	27.2	0.0150	246.4	18.9	0.0069	432.0

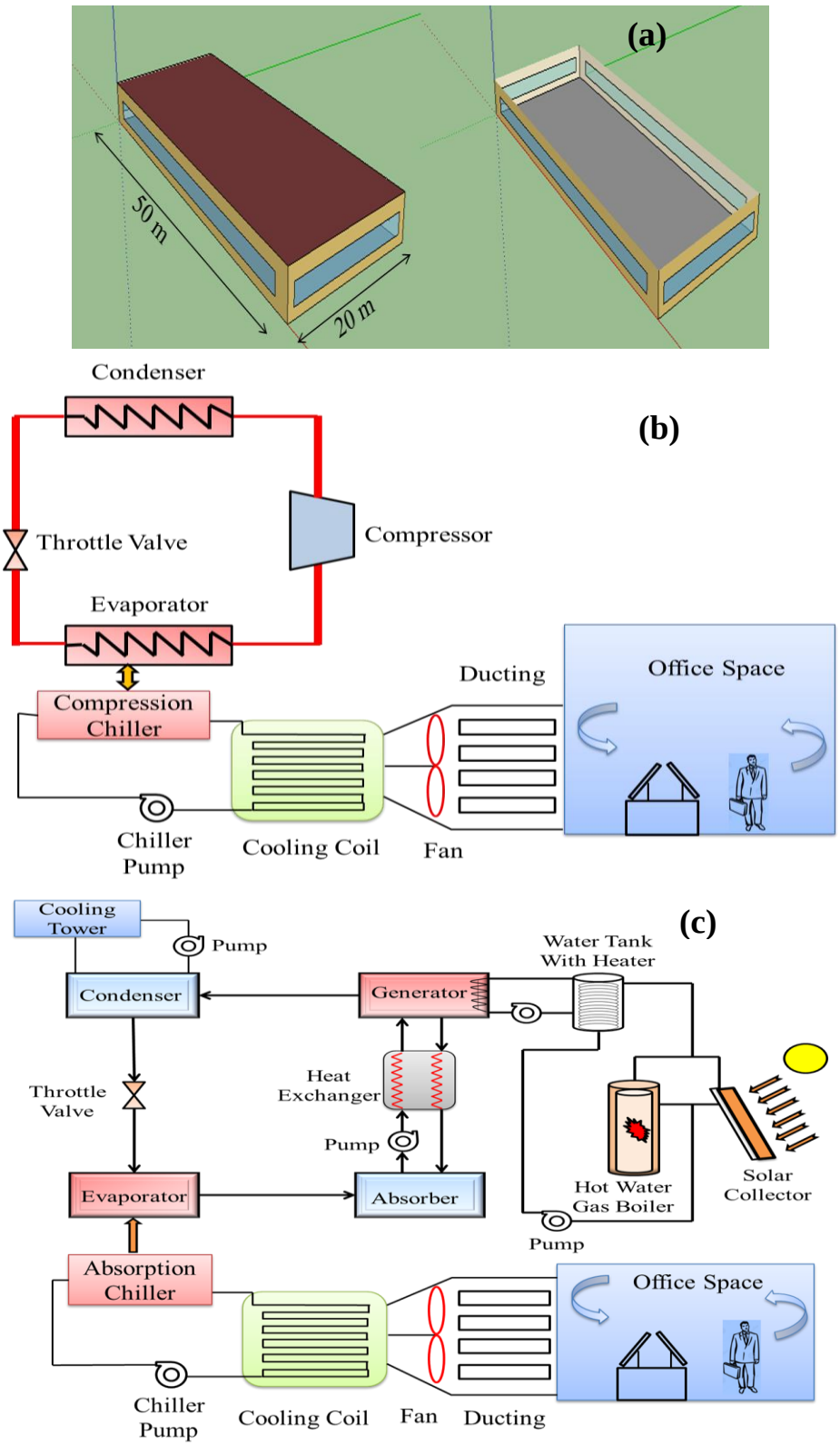

Figure 3.1.5: (a) 3-D Building Geometry for solar-biomass based for VA system analysis, (b) layout for Mode 1 of VC system, (c) layout for Mode 2 of VA system

Table 3.1.2: Building parameters validation of the present simulation study

Input variables	Description	Unit value (Present Simulations)	*NREL* [Deru et al. 2011] and *ECBC* [Khan et al. 2009] values
Computed parameters			
Exterior wall	Outside insulation + Gypsum plaster + Brick 2× 100mm + Gypsum plaster	U = 0.419 W/(m^2·K)	0.440
Roof	Outside insulation + Gypsum plaster + 100 mm light weight concrete + Gypsum plaster	U = 0.428 W/(m^2·K)	0.409
Window	Single glazing	U = 3.004 W/(m^2·K), *SHGC* = 0.296, *VLT* = 0.751	U = 3.30 W/(m^2·K), *SHGC* = 0.25, *VLT*=0.76
Fixed parameters			
Occupancy density	Not applicable (*NA*)	10 m^2/person	9.3-20 m^2/person
Lighting power density	*NA*	10 W/m^2	10.8 W/m^2
Electric equipment power density	*NA*	80 W/person	60-110 W/person
Ventilation	*NA*	20 *CFM*/person	20 *CFM*/person
Window-wall ratio	Area covered by window	40%	40%-60%

Table 3.1.3: Cooling system validation of the present simulation study

S. No.	Parameters	Reference Building *WWR* = 20% [Deru et al. 2011, Khan et al. 2009]	Present Scale down Building *WWR* = 40% [Khan et al. 2009]	Error (%)	Present Scale down Building *WWR* = 20% [Deru et al. 2011, Khan et al. 2009]	Error (%)
1.	Heat gain inside building due to occupants, electric equipment, lights	24827 kWh	24284 kWh	2.23	24394 kWh	1.77
2.	Zone air system cooling energy(Cooling energy supplied by system to building)	36717 kWh	41273 kWh	11.03	37213 kWh	1.33
3.	Fan power	8083 kWh	8119 kWh	0.04	7519 kWh	7.50
4.	Cooling coil total cooling energy	90670 kWh	91560 kWh	0.09	87084 kWh	4.11
5.	Total annual electric energy consumption.	34848 kWh	40119 kWh	13.13	37914 kWh	8.08

3.1.2.1. Mode 1: Conventional vapor compression based building cooling system

In this case, a conventional compression-based chiller system and an AHU are used for installing central air conditioning system for considered building. AHU of this system includes various components such as coils, fan, mixing box for outdoor air, and essential ducting systems. As shown in Figure 3.1.5b, a chiller of COP 3.1 [Deru et al.

2011] delivers chilled water to the AHU's cooling coils and from this coil a large fan delivers cool and dehumidified air into the office space through ducting system.

In the building air conditioning system, the cooling effect is provided by the delivered cooled and dehumidified air exchanging heat with the chilled water at the evaporator section of the coupled chiller. Chilled water gains heat from this air. The used air is a mixture of the outdoor air and the return air. For this purpose, corresponding to the office building, required chilled water temperature ($T_{we,o}$ = 7.5^{o}C), temperature of air from the cooling coil ($T_{a,coil,o}$ = 15^{o}C), and specific humidity ($\omega_{a,coil,o}$ = 0.008 kg/kg of dry air) are well-defined in the Energyplus. These values are in accordance with the standards prescribed by The Trane Air-Conditioning Economics (TRACE® 700) of United States Green Building Council [Trane 2010]. In Mode 1, the achieved chilled water temperature to the cooling coil is 7.22°C that is smaller than the dew point temperature of the surrounding air. A comparative valuation between the defined and the achieved temperature conditions throughout the year is shown in Figure 3.1.6. As shown, in this mode, the attained thermal comfort conditions include average air temperature of 21°C and specific humidity of 0.010 kg/kg of dry air. It is visualized from Figure 3.1.6a that, air is delivered nearly at the specified temperature of 15°C after passing through the cooling coil, whereas, the temperature inside the building is sustained nearly 21°C throughout the year. Total heat load (sensible and latent heat) generated inside the building space due to various components such as electric equipment, lights, windows and people are taken away by the supplied cool air only. Since this total heat load is met only by air, so, this is also a chief cause for the high electrical energy consumption in the central air conditioning system. In this, some share of air is recirculated in the space for catering system requirement. Cooling and dehumidification process of the outdoor air is shown on psychometric chart in Figure 3.1.7. In Mode 1, the main component is chiller. Performance of this chiller is figured in the simulation tool through numerous energy equations and performance curves [EnergyPlus 2017].

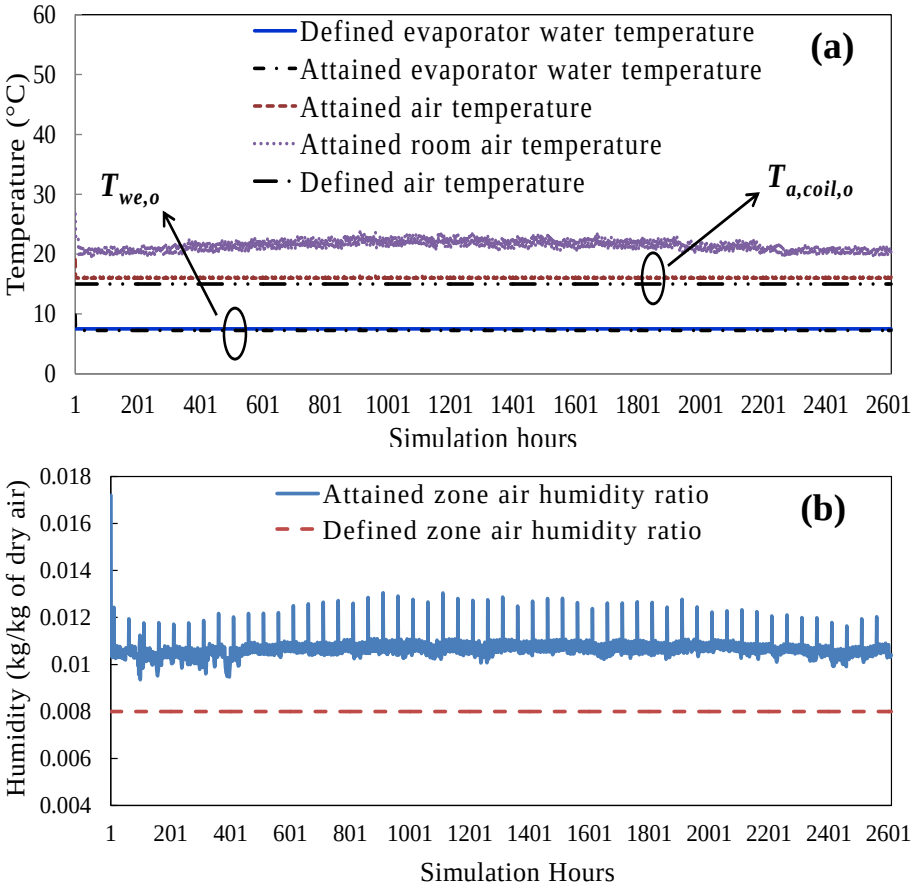

Figure 3.1.6: (a) Comparison of defined and attained temperatures, (b) Comparison of defined and attained temperatures humidities (For modes 1 and 2)

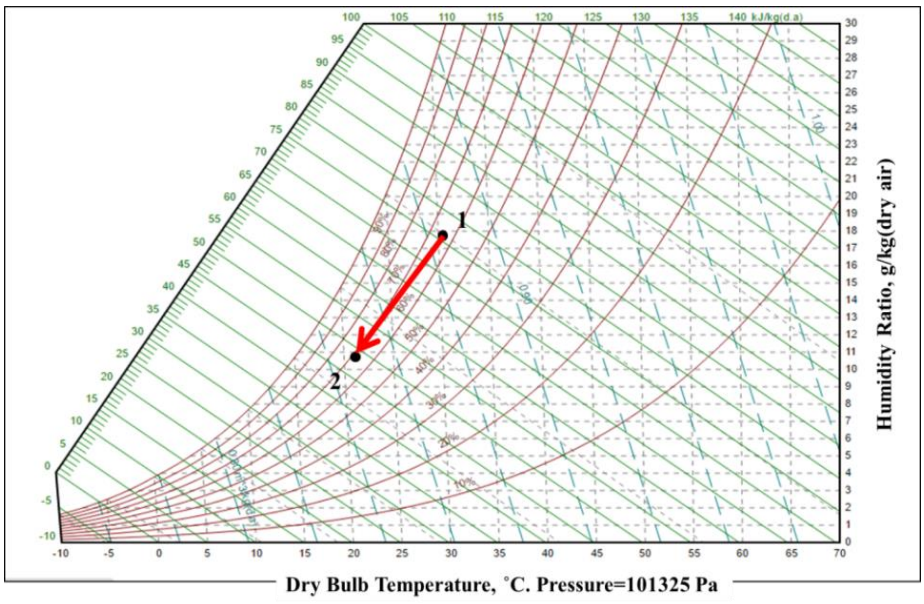

Figure 3.1.7: Psychometric representation of air cooling process

Generally, computations of various parameters for chillers need nominal cooling capacity, evaporator flow rate, and condenser flow rate, as described below [EnergyPlus 2017],

$$Q_c = c_{p,w}\rho_w \Delta T_c V_c f_{size}$$

$$\begin{aligned}&\text{water specific heat}, c_{p,w} = 4.186\text{kJ/(kg}\cdot\text{K)},\\ &\text{water density}, \rho_w = 10^3\text{kg/m}^3,\\ &\text{temperature rise in chilled water loop}, 5.049^{\circ}\text{C} \le \Delta T_c \le 10.565^{\circ}\text{C},\\ &\text{sizing factor of chiller}, f_{size} = 1.0.\end{aligned} \qquad (3.1.1)$$

The water volume flow rate inside the loop, V_c is governed by the ambient conditions and for the present work, it range is mentioned below.

$$1.571\times10^{-4}\ \text{m}^3/\text{s} \le V_c \le 5.425\times10^{-3}\ \text{m}^3/\text{s} \qquad (3.1.2)$$

The water flow rates through the evaporator and the condenser are respectively calculated as follow [EnergyPlus 2017],

$$V_e = V_c \cdot f_{size} \qquad (3.1.3a)$$

$$V_{cond.} = Q_c \cdot (1+1/COP_c)/(\Delta T_c \cdot c_{p,w} \cdot \rho_w) \qquad (3.1.3b)$$

where, *COPc* represents nominal/expected COP from the chiller considered 3.1 [Khan et al. 2009] for the present work. Mode 2 of the building cooling system is discussed below.

3.1.2.2. Mode 2: Vapor absorption based building cooling system

Working of an absorption refrigeration system is similar to a compressor based system. The basic difference between these two is the method of compression. In the compression-based cycle, mechanical/high grade electrical energy is used while in case of absorption system, heat/low grade thermal energy is mainly used. Main parts of absorption cycle are evaporator, absorber, generator/desorber, condenser, expansion device, solution heat exchanger and pump as shown in Figure 3.1.5. In absorption cycle, heat energy either by hot water or steam is supplied to the generator. This heat can be delivered by any thermal heat source or available waste heat. In this work, the triple-hybrid cogeneration of solar collector combined and natural gas fired boiler with an auxiliary heating element supply heat energy to the generator. In Mode 2, an absorption chiller is coupled for air-conditioning in the place of compression chiller. Natural gas-

fired boiler and flat-plate solar collectors are linked in a single loop to supply hot water at the generator side of the chiller (Figure 3.1.5c). In this mode, the solar collectors' area is varied from 400 m^2 to 900 m^2, efficiency of natural gas fired boiler is taken as 85% [Gomri 2013], and the gas-fired boiler capacity is considered as 250 kW. For evaluating the system performance, in Mode 2, the system is modeled for maintaining the same level of thermal comfort as of Mode 1. Generator inlet heat source temperature for the absorption system operation is considered as 70°C and 80°C.

Similar to the previous mode (i.e. Mode 1), in Mode 2 too, the absorption chiller delivers water at 7.22°C to AHU's cooling coil. In this case, four water circulation pumps are used. The first pump circulates water from collector-boiler loop to the water storage tank, whereas, the second one is used for circulation of water to the cooling coil. Third pump is used to circulate hot water from the water storage tank to the generator, and the fourth one is attached to the condenser water loop. During the simulations, EnergyPlus tool uses various heat balance equations, operating curves, input parameters to provide final outputs in the form of energy consumption, COP, temperatures at various points, and mass flow rates. The COP of the absorption system from derived simulation results can be calculated as,

$$COP = \frac{Q_e}{Q_g + w_p} \tag{3.1.4}$$

where, Q_e is chiller evaporator load, Q_g is the heat energy delivered to the generator, and w_p is pump work (considered negligible). These are computed in simulation tool (subscripts *e*/*g* respectively indicate evaporator/generator, *i*/*o* denotes inlet/outlet, *w* denotes water) as,

$$Q_e = m_{we} c_{p,w} \left(T_{we,i} - T_{we,o} \right) \tag{3.1.5a}$$

$$Q_g = m_{wg} c_{p,w} \left(T_{wg,i} - T_{wg,o} \right) \tag{3.1.5b}$$

For both the climates of the present work, various data values obtained from the simulations vary in the range shown below,

$$
\begin{aligned}
&0.148 \text{ kg/s} \le m_{we} \le 5.335 \text{ kg/s} \quad (\text{for evaporator}) \\
&2.994 \text{ kg/s} \le m_{wg} \le 3.965 \text{ kg/s} \quad (\text{for generator}) \\
&13.302\ ^{o}\text{C} \le T_{we,i} \le 17.383\ ^{o}\text{C} \\
&47.588\ ^{o}\text{C} \le T_{wg,i} \le 99.790\ ^{o}\text{C} \\
&35.760\ ^{o}\text{C} \le T_{wg,o} \le 93.720\ ^{o}\text{C} \\
&T_{we,o} = 7.220\ ^{o}\text{C}
\end{aligned}
\tag{3.1.6}
$$

The electrical energy consumption by water heater used in Mode 2 is computed as below.

$$
Q_{w,h} = \frac{\eta_{w,h} \times V_t \times \rho_w \times c_{p,w}\left(T_{wh,o} - T_{wh,i}\right)}{t};\ 16 \text{ m}^3 \le V_t \le 36 \text{ m}^3 \tag{3.1.7}
$$

where, $\eta_{w,h}$ is efficiency of the heater, whereas, V_t is the tank volume simulated by the EnergyPlus. In Eq. (3.1.7), *t* is the total heater operation time in seconds. For the present work, the values of temperatures at inlet, $T_{wh,i}$ and outlet, $T_{wh,o}$ of the auxiliary heater computed by EnergyPlus are as follow,

$$
\begin{aligned}
&35.924^{o}\text{C} \le T_{wh,i} \le 93.760^{o}\text{C} \\
&47.450^{o}\text{C} \le T_{wh,o} \le 99.975^{o}\text{C}
\end{aligned}
\tag{3.1.8}
$$

Fan electrical power consumed in both first and second modes of operation is calculated in the following manner,

$$
Q_f = \frac{f_{pl} \times m_a \times \Delta P}{\eta_f \times \rho_a} \tag{3.1.9a}
$$

where, (for both zones),

$$
2.586 \frac{\text{kg}}{\text{s}} \le m_a \le 6.866 \frac{\text{kg}}{\text{s}} (\text{for Mode 1}),\ 2.594 \frac{\text{kg}}{\text{s}} \le m_a \le 7.094 \frac{\text{kg}}{\text{s}} (\text{for Mode 2}) \tag{3.1.9b}
$$

where, ΔP =900 N/m^2, η_f =0.70, and ρ_a =1.2 kg/m^3 In Eq. (9a), $0.480 \le f_{pl} \le 1.20$ is part load factor that is the ratio of the given and the designed air mass flow rates. Generally, boilers requires nominal heating capacity and water flow rate. Both quantities can be obtained using the user-specified loop sizing data and the loop design flow rates. Nominal capacity of the boiler is defined as [Energyplus 2017],

$$
Q_b = c_{p,w} \cdot \rho_w \cdot \Delta T_b \cdot f_{size} \tag{3.1.10}
$$

where, f_{size} is the sizing factor of boiler taken as 1.0 [Energyplus 2017] and $29.335^{\circ}\text{C} \le \Delta T_b \le 38.405^{\circ}\text{C}$ is the boiler temperature difference.

Next, the solar collector thermal efficiency is defined as the ratio of the useful heat gained by the collector fluid, q to the total incident solar radiation, I on the gross surface area, A of the collector, i.e.,

$$\eta = \frac{\left(q/A\right)}{I} \tag{3.1.11}$$

For Eq. (3.1.11), the following empirical correlation is used [Energyplus 2017],

$$\eta = C_0 + C_1 \frac{\left(T_{w,si} - T_\infty\right)}{I} + C_2 \frac{\left(T_{w,si} - T_\infty\right)^2}{I} \tag{3.1.12a}$$

where (for both zones), $47.559^{o}\text{C} \le T_{w,si} \le 99.975^{o}\text{C}$, and T_∞ (given in Table 1) (3.1.12b)

In Eq. (3.1.12), the subscripts, *s* denotes solar, and *i* represent the inlet condition. C_0 = 0.69, C_1= -3.39, and C_2 = -1.93×10^{-3} are coefficients provided by solar rating and certification corporation [Energyplus 2017]. The design load for the cooling coil is calculated in the following manner,

$$Q_{coil} = m_a \left(h_{a,coil,in} - h_{a,coil,out}\right) \tag{3.1.13}$$

$$h_{a,coil,i} = f\left(T_{a,coil,i}, \omega_{a,coil,i}\right) \tag{3.1.14a}$$

$$h_{a,coil,o} = f\left(T_{a,coil,o}, \omega_{a,coil,o}\right) \tag{3.1.14b}$$

where, $15.882^{o}\text{C} \le T_{a,coil,i} \le 28.223^{o}\text{C}$,

$0.0052\text{kg/kg of dry air} \le \omega_{a,coil,i} \le 0.0153\text{kg/kg of dry air}$, $T_{a,coil,o}$ = 15 °C, $\omega_{a,coil,o}$ = 0.008 (kg/kg of dry air).

The part-load ratio (*PLR*) of an absorption chiller's evaporator is the actual cooling effect (load) divided by the maximum cooling effect available, i.e.,

$$PLR = \frac{Q_e}{Q_{e,\max.}} \tag{3.1.15}$$

For the present work, *PLR* range, the range of evaporator load, and the maximum evaporator load (cooling effect) computed from simulations are indicated below,

$$\begin{aligned} &0.106 \le PLR \le 0.997; \\ &5.394 \text{ kWh} \le Q_e \le 192.219 \text{ kWh}; \\ &138.016 \text{ kWh} \le Q_{e,\max.} \le 192.219 \text{ kWh} \end{aligned} \tag{3.1.16}$$

For both zones, the operating ranges of various parameters indicated in Eqs. (3.1.1), (3.1.2), (3.1.6-3.1.8), (3.1.9b), (3.1.10), (3.1.12b), (3.1.14b), and (3.1.16) are acquired

from simulations at generator temperatures of 70°C and 80°C. Based on the above-mentioned process, EnergyPlus simulates the system performance and provides performance output parameters that are discussed further.

3.1.3. Results and discussion

3.1.3.1. Total annual electric consumption analysis

For attaining the prerequisite thermal comfort within the office building, the total annual electrical energy consumption associated with different modes is evaluated. Figure 3.1.8 shows a comparison of the electricity consumed by different components of air-conditioning system. To fulfill annual thermal load of 183069 kWh (for warm and humid climate) and 134740 (for composite climate), the total annual electrical energy consumption in Mode 1 is 80533 kWh (for warm and humid climate) and 64221 kWh (for composite climate). The obtained COP of the chiller in the Mode 1 is found as 2.84 (for warm and humid climate) and 2.75 (for composite climate). Cooling coil is a heat exchanger that exchanges heat between space air and chilled water. So, there is no need of energy for its working operation. Consequently, the electrical energy consumption in Mode 1 is made only by chiller, chiller pump, and fan. Mode 2 comprises solar collectors, natural gas fired boiler, chiller, pumps, cooling tower, fan, and auxiliary heater. It is clear that in Mode 2, the main contributor to the total electrical energy consumption is water heater. For Mode 2, the effect of considering variable collector areas in the total electrical energy consumption is also represented in Figure 3.1.8. For this comparison, parameters of water heater and natural gas boiler are considered fixed. An increase in the solar collector area reduces the total electrical energy and consumption of natural gas. However, in some case (Figure 3.1.8d), minimal change in electrical energy consumption is perceived beyond a certain value of solar collector area. This is ascribed to the climatic conditions and high values of different generator temperatures. Interestingly, for both warm-humid and composite climatic zones, VACS offers excess energy savings than the compression driven system beyond a certain collector area, particularly when the generator temperature is around 70°C. Conventionally, from the literature [Alobaid et al. 2017] it is revealed that generator temperature for single effect LiBr-water VACS should be above 70°C. It is inferred that too low values of generator temperature will retain inadequate heat to regenerate the refrigerant from the solution. It is vital to note here that the chiller energy consumption includes the energy consumed by both chiller and its pump (i.e. chiller

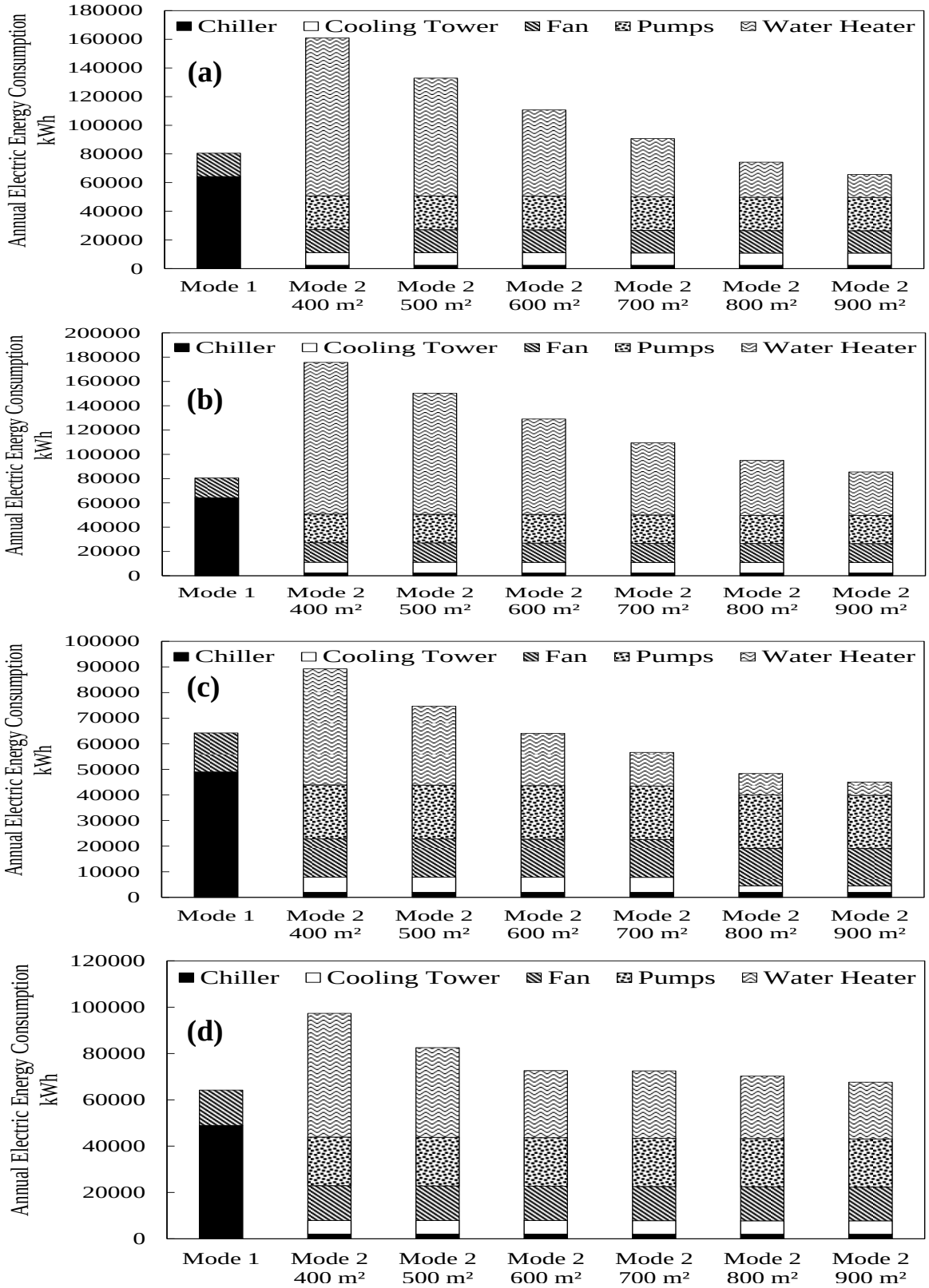

Figure 3.1.8: Total annual electric energy consumption by various components at defined generator temperatures, (a) warm and humid zone at 70°C, (b) warm and humid zone at 80°C, (c) composite zone at 70°C, and (d) composite zone at 80°C

pump in Figure 3.1.5 b, c). Figure 3.1.8 also shows that in Mode 1, major portion of energy (64289 kWh for warm and humid climate, and 48967 kWh for composite climate) is consumed in the chiller, whereas, the least part (16244 kWh for warm and humid climate, and 15254 kWh for composite climate) is contributed by the fan. For Mode 2, the electrical energy consumptions by four pumps other than chiller pump are included under the pump power consumption. Maximum electrical energy savings up to 18.50 % (for warm-humid zone) and 29.8 % (for composite zone) can be ensured by using the triple-hybrid VACS as compared to the compression-based air-conditioning system. The detailed trends of hourly variation in different parameters can be found in the published work [J1].

3.1.3.2. Effect of solar collector area on the supplied cooling load and generator heat input

Figure 3.1.9 displays the amount of cooling load delivered to the office building at different average generator temperatures. The amount of cooling load supplied by the chiller in the subsequent stages of increasing collector area decreases as shown in the figure. In Mode 2, with increasing the solar collector area, there will be decrement in the heat gain from the roof of the building because of the shadow effect, which consequently decreases the overall supplied cooling load.

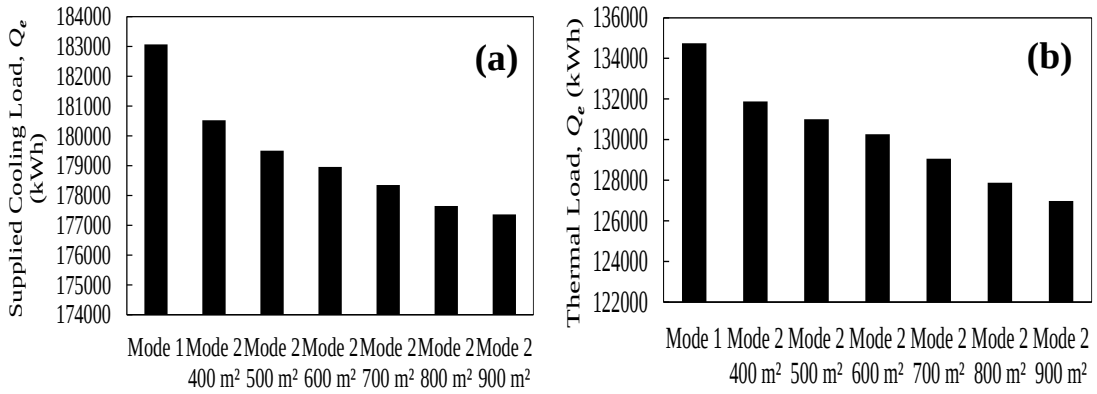

Figure 3.1.9: Cooling load supplied by the system for (a) warm and humid zone, (b) composite zone

3.1.3.3. Effect of solar collector area on COP

Figure 3.1.10 shows, the absorption system's COPs variation against different collector area for different average generator temperatures. It is perceived that the obtained COPs of the present VACS are similar to the experimentally observed COP from the literature

[Alobaid et al. 2017]. For warm and humid climate, Figure 3.1.10a shows that COP of the VACS marginally increases and afterward it decreases as the collector area is increased. However, for composite climate zone, COP decreases continuously with increasing solar collector area (Figure 3.1.10b). This is because COP of VACS is the ratio of evaporator cooling capacity, Q_e and thermal energy supplied to the generator, Q_g. So, for warm and humid climate, when the solar collector area is lesser (i.e. less than 700 m^2), then the delivered heating energy, Q_g reduces more than the corresponding decrement in the evaporator delivered cooling load, Q_e (Figure 3.1.9a). However, for large collector areas (i.e. beyond 700 m^2), heat supplied to the generator, Q_g increases, whereas, the evaporator cooling load, Q_e still decreases (Figure 3.1.9a). For composite zone, the delivered heating energy, Q_g uninterruptedly increases and the corresponding evaporator supplied cooling load, Q_e also decreases (Figure 3.1.9b), that consequently decreases the overall COP of the system.

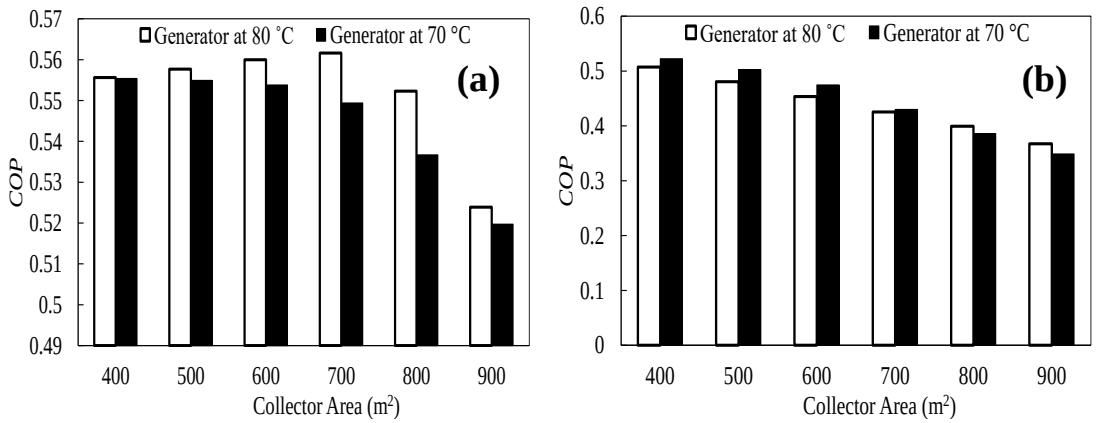

Figure 3.1.10: *COP* of the system at different collector areas and average generator temperatures, (a) warm and humid zone, (b) composite zone

Solar fraction is the basic Performance indicator of the solar energy based system. Solar fraction is defined as the ratio of the energy delivered by the solar collectors (Q_s, kWh) to the total energy supplied/requirement (Q_t, kWh). This solar fraction actually indicates the contribution of the solar energy towards the total energy requirements. This is calculated by using the following equation,

$$\text{Solar fraction} = \frac{Q_s}{Q_t} \tag{3.1.17}$$

Figure 3.1.11 shows the variation of solar fraction at different solar collector areas and generator temperatures. As intuitive, the value of solar fraction increases with increase in collector area. For both cases, the value of the solar fraction is high at the lower generator temperature, since solar collectors are more capable to offer the heating energy at a lower generator temperature as compared to that at a higher one.

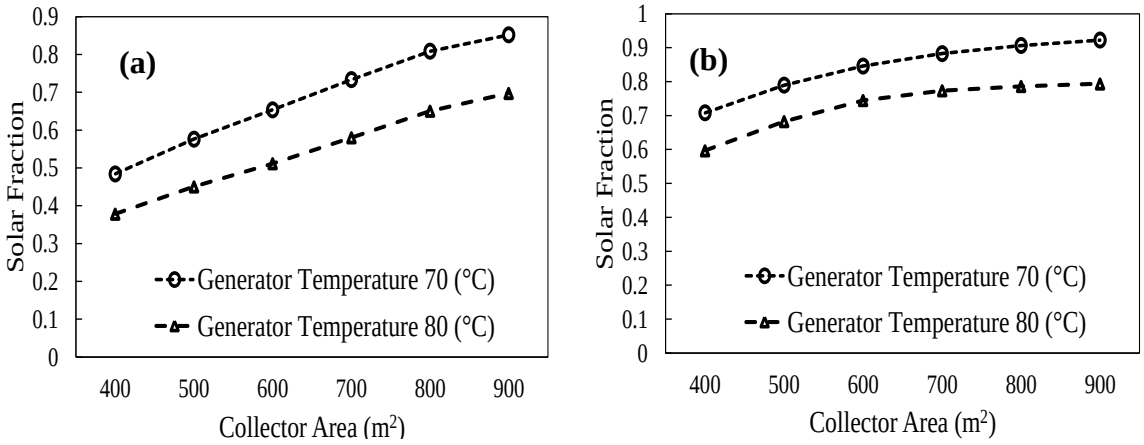

Figure 3.1.11: Solar fraction of the system at different collector areas and average generator temperatures, (a) warm and humid zone, (b) composite zone

3.1.3.4. Replacement study of natural gas with biomass and economic assessment

In this work, natural gas is used as a working fuel in the gas-fired boiler. In the next part of this paper, a calculation is done to compute the equivalent biogas requirement derived from biomass to act as a substitute for the natural gas. The amount of heating energy supplied by the natural gas fired boiler at different generator temperatures and collector areas can be calculated. Here, the quantity of biomass required for fulfilling the maximum requirement of the system is indicated in Table 3.1.4. For example, for warm and humid climate, the maximum total annual heat energy supplied using the natural gas fired boiler is 82020 kWh corresponding to collector area of 400 m^2. Out of this total boiler supplied heating rate, the maximum heating energy supplied in a day is found as 250 kWh on 21 May 2016 (obtained from simulation results by using weather data files). The maximum heat energy (250 kWh) supplied by the gas-fired boiler may be evaluated from Figure 3.1.12. Next, considering the boiler efficiency of 85%, the heat energy required from the fuel is 294.117 kWh, and now, this much amount of energy has to be supplied by biogas. From the literature, the energy content in the natural gas of volume 1 m^3 is 3723 kJ [Wrobel et al. 2013]. In case of biogas, considering the cow dung as a biomass source, 25 kg of dung produces 1 m^3 of biogas,

possessing approximately 22 MJ (or 6.111 kWh) of the heat energy content [Biogas handbook 2008]. Thus, for satisfying the heating requirement of 294.117 kWh, the approximate estimated volume of biogas needed can be as, 48.129 m^3. Finally, the mass of cow dung needed shall be nearly 1203.225 kg. In the similar way, the amount of biogas and biomass required for the different collector areas and generator temperatures can be also figured.

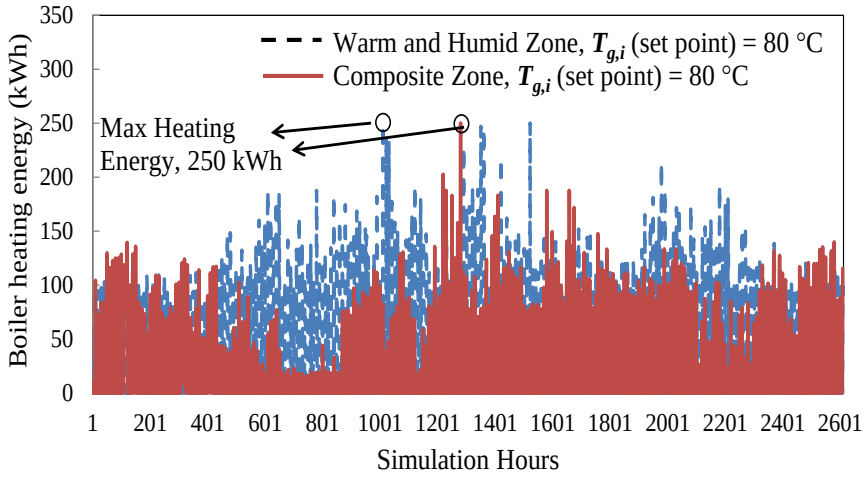

Figure 3.1.12: Heating rate provided by boiler for both climate zones

Table 3.1.4: Evaluation of equivalent biomass (cow dung) required for meeting maximum heating in the *VACS* generator

Zone & generator temperature	Maximum heating energy supplied (kWh)	Required heating energy from boiler (kWh)	Volume of biogas (m^3)	Cow dung required (kg)
Warm-humid zone at 70°C	234.981	276.448	45.237	1130.944
Composite zone at 70°C	199.942	235.225	38.492	962.301
Both zones at 80°C	250.000	294.117	48.129	1203.225

Additionally, on the same building, one another study has also been performed [C1] that contains the same constructional and model input parameters. This work [C1] explores the performance of absorption based air-conditioning system coupled with either solar energy driven system or gas fired boiler. Here, two different cases are

considered in this study, in the first case, VA system is fed by solar collector system and an auxiliary heater. In second case, VA system is fed by the natural gas fired boiler arrangement. Other system details can be found in the work [C1]. The simulations have been done for warm-humid climatic conditions. Simulation results for the annual electrical energy consumption are shown in Figure 3.1.13. Figure 3.1.13a shows the electricity consumed by different components under the condition when VA system is fed by solar collector loop only. Here, it can be observed that, due to environmental conditions the consumption of auxiliary heater is very high. But, in Figure 3.1.13b this heater consumption is nil. The net energy consumed by the gas fired boiler assisted VA air-conditioning system is very less compared to the solar energy based VA system.

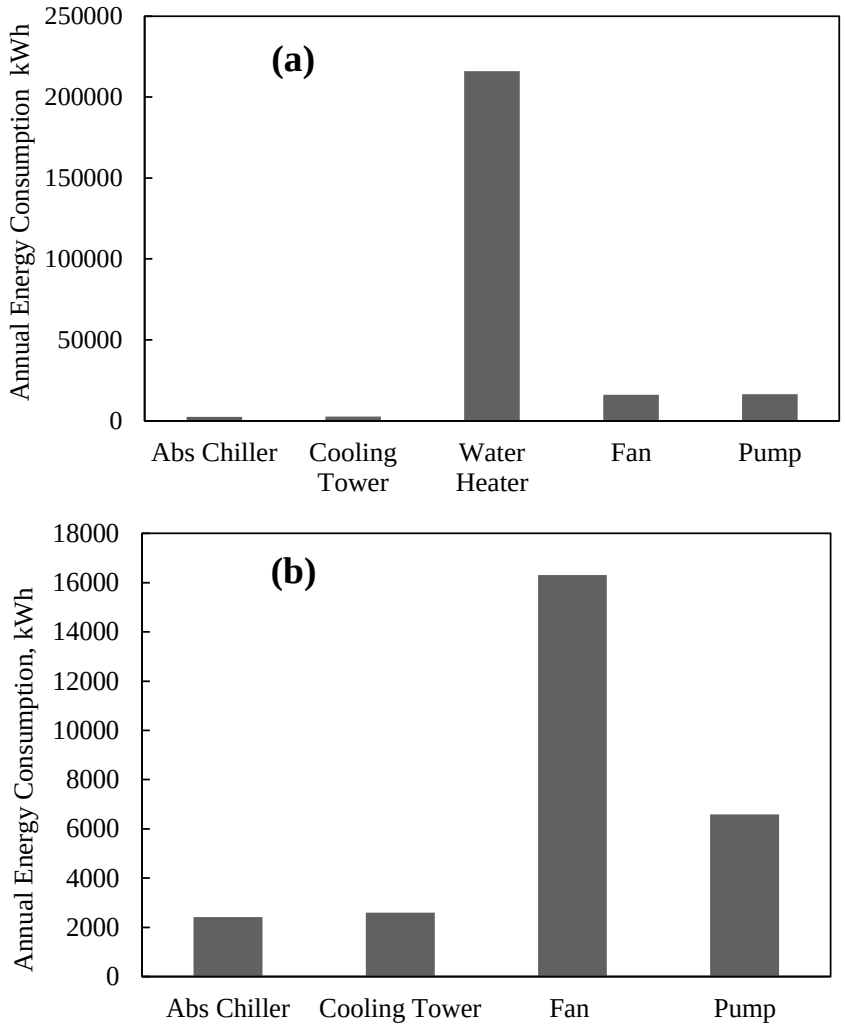

Figure 3.1.13: (a) Energy consumption in solar collector assisted VA system, (b) Energy consumption in gas fired boiler collector assisted VA system

In this work, an economic assessment is also done for the triple-hybrid VA system and a solar PV based VC system. The costs of each installed component for the air-

conditioning purpose are considered as per the peak rated capacity. The costs and capacities can be seen in published article [J1]. This economic assessment reveals the payback period or return on investment (ROI) of the proposed triple hybrid VA system and the solar PV driven conventional VC system. ROI is estimated by using the ratio of additional cost of the system retrofitting to the cost of energy saving per year. It is observed that, when the VC system is operating on solar PV system, then the estimated ROI for the system is around 33.35 years. Whereas, the installation of triple-hybrid VA system in the building provides ROI of around 25.5 years.

3.1.4. Conclusion and summary

In this work, a simulation study using EnergyPlus simulation tool, is performed for assessing the performance of a triple-hybrid vapor absorption cooling system (VACS) for a small office building of 1000 m^2 for different climatic conditions. The building design and the cooling system are well validated with the available standards and documents. Composite and warm-humid climates are considered for the analysis. Simulations are done at different average generator temperature and solar collector areas. The electrical energy consumption patterns of various components along with quantitative heat energy supplied to the generator by various components are discussed. Following conclusions are derived from the present study,

- With respect to a compression-based system, , the proposed triple-hybrid VACS saves up to 18.50 % of the annual electrical energy for warm and humid zone, and nearly 29.80 % of the annual electrical energy can be conserved in the composite environment through proper selection of various components.
- The minimum areas of solar collector for warm-humid and composite zones are found as 700 m^2 and 400 m^2, respectively for maintaining appropriate thermal comfort inside the present office building.
- Natural gas used in the current considered VACS can be substituted with biogas for meeting a given heating requirement in the generator.
- Triple-hybridization is necessary to ensure continuous performance of the system throughout the year. Due to the real aspects such as, space constraints, practically available size of various components and intermittency issues related to solar energy, either one or any two of the three components will not be capable to maintain the required air-conditioning for a uniform thermal comfort level throughout the year.

3.2. Assessment of VC air-conditioning system with desiccant and solar assisted ventilation

3.2.1. Building description and methodology

In the previous studies, the annual energy consumption for each component in the desiccant assisted DOAS under warm-humid climatic conditions was not calculated. Also, the benefit of IEC with respect to VC system and desiccant-assisted VC system was also not found in the previous studies. To fulfill the purpose, in this study, a small office building of total floor area 400 m^2 (20m×20m) with window to wall ratio (WWR) 40% is modelled in the EnergyPlus software. EnergyPlus Simulations are done throughout the year for warm-humid climatic. Building 3-D geometry is presented in the Figure 3.2.1. Working timings are taken from 9:00 to 18:00 hrs. The air cooling unit for the present building is considered to preserve the same thermal comfort level (dry bulb temperature of 21ºC to 26 ºC and specific humidity of 0.008 kg/kg of dry air to 0.010 kg/kg of dry air) throughout the year using three different methods (Cases 1, 2, and 3). In the modeling, occupancy density is 10 m^2/person, light power density is 10 W/m^2, electric equipment power density is 80 W/person and ventilation requirement is 20 CFM/person [Khan et al. 2009]. Before proceeding to the results and analysis of the considered air-conditioning system, validations of the building design and the installed vapor compression system (VCS) are carried out as described in the next sub-section. The validation study for the building model shows acceptable error ranges for different parameters that can be found in the relevant published literature [C3].

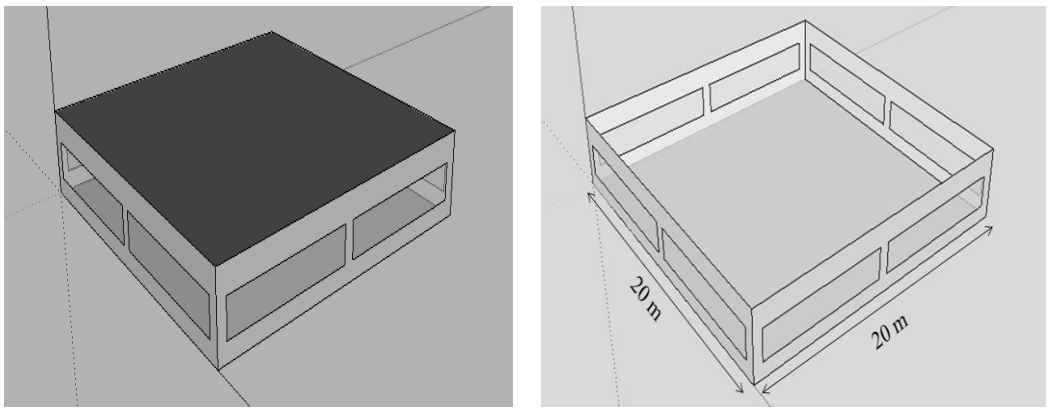

Figure 3.2.1: Building geometry for analysis of solar-desiccant assisted VC system

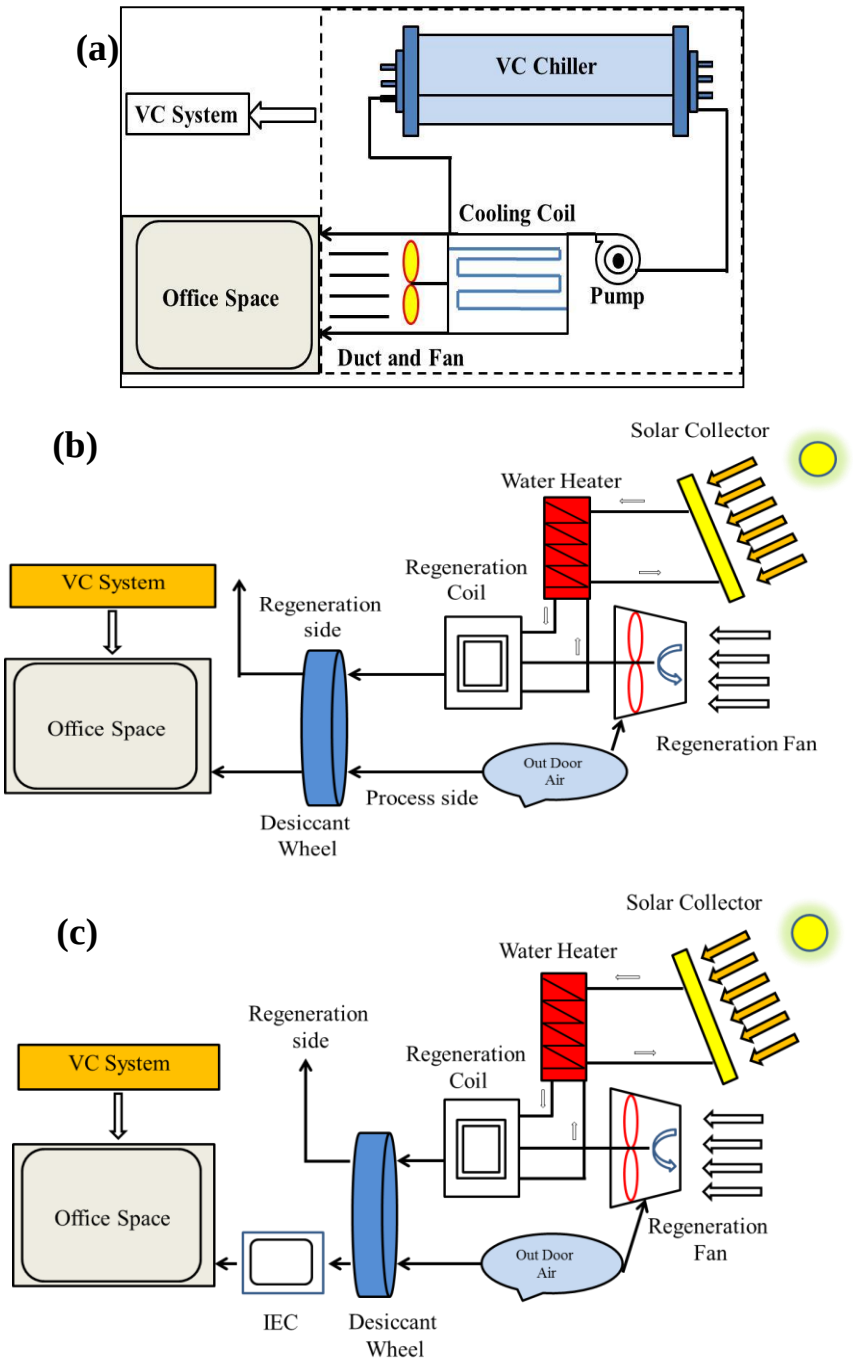

Figure 3.2.2: Layout of the system in (a) case 1, (b) case 2 and (c) case 3

3.2.2. Different modes of operations

In the first case (Case 1), a VCS-based air-conditioning system is considered. This case includes a compression chiller (having COP as 3.1), pump and fan. Schematic diagram of Case 1 is shown in Figure 3.2.2a. In Case 2, a desiccant-assisted DOAS is coupled for separate ventilation along with the conventional VCS. Desiccant is a material that adsorbs the vapor particles of supplied air by the process of chemical dehumidification. As a result, there is a rise in air temperature with reduction in the humidity level of the

air. The process outlet air temperature after passing through desiccant is found as 43°C with specific humidity 8×10^{-3} kg/kg of dry air. This dehumidified air is supplied directly into the building space. Simultaneously, VCS cater the sensible heat load increased due to this effect. Since, desiccant is saturated because of water vapor blocking; it is therefore regenerated using hot air at the temperature of nearly 50°C to 70°C [Khan et al. 2017]. For this, a flat-plate solar collector system having 200 m^2 area is used to supply hot water to the regeneration coil. An auxiliary water heater is also connected for contrary operating conditions like unavailability of sun. Hot water from the collector is provided to the regeneration hot water coil, from where hot air at a temperature of 60°C [Khan et al. 2017] is delivered at the regeneration end of desiccant. An outline of the system for Case 2 is portrayed in Figure 3.2.2b.

In Case 3, for the enhancement in the ventilation cycle of DOAS, an IEC system in the path of process side of DOAS is connected. Design of Case 3 is shown in Figure 3.2.2c. This IEC is used to decrease the temperature of exit air from desiccant wheel at the process side. This decreases the temperature of the dehumidified air up to 28°C that again reduces the additional sensible heat load generated by hot and dehumidified air on the air-conditioning system. This accordingly improves the system performance. The details of the energy/electrical consumption estimation and relevant parameters ranges can found in the published work [C3].

3.2.3. Result and discussion

The connected systems are modelled with the weather data of considered warm-humid climatic zone. To evaluate the energy saving possibilities in cases 2 and 3, these are compared with the conventional VCS. Model is run throughout the year for keeping the same thermal comfort conditions. Simulation results are obtained in terms of total annual electric energy consumed by different components of the system.

Figure 3.2.3 displays the electrical energy consumption pattern of distinct components installed in the system. Complete annual electricity consumption for the conventional case (Case 1) is 32607 kWh, for Case 2 this energy consumption is reduced to 32337 kWh, which is not significant. However, enhancement in the system is realized by coupling the IEC system that leads the energy consumption up to 31752 kWh (i.e. 2.62% savings) for Case 3. Thus, as compared to conventional VCS, electrical energy

saving is very negligible by employing only desiccant system in the ventilation path, but, this can be by using IEC in DOAS.

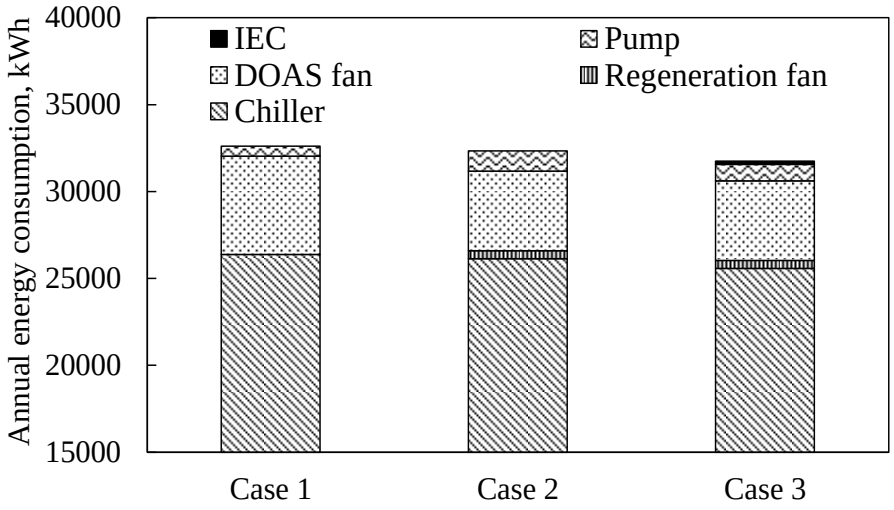

Figure 3.2.3: Comparison of yearly consumption of electric energy

Figure 3.2.4 displays that there is an improvement in COP by amending the conventional VCS (Case 1) with the DOAS (Case 2) and DOAS-IEC (Case 3) systems. However, in Case 3, COP is lesser than Case 2, because due to incorporation of IEC, the heat load removed by the system is reduced along with reduction in electrical energy requirement. This is more beneficial in medium and large buildings and not so relevant in small ones, because in small office buildings, the benefits provided in the form of reduced thermal load is offset by the delivered energy to the evaporative cooler and pump arrangements.

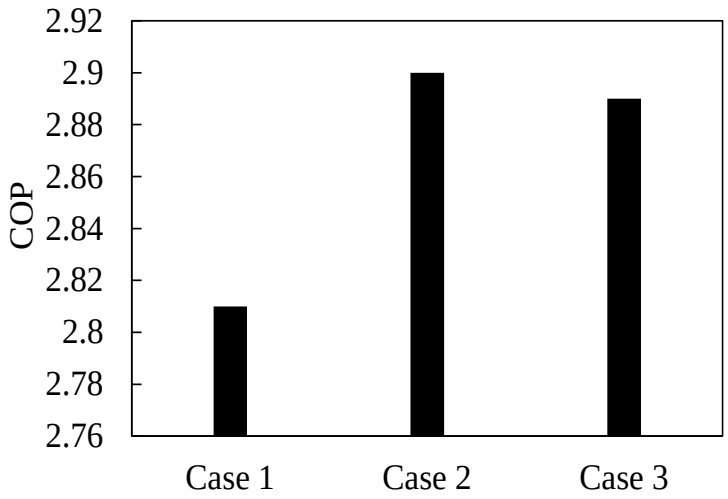

Figure 3.2.4: Comparison of COP for different cases

Additionally, in the published work [C2 and C8], an analysis on the conventional air-conditioning system by using packaged terminal air-conditioner (PTAC) with solar-desiccant assisted DOAS has been carried out on the similar type of building as shown in Figure 3.2.1. PTAC is generally used for 10-20 ton cooling applications. In this work, different building constructional and input parameters are used in the modeling that can be found in the work [C2 and C8] and simulations were run for the warm-humid climate. Two different situations are considered here in this study; conventional case referred as "VC system" and solar-desiccant assisted case referred as "Modified VC system". The electrical energy consumption analysis of the individual installed components for this work is shown in Figure 3.2.5. Here, annual total consumption pattern reveals that installation of desiccant is also beneficial for the PTAC assisted cooling system. This integration of desiccant system with PTAC provides around 5.5% of annual electrical energy savings.

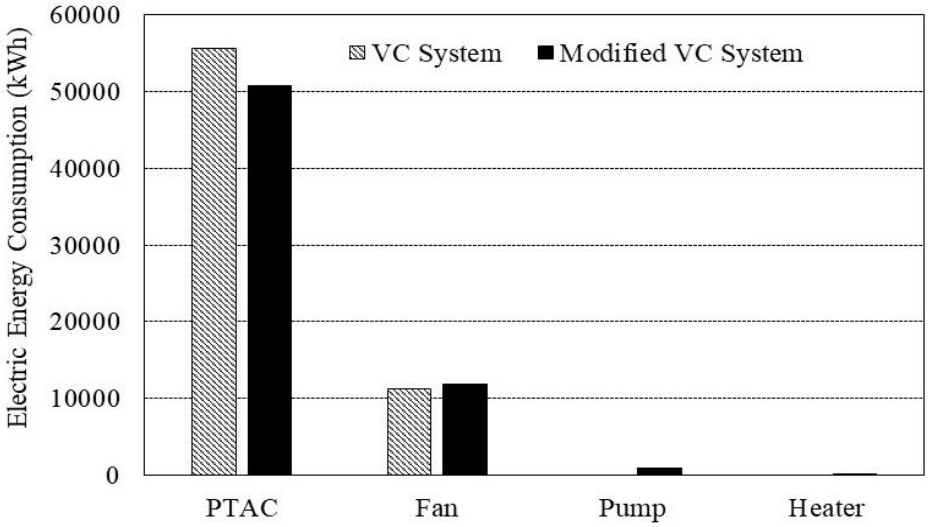

Figure 3.2.5: Annual electricity consumption for VC system and modified VC system

3.2.4. Conclusion and future recommendations

This simulation study demonstrates the impact of using desiccant-assisted DOAS in conjugation with conventional VCS. DOAS is responsible to handle the latent heat load of the supply air that reduces the latent load on the VCS, but increases its sensible load. So, further enhancements in DOAS is done by using an IEC that decreases the annual consumption of electric energy due to VACS by 2.62%. Despite somewhat low energy saving potential, the modified system involving desiccant DOAS and IEC integrated VCS will be beneficial for medium and large-scale buildings. It is recommended that,

further development of this system can be done by using sensible heat recovery wheel in conjunction with DOAS and IEC.

3.3. Assessment of VC and VA air-conditioning systems with desiccant and solar based ventilation unit for hot-dry and composite climates

3.3.1. Building description and methodology

A lot of research has been done independently on VC and VA-based systems. However, in the kinds of literature, the comparative assessment between VC and VA-based methods coupled with desiccant and IEC-based DOAS is unavailable. In this work, a small office building having total area of 400 m^2 (20 m × 20 m) (Figure 3.3.1) is adopted for the investigation. The floor to roof height of the building is taken as 3.1 m. The generated building model is imported in the EnergyPlus simulation [EnergyPlus 2017]. The agreement of the present considered building construction with the available codes and references of ECBC [Khan et al. 2009] and NREL [Deru et al. 2011] has been ensured. The comparison is done in terms of *U*, SHGC, and VLT. Acceptable agreement between the attained and the reference values is highlighted. In this study, two different climatic zones; hot-dry and composite climates are considered. For the building modeling, the considered occupancy density is 9 m^2/person, light power density is 10 W/m^2, electric equipment power density is 75 W per person and ventilation requirement is 9.43×10^{-3} m^3/s for each person. Explanation of systems design is discussed further.

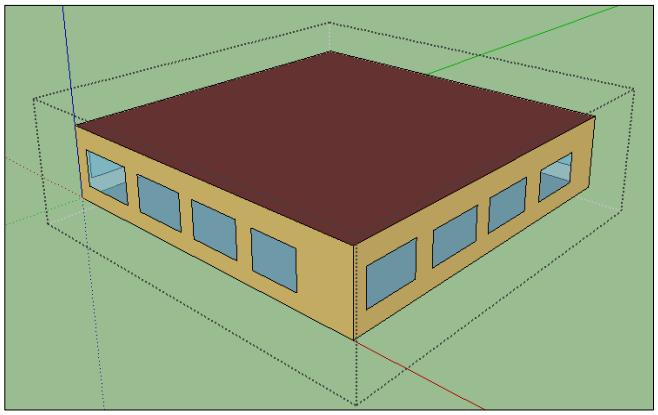

Figure 3.3.1: Schematic layout of the present building for VA and VC system assessment

3.3.2 Methods of operations

3.3.2.1. Configuration 1

A VC system with a DOAS consisting desiccant wheel is modeled in this configuration, as revealed in Figure 3.3.2. The system is designed to keep a desired level of thermal

comfort all over the year. For maintaining the needed building thermal comfort conditions, the VC system provides cold water at 7 ˚C [Trane 2010] to the cooling coil and fan arrangement. From here, cool and dehumidified air is delivered inside the building space at 15˚C and 0.008 kg/kg of dry air. In this case, solar collector system supplies the heat energy in form of hot water for regenerating desiccant wheel. Electrical energy driven auxiliary water heater is also coupled to address the irregularity related with the solar energy. An IEC is coupled to lower the air temperature after passing through desiccant material up to 30 ˚C to supply it within the room. The validation of the installed VC system with the available reference building model [EnergyPlus 2017] for hot-dry climate condition is presented can be found in published work [C4]. It is worth to mention here that the reference building is of 1000 m^2, thus, for the comparison purpose, the parametric values of the same are scaled down to 400 m^2 for evaluating it with the present building.

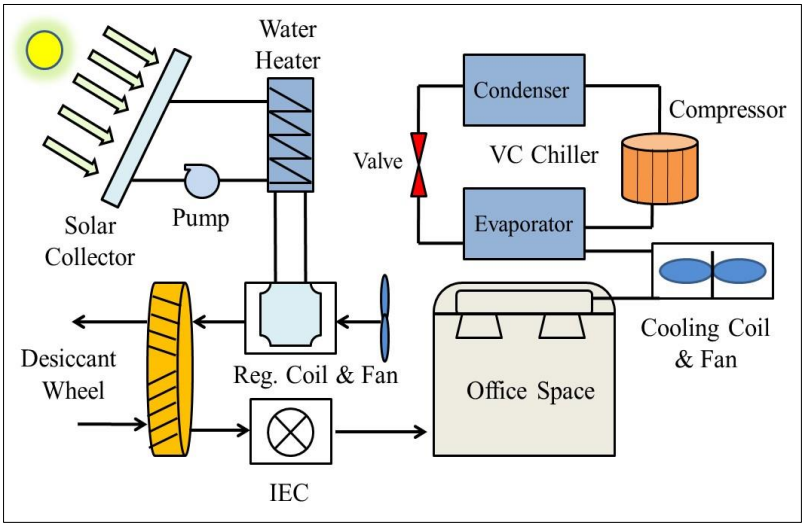

Figure 3.3.2: System layout for configuration 1 of air-conditioning

3.3.2.2. Configuration 2

Here, a VA system is used in the place of VC system of the configuration 1 (Figure 3.3.3). In this VA based system, supply some kind of heat energy needed to be at the generator side for functioning of the VA system. In the present analysis, the essential thermal energy is accomplished with the biomass-based boiler. The boiler delivers hot water at 80 ˚C to the generator of VA system. For satisfying the given thermal comfort, other components of this configuration are the same as configuration 1. In configuration 2, roof area of around 300 m^2 is used for the solar collector installation to regenerate the desiccant. Therefore, the necessary heat energy requirement in the generator side

has to be sustained by boiler system. This is because the remaining available roof area of 100 m^2 will not be sufficient to meet the necessary heat load for generator of VA system through solar collectors.

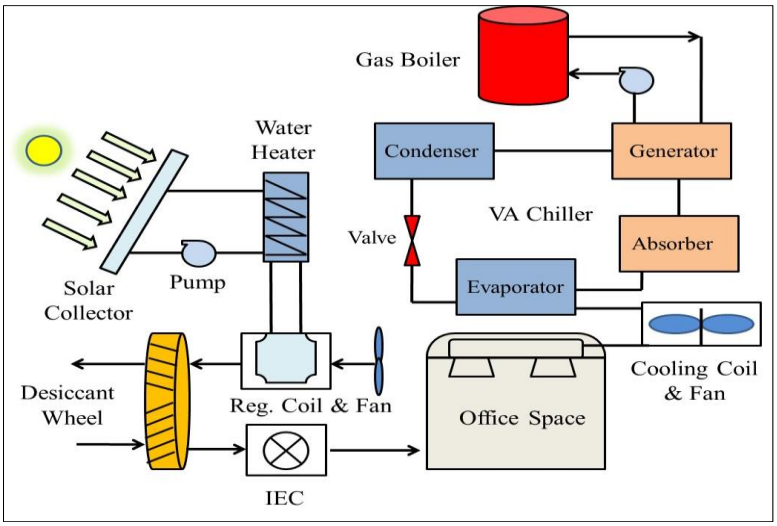

Figure 3.3.3: System layout for configuration 2 of air-conditioning

3.3.3. Results and discussion

Simulations are completed for both the conferred configurations under hot-dry and composite climatic conditions. Variable environmental circumstances affect the system performance in terms of energy consumption and COP. EnergyPlus simulations are accomplished for a whole year in order to sustain the thermal comfort conditions.

Figure 3.3.4 shows the yearly electricity consumption pattern for the two different weather conditions. Figure 3.3.4a outline pertains to hot-dry climate zone. From Figure 3.3.4 it is well-highlighted that the total energy outflow occurring in a year for configuration 1 is more as compared to that configuration 2. From the analysis, total electricity consumed is found as 32139 kWh and 17171 kWh in configurations 1 and 2, respectively within a year for hot and dry climate zone. Major reduction in electrical energy requirement for configuration 2 is due to the addition of VA system. However, in configuration 2, pumps' power consumption is higher than configuration 1. This is because; one additional pump is added to circulate the hot water from boiler to the generator of the VA system. In configurations 1 and 2, the water heater is requiring electricity because of the incapability of the solar collector system to fulfil the needed thermal energy requirement, particularly during adverse climates.

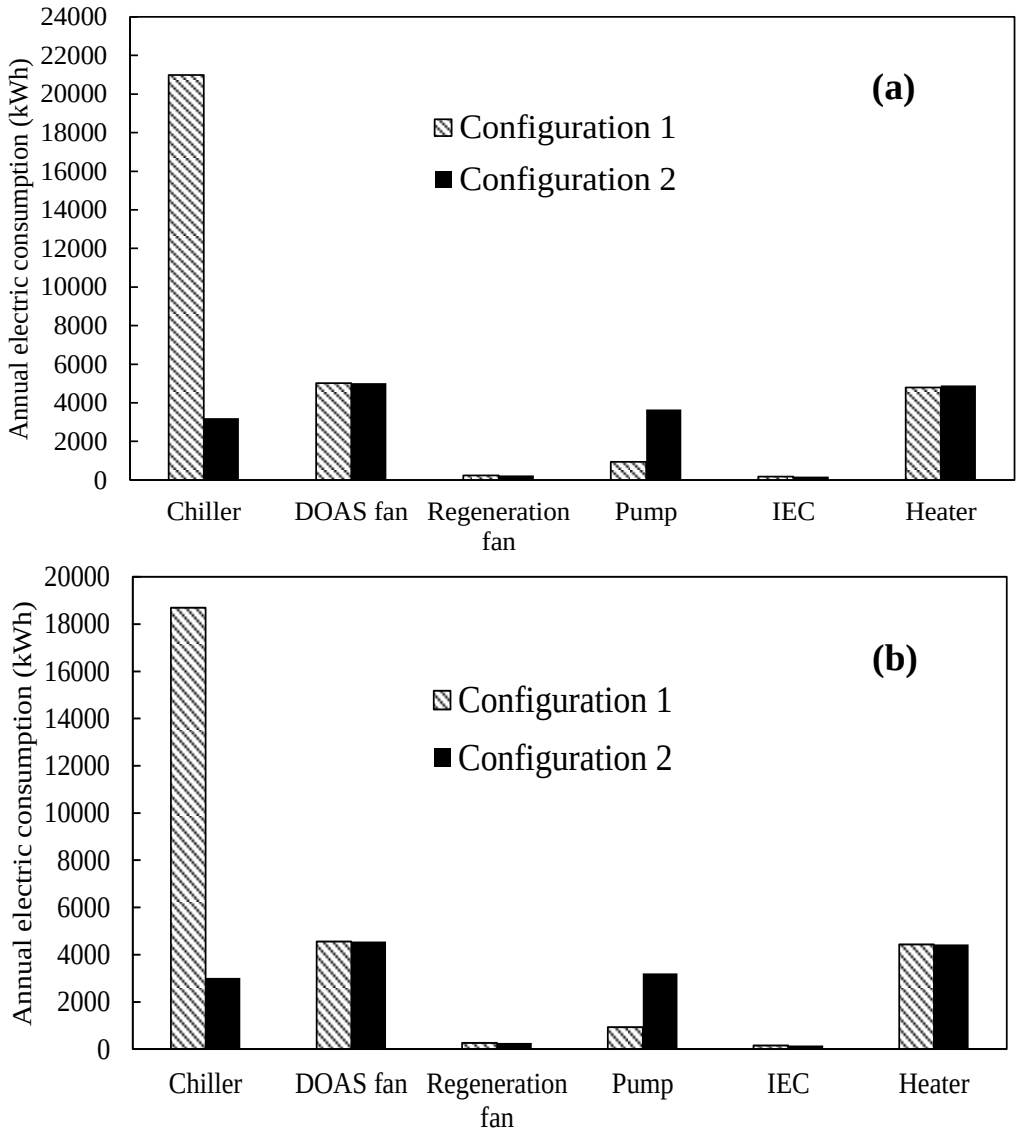

Figure 3.3.4: Annual electric energy utilization details (a) hot-dry weather (b) composite weather

The annual electrical energy consumption for configuration 1 is 29047 kWh and the same for configuration 2 is 15644 kWh for the composite weather (Figure 3.3.4b). From Figure 3.3.4 it is well-observed that the net electricity consumed in both the configurations is lesser for the composite weather. This is due to the environmental conditions of these two locations. It is perceived that configuration 2 results in 46.57% electric energy savings than configuration 1 for the hot-dry weather. Furthermore, for the composite weather, this value is around 46.14% that is ascribed due to the difference in environmental conditions.

3.3.4. Conclusions

This study demonstrates the effect of using desiccant-assisted ventilation in VC and VA based air-cooling systems for composite and hot-dry weather conditions. Here, solar collector supply heat energy to the desiccant side, whereas biomass-based boiler system is added to meet the VA-system requirements. Electricity based heat is used only for emergency purpose to address any disruption in the availability of solar and bio energy. For the present objective, EnergyPlus simulations are done for a complete year. From the results of this present study, it is shown that the usage of VA along with desiccant based system provides surplus energy savings with respect to the VC based system. Electrical energy saving potential of VA based system for hot-dry weather condition is 46.57%, and the same for composite weather is nearly 46.14% compared to VC-based system. Apart from this, it is also established that the VA system would be more beneficial under hot-dry climates in comparison with the composite climates.

3.4. Energy saving assessment of triple-hybrid vapor absorption building cooling system under hot-dry climate

3.4.1 Building design and system description

This study includes the performance assessment of a triple hybrid VA-based building cooling system under hot-dry climatic conditions, and the novelty aspect is somewhat similar to that deliberated in Section 3.1. To meet the aim of this study, two different kinds of air-cooling setups are added in the small office building model which are discussed below. The concerned 3-D building geometry is shown in Figure 3.4.1a. Here it includes a single zone having 1000 m^2 of total floor area. The construction parameters of the building geometry (wall, floor, roof, and window) are in accordance with the specified benchmark data of ECBC [Khan et al. 2009]. Here, in this study, the building's essential input parameters follows standard values [Khan et al. 2009 and Deru et al. 2011] as shown in published literature. This simulation study is subjected to the climatic conditions of hot and dry climate. This climatic zone possesses air relative humidity as low as 20% with a maximum temperature of around 45 ºC. Hot and dry climatic zone attributes to clear sunny days that provide more potential to use solar energy. The intensity of solar radiation is also quite high throughout the year. The details of different modes of operations are discussed below.

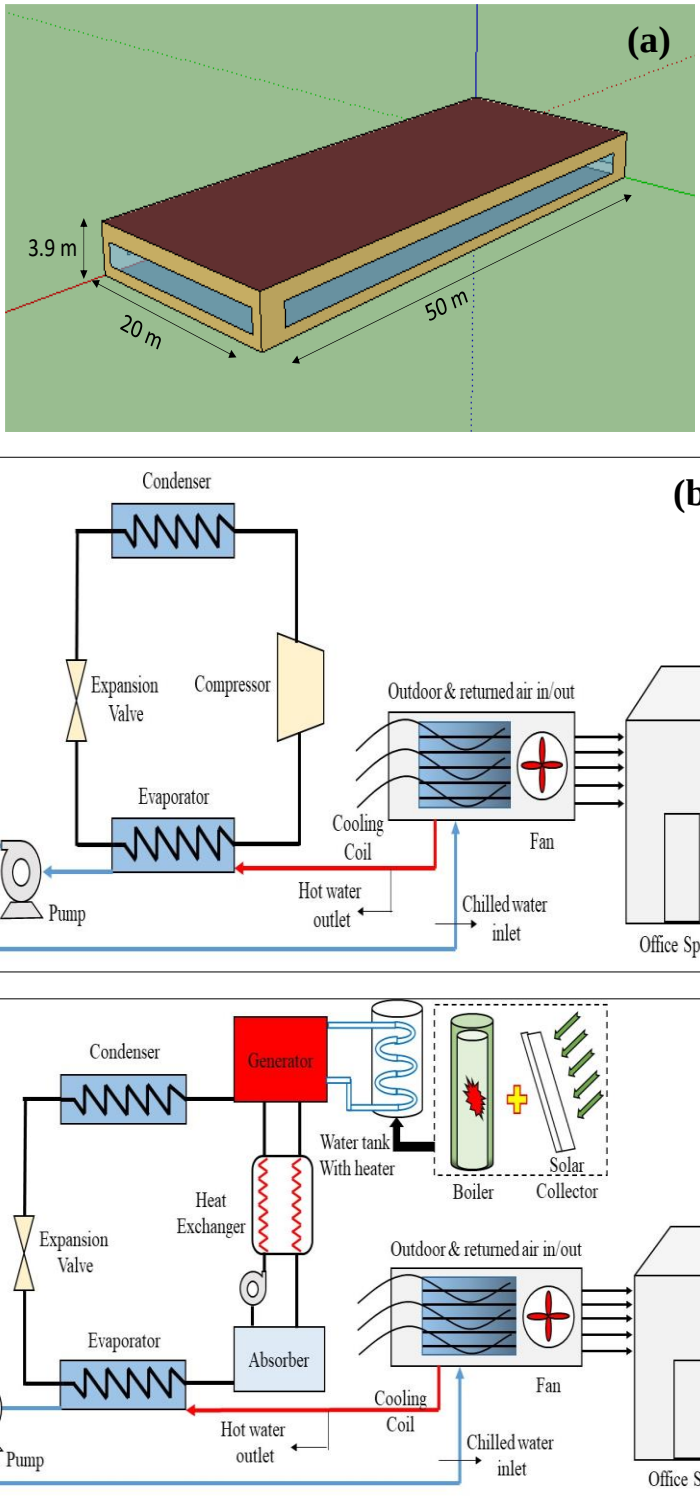

Figure 3.4.1: (a) building model for analysis of triple hybrid VA system, (b) case 1 conventional design and (c) case 2 VA design

3.4.1.1. Case 1: (Vapor compression air-conditioning system)

Here, VC cycle driven air-conditioning unit is installed in this case (as discussed earlier). The layout of this case 1 is shown in Figure 3.4.1b. The installed air-conditioning system of this case is validated with available reference model of EnergyPlus tool by scaling down the present building model to the available small office model of 500 m^2 floor area. Both of these models are validated for the same input parameters. Here in this study, the space thermal comfort conditions are kept identical in both modes of operation. The details of energy consumption estimation and required parameters can be referred from section 3.1.2.1 and also found in published work [C6].

3.4.1.2. Case 2: (Vapor absorption air-conditioning system)

Here, only VC chiller of case 1 is replaced with VA based chiller. Other remaining functional parameters are kept the same as case 1. The plan layout of the air-cooling setup is depicted in Figure 3.4.1c. In this study, solar collectors with different collector area and biomass driven boiler are used for supplying the heat energy (hot water) at the generator. The hot water temperature is varied between 70 °C – 80 °C. The area of solar collector is changed from 400 m^2 to 500 m^2. Biomass boiler is coupled in the hot water circuit with solar collectors to contribute under unfavorable conditions. Further, to ensure hurdle free operation, an auxiliary heater is also coupled.

3.4.2. Results and Discussion

The purpose of this study is to carry out a quantitative analysis of a triple hybrid absorption-driven air-cooling system in terms of thermodynamic and electrical aspects against the conventional system. For both of the operational modes, simulation results are discussed next.

Figure 3.4.2 shows the annual electrical energy consumption analysis of both the modes which includes energy consumption of individual components like chiller, cooling tower, fan, pump, and heater.

In cases 1 and 2, the chilled water circulation (pump of AHU) consumption was small, so it was added in to the chiller energy consumption itself. The net annual electricity consumption in case 1 is 72951 kWh. Here, the major contributor is VC chiller. In case 2 with 400 m^2 solar collector area (generator temperature 70 °C), the net annual electricity consumed is around 68679 kWh. Here the energy consumption shared by the auxiliary heater is quite high because solar and biomass boiler were not capable to fulfill

the system requirements. However, in case 2 with 500 m^2 solar collector area, the net electricity demand is around 48064 kWh (at generator temperature 70 °C). By using 400 m^2 and 500 m^2 collector area, around 5.8% and 34.1% of annual electrical energy savings can be attained with respect to the conventional system (Figure 3.4.2a). It can also be noticed that the net auxiliary heating energy requirement for the lower generator temperature with 500 m^2 solar collector case is nil (Figure 3.4.2a).

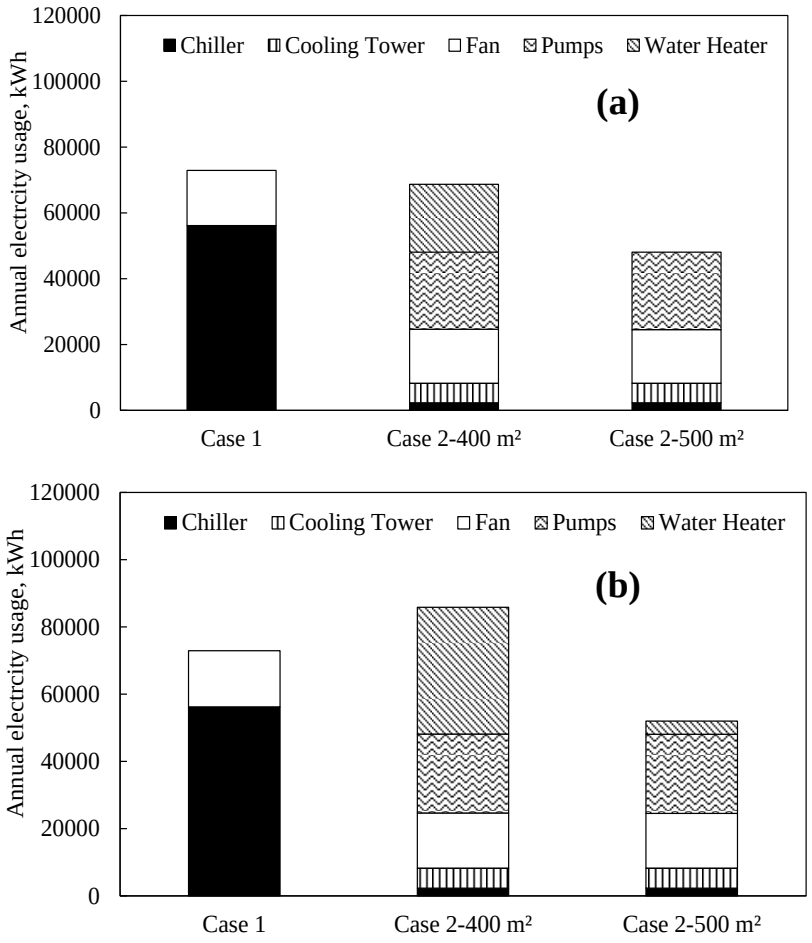

Figure 3.4.2: Net annual electricity consumption at generator temperature of (a) 70 °C, (b) 80 °C

In case 2, the contribution of VA chiller is very small. When the generator temperature is 80 °C, the net electricity consumed in 400 m^2 and 500 m^2 solar collector area cases are 85858 kWh and 52005 kWh, respectively (Figure 3.4.2b). This results in 28.7% of energy savings with only 500 m^2 collector area. Here, in the case of 80 °C generator temperature, the heat energy demand is increased at the generator side, consequently, that is being supplied by the auxiliary electric heater. Hence, in this case, a collector area of 400 m^2 is not sufficient to provide enough heat energy and due to this, auxiliary share has been increased. So, it does not provide preferred energy savings.

Nevertheless, increase in the generator temperature (70 °C to 80 °C) increases the COP of the VA chiller from 0.50 to 0.52.

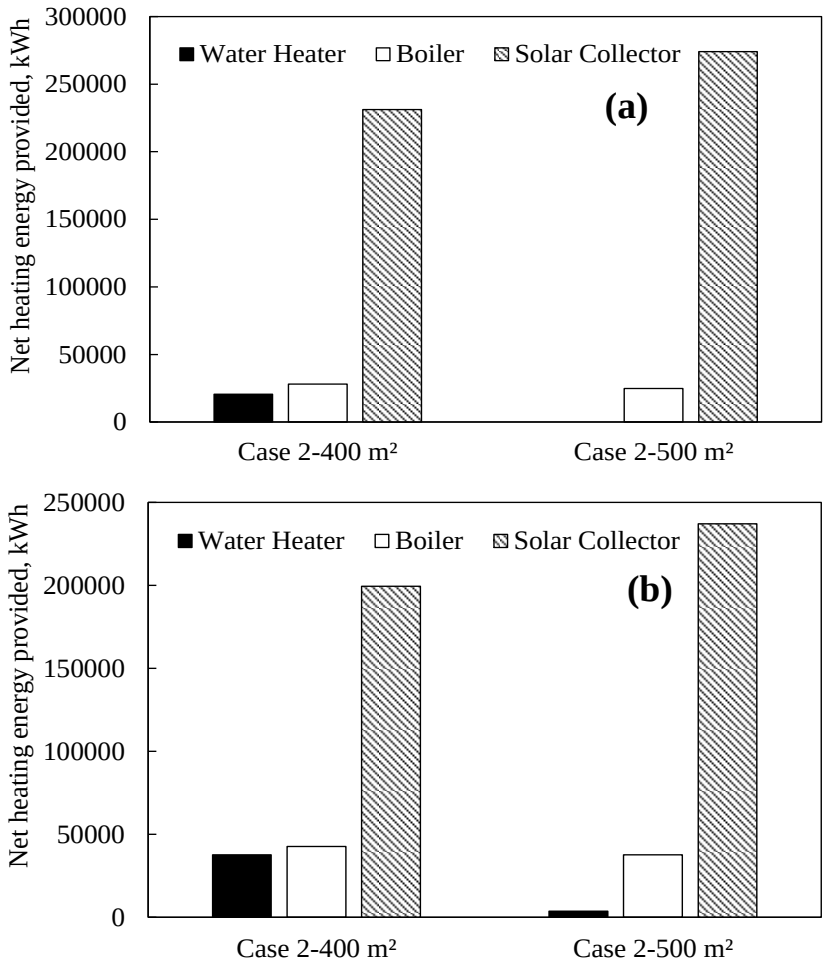

Figure 3.4.3: Fractional heating energy provided by components at generator temperature of (a) 70 °C, (b) 80 °C

Figure 3.4.3 shows the fractional amount of heating energy supplied by the individual components installed in the hot water circuit of the absorption system. It can be noticed that at generator temperature of 70 °C, the quantity of heating energy delivered by the auxiliary heater is nil (Figure 3.4.3a), which means that the whole system is fully renewable energy driven. From Figure 3.4.3 it can be perceived that, as the generator temperature increases, the contribution of the solar collector energy reduces and that causes more contribution of auxiliary heater.

3.4.3. Conclusions

In this study, an assessment has been carried out on a small office building to analyze the energy saving potential and thermal performance of a triple-hybrid absorption-

based building cooling system against a conventional compression-based system. Here, two cases are studied for the absorption system, first when solar collector area is 400 m^2 and the second with 500 m^2. Further, the generator temperature is varied from 70 °C to 80 °C. It can be revealed that, for hot-dry climate, VA-based systems can be fully operated by renewable energy-based resources under the condition of 70 °C generator temperature. With increasing the generator temperature, COP of the system can be enhanced, but it can also increase the dependency of the system on high grade energy. The maximum electrical energy savings of absorption system can be achieved up to 34.1% against conventional system.

3.5. Performance analysis of evaporation and heat wheel-based building air conditioning systems

3.5.1. Building and model details

The literature survey reveals that the comparative performance assessment between the IEC and heat recovery device-assisted DOAS with the VC system is not done yet. In this context, this work has been done. As indicated (Figure 3.5.1), a building consisting of carpet area 511 m^2 along with five zones and 0.40 window-to-wall ratio (WWR) is studied here. For each person, the ventilation demand is taken to be 20 cubic feet per minute [Khan et al. 2009 and Deru et al. 2011]. The present air-conditioning model is also compared with reference model by the same process as discussed earlier. From the comparative study it can be observed that the maximum error between these two system models is below 12% as discussed in published literature.

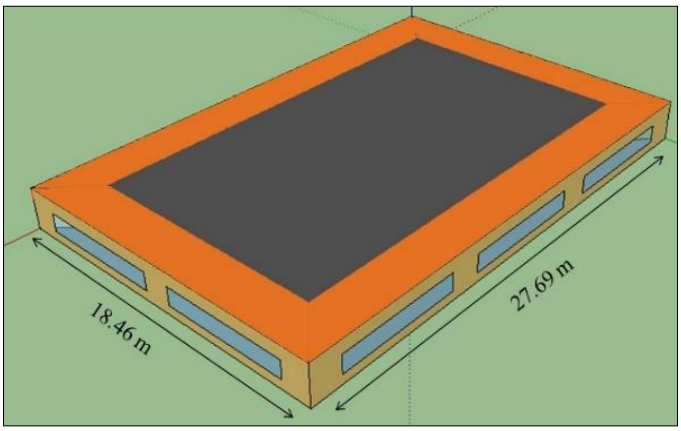

Figure 3.5.1: Building for analysis of VC system with sensible heat wheel and IEC

In the present work, a VC based chiller has been used for building air-conditioning. Besides this, a desiccant material is also provided that also supplies air under

dehumidified condition to reduce the energy/thermal load on the system. Heat energy in the form of hot air is required for regeneration purpose which is coming either from direct heater or any heat exchanger. In this work, a regeneration coil with a fan in front of this regeneration coil is provided to supply hot air. Because of dehumidification process, air coming out of the desiccant gains temperature (process 1 to 2 in Figure 3.5.2 and Figure 3.5.3) before the same is supplied to the room. Here, air attains a temperature of nearly 48 °C along with humidity of approximately 8.0 kg/kg of dry air after emerging from the desiccant material. The process side air follows path 1-2-3 (shown by solid arrow lines), and the regeneration side air follows path 4-5-6 in mode 1 and 4-5-6-7 in mode 2 (indicated by dotted arrow lines). Now for decreasing this temperature, two strategies have been studied here. In the first strategy (Mode 1), an IEC arrangement with effectiveness of 70 % has been provided along air flow route as indicated by Figure 3.5.2. Here, ambient air has been used for both the process side (Node 1 in Figure 3.5.2) as well as regeneration end of DOAS (Node 4 in Figure 3.5.2). In the second strategy (Mode 2) indicated by Figure 3.5.3, a heat wheel of 70 % effectiveness has been incorporated along the process side as well as the regeneration end of DOAS. A heat wheel is a typical heat exchanger which exchanges heat between two air streams. There is sensible heat transfer between the exhaust and supply air streams. Here, return air out of the conditioned space has been used at the regeneration side. Heat wheel serves as thermal energy exchanging unit between the supply and returned air. The temperature of the supply air after flowing out of the indirect evaporation cooler and thermal energy recovery wheel fluctuates in the range of 24 °C-27 °C. For regenerating the desiccant material, a loop of flat plate solar collectors having an area of 400 m^2 is provided. This loop provides hot water at 80 ºC to the regeneration coil and from here, hot air at around 60 ºC is supplied at the regeneration side of desiccant wheel through fan arrangement. Further, electricity-based auxiliary heating is also included for running the system without any interruption in case of insufficient availability of solar energy. It is worth to mention here that auxiliary energy need may also be met by biomass based systems. Further design details about the related to the chiller and other component details can be found in a previously published work [J6 and C5]. The psychrometric representation of the path followed by air in two of studied strategies can also be found in the work [J6 and C5].

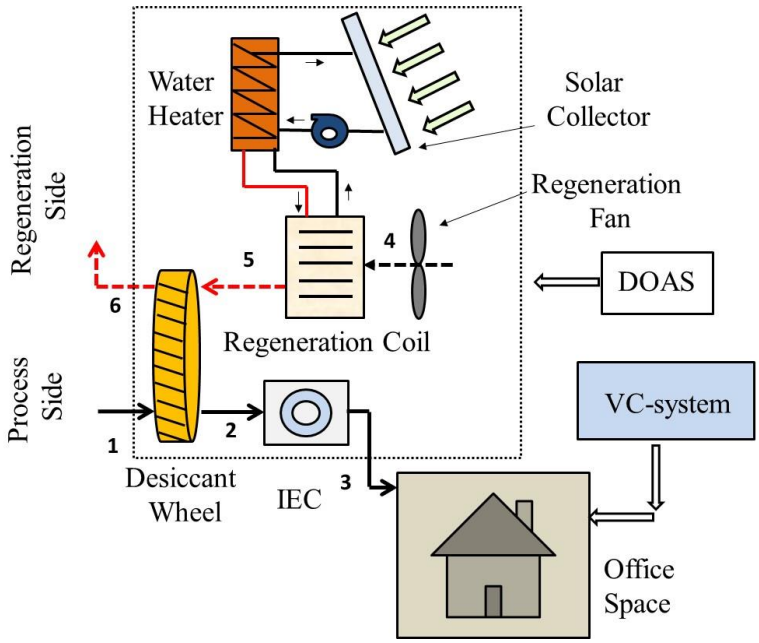

Figure 3.5.2: Schematic design of first strategy (MODE 1)

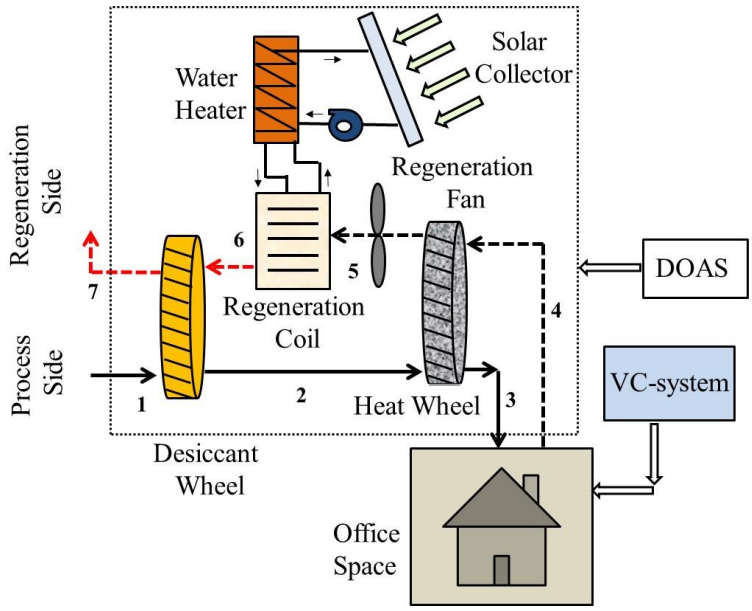

Figure 3.5.3: Schematic design of second strategy (MODE 2)

3.5.2. Results and discussion

The purpose of the air-conditioning system is to sustain an acceptable level of thermal comfort regardless of the dynamic outside weather conditions.

The installed system maintains the required thermal comfort conditions throughout the year [J6 and C5]. To determine electrical energy savings attained due to various arrangements done inside the DOAS, present results are evaluated through Figure 3.5.4.

For Strategy 1, net yearly usage of electricity has been found to be 26229 kWh, whereas, for Strategy 2, the same has been found to be only 24970 kWh against the composite climate. The total annual energy consumption of standalone VC chiller is around 18695 kWh and 18590 in Modes 1 and 2, respectively. The difference in energy consumption by different fans is not of much significance. The major impact of using heat recovery wheel in Mode 2 was on IEC and auxiliary heater. Further, it may be highlighted that by introducing a heat wheel instead of indirect evaporation cooling arrangement, electricity usage in auxiliary heating, pumps, and regeneration fans can be reduced. By this practice, net electricity requirement is found to decrease by 1259 kWh. This can be attributed to the fact that the provision of heat wheel decreases the thermal energy demand towards the regeneration end of desiccant material. Consequently, the usage of a heat wheel instead of an indirect evaporation cooling arrangement can lead to nearly 5.04 % savings in the annual electricity demand. As the addition of heat wheel in place of IEC in Mode 2 enhances the energy performance of the system, the economics related to the proposed modification shows less initial capital investment. For the same air flow rate, the cost of the heat recovery wheel [29] is less than that of IEC [30], so it is obvious that proposed modification to the system will be economically suitable.

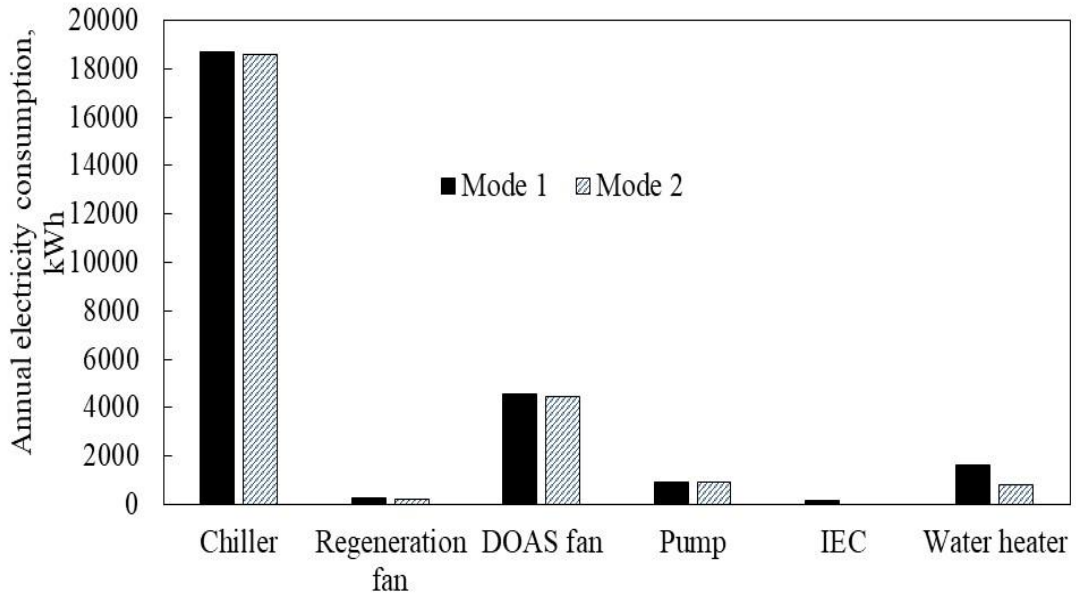

Figure 3.5.4: Electrical energy patterns indicating negligible energy consumption by heat wheel

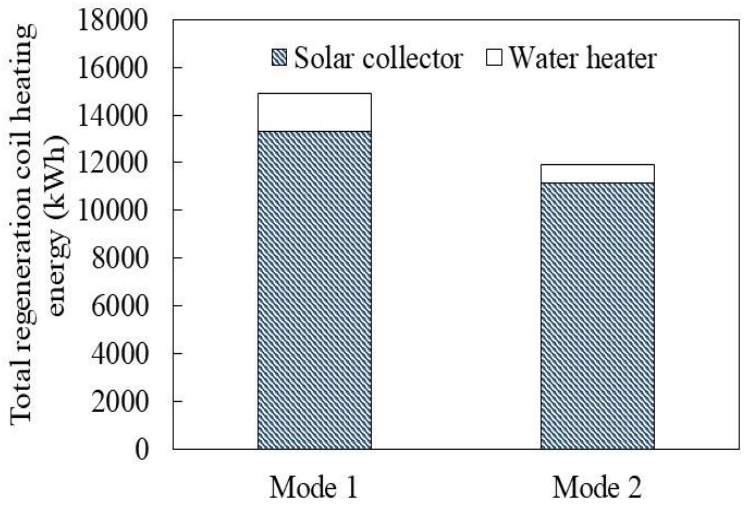

Figure 3.5.5: Regeneration heating energy requirements in both strategies (Modes 1 and 2)

Figure 3.5.5 demonstrates the total thermal energy demands for the regeneration purpose on the yearly basis for strategies 1 and 2 that is fulfilled by solar collector and auxiliary heating arrangement. The amount of total thermal energy delivered by the solar collector and auxiliary heater is 13294 kWh and 1620 kWh, respectively. However, in Mode 2, the solar collector loop supplies 11124 kWh of thermal energy and the auxiliary heater provides 796 kWh of thermal energy. As intuitive, with reference to the first strategy, in the second strategy, the amount of total thermal energy delivered to the regeneration coil reduces by nearly 2994 kWh (Figure 3.5.5). In Mode 2, the net heat energy supply at the regeneration end is reduced due to incorporation of heat recovery wheel. That is using low temperature return air from the office space to reduce the temperature of outgoing process air from desiccant wheel.

3.5.3. Conclusions

This study revealed the working characteristics of two modified strategies related to desiccant-based DOAS when incorporated to a VC air-conditioning system operated in a composite weather conditions. A small 511 m^2 building is studied wherein the studied modification along the air flow route of the DOAS has been realized by two different strategies, namely Mode 1 and Mode 2 consisting of indirect evaporation cooler and heat wheel, respectively. The present simulations indicate that the provision of heat wheel instead of indirect evaporation cooler is capable of saving the air-conditioning system's yearly electricity up to 5.04 %. Further, as compared to the indirect evaporation cooler strategy, the value of solar fraction is determined to be more with

the heat wheel-based strategy. The proposed heat wheel-assisted strategy reported here for air-conditioning of small-scale buildings is predicted to be more advantageous for large-scale buildings.

3.6. Comparative performance assessment of multi-stage absorption air-conditioning under warm-humid climate

3.6.1. System description and building model

Significant research effort has been put forward in the past years for performance improvement of single and double-effect VA systems. However, none of the studies presented a quantitative analysis of the electrical and thermal energy performances of single and double-staged VA systems with those of the compression-based system for air-conditioning. In this context, the objective of this work is to estimate the annual electrical and thermal energy aspects of the different air-conditioning method (single-stage VA system, double-stage VA system, and vapour compression system) and calculate the energy savings. These air-conditioning units are installed in a small office building and performance valuation is done using the Energyplus tool [EnergyPlus 2017]. The concerned a single-storey small office building has total floor area of 1000 m^2. Its building 3-D geometry is revealed in Figure 3.6.1. The building envelope parameters (wall, roof, and window) follow standard identified benchmark details provided by ECBC [Khan et al. 2009]. The present simulation study is done for the warm-humid climatic conditions. The details of different air-conditioning setups are deliberated next.

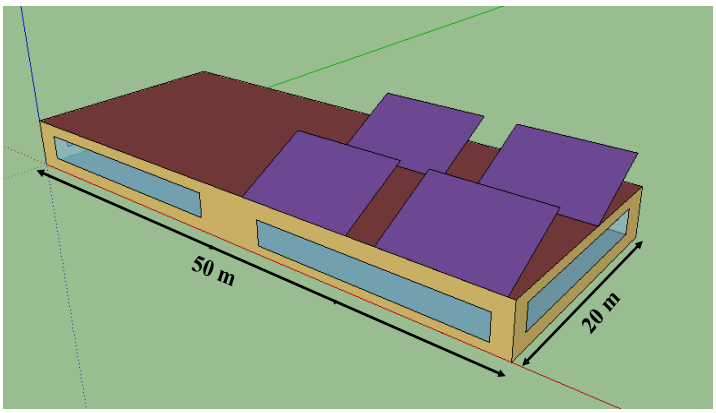

Figure 3.6.1: 3-D building model with solar collector on roof for multistage VA system

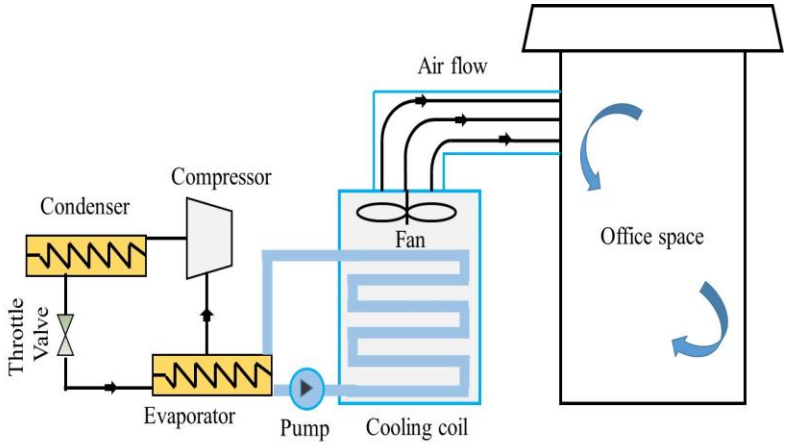

Figure 3.6.2: Layout of the compressor-based air-conditioning unit

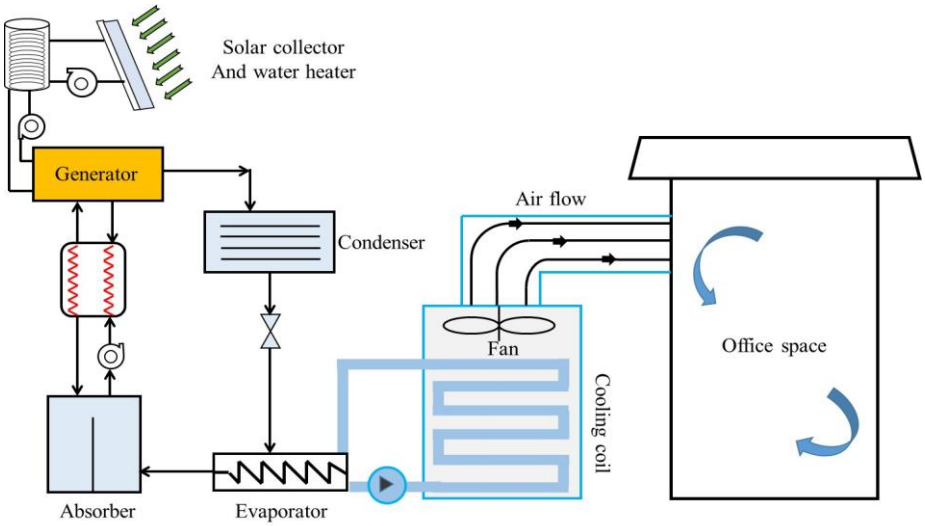

Figure 3.6.3: Layout of single-stage *VA*-based air-conditioning unit

3.6.1.1. Case 1: Compressor-based air-conditioning unit

A central air-conditioning system that comprises an arrangement of pipes, chiller, fan, etc. is modeled. In this mode of air-conditioning, a same working setup is installed as discussed in the earlier studies. The schematic plan of case 1 is shown in Figure 3.6.2. A validation study also has been performed in order to check the functioning of the installed air-conditioning unit [C7]. This validation study also represents satisfactory variations in the parameters (except annual electrical energy consumption) for the other modes (single/double staged absorption) of operation. The assessment method of the energy consumption by installed components and ranges of different parameters for all the considered can be calculated as prescribed in section 3.1.2.1 and can also found in published work [C7].

3.6.1.2. Case 2: Single-stage absorption based air-conditioning unit

Here, a single-stage VA chiller is installed with the AHU. In this mode, other identified parameters remain the same as of Case 1. The schematic arrangement for this case is shown in Figure 3.6.3 This VA chiller delivers chilled water at the same conditions as that of Case 1. Here, in the single-stage VA system, the flat-plate solar collector loop that has a total collector area of around 500 m^2 delivers required thermal energy in the form of hot water at 80 ºC temperature at the generator of the VA chiller. An auxiliary electrical heater is also coupled inside the hot water storage tank for addressing any solar energy related deficiency.

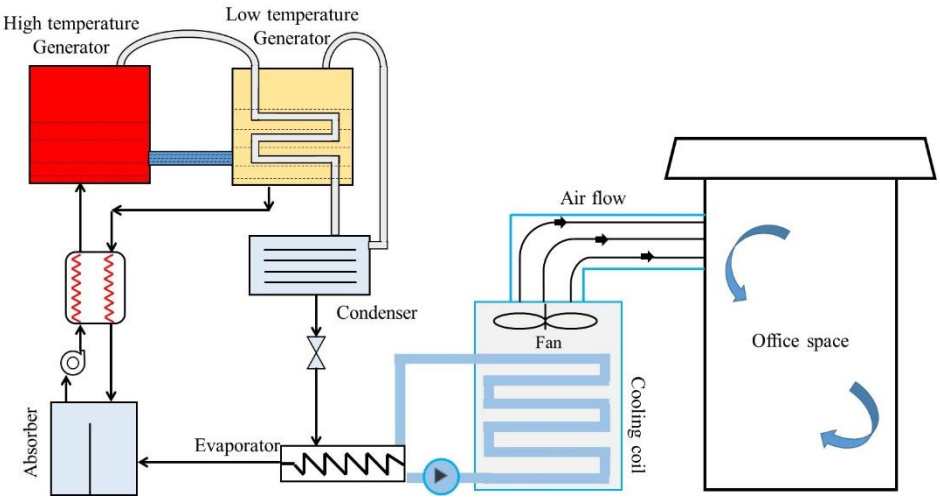

Figure 3.6.4: Layout of double-stage *VA*-based air-conditioning unit

3.6.1.3. Case 3: Double-stage absorption-based air-conditioning system

Here, a double-staged direct fired VA chiller is connected with the AHU. This chiller (double-staged) is also liable for performing the same functions as of the earlier ones (compression chiller and single-staged VA chiller). The component arrangement is shown in Figure 3.6.4. In the double-stage VA chiller, there are two vapor generators: low and high temperature generators. Primarily, the solution mixture is pumped into the high temperature generator (First generator) where high temperature thermal energy separates the refrigerant from mixture, then this mixture is sent to the low temperature generator (second generator). Inside low temperature generator (i.e. second generator), high-temperature steam coming from the first generator is used to regenerate some part of the solution available inside the first generator. Thus total vapor/refrigerant is sent to the condenser section, and it goes through the complete cycle. Here, natural gas has been used as the preliminary fuel of double-stage VA system. Apart from natural gas,

an equivalent amount of biomass/biogas may also be used for the same thermal energy need. The performance parameters of the double-stage VA system can be estimated as follow,

$$COP = \frac{Q_C}{Q_{Gas}} \tag{3.6.1}$$

$$Q_{Gas} = \dot{V}_{Gas} \times LHV \tag{3.6.2}$$

where, $\dot{V}_{Gas}$ m^3/s is the volume flow rate of gaseous fuel and LHV indicates its lower heating value. The pump work is neglected in this study for the calculation of the COP of the chiller.

3.6.2. Results and discussion

The objective of this study is to quantify and compare electrical and thermodynamic performances of single and double-stage VA air-conditioning systems against the conventional cooling technique. The simulation model runs for the weather file of warm-humid climate. All of the considered air-conditioning designs perform the same functioning in terms of maintaining air humidity level, temperature and ventilation [C7].

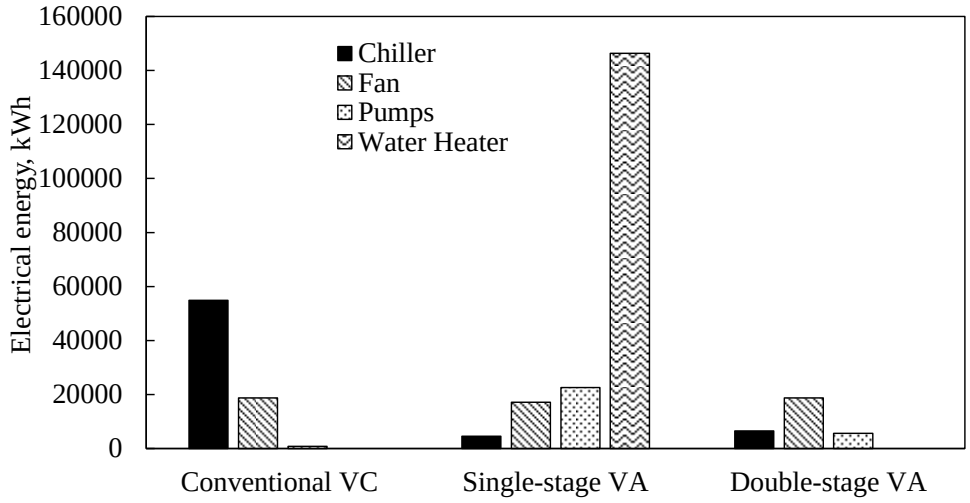

Figure 3.6.5: Annual electrical energy analysis of various systems

Next, Figure 3.6.5 indicates the total annual electrical energy consumption pattern by each component of the installed air-conditioning unit. From Figure 3.6.5, it can be observed that there is a very high difference in the electricity consumption by the compression and absorption chillers. However, the difference in electricity consumption by single-stage and double-stage chillers is not noteworthy. The fan

electricity consumption is almost the same in all of the three considered systems. The pump energy consumption is very less in conventional compression-based system whereas, this is relatively high in case of single-stage VA system. This is because in the single stage VA system, additional pumps are connected in the solar collector loop. From Figure 3.6.5, it is observed that the auxiliary heater energy consumption is very high in the single-stage VA system, because the accessible solar energy is not sufficient to fulfill the requisite thermal demand of the generator. However, there is no auxiliary heater in double-stage because complete heat energy is supplied by firing the gas. The total annual electricity consumed by the compression-based system is 74451 kWh, single stage *VA*-based system consumes 190692 kWh, and the double-stage VA-based system consumes around 30910 kWh. The total electrical energy savings attained by the double stage VA system in comparison with compression driven system is 58.4% and with single stage system this value is 83.7%.

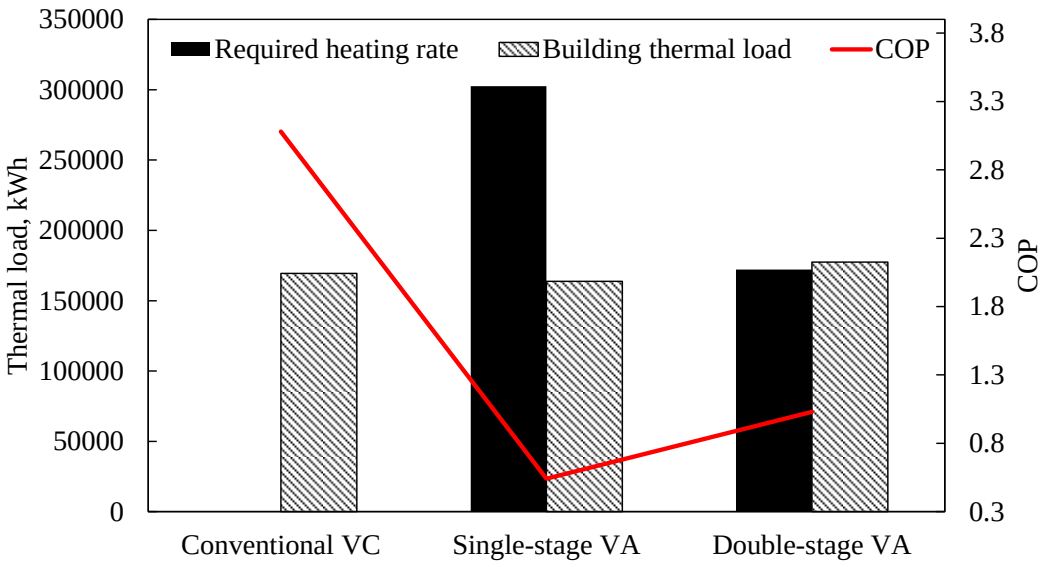

Figure 3.6.6: Annual heat energy required and building thermal load catered by different air conditioning systems

Figure 3.6.6 displays the annual building thermal load catered by all three configurations and the thermal energy requirement at the generator of the single-stage and double-stage VA systems. The catered building thermal loads in the case of compression, single-stage and double-stage VA are 169359 kWh, 163808 kWh and 171530 kWh, respectively. Further, from Figure 3.6.6 it can be noticed that thermal energy required at the generator side of the double-stage VA system is lesser as compared to that of the single-stage VA system.

Table 3.6.1: Unmet hours for configurations in all studies

S. No.	Building area	System type (Configuration details)	Unmet hours (Climate)
1.	1000 m^2	Conventional VC system	10 (Warm-humid) 63 (Composite)
		Solar-natural gas assisted VA system (700 m^2 collector area and 70 °C generator temperature)	35 (Warm-humid) 40 (Composite)
2.	400 m^2	Conventional VC system	11 (Warm-humid)
		Conventional VC system with desiccant DOAS	5 (Warm-humid)
		Conventional VC system with IEC-desiccant DOAS	4 (Warm-humid)
3.	400 m^2	Conventional VC system with IEC-desiccant DOAS	12 (Hot-dry) 163 (Composite)
		Conventional VA system with IEC-desiccant DOAS	14 (Hot-dry) 186 (Composite)
4.	1000 m^2	Conventional VC system	8-55 (Hot-dry)
		Solar-natural gas assisted VA system (500 m^2 collector area)	11-50 (Hot-dry)
5.	511 m^2	Conventional VC system with IEC-desiccant DOAS	194 (Composite)
		Conventional VC system with SHRW-desiccant DOAS	105 (Composite)
6.	1000 m^2	Conventional VC system	10 (Warm-humid)
		Single-stage VA system	20 (Warm-humid)
		Double-stage VA system	10 (Warm-humid)

This is because in double-stage VA, heating energy is supplied at a higher temperature as compared to that of the single-stage and heat energy accompanying with refrigerant coming from high temperature generator is reused in the low temperature generator. The amount of annual required thermal energy in single and double stage VA systems are 302622 kWh and 172214 kWh, respectively. Due to this, the COP of the double stage VA system is found as 1.03, whereas, for the single stage it is around 0.54. The estimation of COP for different configurations includes different parameters, like: for compression chiller, chiller cooling capacity and compressor electric consumption is required, for absorption chiller cooling capacity, generator heat input and pump power is required, The COP of the commercial single-stage VA system is less than 1 because the amount of required heating energy is more compared to the produced cooling effect. Further, the details of unmet hours of various simulation models for different configurations of air-conditioning modes are shown in Table 3.6.1. Here, the ranges of unmet hours (varies between 1-300 hours) according to the climate, solar collector area, system technology etc. for each of the considered configurations in chapter 3 falls under the specified range (Unmet load hours troubleshooting guide, 2013, and Chiu and Krarti, 2021) for a system working throughout the year.

3.6.3. Conclusion

In this work, a comparative assessment has been done between compression and VA-based air-conditioning units under warm-humid climate. Using EnergyPlus simulation tool, thermal and electrical characteristics have been deliberated by considering three different air-conditioning modules based on compression, single-stage VA, and double-stage VA strategies. The simulation results portray that, double-stage VA technique is able to save nearly 58.4% of annual electrical energy compared to the compression-based techique, whereas 83.7% electrical energy can be saved with respect to the single-stage VA mode. The supplied cooling energy in the case of single-stage VA system is lesser compared to the other two configurations due to the shading effect of the solar collectors. From this study, it can be clearly perceived that the amount of net heat energy required for running the absorption system is less in the case of double-stage chiller. The COP of the compression, single-stage, and double-stage VA modes are 3.08, 0.54 and 1.03, respectively. Net thermal energy input to the generator of double-stage VA is found to be lesser than the catered cooling load thus yielding a higher COP than that of single-staged VA. Based on the annual energy savings and COP, it can be

concluded that two-staged VA design delivers enhanced performance under the prescribed operating conditions compared to other two techniques.

CHAPTER 4

*ABSORPTION BASED RADIANT COOLING SYSTEM WITH DESICCANT DEHUMIDIFICATION

This chapter investigates the feasibility of a decoupling strategy (separation of cooling and ventilation task) by adding a vapour absorption (VA) based system. This study introduces the concept of integrating radiant cooling systems with VA-based cycle. This study has been done on a large-scale office building subjected to warm-humid climatic conditions. Conventionally, a typical radiant cooling system operates on a compression-based approach and uses expansion coils for the ventilation unit. Here, this study presented a radiant cooling system with a triple hybrid VA chiller for the cooling unit and the addition/coupling of a desiccant and indirect evaporative cooling unit with a ventilation unit. A comparative analysis of the presented system with the conventional units is also shown for evaluating various performance parameters and energy savings.

4.1 Building description and methodology

A lot of studies reported the study of the radiant cooling system with VC-based chiller. However, very few studies of the radiant cooling system with a VA-based system are available, but those were only for small-scale capacity applications. Large-scale radiant cooling systems with VA systems will involve various challenges like space constraints, components sizing, availability of heat energy sources, etc., if it operates merely on solar energy as the heating source. Intuitively, intermittency associated with solar energy due to fluctuating weather conditions affects the system's performance. Therefore, the present work analyzes the performance of triple hybrid solar, biogas, and auxiliary heater-based absorption radiant cooling system integrated with desiccant dehumidification methodology for a large-capacity office building. This study aims to assess the energy-saving potential of a triple-hybrid VAC-based radiant building cooling system integrated with desiccant-based dehumidification. A medium

* Content presented in this chapter can be found in the publication J2

office building model is developed in EnergyPlus [EnergyPlus 2017] to meet the requirement. The building (Figure 4.1) consists of four floors with a total area 5000 m^2. In other words, the total combined area is 5000 $m^{2,}$ or the area per floor is 1250 m^2. The building layout includes one core and four perimeter zones on each floor. Construction of the building envelope, windows, etc., is per the ECBC [Khan et al. 2009]. The installed radiant system includes roof-floor embedded pipes with a total radiant surface area of 6250 m^2, an AHU, solar collectors, and gas-fired boiler. An auxiliary electric heating element is also provided to address any contingent issues related to solar and biogas energy. In this study, three systems (case 1, case 2, and case 3) are compared to show the VAC radiant cooling system's energy-saving potential under different operational strategies. Case 1 is a conventional vapor compression chiller (VCC) radiant cooling system with conventional VCC-DOAS, Case 2 is a hybrid VA radiant cooling system with conventional VCC-DOAS, whereas Case 3 is a hybrid vapor absorption chiller (VAC) radiant cooling system with desiccant-assisted VCC-DOAS. As per the availability of the roof area of the present building model, we have used 500 m^2 and 1200 m^2 of the total roof area for installing solar collectors in cases 2 and 3, respectively. On the roof portion of the current building model, we have used 500 m^2 and 1200 m^2 of the total roof area for installing solar collectors in cases 2 and 3, respectively.

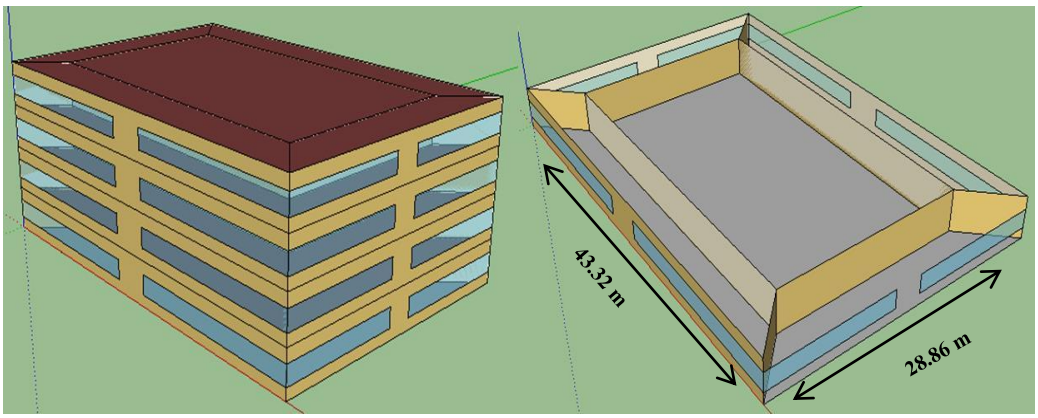

Figure 4.1: 3-D building geometry with internal cross section

4.1.1. Case 1: Conventional VCC based radiant cooling system with VCC-DOAS

In this case (Figure 4.2), both the radiant cooling system and DOAS are equipped with conventional VCC. Radiant system is operated by VCC named “Radiant VCC” and DOAS is operated by VCC named as “DOAS VCC”. Both chillers possess a defined

COP of 3.1. “Radiant VCC” is defined as supplying chilled water to the radiant chilled water pipes at a temperature 15°C, which maintains the radiating surfaces at a temperature of around 17°C-20°C. In this study, a pre-validated low temperature radiant variable flow template is used for designing the radiant cooling system [Chantrasrisalai et al. 2003]. Radiant cooling system caters the maximum portion of the building sensible load. Chilled water from the “DOAS VCC” at temperature 7°C [Trane 2010] is supplied to the AHU’s cooling coil to meet the remaining sensible and latent loads. To prevent condensation on the radiant surface, this DOAS provides effective dehumidified air at the temperature of nearly 12°C with humidity of 0.008 (kg/kg of dry air) inside the office space. Performance of VCC and other associated components in the EnergyPlus is computed by solving various fundamental equations as shown in section 3.1.2.1 and values of different parameters can be found in the published work [J2].

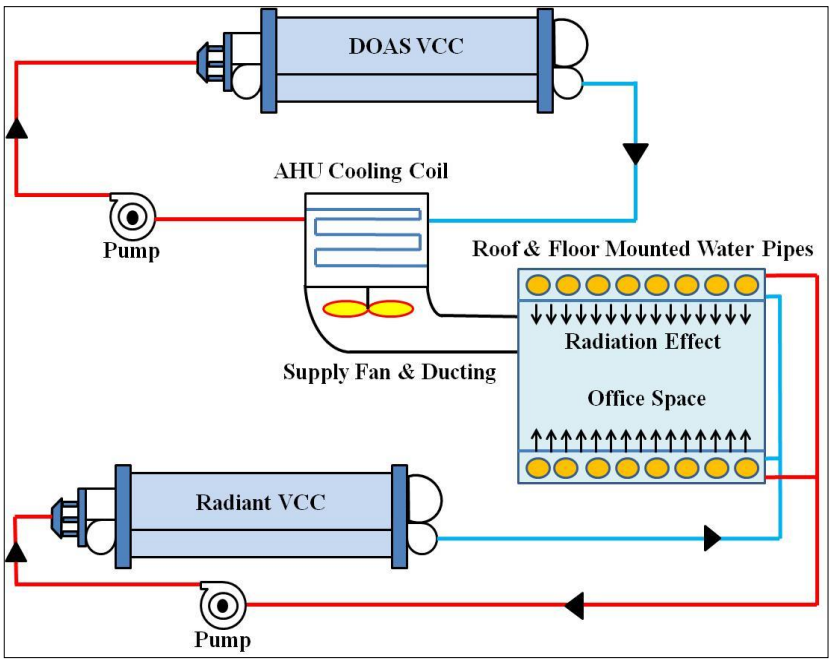

Figure 4.2: System layout for case 1

Radiant cooling system extracts heat load from space through convection and radiation. This system cools air directly (by convection process) and indirectly by cooling the enveloping surfaces of the building (like: wall, roof, and floor). To calculate the capacity of the radiant cooling system, heat transfer between the space and chilled ceiling system has to be evaluated. Radiant cooling system mainly exchanges heat convectively with space air and radiantly with other building surfaces. Furthermore, the conduction phenomenon also occurs during heat transfer within the chilled ceiling.

EnergyPlus solves various heat balance equations of conduction, convection and radiation processes to assess the performance of the radiant cooling system. Knowing multiple input parameters such as, water inlet temperature, water mass flow rate, etc., surface heat flux is calculated by a standard conduction transfer equation shown below [EnergyPlus 2017],

$$\text{Surface heat balance} = \sum_{j=1}^{M} X_{k,j} T_{1,t-j+1} - \sum_{j=1}^{M} Y_{k,j} T_{3,t-j+1} + \sum_{j=1}^{k} F_j q''_{1,t-j} + \sum_{j=1}^{M} W_j q_{source,t-j+1} \quad (4.1)$$

where, X, Y, F and W the conduction transfer functions (CTF), M is the finite number defined by order of conduction transfer function, q_1'' is the heat flux at the inner surface of the multilayer envelope, q_{source} is the internal heat source, and k is the order of CTF. CTFs are constant values that are required to be determined, as discussed in [EnergyPlus 2017]. Calculating CTFs requires various parameters such as thermal conductivity, thermal diffusivity, thickness, density, and all other thermo-physical properties of construction material. EnergyPlus deals with parameters like the required mass flow rate of water through the radiant system and the needed tubing length for sizing calculations of the cooling system. In this study, only chilled water flows through the tubing circuit of radiant system, so the chilled water flow rate through radiant tubing $\dot{V}_R$ is calculated in the following manner [EnergyPlus 2017],

$$\dot{V}_R = \frac{Q_{des.}}{\Delta T_R \times c_{p,w} \times \rho_w} \quad (4.2)$$

where, 5.43°C$\leq \Delta T_R \leq$6.37°C (for all three cases) and 10.42 kW$\leq Q_{des.,1} \leq$73.39 kW. Hydronic tubing length in the design of radiant system is calculated in the following manner [EnergyPlus 2017],

$$\text{Tube length} = \frac{\text{Total surface area}}{\text{Tube spacing}} \quad (4.3)$$

where, total surface area is 6250 m^2 and tube spacing is taken as 0.15 m. Next, fan power consumption for the transportation of air inside the space is calculated as [EnergyPlus 2017],

$$w_f = \frac{\dot{V}_a \times \Delta P_f}{\eta_f} \quad (4.4)$$

where, $w_f = w_{f,1,DOAS,VCC}$ and η_f =0.70. In Eq. (4.4), $\Delta P_f \left(= \Delta P_{f,DOAS,VCC}\right)$ =900 N/m^2 (same for case 1, 2 and 3) and 2.10 m^3/s $\leq \dot{V}_a \left(= \dot{V}_{a,DOAS,VCC}\right) \leq$ 4.72 m^3/s (same for all three cases). The cooling coil designed load is obtained as below [EnergyPlus 2017],

$$Q_{coil,DOAS,VCC} = \rho_a \dot{V}_{a,DOAS,VCC}(h_{a,i,coil} - h_{a,o,coil}) \quad (4.5a)$$

where,

$$h_{a,i,coil} = f\left(T_{a,i,coil}, \omega_{a,i,coil}\right) \text{ and } h_{a,o,coil} = f\left(T_{a,o,coil}, \omega_{a,o,coil}\right) \quad (4.5b)$$

$$30°\text{C} \leq T_{a,i,coil} \leq 38.14°\text{C},\ T_{a,o,coil} = 12\ °\text{C} \quad (4.5c)$$

$$0.003 \text{ kg/kg of dry air} \leq \omega_{a,i,coil} \leq 0.020 \text{ kg/kg of dry air and}$$
$$\omega_{a,o,coil} = 0.008 \text{ kg/kg of dry air} \quad (4.5d)$$

Parameters mentioned in Eq. (4.5) remain the same for cases 1, 2 and 3.

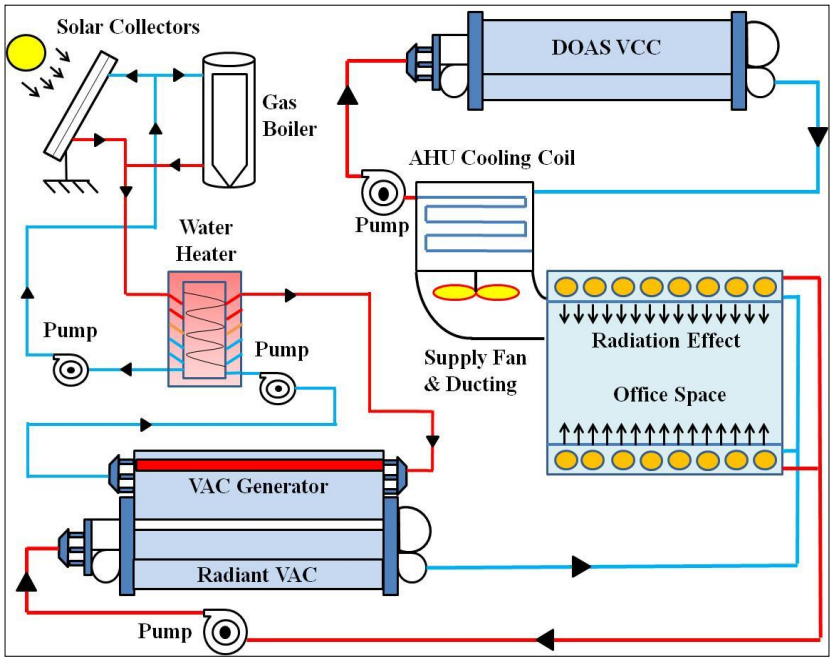

Figure 4.3: System layout for case 2

4.1.2. Case 2: Hybrid VAC based radiant cooling system with VCC-DOAS

In this case (Figure 4.3), the installed radiant cooling system is the same as in case 1 but, conventional VCC is replaced with VAC-based chiller named "Radiant VAC" to supply the chilled water to radiant piping system. A single-effect LiBr-water based absorption chiller is used, whereas DOAS is equipped with the earlier "VCC DOAS". In this case, both flat plate solar collectors (500 m^2 collector area) and biogas-fired

boiler (η_b = 85%) are also installed in the system to supply heating energy at the generator side of the Radiant VAC. Along with this, a small auxiliary water heater with a storage tank is also coupled to compensate for any deficiency and address any contingency in the availability of solar and biogas. Generally, hot water temperature on the generator side varies between 70°C-90°C for LiBr-water VA system [Saleh et al. 2014]. Here, a triple hybrid loop of solar collectors, biogas fired boiler and a heater is used to supply the hot water to the storage tank at a temperature of 80°C. From the storage tank, hot water is sent toward the generator side of Radiant VAC and recirculated in the loop. The energy performance of the absorption chiller and other associated components can be evaluated as discussed in section 3.1.2.2 and parameters values can be found in published work [J2].

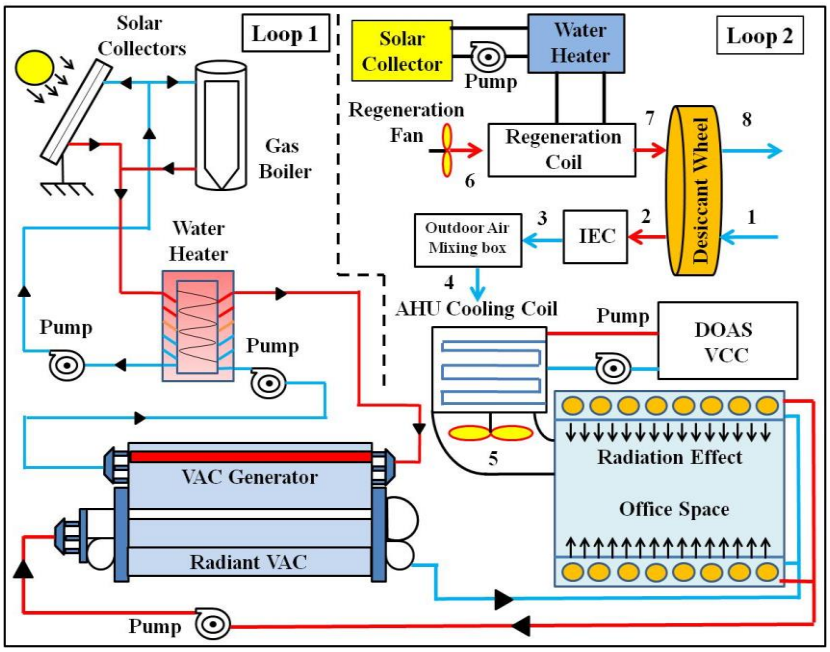

Figure 4.4: System layout for case 3

4.1.3. Case 3: Hybrid VAC based radiant cooling system with desiccant-assisted VCC DOAS

In this case, the installed radiant cooling system and VAC are the same as of case 2 (Loop 1 of Figure 4.4). For dehumidification of air, a desiccant wheel is used (termed as process side node 1 to node 5). To reduce the temperature of the supply air, an IEC is used in the path of supply air passing through the desiccant as shown in Figure 4.4 (Loop 2). Depending upon the environmental condition, IEC cools air temperature in

the range of 28°C-38°C. Use of desiccant wheel reduces the total load on VC-DOAS chiller. However, during dehumidification, desiccant wheel gets clogged with the adsorbed moisture particles from the process supply air. So, to ensure the continuous operation of desiccant material, it needs to be regenerated (termed as regeneration side node 6 to node 8). In this case, hot water at 80°C from separate solar collectors (700 m^2 collector area) is supplied to the regenerator hot water coil. A fan is used to supply hot air at 60°C to regenerate the desiccant [Khan et al. 2017]. As can be inferred from Figure 4.1, the total available roof area is 1250 m^2, and in case 3, we have installed solar collector system on roof area of 700 m^2 for Loop 2 [Khan et al. 2017]. As we cannot cover the complete roof for the installation of solar collectors, therefore, we have chosen 500 m^2 solar collector area for Loop 1. In Loop 2, a solar-auxiliary water heater system is installed for the regeneration of desiccant material, whereas a hybrid solar-biogas boiler and auxiliary heating systems are installed in Loop 1. This is done because of the constraints in the space availability, intermittency issues with solar energy, and to fulfil the energy requirement for continuous functioning of the absorption system. IEC provides a way of improved modeling that includes performance curves for the pump and the fan installed inside it. Power consumption of IEC components is computed as follows [EnergyPlus 2017],

$$w_{f,IEC} = w_{f,IEC,des.} \times \frac{\dot{V}_{a,IEC}}{\dot{V}_{a,IEC,des.}} \tag{4.6}$$

$$w_{p,IEC} = w_{p,IEC,des.} \times \frac{\dot{V}_{a,IEC}}{\dot{V}_{a,IEC,des.}} \tag{4.7}$$

where, 1.92 $m^3/s \leq \dot{V}_{a,IEC} \leq 4.72$ m^3/s , $w_{f,IEC,des.}$ = 1179 W, $w_{p,IEC,des.}$ = 700 W and $\dot{V}_{a,IEC,des.}$ = 3.93 m^3/s are calculated from EnergyPlus simulations [EnergyPlus 2017]. In case 3, respective thermal loads imposed on absorption-based radiant chiller and generator remain the same as case 2, i.e., $Q_{c,3,Radiant,VAC} = Q_{c,2,Radiant,VAC}$ and $Q_{g,3,Radiant,VAC} = Q_{g,2,Radiant,VAC}$. Therefore, *COPs* of "*Radiant VAC"* for cases 2 and 3 will be the same. Using the above equations, EnergyPlus computes the total power consumption, *TPC* (in W) by adding the energy consumption of individual components [J2].

Considering working time of 9 hours (i.e., 9:00 am to 06:00 pm) per day along with 290 working days (excluding Sundays and other holidays) in a year, the total simulation

hours is considered as 2601. Finally, the total annual electric energy consumption, *AEC* (in MWh) is computed in the following manner,

$$AEC = \frac{\sum_{i=1}^{n} TPC_i}{10^6} \text{; where, } n\text{=2601 hours} \tag{4.8}$$

4.2. Results and discussion

The objective of this study is to evaluate the energy saving potential of triple-hybrid "Radiant VAC" with/without desiccant wheel (cases 2 and 3) with the conventional "Radiant VCC" (case 1). For all three cases, simulations are performed for warm and humid climatic zone. Results obtained from the simulations are discussed in sections 4.2.1, 4.2.2 and 4.2.3.

4.2.1. Annual electric energy consumption and supplied cooling load pattern

The main concern of this study is related to the total electric energy consumption for all three cases to ensure the same level of thermal comfort throughout the year (25°C-27°C dry bulb temperature with specific humidity 0.008-0.010 kg/kg of dry air) inside the office space. A comparison of annual electric energy consumption is shown in Figure 4.5. It is highlighted that in case 1, the major portion of electric yearly energy (238 MWh) is consumed in VCC-DOAS and its pump supplying chilled water to the cooling coil of the AHU. This, in turn, supplies dehumidified air to the office space. However, "Radiant VCC" consumes very less energy as compared to "DOAS-VCC". In case 2 energy consumption portion of radiant chiller is reduced because "Radiant VCC" is replaced with "Radiant VAC". DOAS fan energy, $w_{f,DOAS}$ consumption in all three cases is found nearly equal as already highlighted earlier in Eq. (4.5). Regeneration energy includes energy consumptions of water circulation pump in the solar-biogas boiler loop and auxiliary heater. It is clear from Figure 4.5a that regeneration energy in case 3 is more as compared to case 2, because in case 3 regeneration energy includes two water heating loops (Loop 1 and Loop 2): one for "Radiant VAC", whereas, another for desiccant wheel regeneration. In case 3, desiccant wheel is used for dehumidification of the supplied air, which reduces the electric energy consumption of DOAS VCC. However, due to the involvement of additional components (water heater, pump, and fan) in Loop 2 along with desiccant wheel, the electrical energy for regeneration increases in case 3. In case 3, minor energy consumption occurs in the IEC. It is noticed that using desiccant material in case 3,

electric energy savings up to 13.2% and 9.1% can be achieved with respect to the conventional radiant system (case 1), and non-desiccant based absorption system (case 2), respectively. The cooling load supplied by chillers in all cases for maintaining the specified thermal comfort inside the building is shown in Figure 4.5b. As highlighted in the figure, the cooling load provided by the cooling system is decreasing continuously because, in case 2 and case 3 solar collector systems are installed on the roof due to which there is reduction in the total heat gain inside the building from the roof. It can also be noted (Figure 4.5b) that radiant cooling system caters 12-15% of the total cooling.

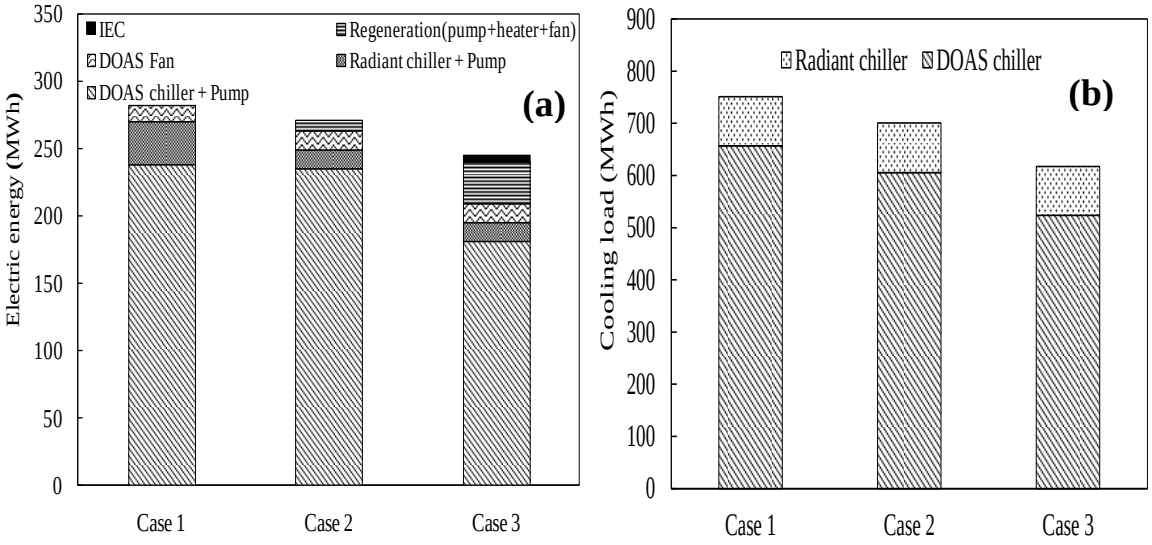

Figure 4.5: (a) Comparison of annual electric energy consumption in all three cases, (b) Cooling load supplied by the chillers in different cases

4.2.2. Analysis of solar fraction and heat energy contributed by different components

This section shows the contribution of solar energy in the total heating energy supplied to the system for desiccant regeneration and to the generator of the absorption system (cases 2 and 3). Water heater tank temperature is specified at 80°C to supply the required heating energy (through hot water). In this analysis, the term solar fraction is considered as the performance parameter of solar collector system. Solar fraction is defined as the ratio of heating energy provided by solar collectors to the total heating energy provided by all components. In this study, solar collector of 500 m^2 area is taken for the simulation purpose in the "Radiant VAC" of case 2 and case 3 (Loop 1), whereas 700 m^2 collector area is considered for desiccant regeneration in the ventilation cycle of case 3 (Loop 2). Figure 4.6 shows the value of solar fraction obtained from the simulation results for different cases. It is evident from the figure that the value of solar

fraction in case 3 (Loop 2) is higher because in this case solar collector area is large (700 m^2). Additionally, in case 3 (Loop 2), along with solar collector, only the auxiliary electric heater is coupled, increasing the solar fraction due to the absence of a biogas boiler. The contribution of the biogas boiler is observed as negligible, and owing to the unnecessary costs involved in its operation and installation, it is not included in this loop. In case 3 (Loop 1) the amount of solar fraction is somewhat lesser than in case 2. This is because the required heating rate at the generator side becomes lesser due to the shading effect by the additional solar collector (700 m^2) of Loop 2. This causes less heat gain inside the building. Consequently, heating energy supplied by the solar collector of an area of 500 m^2 marginally decreases. Thus, a relatively lesser solar fraction is obtained in Loop 2 of case 3 than case 2.

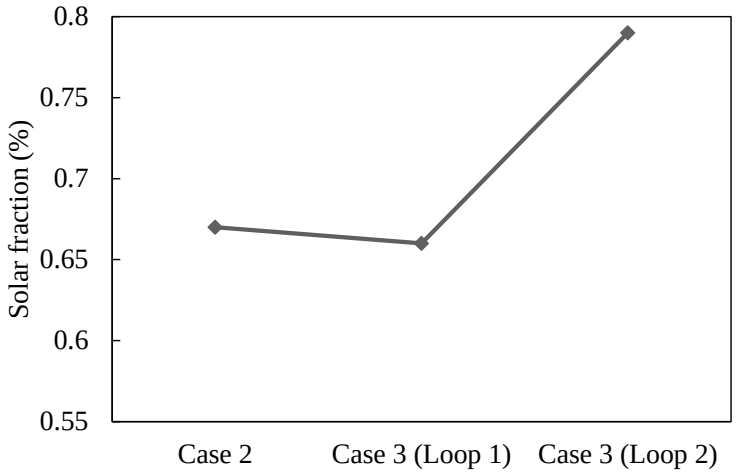

Figure 4.6: Solar fraction for different cases

Heat energy provided by the hybrid solar-biogas fired boiler and auxiliary water heater system (Loop 1) and solar-auxiliary hot water heater system (Loop 2) of case 3 is shown in Figure 4.7. It can be seen from Figure 4.7a that the contribution of solar collector water heating system keeps changing with months throughout the operation time. In order to meet the required heating rate at the generator side of the "Radiant VAC", it is necessary to operate the system in Loop 1 with a combined solar collector and biogas boiler in conjunction with a separate auxiliary electric heater. An auxiliary heater is needed to account for any available solar energy and biomass deficiency. It can be envisaged from Figure 4.7a that the solar collector supplies the maximum portion of heating energy. However, if we remove the biogas boiler, then the solar collector itself (comparatively having less area of 500 m^2) would be unable to fulfill the required heating rate. Consequently, the auxiliary water heater will consume more electric

energy, resulting in negative energy savings. Biogas boiler cost is only one-time capital investment, and the operating and fuel cost of biogas is relatively low.

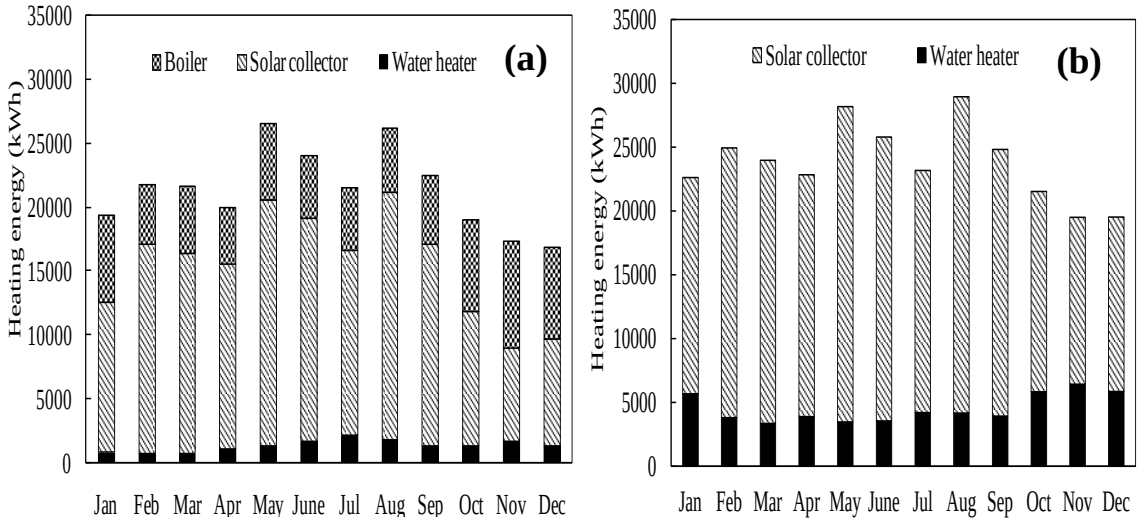

Figure 4.7: Partitioned heating energy provided by water heating system in (a) Loop 1, (b) Loop 2

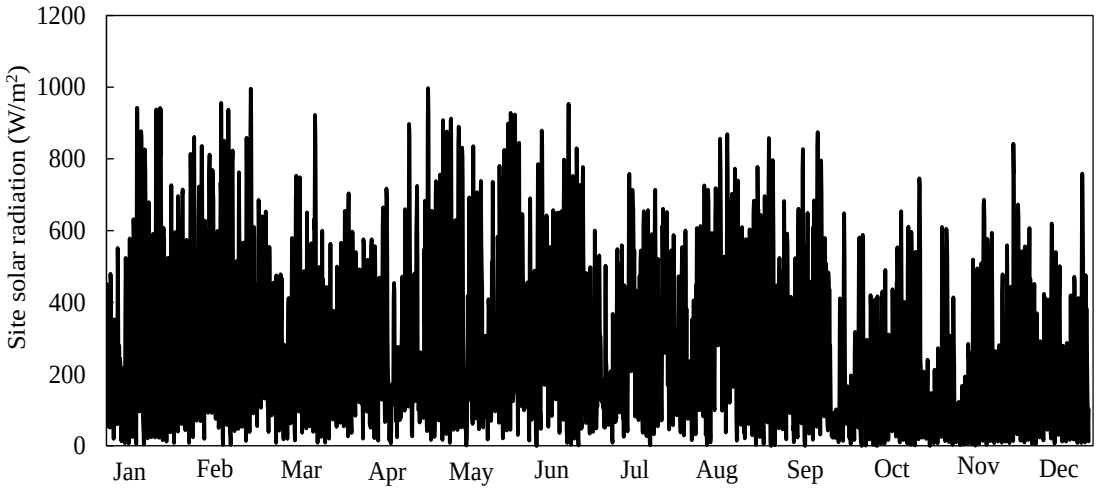

Figure 4.8: Site outdoor available solar radiation throughout the year

Variation in heating energy supplied by the solar collector system is in accordance with the available solar radiation at the site, as shown in Figure 4.8. As indicated in Figure 4.7, the heating energy provided by the solar collector system is least for the month of November because the available average monthly solar radiation for this month is lower compared to other months (Figure 4.8). A similar observation is made in Figure 4.7b. The requirement of the equivalent biomass required to supply the biogas can be computed as shown in Table 4.1. The simulation results show that the maximum amount of heating energy supplied by the biogas boiler system is around 243 kWh. Cow

dung is considered as biomass resource which produces 0.04 m^3 of biogas per kg of cow dung containing 0.244 kWh of heating energy [Seadi et al. 2008].

Table 4.1: Calculation of biomass requirement for desired heating energy

Operating Temperature (°C)	Heat energy supplied (kWh)	Heating energy at boiler (kWh)	Biogas volume (m^3)	Weight of cow dung (kg)
80 °C	243	285.88	46.86	1171.63

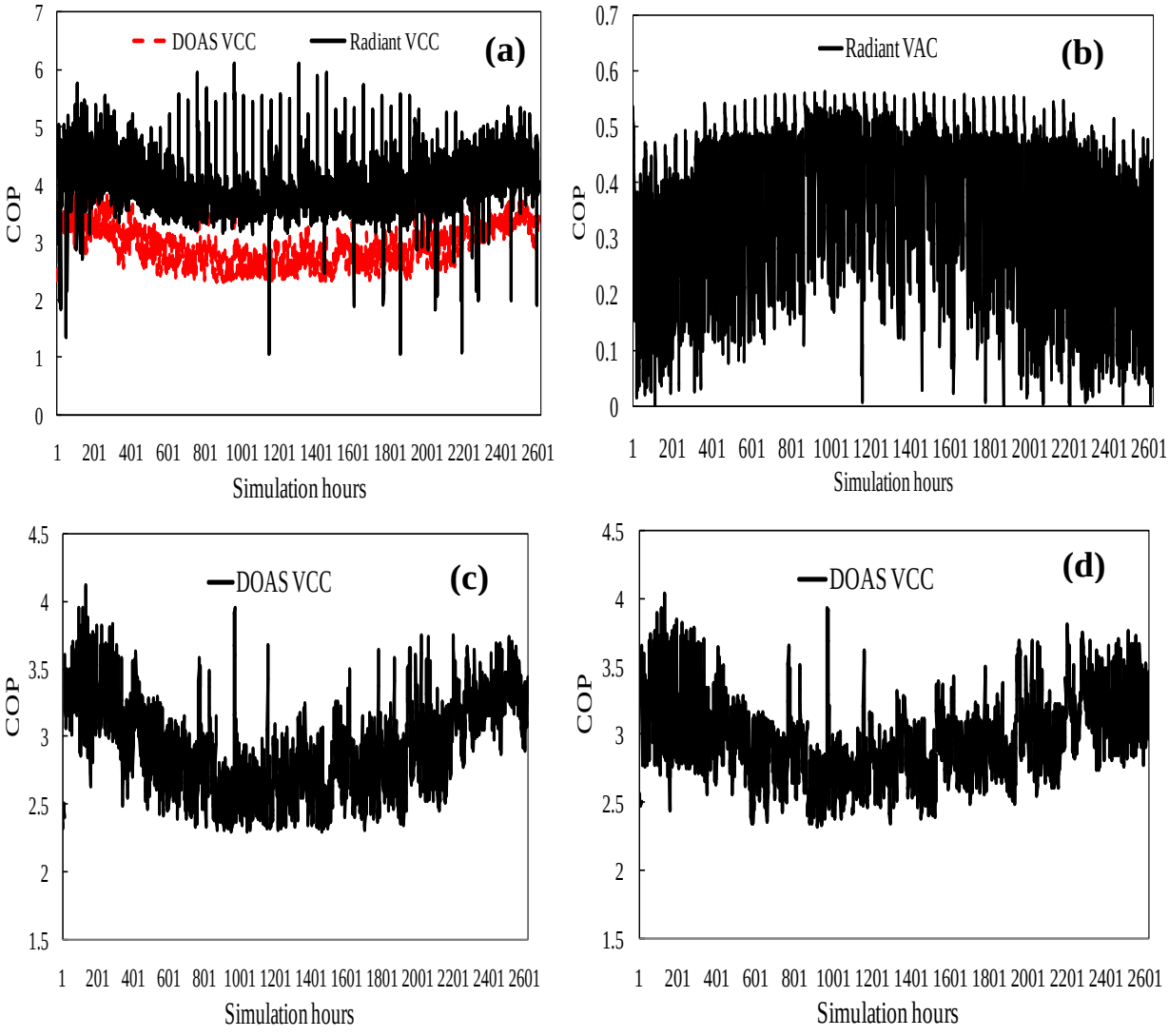

Figure 4.9: Hourly variation *COP* (a) Case 1 (b) Cases 2 and 3 (c) Case 2 (d) Case 3

4.2.3. Analysis of coefficient of performance parameters and cost assessment

Based on the variation of generated building heat load patterns throughout the year, COP of chillers varies accordingly. Figure 4.9 shows the hourly variation in the COP

of “DOAS VCC” and “Radiant VCC” for different systems. It is already discussed earlier that COP for “Radiant VAC” is identical for cases 2 and 3, whereas, for case 1 it does not exist. It is envisaged from Figure 4.9 that the obtained average COP of the “DOAS VCC” is 2.90, whereas the same for “Radiant VCC” and “Radiant VAC” are 3.97 and 0.33, respectively. Additionally, the details of the unmet hours for each of the considered configurations are shown in Table 4.2. For each of the designed air-conditioning system the unmet hours falls under the specified range (Unmet load hours troubleshooting guide, 2013) for a system working throughout the year.

In this work also, an economic analysis is performed to estimate the ROI of the installed systems. The details related to peak rated capacities and cost of different installed components obtained from the simulation results are available in published work [J2]. Here, the costs associated with operation and maintenance are neglected because these marginally vary between different systems. The total estimated costs for the installed system are 3125000 INR (USD 44642.85), 5721600 INR (USD 81737.14), and 8508800 INR (USD 121542.85) for case 1, case 2 and case 3, respectively. As per the cost of energy savings, the ROI of case 2 with respect to case 1 is around 23.29 years, and ROI of case 3 against case 1 is around 14.59 years [J2].

Table 4.2: Unmet hours for assessment of radiant cooling system based configurations

S.No.	Building area	System type (Configuration details)	Unmet hours (climate)
1.	5000 m^2	Conventional VCC based radiant system with VCC-DOAS	10 (Warm-humid)
		Hybrid VAC based radiant cooling system with VCC-DOAS	179 (Warm-humid)
		Hybrid VAC based radiant cooling system with desiccant assisted VCC-DOAS	152 (Warm-humid)

4.3. Conclusion

In this study, the energy-saving potential of a novel triple-hybrid vapor absorption chiller (VAC) based radiant cooling system with desiccant dehumidification is

proposed for large-scale capacity office buildings. Using EnergyPlus simulation, a conventional vapor compression chiller (VCC) based radiant cooling system is compared with different variants of VAC based radiant cooling system. Solar collectors, biogas-fired boiler, and auxiliary electric heater are used to supply the heat energy required to maintain uniform thermal comfort inside a medium office building situated in warm and humid climate zone. It is apparent from the present study that with DOAS using triple-hybrid Radiant VAC without desiccant, nearly 9.1% of electrical energy savings can be acquired against a conventional Radiant VCC system. It is also concluded that using triple-hybrid Radiant VAC system with desiccant, 13.22% electrical energy savings can be obtained concerning Radiant VCC based system. The present absorption radiant cooling system design can address the harmful effect of conventional compression based HVACs on the environment.

CHAPTER 5

*AIR-CONDITIONING METHODS FOR ELECTRIC GRID INDEPENDENCY

This chapter deals with the investigation of different air-conditioning configurations for attaining the net zero energy /grid independent building target. A grid independent building refers to a building that generates energy equivalent to the requirement which can also be refereed as grid independent building. Solar photovoltaic (PV) system is installed for power generation. This simulation study shows the potential of VC and VA driven systems to attain the grid independent status under different climatic conditions. The outcomes presented in this chapter show various evaluation parameters such as: the percentage of target achieved, energy analysis, performance analysis etc. An emission included in this chapter shows the GHG emission potential by using different air-conditioning techniques.

5.1. Methodology, building description and building parameters validation

This section presents the methodology for the performance evaluation of nearly/net zero energy building/grid independent building under changing operating conditions with different design configurations. From the above-discussed literature survey, it is observed that in the area of net-zero-energy buildings, substantial research has been done. Still, the influence of different radiant cooling-based air conditioning strategies incorporating renewable energy-based sources is missing. Apart from this, the suitability of building's net zero condition concerning the air-conditioning system's outside environmental aspects is also not discussed yet. To fulfill this purpose, in this study, we have taken a medium office building of 4981 m^2 of total floor area with three-floor layout (Figure 5.1). The set of solar collectors and solar PV systems are provided on the roof having different areas. Each floor involves five regions and consumes nearly 1660 m^2 of area. Recommended benchmark data (occupancy, equipment power, lightning power, window-to-wall ratio, ventilation requirements, schedules and *U*

* Content presented in this chapter can be found in the publications J3

values) provided by the ECBC [Khan et al. 2017] and NREL [Deru et al. 2011] are used as input factors for the model as well for the building structure validation. The relevant physical parameters necessary for the modeling are taken from ECBC, NREL and American Society of Heating Refrigeration and Air-conditioning Engineers (ASHRAE) standards.

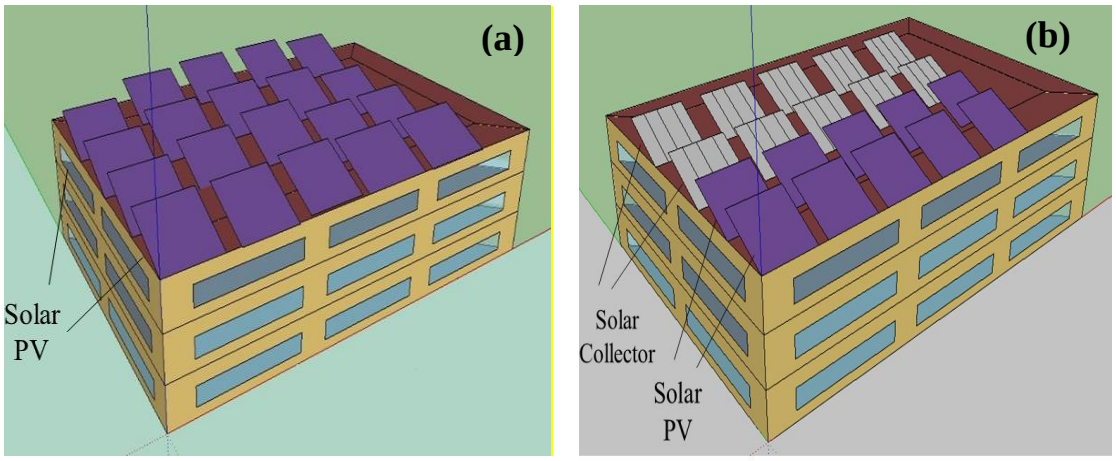

Figure 5.1: Building model layout for grid independency study (a) Roof area covered by solely solar *PV* (configurations 1 and 3) (b) Roof area covered with both solar collector and *PV* (configurations 2 and 4)

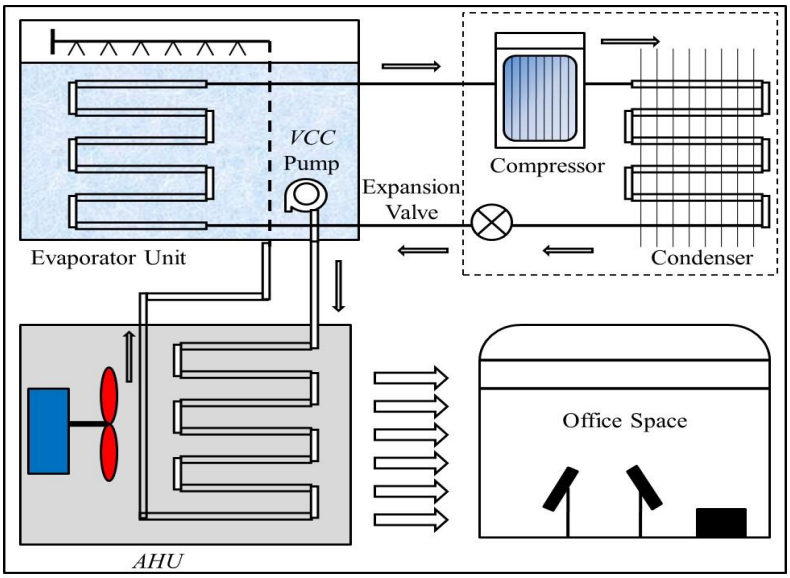

Figure 5.2: Air-conditioning layout of configuration 1

5.2. System description

In this simulation study, four different types of central air-conditioning configurations are modelled to maintain equal desired thermal comfort inside the building space under different climatic conditions. These configurations are incorporated with VC system, VA system, VC-based radiant air-conditioning system with VC-DOAS and VA radiant

air-conditioning system with VC-DOAS. In this study, three major environmental conditions comprising warm-humid, composite and hot-dry environments are analyzed. The configurations details are discussed in sections 5.2.1, 5.2.2, 5.2.3 and 5.2.4.

5.2.1. Configuration 1 (VC-based air-conditioning system)

In this configuration, the air-conditioner includes conventional vapour compression chiller (VCC) for maintaining the required thermal comfort conditions. For this purpose, a central air-conditioning system is installed in the building model using standard modules of EnergyPlus. A layout of this configuration is shown in Figure 5.2. In this configuration, a central VC-based water chiller is modelled for pumping the chilled water between 7-8°C to the cooling coil of the outside air handling unit (AHU) [Trane 2010]. This chilled water coming through evaporator unit is accountable for cooling and dehumidifying the supplied air on the surface of AHU'S coil. The temperature of the air delivered after flowing over the AHU varies in the 12-14°C. Cold air meets the heat generated inside the building due to occupancy, window heat gain, heat stored by construction material and electric loads, which in turn maintains the space temperature in the range 19-26°C along with specific humidity between 0.004-0.012 kg/kg of dry air. In this configuration, one pump is used for the chilled water circulation in cooling coil. Next, for fulfilling the requirement of grid independent building, solar PV system is installed on the roof of the building. Here, around 1400 m^2 (i.e., 84% approx.) of the roof area is used for installing solar PV and the remaining roof area for the inverter system and wiring etc. In this study, average cell efficiency is taken as 20% [PV Cell efficiency 2019]. The electricity obtained from solar PV is used for building lighting, air-conditioning, and in meeting other demands of the building. The generation of electricity by solar PV depends on the outside weather conditions and location. Either batteries or direct grid connection can be used to address any deficiency in energy supply.

5.2.2. Configuration 2 (VA-based air-conditioning system)

In this mode of operation, instead of VCC of configuration 1, a triple-hybrid vapour absorption chiller (VAC) is installed for supplying the chilled water in the range 7-8 °C towards AHU coil (Figure 5.3). As the operation of absorption chiller invariably requires thermal energy in generator, in this study, the same is supplied with the aid of solar collector and biomass driven boiler in addition to a supplementary electrical

heater. This supplementary heater enables the system to work under adverse conditions, including insufficient availability of solar and biogas energy sources. As indicated in Figure 5.3, solar collector and biogas boiler operate in a single loop to supply hot water at nearly 80 °C to generator of the VAC [J1]. In this configuration, 700 m^2 of roof space is equipped with flat plate solar collectors, whereas 700 m^2 roof is further covered by solar PV system. As expected, in this case, the electricity generation by solar PV would be reduced as the PV installation area is lesser than configuration 1. In this configuration, one pump is used for cooling water circulation, and two pumps are used for water circulation toward the generator of VAC. The validation study for the installed VC and VA based system is done as per the procedure discussed in section 3.1.2.1 and 3.1.2.2. The results of the validation study can be found in the published work [J3].

5.2.3. Configuration 3 (VCC-Radiant with VCC-DOAS based air-conditioning system)

Compared with conventionally used compression-driven cooling systems, radiant air-conditioning systems offer better performance in terms of electrical energy savings for air-conditioning [Scoccia et al. 2018]. In this study, the radiant air-conditioning system's piping is embedded within the floor and the roof of the building structure, as shown in Figure 5.4. EnergyPlus provides a set of templates for radiant cooling system that are extensively pre-validated [Chantrasrisalai et al. 2003], and these templates are used to model the radiant cooling system. Further, the literature reveals that the radiant cooling system is capable of satisfying around 10%-30% of the total building thermal load [Wojtkowiak et al. 2019 and J2], therefore in our case, the radiant system is handling 19% of the total building thermal load, which verifies that the system is working satisfactorily. Figure 5.4 shows the layout of the radiant air-conditioning system with a separate *DOAS*. In this configuration, both radiant air-conditioning system and *DOAS* operate by the *VCC*. The working of VCC in DOAS is the same as that of configuration 1, while radiant VCC supplies chilled water at 15 °C to the embedded water piping of the radiant cooling system. DOAS delivers chilled and dehumidified air through the duct inside the building space using diffusers. The radiant cooling system is responsible for catering to the maximum part of the sensible part of the total thermal load, while DOAS caters the remaining sensible and latent heat loads. Thus, the complete load is catered by the combined DOAS and radiant systems. DOAS is designed to ensure that the indoor air temperature is always maintained higher than

the air dew point at the radiant surface. This is required to eliminate the condensation problem. Since, in this configuration, no heating energy is needed in the air-conditioning system so, the maximum area of the roof can be utilized for electricity generation. So, a solar PV array of around 1400 m^2 area is installed on the roof of the building [Kreider JF 2000].

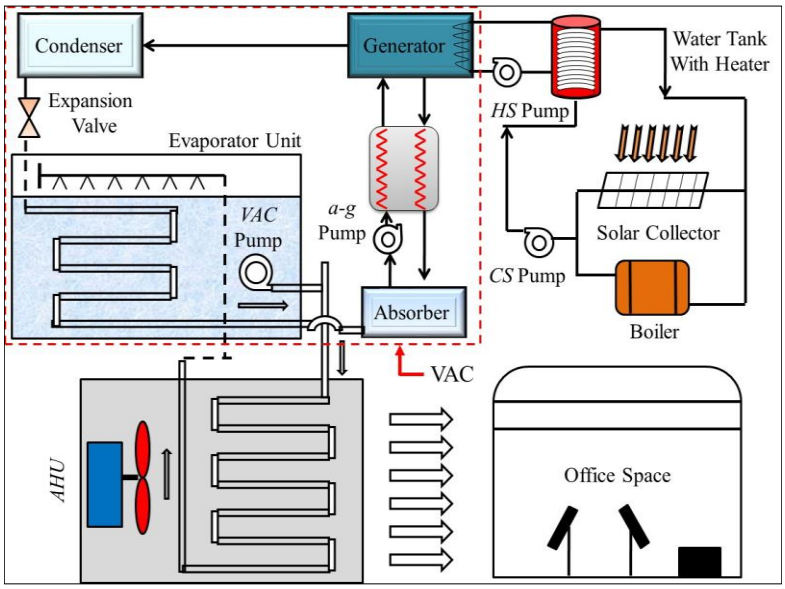

Figure 5.3: Air-conditioning setup layout of configuration 2

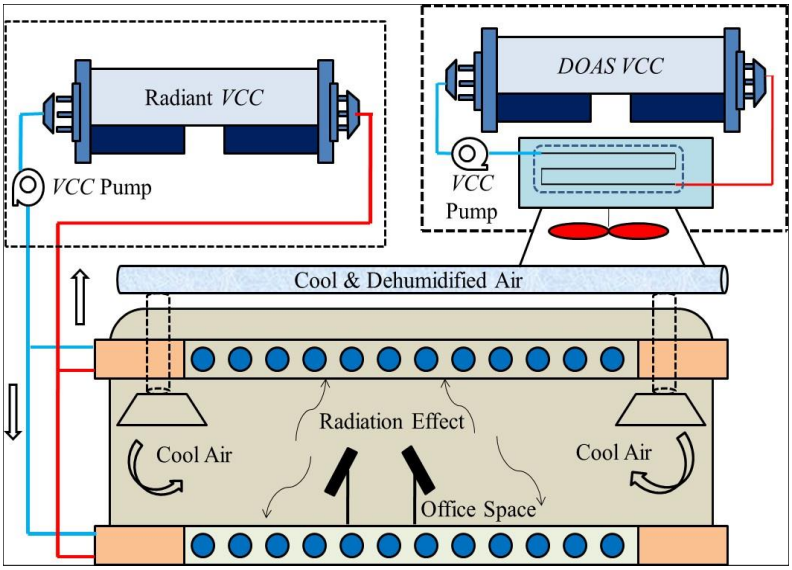

Figure 5.4: Air-conditioning setup layout of configuration 3

5.2.4. Configuration 4 (Radiant VAC with VCC-DOAS based air-conditioning system)

Here, radiant VCC of configuration 3 is replaced with triple-hybrid radiant VAC (Figure 5.5). Installation of absorption system with radiant cooling system in place of

compressor driven system improves the system performance [J2]. The VAC supplies the chilled water for fulfilling the necessary requirements of the radiant piping structure embedded within the building. This VAC is driven by solar collector and biomass-operated boiler along with a supplementary electrical heater for meeting the functional requirements of the absorption chiller. In order to investigate the building performance for the fully grid independent condition, solar PV system and solar collectors are installed on the roof on the building. In this case (i.e., VAC is used), 700 m^2 area of the roof is occupied with solar collectors for hot water, whereas another 700 m^2 of the roof space is provided with solar PV system for electricity generation. In this study, DOAS is not operated by VAC, because DOAS caters major portion of the total thermal load of the building. So, suppose we install VAC for DOAS along with radiant VAC chiller. In that case, additional roof space will be required for the installation of more solar collectors for VAC of DOAS, and installing more solar collectors on the roof is not possible in this case. EnergyPlus computes the performance of various components (chiller, pump, fan, heater, solar PV, solar collectors, cooling and heating coils, biomass boiler and related connectors) aided through several heat balance equations as discussed in the section 4.1.1 and required ranges of different parameters can be found in published work [J3].

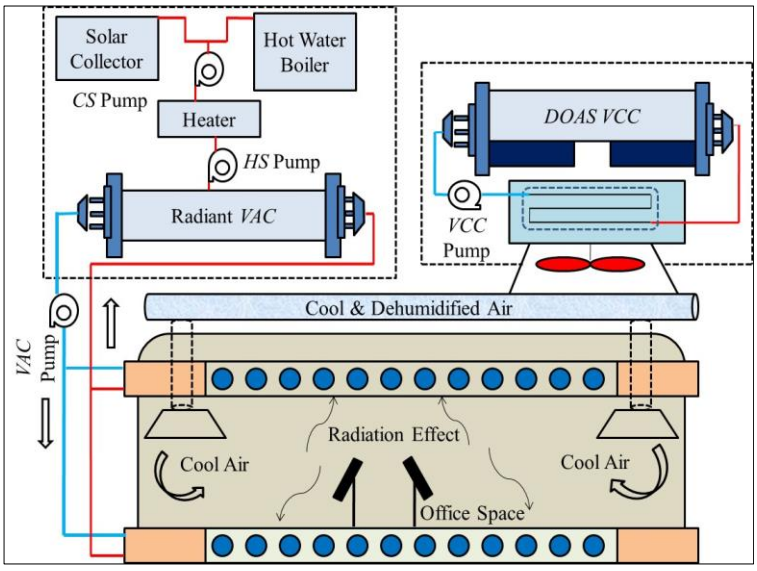

Figure 5.5: Air-conditioning setup layout of configuration 4

5.3. Results and discussion

This simulation study investigates the performance of different configurations of air-conditioning systems to realize the target of grid independent building under different

environmental conditions. For this purpose, simulations were done with weather files of these environment regions and details are available in the work [J3]. Results acquired from the simulations are analyzed, and the contribution of solar PV-generated electricity towards the energy requirements of the building to realize grid independent status is assessed. Simulations show some exciting outcomes for the studied configurations and suggest the requirements for achieving the grid independent building target. Further details are discussed next. All simulations are done to maintain the same desired level of thermal comfort (air temperature between 20-28 °C and humidity level in the range 0.0045-0.013 kg/kg of dry air [Kreider JF 2000] irrespective of the environmental conditions which are shown in published work [J3].

5.3.1. Energy consumption analysis

For a grid independent building, the building's energy generation (electricity) should be comparable or in accordance with its energy demand. The office building has various energy-consuming components like lights, electric equipment, and air-conditioning system's tools (fan, pumps, chiller, and heater). The total annual electrical energy consumption analysis of lighting, chiller, fan and pump relating to configurations 1 and 2 are available in the published work [J3]. Here, only configurations 3 and 4 are discussed in order to estimate the energy savings offered by the configuration 4.

The total annual energy consumption analysis for configuration 3 is shown in Figure 5.6. Since, in this case, the air-conditioning unit is bifurcated into two separate systems (radiant cooling system and DOAS), both of these systems are simultaneously operated to accomplish the required indoor comfort level. Here, the radiant cooling system is operated by VCC and DOAS is also coupled with VCC. It is established that, for all three environmental conditions, energy consumption of radiant VCC is lesser as compared to the VCC-DOAS. This is because out of the total thermal load (sensible and latent), the sensible load met by radiant cooling system is relatively lesser than that taken care of by the VCC-DOAS. Loads due to electrical appliances will remain the same as in the earlier cases (configurations 1 and 2). Energy consumptions of both the chillers (Radiant VCC and VCC-DOAS) are higher for the warm-humid environment because of the environmental conditions concerning the particular place. It is also observed that the radiant cooling system with DOAS consumes lesser electricity than that consumed in VC and VA systems. This is applicable for the all operating environments considered in this study. Compared with configuration 1, this

configuration (i.e., radiant VCC with VCC-DOAS) provides nearly 16%, 14% and 13% electric power savings for warm-humid, composite and hot-dry environments. Furthermore, with reference to configuration 2, 64%, 51% and 46% electricity energy savings is achieved under warm-humid, composite and hot-dry weather conditions, respectively.

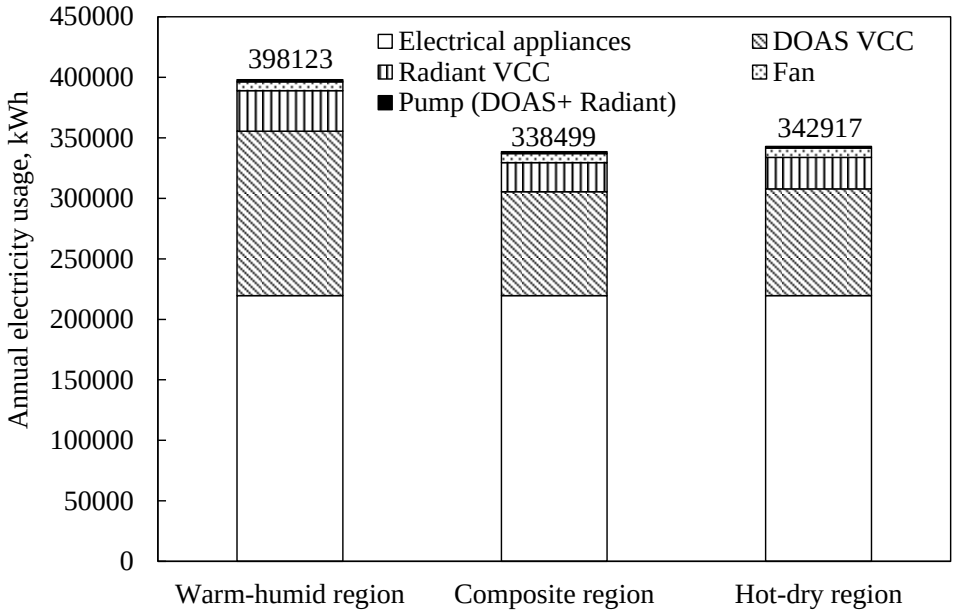

Figure 5.6: Annual electric energy consumption for configuration 3

Figure 5.7 presents the yearly energy analysis relating to configuration 4 of the air-conditioning system. Only the radiant air-conditioning system is coupled with the VAC in this configuration, whereas DOAS is operated under the VCC framework. So, as intuitive, the electricity consumption by the radiant VAC is much less than the VCC-DOAS. Here, total annual electricity requirements are 385045 kWh, 319839 kWh and 327331 kWh for warm-humid, composite and hot-dry conditions, respectively. It is also highlighted that very less energy is consumed by the pumps which are installed at the refrigerant regeneration side assisted by solar collector, biomass boiler, VCC pump, VAC pump and supplementary heating element (Figure 5.7). Studies [Wojtkowiak et al. 2019 and J2] reveal that by incorporating the renewable energy-based desiccant system and other evaporative cooling arrangements, energy efficiency will further improve. However, this study intends to achieve the grid independent energy building target. Thus, incorporating such efficiency improvement mechanisms will affect solar PV energy generation due to limited space availability in the building roof. This is because additional area/space should be provided for installing solar collectors to regenerate the desiccant material. Here, this configuration (i.e., triple-hybrid radiant

VAC with VCC-DOAS) gives maximum electric power savings of nearly 19% against configuration 1, 65%, against configuration 2 and 5% against configuration 3.

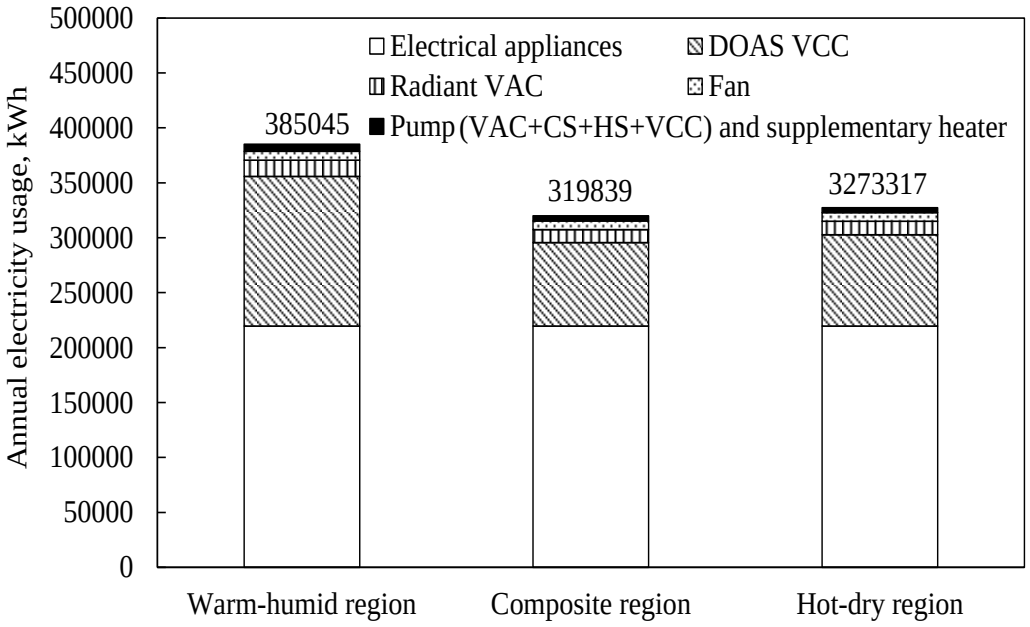

Figure 5.7: Annual electric energy consumption for configuration 4

5.3.2. Solar PV electricity generation and requirement

This section deliberates on the essential aspect of attaining a building's grid independent target. To ensure the building to be nearly grid independent, the generation of electrical energy should be in accordance with the building's energy demand. The required load of the building that is fulfilled by it shows the percentage of grid independency attained. It is reported that, for a building to suit grid independent energy criterion, 50-90% of the total energy demand should be catered by the building only. The hour-wise solar PV electricity generation is discussed in the published work [J3]. The energy generation via solar PV shall depend on the environmental conditions and the area covered by solar PV system. Therefore, in this study, based on the availability of roof space (700 m^2 for configurations 2 and 4, and 1400 m^2 for configurations 1 and 3), in configurations 2 and 4, lesser area will be available than that corresponding to configurations 1 and 3. This is because solar collector system is installed in configurations 2 and 4 to satiate the functional requirement of VA system.

Figure 5.8 compares the net/annual electric energy requirement and the net/annual electric energy generated using solar PV. This figure shows the level of energy mismatch between the demand and the supply sides. Figures (Figure 5.8a and Figure 5.8c) concern to the configurations 1 and 3, whereas, Figure 5.8b and Figure 5.8d relates

to configurations 2 and 4. Figure 5. 9 presents the summary of grid independent targets achieved by the different configurations under various environmental conditions. It is envisaged that VC based (conventional and radiant) air-conditioning system is a more suitable choice than the VA based system for achieving building's grid independent status.

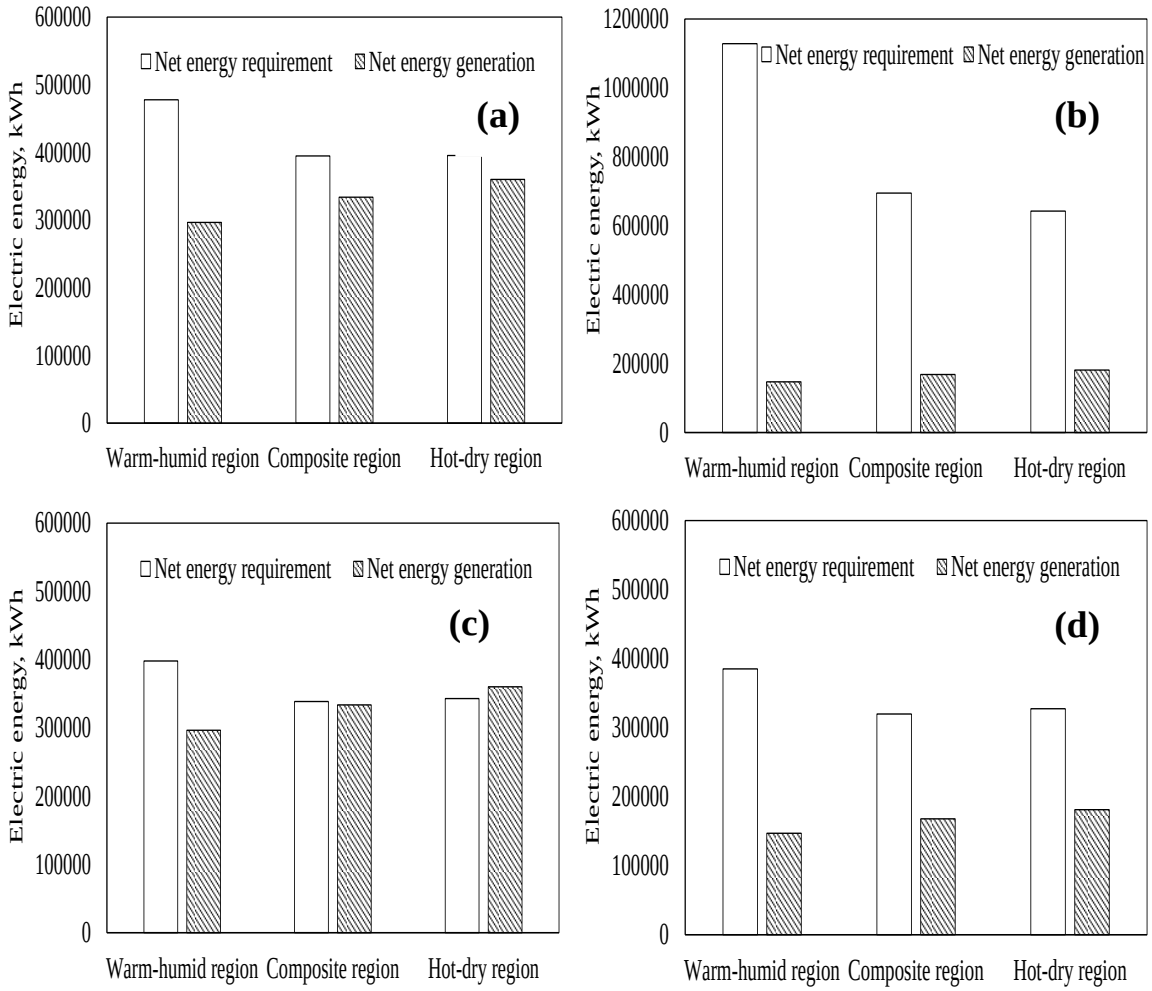

Figure 5.8: Net energy requirement and net energy generation (a) configuration 1, (b) configuration 2, (c) configuration 3 and (d) configuration 4

5.3.3. Emission and cost analysis

For a building, apart from the target of grid independent achievement, it is also appropriate to become nearly/net zero carbon during its operation. Here, solar PV based generation enables towards acquiring carbon neutrality. It may be visualized that the usage of biogas based system is carbon neutral [Paolini et al. 2018]. This study uses solar PV to supply energy according to requirement. But, the solar PV system cannot continuously fulfil building's energy demand due to some constraints (for example:

space, solar radiation availability etc.). In such a scenario, grid-connected energy becomes inevitable. Therefore, greenhouse emissions will be generated. Based on the past available data, emissions of gases like CO_2, SO_2 and NO_x are studied for different configurations under considered climates (Figure 5.10).

It is assumed that these emissions from conventional coal fired vary as, CO_2 : 0.91 to 0.95 kg/kWh, SO_2: 6.9×10^{-3} to 7.2×10^{-3} kg/kWh, and NO_x: 4.0×10^{-3} to 4.3×10^{-3} kg/kWh [Mittal et al. 2012]. Based on the average values of the above data and additional grid energy requirements, Figure 5.10a shows CO_2 emissions, Figure 5.10b shows the SO_2 emissions and Figure 5.10c shows the NO_x emissions against different configurations and climatic conditions. It is revealed that configuration 2 results in the highest emissions under warm-humid climate.

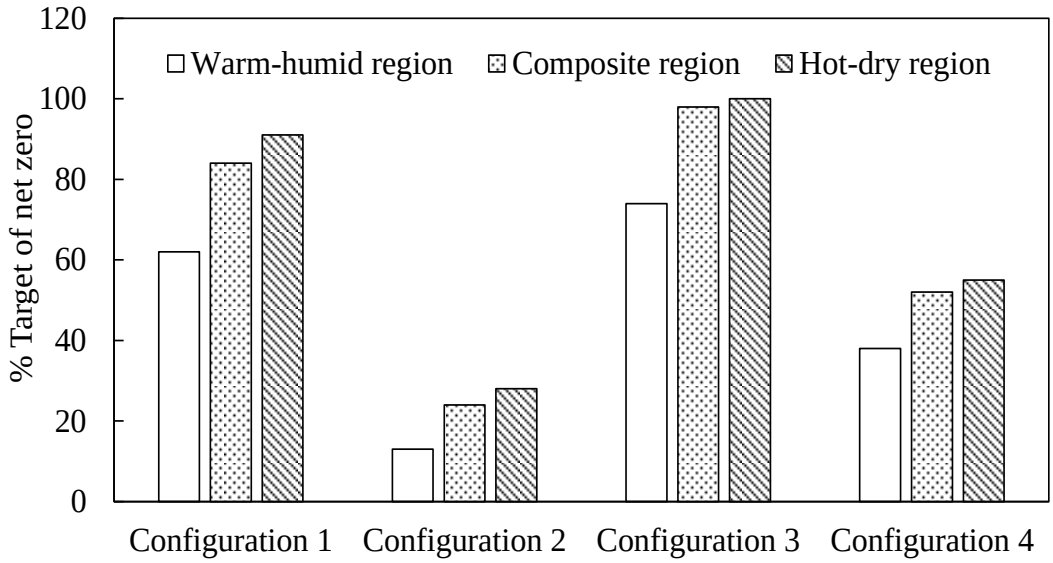

Figure 5. 9: Target of grid independency achieved by different configurations

On the other hand, it is highlighted from Figure 5.10 that all of the emissions are lower as for the configuration 3 as compared to those corresponding to other configurations.. Although configuration 3 is ideal for hot-dry climate, for warm-humid region, configuration 3 results in 89.6% lesser emissions of CO_2, SO_2 and NOx than those emitted by configuration 2. Furthermore, in composite region, 99.3% reduction in CO_2, SO_2 and NOx takes place with configuration 3 as compared to that with configuration 2. Additionally, the details of the unmet hours for each of the considered configurations are shown in Table 5.1. The unmet hours for each of the air-conditioning system falls under the specified range (Unmet load hours troubleshooting guide, 2013) for a system working throughout the year.

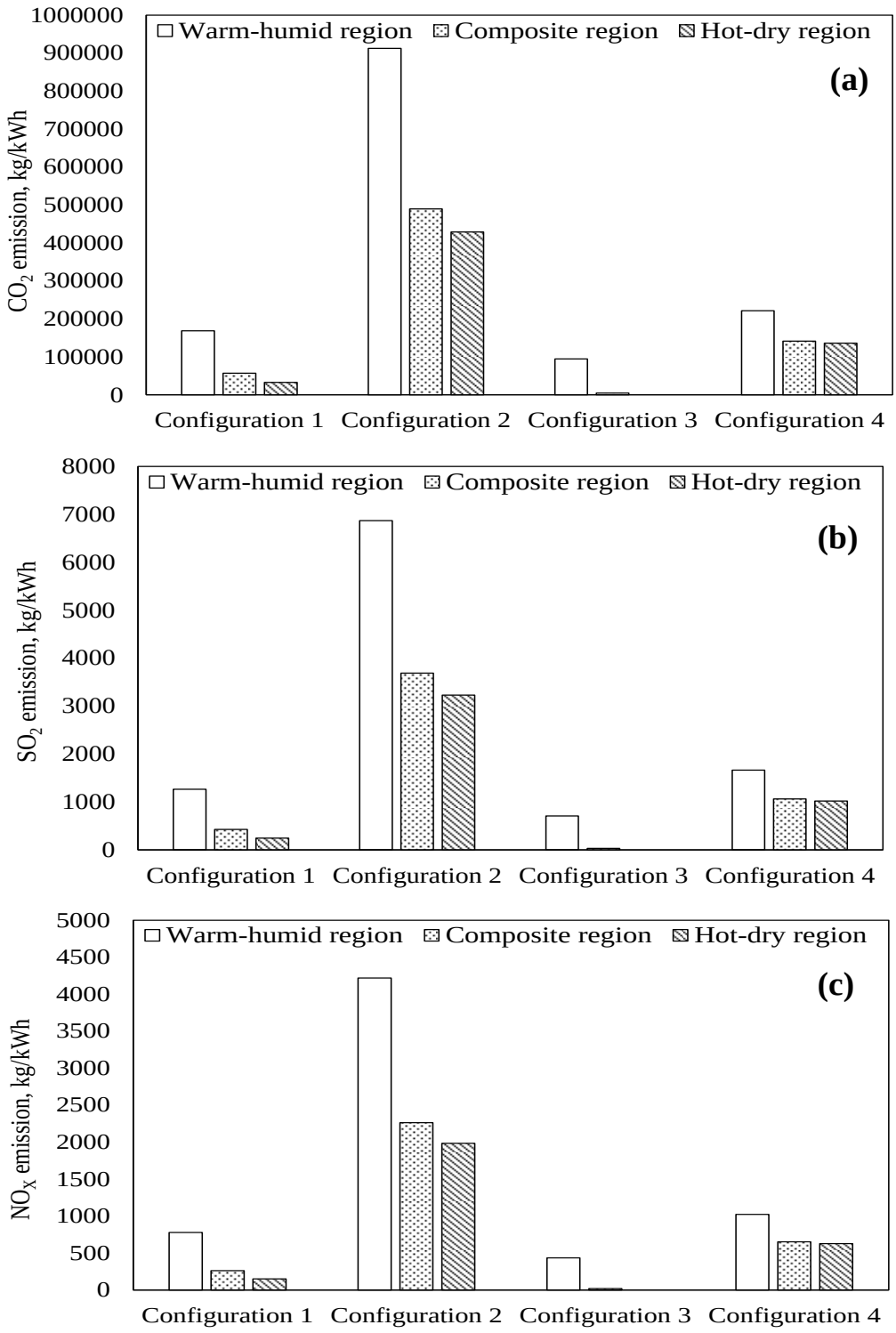

Figure 5.10: Emission analysis for different configurations (a) CO_2 emission (b) SO_2 emission and (c) NO_x emission

Here, the cost assessment has been done for estimating the ROI for the above-discussed four configurations. The maximum capacities and costs of all the installed components like chiller, pump, fan, heater, solar collectors, boiler, radiant system, PV system and inverter are obtained from EnergyPlus simulation results and these can be found in the

published work [J3]. The total cost estimation of each considered system reveals that the cost of radiant VCC with DOAS-VCC is highest, but the energy savings were more with this case only. So, as per the cost of energy savings the ROIs of configuration 3 with respect to the configuration 1 for warm-humid, composite and hot-dry climate are 5.73 years, 8.11 years and 8.69 years, respectively.

Table 5.1: Unmet hours for grid independent building analysis

S.No.	Building area	System type (Configuration details)	Unmet hours (climate)
1.	4981 m^2	Conventional VC system	10 (warm-humid), 55 (hot-dry) 186 (composite)
		Solar-gas assisted VA system	4 (warm-humid), 35 (hot-dry) 118 (composite)
		VC radiant with VC-DOAS air-conditioning system	137 (warm-humid), 108 (hot-dry) 181 (composite)
		VC radiant with VC-DOAS air-conditioning system	112 (warm-humid), 88 (hot-dry) 140 (composite)

5.4. Conclusion and recommendation

In this work, EnergyPlus based analysis has been done for a medium capacity building to achieve the status of grid independent building. The focus of the present work is to assess the suitability of four different air-conditioning strategies under various environmental conditions towards electric energy savings, achievement of grid independent and emissions of greenhouse gases. In particular, the current study considered conventional VCC, VAC, radiant VCC with VCC-DOAS and radiant VAC with VCC-DOAS. The following conclusions are made from the present study,

- VAC-based radiant air-conditioning system with VCC-DOAS is an energy efficient option, but, it does not fulfil the criterion of grid independent and net

zero carbon building. However, VCC-based radiant cooling system with VCC-DOAS fulfil the requirements of grid independent building to 98% and 100% for composite and hot-dry environments, respectively. Under warm-humid condition, only 74% of the grid independency target is attained with this configuration.

- With the objective of grid independent building design, compromise on collector area for VAC-based system is essential. Due to this, electrical energy consumption in triple-hybrid VAC is considerably high than conventional VCC. However, radiant VCC with VCC-DOAS results in 13%-16% electricity savings with respect to conventional VCC. Further, radiant triple-hybrid VAC with VCC-DOAS requires 17%-19% lesser electrical power than the conventional VCC.

- With any configuration of air-conditioning, the possibility of attaining the grid independent energy building target is always minimum under warm-humid environmental condition. This is followed by composite environment, whereas, hot-dry environment is most suitable for grid independent energy buildings.

- Emission analysis shows that 89.6% and 99.3% lesser emissions of CO_2, SO_2 and Nox can be ensured by the radiant and DOAS based conventional VCC-based system under warm-humid and composite conditions, respectively. Moreover, for hot-dry climate, the energy requirements can be fulfilled solely by renewable sources, thereby resulting in insignificant emissions of greenhouse gases.

CHAPTER 6

*ANALYSIS OF SOLAR ENERGY-BASED VARIABLE REFRIGERANT FLOW SYSTEMS

This chapter investigates the solar energy-based VRF based air-conditioning system. In the VRF system, a single outdoor unit drives multiple indoor evaporator units. Each indoor unit can cater different thermal load conditions. A VRF system comprises a variable-speed compressor system that allows different refrigerant flow rates through different indoor units. This VRF system is coupled with a desiccant-assisted DOAS unit that serves the purpose of decoupling. A solar collector system loop is installed to fulfill the desiccant regeneration requirement. The simulation study compares this modified VRF system with the conventional VRF system and VAV under different climatic conditions. Results of this show better performance of the proposed system compared with other considered systems.

6.1. Methodology and system operations

In the previous literature, the addition of desiccant material with the VRF system is highlighted, but in those studies, the desiccant was embedded with the chiller's heat exchangers itself. However, the detached integration of desiccant wheel-based DOAS with the VRF system is nowhere mentioned. Thus, this study is directed to analyze the VRF system performance under diverse climatic conditions by integrating a solar-desiccant-based ventilation unit. The discrepancy in the energy consumption of the VRF system is dependent on climate, building operation and schedules etc. By fixing the building specifications, operation, schedule, occupancy, power density, and equipment usage, this analysis has been focused to suit variable climatic conditions. The effect of integrating the desiccant heat exchanger with the VRF system is analyzed using the Energyplus simulations (EnergyPlus, 2017). Solar thermal energy is used for the desiccant regeneration for the continuous working of the desiccant-assisted DOAS.

* Content presented in this chapter can be found in the publications J7

This study compares the proposed air-conditioning system's electrical and thermal energy performances with conventional VRF and VAV systems. In this context, three different modes of air-conditioning systems are modeled and simulated for warm-humid, composite and hot-dry climates. These are discussed in the subsequent sections.

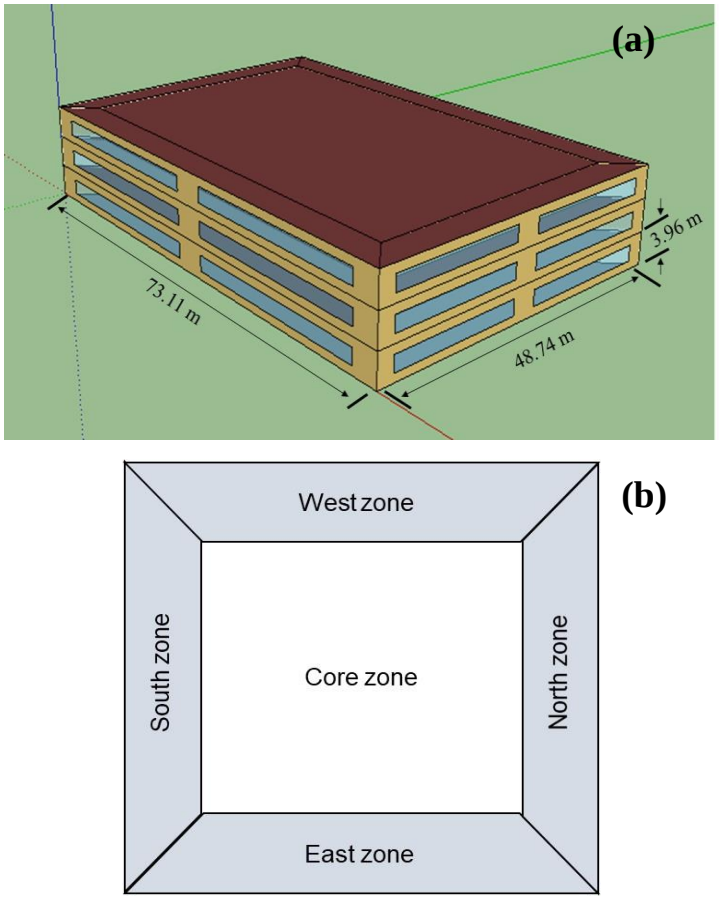

Figure 6.1: Large scale office building geometry for VRF system

6.2. Building description

A large-scale office building is considered for analyzing the energy performance of the suggested system. The present office building consists of three floors with a total floor area of 10690 m^2. Each floor is divided into five zones involving east, west, north, south, and core zones. The considered building structure is shown in Figure 6.1. Each floor is of 48.74 m × 73.11 m with a ceiling height of 3.96 m and occupies 3563 m^2 of the floor area. The largest side walls of the office building are south and north-faced. Only outside walls consist of transparent windows that cover around 40 % of the total wall area. The considered building involves an average infiltration rate of 0.09 air change per hour (Ji et al., 2020), which means the infiltrated air constitutes about 9 % of the total air intake through ventilation. The constructional parameters of the building

envelope comprising wall, roof, and floor and *U* values are illustrated in work [J7]. The properties of window material glazing (SHGC, *U,* and VLT) are directly defined manually according to the references (Khan et al., 2017) and no shading device is used in the present modeling. These parameters complies with the standard data (Khan et al., 2009, Deru et al., 2011) and are under specified limits suggested by the references. Other simulation parameters for the building model related to the occupancy level, light, electrical equipment density can be found in published work [J7]. Throughout the year, the simulation working hours for the office building are considered from 9:00 hours to 18:00 hours.

6.3. System description

6.3.1. Mode 1- Conventional central all-air conditioning system

A central air-conditioning system in the office building includes a compression chiller, ducting arrangements, cooling coil, flow pumps, fan, and controls. The schematic layout for this mode is shown in Figure 6.2a. A compression chiller supplies chilled water at 7.5 ºC to the cooling coil that generates cool and dehumidified process air (Trane 2010). This air is distributed throughout the building using the variable speed fan. The supply air temperature varies in the range of 11 ºC -15 ºC. The cool air is catered to the thermal load generated due to occupancy, lightening, infiltration, solar heat gains, and electric equipment. In this mode, the single system handles both latent and sensible thermal loads generated inside the building. The air-conditioning system maintains the same level of thermal comfort environment inside the office space throughout the year. The installed central air-conditioning unit is well-validated against the reference building model available in the Energyplus documentation as shown in published work [J7]. The schedules of the office occupancy, electric equipment, and lightning for all the modes of operations are shown in Figure 6.3. The fresh air intake is maintained through the ventilation rate. For both the models (present and reference), simulations are done for warm-humid climate and different results are compared. The comparative analysis shows that the associated errors are within an acceptable range and the air-conditioning model in the present building is working well. In Mode 1, the chiller is the key component for building air conditioning. The performance of this chiller and other associated components are evaluated by solving various energy equations and using performance curves as discussed in section 3.1.2.1.

6.3.2. Mode 2: conventional variable flow refrigerant air conditioning system

A VRF system is essentially a multi-split air-conditioning system that distributes the refrigerant to each indoor unit from a single outdoor unit. Figure 6.2b shows the schematic layout of the installed VRF system. The design of the VRF includes individual indoor evaporator unit for each of the zones and the condenser unit is installed outside. A VRF heat pump-based unit is installed in the building using the modules of Energyplus. This unit supplies either cooling or heating at a time. This VRF system (i.e., Mode 2) is also designed to maintain the same level of thermal comfort condition as specified for the Mode 1. The refrigerant distribution for each evaporator unit depends on the set point air temperature, thermal load and humidity requirements prevailing within the relevant sub-domains. The literature reveals that only the VRF-based system may not fulfill the building air-conditioning requirements (temperature, humidity and air quality) and under some circumstances, additional ventilation may be required to maintain freshness in the air. This is because the VRF system only recirculates the indoor air. So, a separate ventilation unit comprising a fan is coupled to this mode for maintaining the indoor air quality. In the VRF system, for estimating either the individual or the total capacity of the installed indoor unit, capacities of each indoor sub-units are needed to be calculated. This is done using the following equation (Aynur et al., 2010c),

$$Q_{IU,2} = \dot{m}_{ref,IU,2} \cdot \left(h_{ref,in,2} - h_{ref,out,2}\right) \tag{6.1}$$

$$Q_{Total,2} = \sum_{n=1}^{N} \dot{m}_{ref,IU,2} \cdot \left(h_{ref,in,2,n} - h_{ref,out,2,n}\right) \tag{6.2}$$

where, 4.5 kg/s $\leq \dot{m}_{ref,IU,2} \leq$ 18.4 kg/s. The concept of enthalpy potential can be used for quantifying the heat transfer between the space air and refrigerant within the cooling coil. The enthalpy balance between the air and refrigerant requires various parameters like heat exchange surface area, convective heat and mass transfer coefficients of air and refrigerant sides, and dimensionless flow parameters. Using the suggested method, the final enthalpy drop of the air and enthalpy rise of the refrigerant inside the cooling coil can be estimated (Khamis Mansour and Hassab, 2012). Temperature and humidity values have been indicated in the respective plots discussed later. The COP or the performance factor of the VRF system can be estimated as (Aynur et al., 2010c).

$$COP_{VRF,2} = \frac{Q_{Total,2}}{\sum_{n=1}^{N} W_{VRF,2,n}} \tag{6.3}$$

$$\text{where, } W_{VRF,2} = W_{OU,2} + W_{IU,2}$$
$$W_{OU,2} = W_{compressor,2} + W_{f,2} + W_{controller,2} \quad (6.4)$$

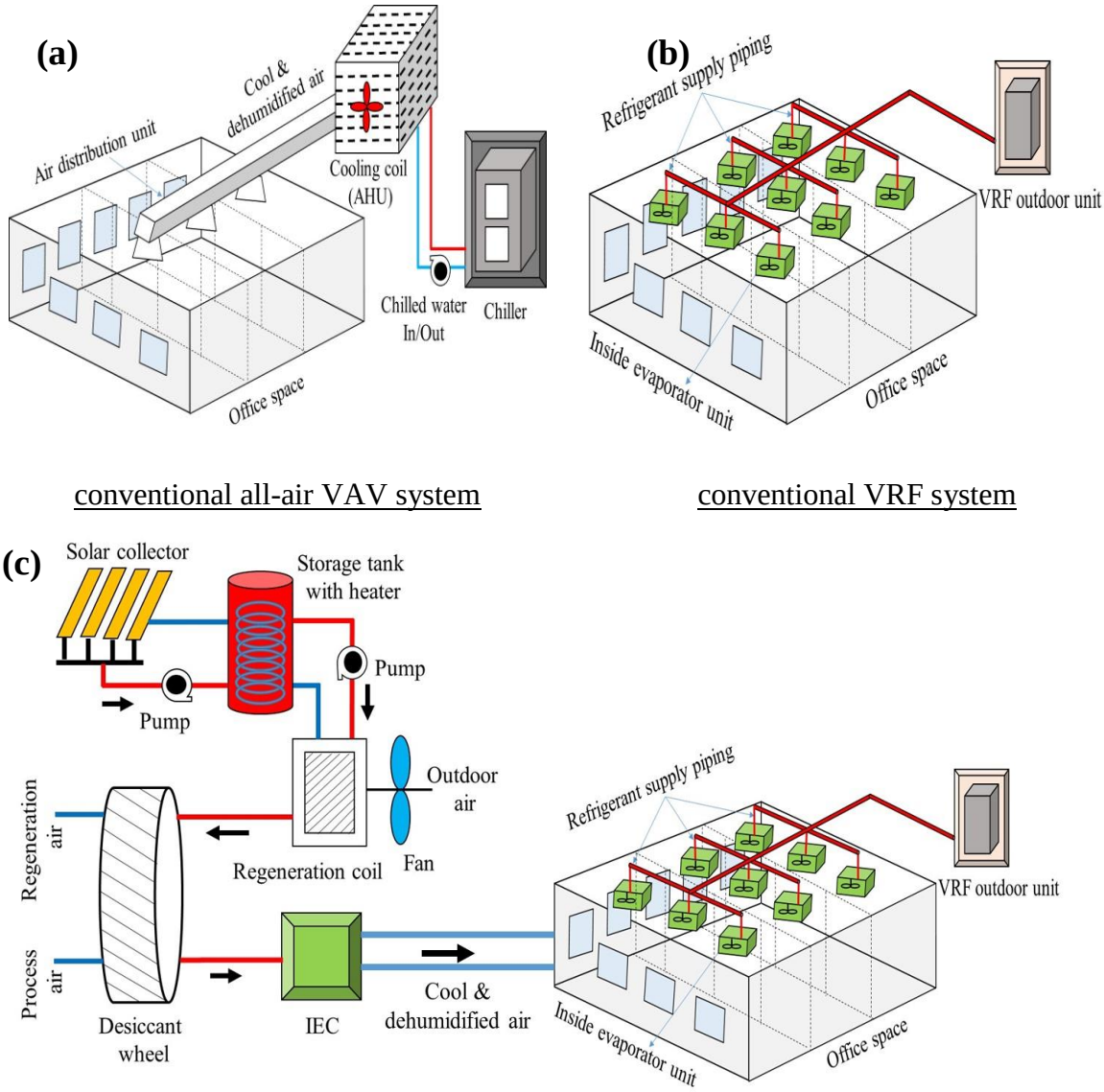

conventional all-air VAV system

conventional VRF system

proposed VRF system with solar energy-based desiccant-assisted DOAS

Figure 6.2: Schematic layouts of the air-conditioning systems studied

6.3.3. Mode 3- Desiccant assisted variable refrigerant flow air-conditioning system

In this mode of operation, a separate ventilation unit is coupled with the conventional VRF system. In this unit, a desiccant-assisted heat exchanger is installed, which dehumidifies the outdoor air to the desired level of humidity control. After some operation, it will become saturated and further adsorption will not be observed, so desiccant regeneration is invariably required. For this purpose, a loop of solar collector

system having total collector area of 1780 m^2 is installed on the roof of the office building. This solar collector supplies hot water to the hot water storage tank in which an auxiliary heater (electrically heated) is installed to address any solar energy intermittency issue. This hot water at 80 ºC is supplied to a heating coil, from where hot air at around 60 ºC is supplied for the desiccant regeneration. The schematic layout of this setup is shown in Figure 6.2c. As the desiccant dehumidifies the outdoor air, temperature of this air increase due to chemical dehumidification process. So, the high temperature of this supply air is reduced by using the IEC. The desiccant-assisted DOAS caters the maximum portion of the latent load. This combined system i.e., desiccant-assisted DOAS and VRF caters the total thermal load of the office building. By solving various heat and mass balance equations inside the engine of EnergyPlus tool, outputs in various forms are obtained are shown in published work [J7].

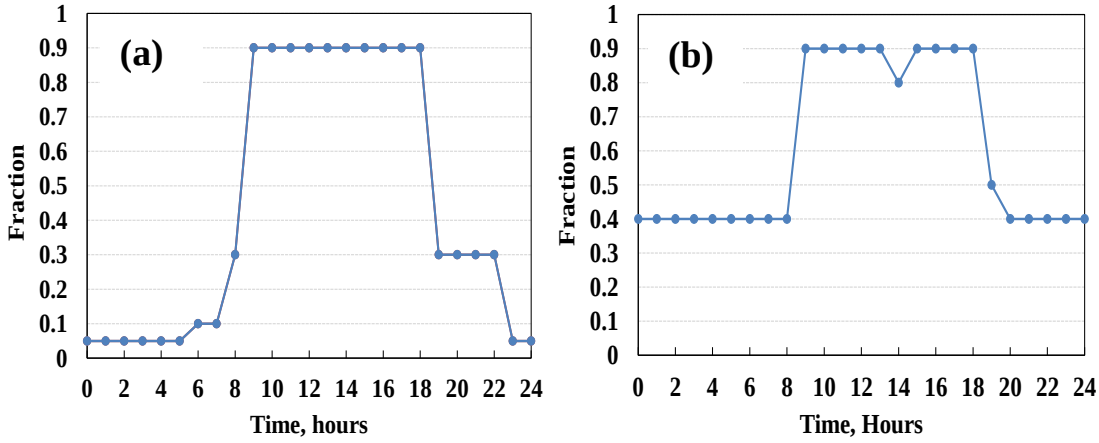

(a) Light schedule (b) Electric equipment schedule

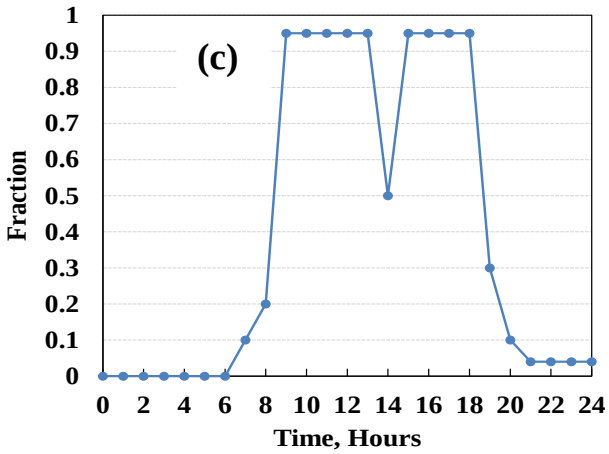

(c) Occupancy schedule

Figure 6.3: Various operational schedules for EnergyPlus models

6.4. Results and discussion

The current study modifies the design of the existing/conventional VRF systems by integrating a desiccant-based DOAS in which solar energy has been used for regeneration. Energyplus simulation results for evaluating the thermal and electrical performances of the proposed system, as well as the conventional ones, are presented in this section. The predicted mean vote (PMV) and percentage of person dissatisfied (PPD) are important indices of the maintained thermal comfort conditions inside the office space and variation of these parameters are discussed in the work [J7]. Results are compared in terms of different climates. Various outcomes of this study are discussed next.

6.4.1. Thermal load analysis

Figure 6.4 shows the monthly variations in the average thermal load generated inside the building and the cooling potential supplied by the respective air-conditioning modes. The pattern of thermal load generated and cooling provided by the system vary according to the climatic conditions. Figure 6.4a shows the variational pattern for the warm-humid climate. From this figure, it can be observed that during the whole year of operation, for Modes 1 and 2, the supplied cooling is always more than the generated load. However, for Mode 3, this holds well only during the period of March to November. This is because in Mode 3, the net load on the VRF is decreased due to the addition of desiccant that takes away a major portion of the latent heat load, which is not the case for Modes 1 and 2. This is so, because under warm-humid climate the variation in outdoor air temperature is not as significant as in composite and hot-dry climate. Under the composite and hot-dry climatic conditions (Figure 6.4b and Figure 6.4c) the supplied cooling load during relatively colder seasons (November to March) is less compared to the generated load for all of the studies modes, because during this season, the temperature of the indoor is required to kept higher than that of the surrounding.

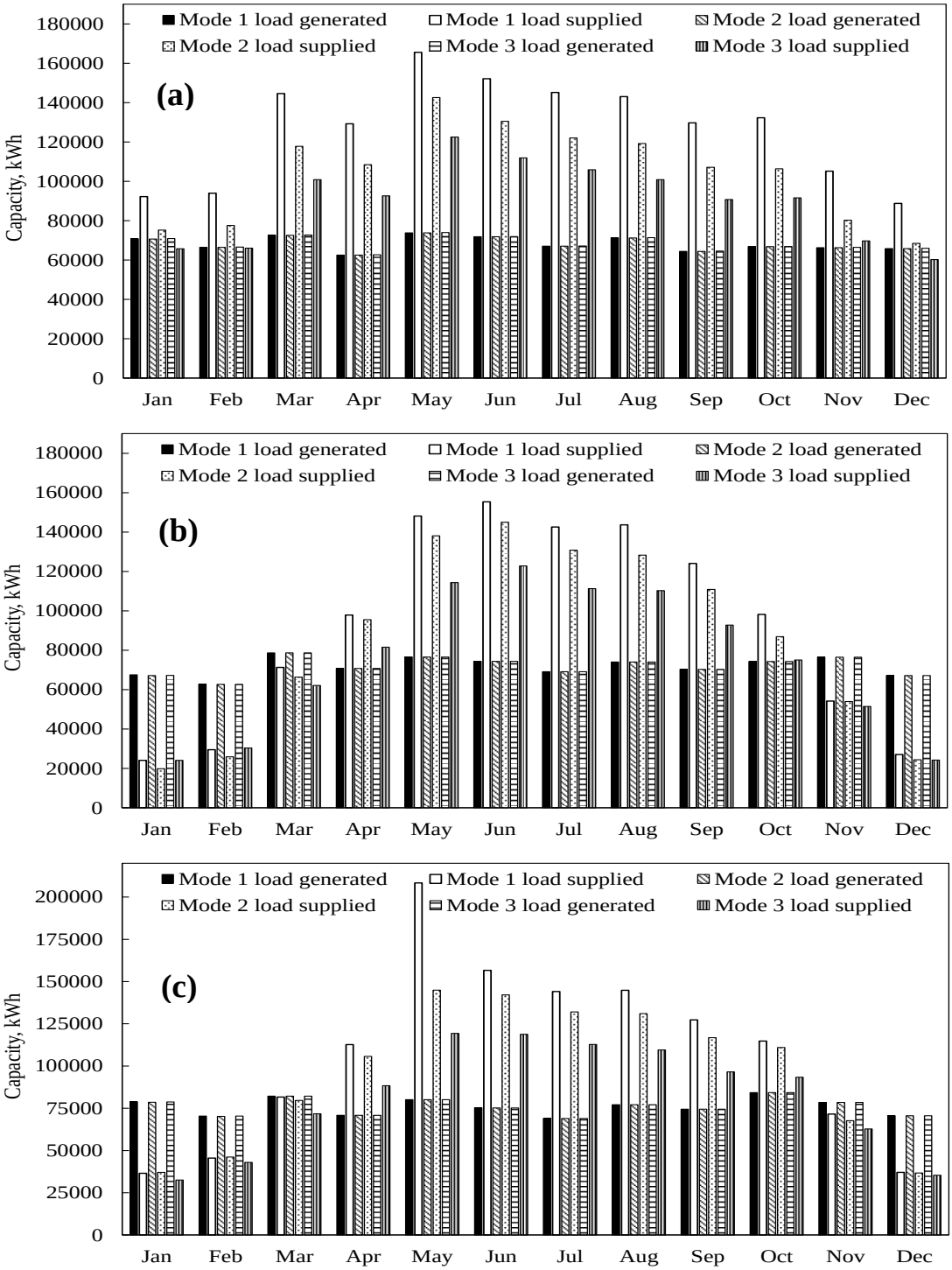

Figure 6.4: Monthly variation of thermal load generated inside building and supplied by air-conditioning systems (a) warm-humid, (b) composite, (c) hot-dry

6.4.2. Electrical and thermal energy performance & cost assessment of the system

This section shows the variational patterns of different components involved in each mode of operation's total annual electricity consumption. These include chiller, fan,

pumps, VRF system, IEC, and heater. Flow pump refers to the chilled and hot water circulation in their respective units. Figure 6.5a shows the electrical energy performance for Mode 1. In all the working modes, the major portion of electricity is consumed by the compression chiller. Among the three climates, the maximum electricity consumption occurs in warm-humid climates followed by hot-dry and composite climates. This is attributed to the high cooling demand in warm-humid climate. Figure 6.5b shows the pattern for Mode 2. In this mode, only VRF chiller and fan consumptions are associated with building air-conditioning. In this case, too, maximum energy consumption is shown by warm-humid climate. Figure 6.5c shows the data values for Mode 3 under different climatic conditions. From this figure it is observed that the auxiliary heater is consuming electricity in warm-humid climate only, whereas its consumption is nil for composite and hot-dry climates. This is because in these two climates solar energy is sufficiently available to fulfill the regeneration requirement of desiccant material, but the same is not possible for warm-humid climate for the given solar collector size (1780 m^2 occupying nearly 50 % of the roof space). However, auxiliary heater energy consumption for warm-humid climate can be reduced by employing additional solar collectors on the roof, but for consistency in comparison between different climates, uniform proportion has been considered. In this case, warm-humid climate also possesses more energy consumption than the other two climates.

Figure 6.6 shows the total electricity consumed by the each air-conditioning system under different climatic conditions. The annual electrical energy consumption under the warm-humid climate by Mode 1, Mode 2, and Mode 3 are 558601 kWh, 469571 kWh and 424747 kWh, respectively. For warm-humid climate Mode 3 is capable of saving 9.5 % and 23.9 % of annual electrical energy against Mode 2 and Mode 1, respectively. These values for composite climate for Mode 1, Mode 2, and Mode 3 are 428742 kWh, 407897 kWh and 369478 kWh, respectively. Under the composite climatic conditions, the proposed system (Mode 3) is found to save 9.4 % and 13.8 % of energy with respect to the Mode 2 and Mode 1, respectively. For the hot-dry climate, Mode 1, Mode 2, and Mode 3 respectively consume 477508 kWh, 445835 kWh and 393770 kWh of annual electricity. Here, Mode 3 saves around 11.6 % and 17.5 % of yearly electricity compared to Mode 2 and Mode 1, respectively.

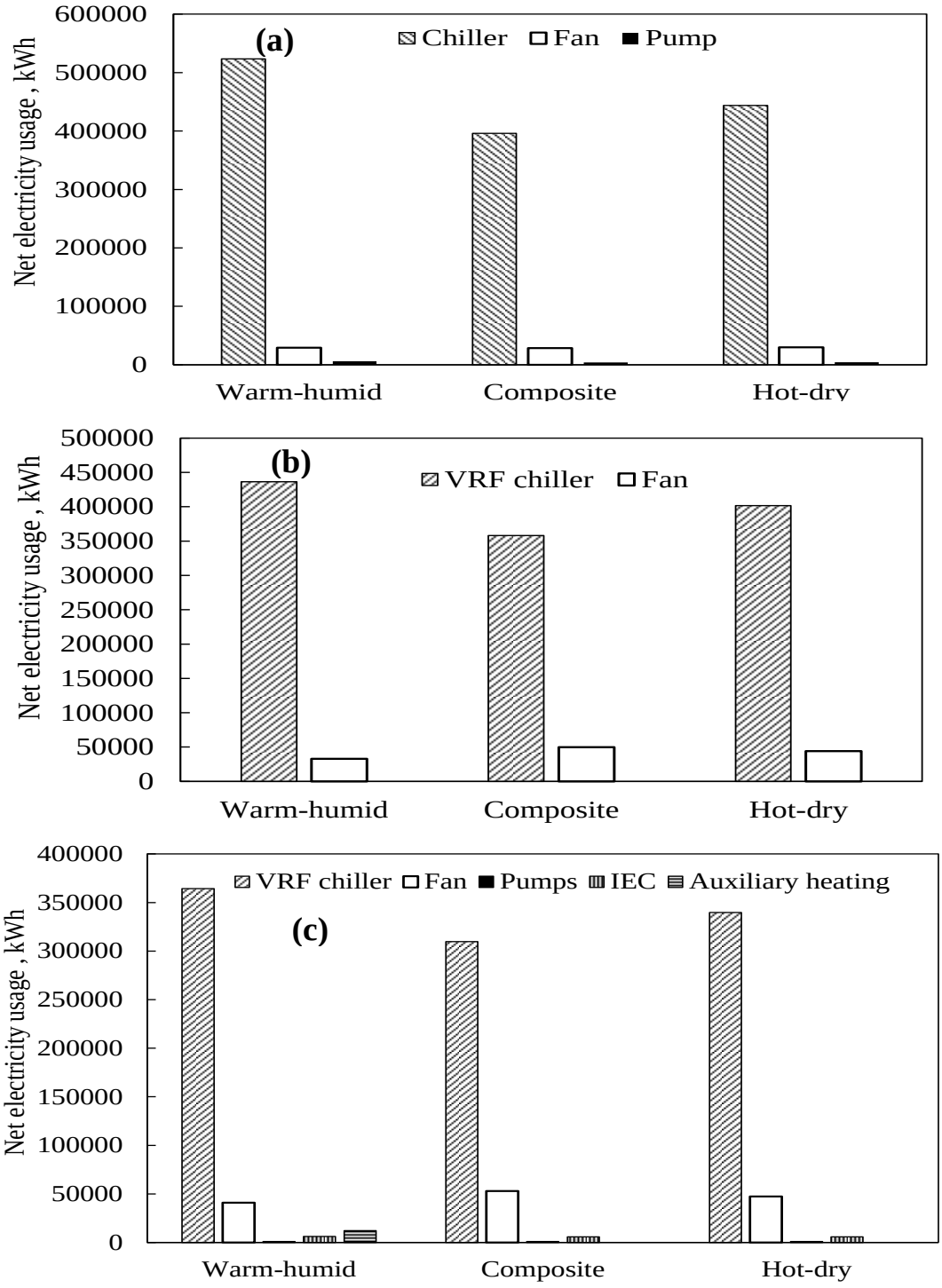

Figure 6.5: Annual electricity usage breakdown in different components (a) Mode 1, (b) Mode 2, and (c) Mode 3

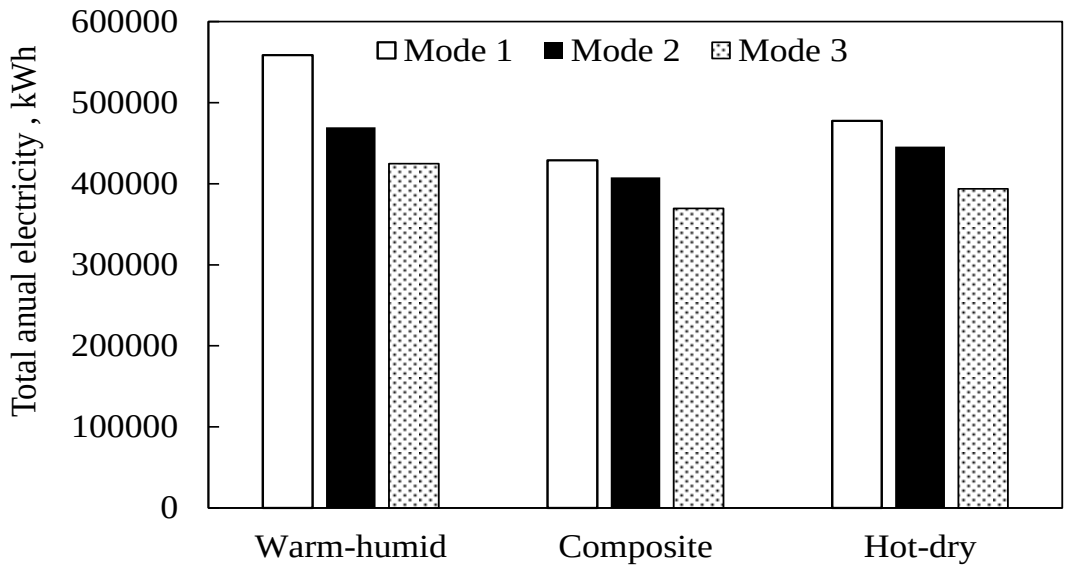

Figure 6.6: Analysis of net annual electricity consumption

The regeneration fan creates hot air at the temperature around 60 ºC from the hot water coming from solar collector loop at 80 °C and desiccant material is regenerated as hot air passes over it. For the proposed mode (Mode 3), Figure 6.7 shows the annually required heating energy at the regeneration coil and the supplied heating energy through solar collector and auxiliary heater. It is observed that for the warm-humid climate, the annual consumption of auxiliary heater is around 12131 kWh, because solar collector is unable to fulfill the required heating demand. The total requirement for this case is 479150 kWh and out of this solar collector gives around 467019 kWh of heating energy. So, the required difference is fulfilled by the auxiliary heating system. For the composite climate, the required heating demand for the desiccant regeneration is around 263695 kWh, whereas solar collector at this condition supplies 637700 kWh of thermal energy. Thus, the consumption of auxiliary heater is zero. For hot-dry climate too, solar collector is supplying surplus heating energy of 830801 kWh against the net demand of 231524 kWh only. For the given solar collector area, the surplus solar energy available from the composite and hot-dry regions may be effectively stored for other purposes. So, it may be concluded that the net solar collector area requirement in composite and hot-dry climate is very less compared to that of the warm-humid climate. Even the installation of half of the collector area or lesser (around 890 m^2) is also sufficient to operate this system efficiently and that will also reduce the initial capital investment. The performance of the solar collector system can be defined in terms of solar fraction. This term shows the contribution of solar energy towards the net energy requirement (J1). The estimated value of solar fraction under the warm-humid climate is around

0.97. In contrast, the solar fraction can be greater than one for other climates (composite and hot-dry). Still, for the representation, its maximum value is kept as one because excess energy is available in those climates.

Table 6.1: Unmet hours for VRF air-conditioning system assessment

S. No.	Building area	System type/Configuration	Unmet hours (climate)
1.	10690 m^2	Conventional all-air VAV system	5 (warm-humid), 15 (composite), 12 (hot-dry)
		Conventional VRF system	17 (warm-humid), 22 (composite), 57 (hot-dry)
		Solar-desiccant assisted VRF system	12 (warm-humid), 19 (composite), 51 (hot-dry)

The installed air conditioning system operates for 9 hours a day, and throughout the year total working days are around 289 days, excluding the holidays and weekends. So, the running hours of the system are around 2601 hours (J2). Therefore, using the simulation outcomes, it is observed that unmet hours are different for different operating conditions as shown in Table 6.1. The unmet hours for each of the air-conditioning system falls within the specified range (Unmet load hours troubleshooting guide, 2013). Figure 6.8 shows the variation of these unmet hours under different operating modes for considered climatic conditions. From this figure, it can be highlighted that the same type of installed system is not performing equally in all climates, but, it varies according to the climatic conditions. Air conditioning systems under the warm-humid climate is performing for the longest time. For any climate, the unmet hours under the Mode 3 are somewhat more compared to Mode 1, but lesser than Mode 2. The variation in the unmet hours, affects the overall thermal and electrical performances of the installed air-conditioning systems.

In this work also, an economic analysis has been done for estimating the ROI for all of the considered modes of operations subjected to different climatic conditions. The values of peak rated capacities and costs of different components can be found in published work [J7]. The ROI of this work is highly dependent on the area of solar

collector. The solar collector area can be reduced up to 50% that will influence the ROI significantly. According to the cost of energy savings, the estimated ROI of the Mode 3 with respect to Mode 1 with 1780 m^2 collector area for warm-humid, composite and hot-dry climatic condition is around 6.19 years, 13.98 years, 9.90 years respectively. Whereas, the ROI of Mode 3 with respect to Mode 2 varies between 13-17 years according to climatic conditions.

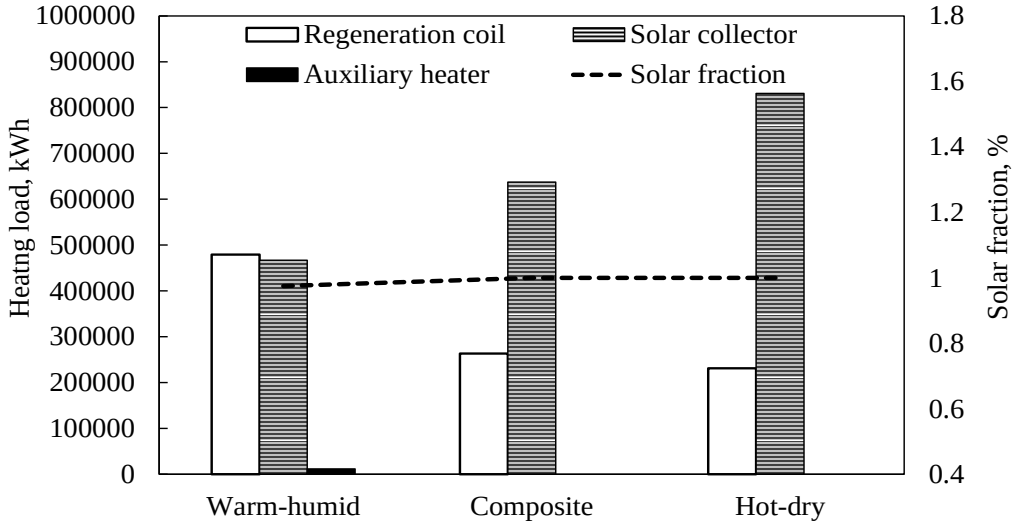

Figure 6.7: Heating energy requirement and supplied with solar fraction

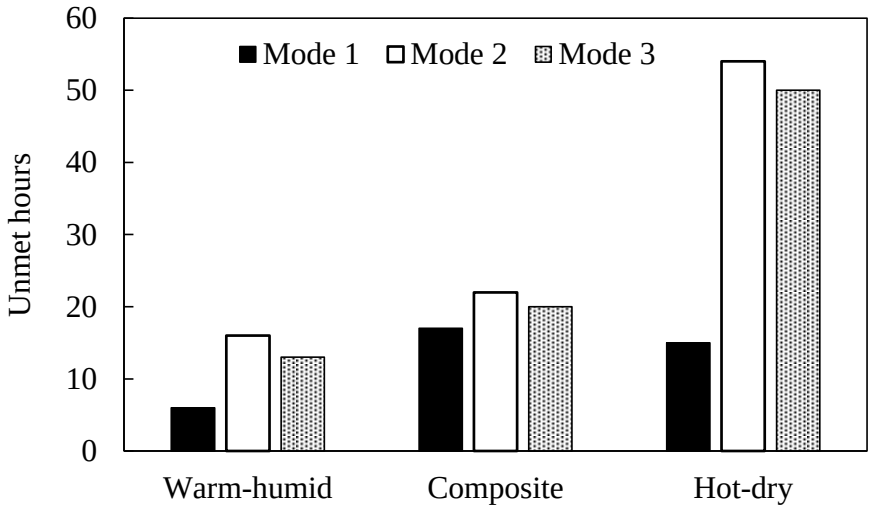

Figure 6.8: Simulation unmet hours under different operating conditions

6.5. Conclusion and recommendations

Integrating a solar energy-based desiccant-assisted VRF air-conditioning system is proposed for a large-scale building cooling. Performance comparison has been made with conventional all-air/ VAV and conventional VRF in terms of electrical energy consumption and thermal aspects for three distinct climatic conditions. It is found that

the supplied cooling energy by the proposed VRF system is lesser compared to the conventional all-air/VAV and VRF systems. Further, from the perspective of using renewable energy-based resources for building air-conditioning, this study provides attractive energy savings and cost ways. Following conclusions are drawn from this study,

1. The proposed solar energy-based desiccant-assisted VRF saves around 23.9 % and 9.5 % of electrical energy compared to the conventional all-air/VAV and VRF system, respectively under warm-humid climate. Under composite climate these saving are 13.8 % and 9.4 %, respectively, whereas, these savings for hot-dry climate are 17.5 % and 11.6 %, respectively.
2. For warm-humid climate, desiccant enables the proposed system to supply less cooling load than that is needed for certain cold periods of the year, whereas conventional designs provide more cooling energy than required.
3. For hot-dry and composite climates, the part load ratio and cooling load follow a similar trend in all modes of operation. However, for warm-humid climate, a definite trend is not observed which is attributed to narrow variations in the psychrometric properties of outdoor air.
4. Surplus solar energy is available for regeneration of the desiccant in composite and hot-dry climates, whereas, for warm-humid climates, 97 % of the desiccant heating demand is fulfilled by solar energy.
5. The total supplied cooling load and annual electrical energy requirement are high in warm-humid climate followed by composite and hot-dry climates. Further, the suggested system fulfills the air-conditioning requirements for the longest time under the warm-humid climate.

The present work shows the energy saving potential of the proposed air-conditioning setup by integrating solar energy with desiccant material in a VRF system. The system provides better thermal comfort and lesser energy requirement under high humidity and temperature conditions than other VRF designs.

CHAPTER 7

*EXPERIMENTAL STUDY OF HYBRID VAPOUR ABSORPTION SYSTEM

This chapter exhibits the experimental analysis of the developed working model of vapor absorption system at the lab scale in IIT Ropar transit campus. This chapter is divided into two subchapters which show different kinds of analysis of the developed system using the experimental data.

From the discussion in chapter 5, it is perceived that for a building to be grid independent, the best suitable air-conditioning system is compression driven only. However, in this chapter, suitability of the absorption based system for attainment of target of grid independency is highlighted experimentally. In this direction, the first subchapter (section 7.1) demonstrates the working of the developed actual working model under different operating conditions such as: solution concentration and generator temperature. In this work, solar and biomass-based energy resources have been coupled with the absorption system which makes this test assembly as the grid-independent unit. Paddy straw, wooden chips, and waste biomass have been used to run the biomass gasifier. The end application of the absorption system in this work is used to cool a test chamber. Experimental results revealed the acceptable working of the developed system.

Second subchapter (section 7.2) establishes empirical correlation generation for the developed absorption system based on the experimental data. Minitab software has been used for generating these correlations. This chapter shows the relationship between evaporator load and evaporator temperature in equations with the variables: generator temperature, solution concentration, and hot water mass flow rate. This chapter's results also show the acceptability of correlations compared with other literature.

* Content presented in this chapter can be found in the publications J4 and J5.

7.1. Experimental analysis of triple hybrid single effect LiBr-water absorption air-conditioning system

7.1.1. Setup components and description

It was observed from the literature survey that the absorption chiller-based air-conditioning are either fully or partially grid dependent. However, a fully grid-independent absorption-based air-conditioning system is not discussed previously. In this direction, a test bench has been conceptualized and fabricated to study the operation of a triple-hybrid biomass and solar energy based absorption air-conditioning system. This facility (Figure 7.1.1) includes various components. Figure 7.1.1a shows the schematic layout of the designed test bench and Figure 7.1.1b shows the actual image of test bench at the site. For instance: the LiBr-water based absorption chiller is used for air-conditioning the test chamber. This single-effect absorption chiller is fabricated in the laboratory. The distinguished aspects of this chiller is that the condenser is air-cooled, whereas, the absorber is water-cooled with the aid of cooling tower of biomass gasifier. In the gasifier, the cooling tower cools the generated syngas from the cyclone filter by enabling it to pass through various filters (sawdust filter and cotton filter). Otherwise, high-temperature syngas can deteriorate these filters materials. The thermal capacity of the gasifier is 15 kW with 5 kW electricity generator. The exhaust waste heat of the electricity generator is used for heating the water of hot water storage tank that supplies hot water to generator of absorption chiller. The electricity generated from the biomass genset is used for running the water circulation pumps, vacuum pump, lights, FCU, auxiliary heater and other associated electrical appliances shown in Figure 7.1.1a. This practice allows the system to approach closer towards the electric grid independent objectives. A parabolic trough solar collector (PTSC) is also coupled to supply hot water to the hot water storage tank. At favorable operating conditions (i.e., clear sunny day, moderate wind speed, availability of sufficient solar irradiation and without shading effect), the maximum thermal output of the PTSC is around 10 kW. Temperature sensors and flue gas sampling nodes at various positions are provided, as indicated in Figure 7.1.1a. A vacuum pump is used to create vacuum inside the chiller's interconnected assembly. Two vacuum gauges are installed in the absorber and generator tanks. The heat source circuit consists of hot water storage tank, pump and electrical heating element. All water circulation pumps are of 0.37 kW capacities. To test the developed system's performance, a test chamber, having size (length 3.04 m ×

width 3.04 m × height 2.59 m) is fabricated. Insulations are applied on the inner walls, roof and floor of the test chamber to reduce the heat gain inside the room from the surrounding. From Figure 7.1.1a, it can be seen that thermal energy to the absorption chiller's generator side is supplied from a hot water storage tank of 0.18 m^3. A FCU is installed inside the test chamber for the air-conditioning, which is essentially a water-air heat exchanger.

7.1.2. Methodology and experimental procedure

This study assesses the feasibility and performance of the developed triple-hybrid air-conditioning system using solar and biomass-based resources. Here, the performance parameters are chiller's COP, cooling capacity, heating energy requirement, developed thermal comfort conditions, fractional heating energy supplied by solar and biomass resources, economic perspectives and associated emissions. Further, the absorption chiller performance is evaluated with two different concentrations (54 % and 58 %) of LiBr-water solution with three T_G ranges: 60 °C, 70 °C and 80 °C. These ranges have been selected based on the available heat source. The 54 % concentration is initially considered based on market availability. However, according to the literature Prasartkaew (2014), 58% concentration is selected for obtaining better output from the system, so enrichment in the existing solution has been done using additional LiBr salt. Within 54 % to 58 % concentration, the problem of crystallization is very less over a wide range of temperature, while beyond 58 % concentration proper attention is required to eliminate the crystallization problem, especially at low temperatures (Prasartkaew 2014). In the present work, various instruments are involved, such as, thermocouples, flue gas analyzer, humidity measuring device, and the meter for measuring electrical parameters. The required mass flow rates are manually monitored and adjusted by controlling the flow through the valves. This is done by collecting a certain amount of liquid for a specified time period. Experiments are done for catering the artificially generated cooling load of 4±0.5 kW using filament bulbs and due to heat interactions between room metal envelope and inside air, since any insulation cannot be perfect. This artificial load is applied until the room temperature ($T_{R,a}$) reaches up to 36 °C. This temperature value is selected, because during the summer period generally inside $T_{R,a}$ is achieved around this value for the prevailing weather conditions. Heated water from the storage tank is delivered to system generator by hot water circulator for maintaining different T_G (60 °C, 70 °C and

80 °C). A validation study has also been performed for the developed absorption system against the available reference model and the various equations used for the energy consumption evaluation with related parameters ranges are shown in the published work [J4].

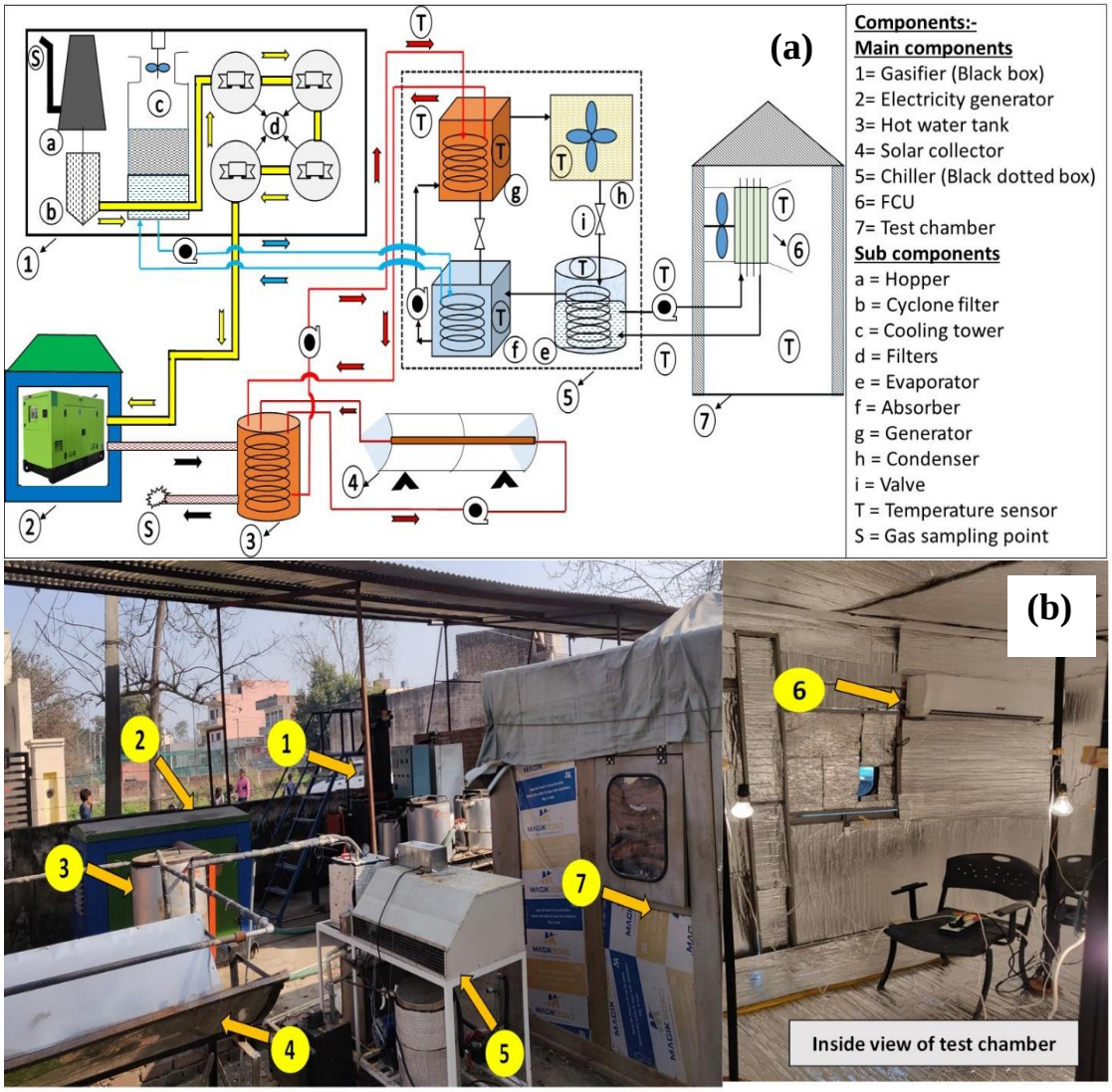

Figure 7.1.1: (a) Schematic of experimental setup, (b) Actual image of test bench

Various assumptions considered before evaluating the system performance are mentioned below,

1. All experiments are carried out under steady-state conditions.
2. Steady-state is attained when the difference between two successive temperature values at the same location is within 0.1 ºC.
3. Generated load and supplied cool air are uniformly distributed inside the room.
4. Hot water circuit is well-insulated so that there is no heat loss from the piping and water storage tank.

5. Starting specified conditions (initial room and chilled water temperature) varies within ±1 ºC.

7.1.3. Analysis of results

7.1.3.1. System performance analysis

The developed absorption-based air-conditioning system is tested for six days at different T_G (60 ºC, 70 ºC and 80 ºC) with varying concentrations of LiBr-water solution (54% and 58%). Experiments are performed for the first 3 days with 54 % LiBr-water concentration, whereas for the next 3 days, evaluations are done with 58 % concentration. The initial conditions (circulating chilled water temperature, T_{CW} of 23±1.0 ºC and $T_{R,a}$ of around 36±1.0 ºC) during all experiments were held same. For this purpose, multiple replicates of the final $T_{R,a}$ are taken to ensure the data accuracy against different concentrations and T_G. Figure 7.1.2 show the variation of T_{CW} provided to the evaporator (during pull down and response periods) and the temperature (T_{RCW}) of the water that is returned from the FCU after providing the cooling effect inside the test chamber. Pull down period is the time required for chiller evaporator section in which water is being made reusable for cooling purpose, whereas, response period is the time for the actual air-cooling accomplished by FCU. Heat gained from room by the circulating chilled water needs to be completely rejected at the evaporator section (i.e., by evaporation of water refrigerant) of the absorption chiller. The evaporation rate of water refrigerant from the chiller is a function of vacuum pressure. Here, the rate of heat gained and heat removal are not exactly equal; consequently, the temperature difference between the chilled water and returned chilled water decreases continuously, due to this further air-cooling could not be realized after a certain time. Thus, the system's pull down is necessary.

Results with the 54% concentration conditions can be found in the published work [J4]. Here, results with the 58% concentration condition are discussed for different parameters. With 58% concentration, Figure 7.1.2 shows the number of experiments performed in a single day of working at a particular T_G. For the solution with the 58% concentration, three set of trials can be attained by considering the same initial conditions (around T_{CW} =23±1 ºC and $T_{R,a}$ =36±1 ºC). During the experiments, within hours 11:00-12:15, T_{CW} are14.8 ºC, 14.6 ºC and 13.8 ºC for T_G =60 ºC, 70 ºC and 80 ºC, respectively (Figure 7.1.2a-c). That means the performance of the developed system

is improved in terms of reduced pull down time/fast start-up time and temperature reduction of chilled water by using 58 % concentrated solution as compared to the 54 % concentrated solution, due to which, three sets of experiments could be performed. Thus, from Figure 7.1.2c it can be observed that the initial pull-down period is lesser compared to the other two cases (i.e., Figure 7.1.2a and b). For the lowest T_{CW}, the average final $T_{R,a}$ can be achieved up to 28.2 ºC (Figure 7.1.3c) with minimum value 27.5 ºC against T_G =80 ºC. Further, the temperature profiles for other set of trials can be investigated from Figure 7.1.2.

From Figure 7.1.2, it is also observed that there is a decrement in the temperature difference between T_{CW} and T_{RCW} profiles for each response period. Apart from this, it has been observed that, during all sets of experiments, the average cooling water temperature (water circulated from cooling tower to absorber) varies between 23 ºC to 28 ºC and after removing the heat from the absorber, its temperature is raised between 1 ºC to 2 ºC only.

Figure 7.1.3 show the temperature profiles of $T_{R,a}$ for two different concentrations of LiBr-water solution. The figures are shown for each hour of experiment along with replicates for a single day, where a single replicate only consists of 60 minutes of the response time period. As per the standards (Kreider 2020), the final conditions of the room should be matched with the specified thermal requirements (21-28 ºC temperature with 55-65 % humidity level). Figure 7.1.3 shows these temperature profiles for 58 % concentrated solution. From Figure 7.1.3c it can be projected that using 58% concentrated solution, the minimum average temperature of 28.2 ºC (with lowest value of 27.5 ºC) at T_G =80 ºC can be acquired. However, at low T_G, the final attained $T_{R,a}$ is quite high (Figure 7.1.3 7a, b), because at low T_G, the T_{CW} is also high that results in less thermal load catering capability. Additionally, the average humidity level inside the chamber has been observed in the range of 38 % to 60 %. These air-conditioning levels lie within the range of standard thermal comfort conditions (Kreider 2020).

The performance of the developed absorption based air-conditioning system is calculated on the basis of measured data values and using of section 3.1.2.2. Here, in this experimental study, the pump work needs to be added at the denominator of COP calculation, but this parameter's value is very small. So, we have neglected this for calculating the COP.

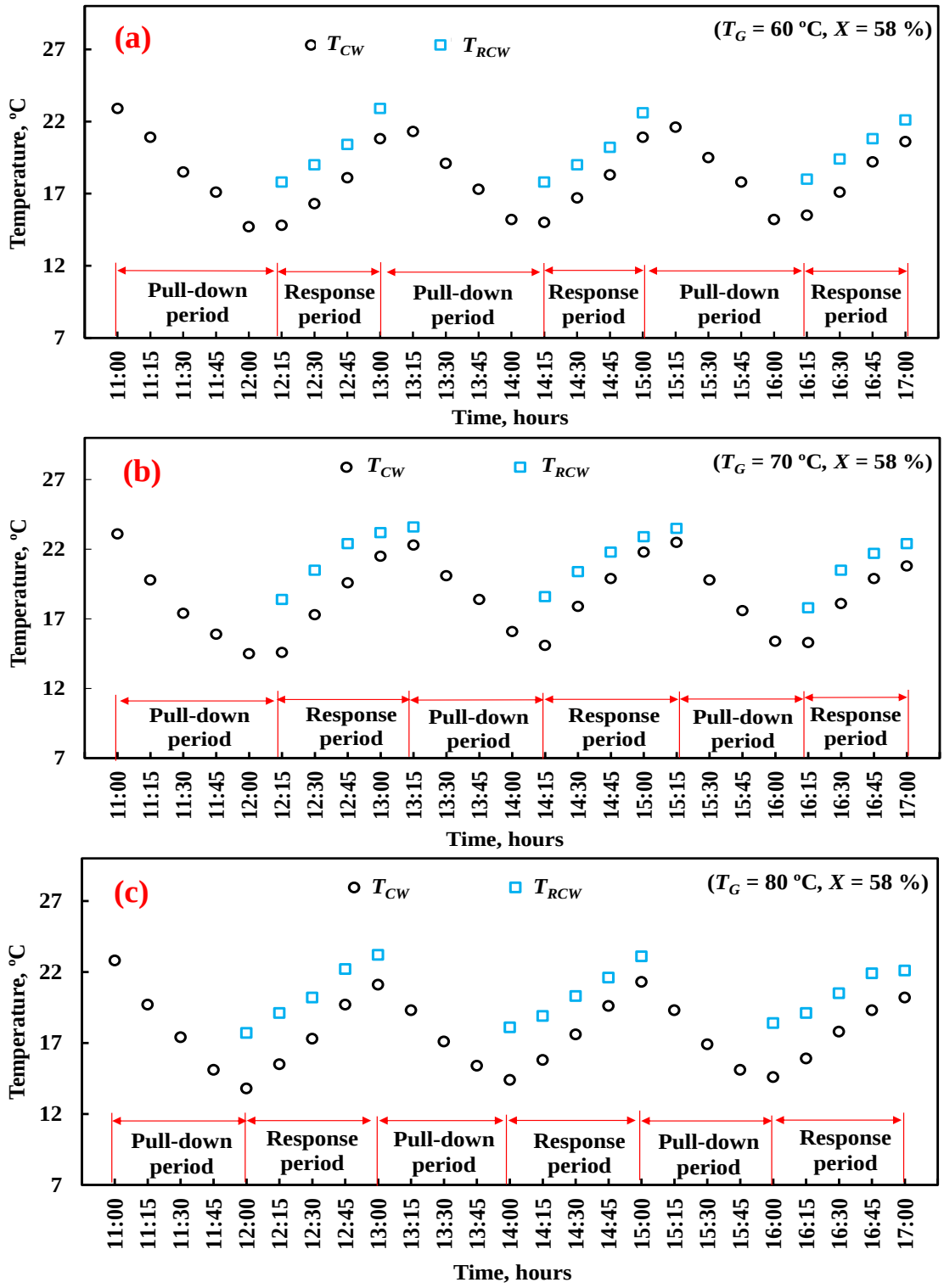

Figure 7.1.2: Chilled water temperature profiles with 58 % solution for (a) Day 4 (b) Day 5 and (c) Day 6

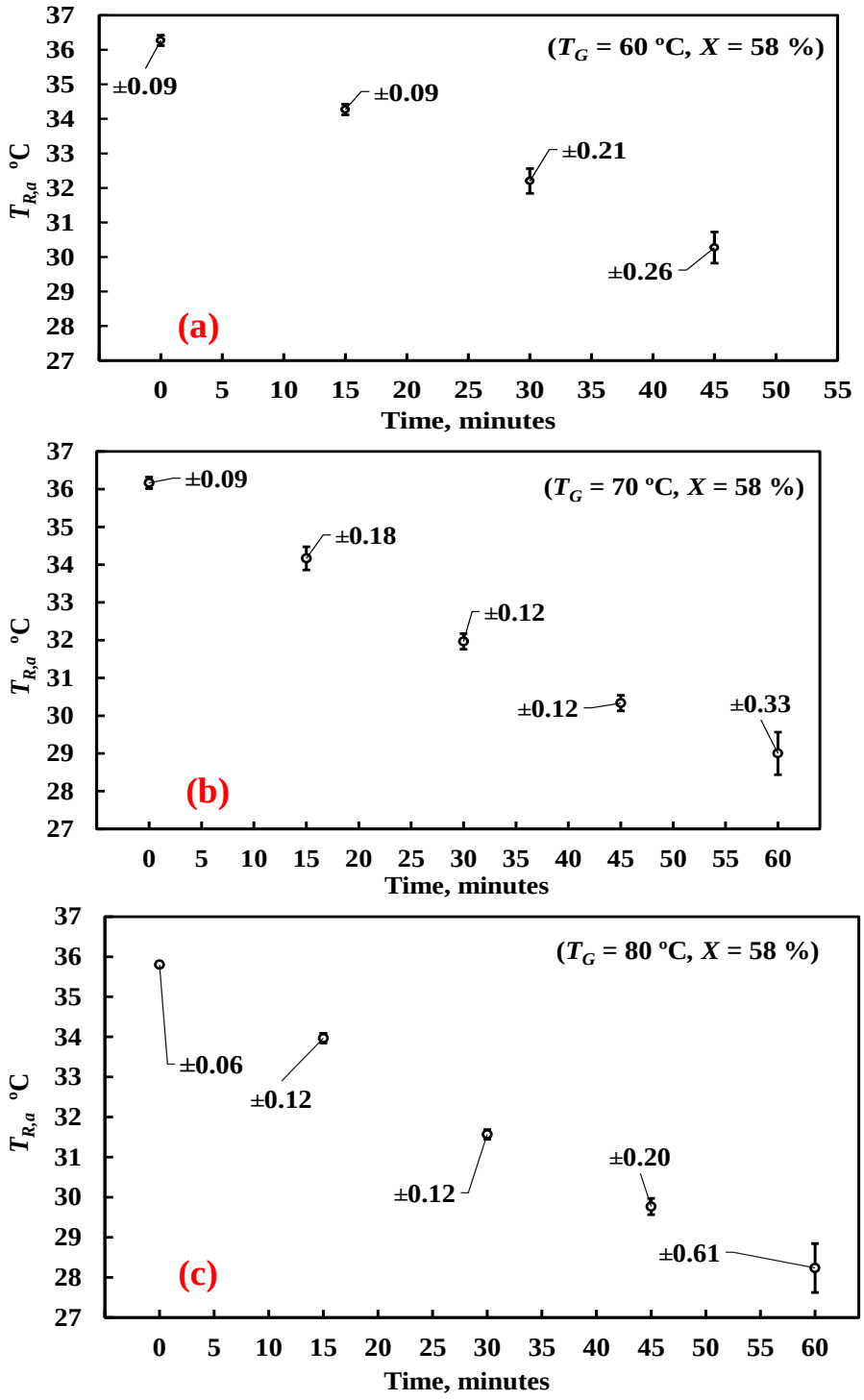

Figure 7.1.3: Room air temperature during response period with 58 % solution (a) Day 4, (b) Day 5 and (c) Day 6

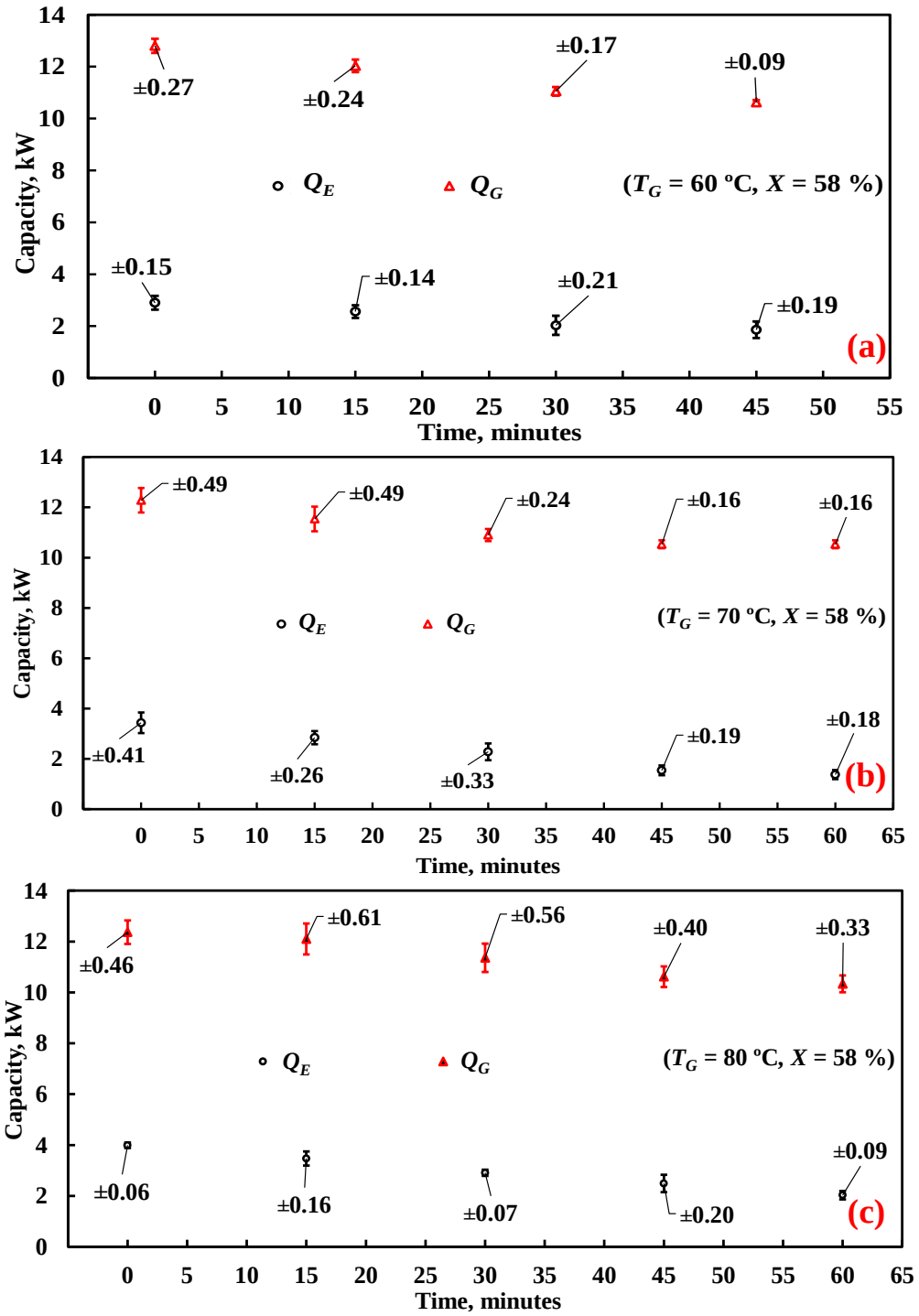

Figure 7.1.4: Average generator load and evaporator load during response period of the system with 58% solution (a) Day 4, (b) Day 5, and (c) Day 6

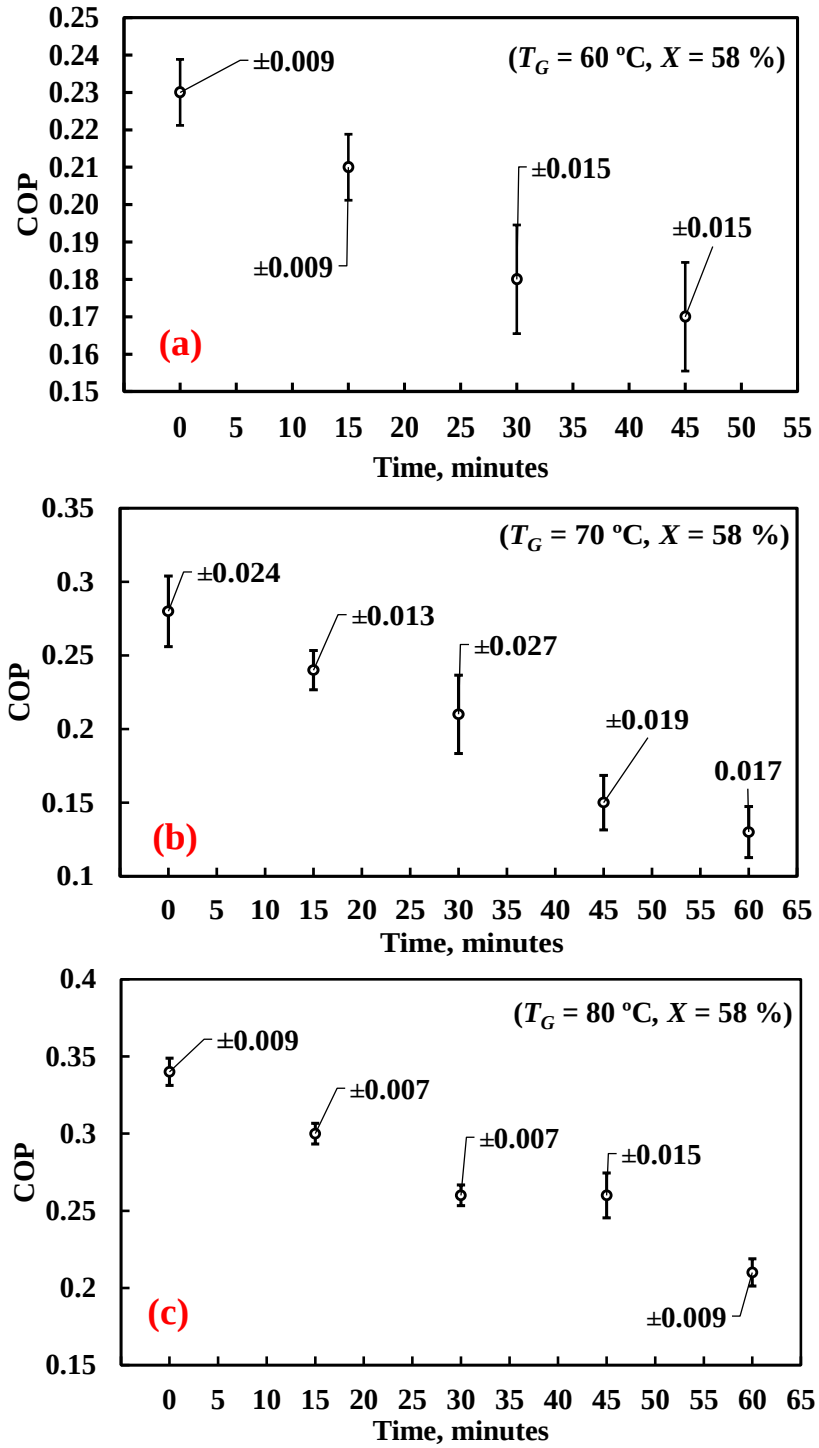

Figure 7.1.5: Average COP of the system during response period with 58 % solution (a) Day 4, (b) Day 5, and (c) Day 6

Figure 7.1.4 depict the performance parameters of the developed system in terms of evaporator load and generator load for both the considered cases of concentration (58 %) at different T_G. These graphs have been plotted during the actual air-conditioning period at different operating hours. Further, Figure 7.1.4 shows these profiles

corresponding to the three response periods concerning 58% concentration condition as observed in Figure 7.1.2. From Figure 7.1.4 it can be observed that, the heat provided to the generator slightly reduces, while evaporator's load profile decreases relatively more with time. This is because of the reduction in temperature difference between chilled water and returning chilled water during the response period (please refer to the response period of Figure 7.1.2). However, the highest evaporator load of 4.09 kW is catered with 58 % concentration at T_G = 80 ºC. Figure 7.1.5 show the COP variation during the response period for each considered case. It also highlights that the working of the present chiller is in accordance with the available studies. It is revealed by Prasartkaew (2014) and Kefti et al. (2017) that with increase of T_G, the system COP also enhances. So, in this study too, similar trends are obtained in terms of COP at different T_G. Further, with 58 % concentrated solution, the average COP is obtained as 0.19, 021 and 0.25 with T_G of 60 ºC, 70 ºC and 80 ºC, respectively. From these figures (i.e., (Figure 7.1.5a, Figure 7.1.5b and Figure 7.1.5c), it can also be noticed that, at the same T_G, enrichment in the solution concentration 54% to 58% improves the system COP. Here, with reference to 54 % concentration, COP of the system is enhanced by 35.7 %, 23.5 % and 31.5 % at T_G of 60 ºC, 70 ºC and 80 ºC, respectively when 58 % concentration is used. During the experiments, highest instantaneous COP at a certain point of time with 58 % concentration and 80ºC generator temperature conditions is obtained as 0.34 (Figure 7.1.5c). Here, due to the reduction in evaporator capacity during the complete set of experiment, COP of the system also shows downwards slope during response time.

A net zero/grid independent energy building is the one for which its on-site renewable energy (solar, biomass, wind and other resources) based power generation is capable to fulfil its own energy demand as discussed by Hossaini et al. (2015) and J3. In this study, the biomass gasifier is used for both on-site and off-site energy generation. For grid independency assessment, the electricity consumed and generated by the test bench during a day is studied in Figure 7.1.6. During the actual experimental time of 6 hours, the quantity of electricity generated using biomass gasifier is around 30 kWh. However, the amount of electricity generated depends upon the operating hours of gasifier. This generated electricity is consumed by various installed components of the test bench. The total energy consumed by the installed components (FCU, lights, pumps, heater, chiller and cooling tower) during the operation is observed around 23.5 kWh. Here, the pumps consumption includes: hot water circulation pump, solar collector loop pump,

chilled water circulation pump, and cold water circulation pump. Further, cooling tower consumption comprises a fan motor and its separate water circulation pump. So, it can be observed from Figure 7.1.6 that the grid-dependency of the developed test bench is zero i.e., the objective of grid independency is possible in a complete manner. Moreover, it is capable of generating surplus energy that can be used further. Moreover, the present system's solar fraction and emission analysis are also discussed in the published work [J5].

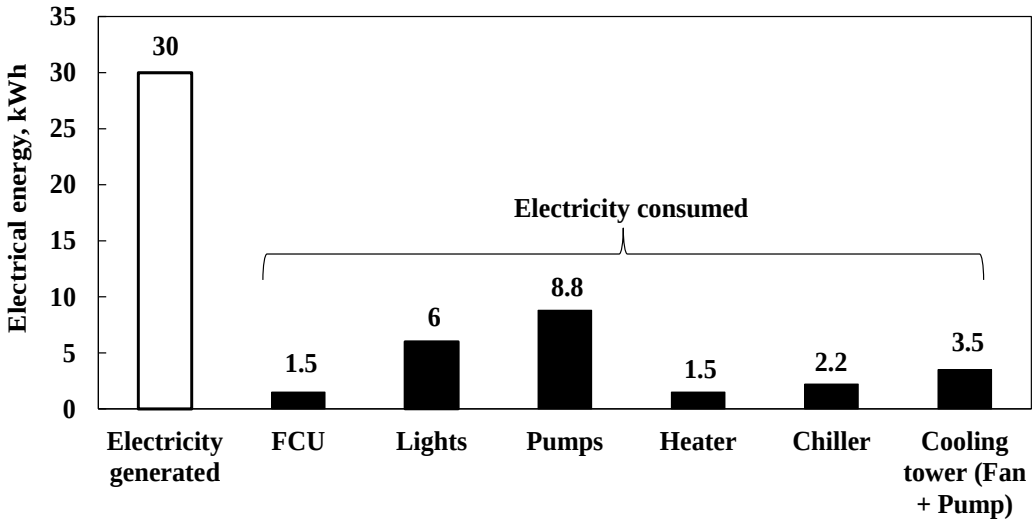

Figure 7.1.6: Electrical energy analysis for a day

7.1.4. Empirical correlation generation and cost assessment

In this work, a response surface analysis has also been performed for developing an empirical correlation between the amount of thermal power supplied by the combined solar and biomass based resources with respect to the net cooling capacity of the present absorption chiller. The response surface method is a statistical technique employed for deriving a relationship among the system's independent and dependent parameters. For this purpose, the thermal loads supplied by the solar collector and biomass gasifier are taken as the independent variables, whereas the chiller's cooling capacity is considered the dependent variable. The total heat content supplied at the generator side of the absorption chiller consists of solar collector, waste exhaust heat from the biomass-operated genset, and the auxiliary heater operated by electricity generated from biomass driven genset. So, the independent variables for the response surface analysis are designated as Q_{ST} (for thermal power by the solar collector), and Q_{BT} (for thermal power of the biomass based sources). The, the dependence of the chiller's cooling capacity or evaporator load (Q_E) can be designated as,

$$Q_E = a_0 + a_1 Q_{ST} + a_2 Q_{BT} + a_{11} Q_{ST}^2 + a_{22} Q_{BT}^2 + a_{12} Q_{ST} Q_{BT} \quad (7.1.1a)$$

a_0 = -8.30, a_1 = 82.70, a_2 = -10.58, a_{11} = - 44.70, a_{22} = 0.2643, a_{12} = 4.48 (7.1.1b)

where, the a_i (i=1, 2) is the regression coefficient. The values of these coefficients are computed using the Minitab and the correlations can be generated using the functional templates. For estimating the correlation and its coefficients in the Minitab, data set of experimentally-obtained independent parameters are fitted with the respective outcomes of the experiments (i.e., the dependent variable). So, in this study, 15 different input data sets for are considered for the optimized case (X = 58% and T_G = 80 °C). For this condition, the input data for the independent parameters vary as, 1.25 kW ≤ Q_{ST} ≤ 1.50 kW and 7.94 kW≤ Q_{BT} ≤ 11.55 kW, whereas, the dependent parameters varies as 1.897 kW ≤Q_E ≤ 4.10 kW. The value of the coefficient of determination/Correlation coefficient (R^2) obtained from the Minitab is found as 92.13%.

Here in this work, cost analysis is performed in order to investigate the economic aspects related to fabrication of the developed test bench against the conventional coal-based system. The associated costs with taxes of the components, maintenance, and man power are shown in the published work [J4]. The total cost of the fabricated test bench is around 1145570 INR. The ROI of this work, as per the cost of energy savings is varying between 9-12 years.

7.1.5. Uncertainty analysis

In every experiment the obtained data values are not absolutely accurate but with some errors due to equipment, recording methods, human error, and others. Therefore, uncertainty analysis is important to estimate the associated errors. For example, as shown in Eq. (7.1.2), ϕ any final outcome of any parameter of interest is a function of some other dependent variables.

$$\phi = f(Z_1, Z_2, Z_3 \ldots\ldots Z_n) \quad (7.1.2)$$

Let, ξ_Z is absolute uncertainty in the independent quantity, Z. The absolute uncertainty for ϕ (i.e., ξ_ϕ) is estimated as Eq. 12 using the procedure of Moffat (1982). The associated uncertainties with various parameters at particular conditions are shown in Table 7.1.1.

$$\xi_{\phi} = \left[\left(\frac{\partial \phi}{\partial Z_1} \times \xi_{Z1} \right)^2 + \left(\frac{\partial \phi}{\partial Z_2} \times \xi_{Z2} \right)^2 + \left(\frac{\partial \phi}{\partial Z_3} \times \xi_{Z3} \right)^2 + ... + \left(\frac{\partial \phi}{\partial Z_n} \times \xi_{Zn} \right)^2 \right]^{0.5} \quad (7.1.3)$$

Table 7.1.1: Uncertainty in various parameters; T_G = 80 °C, X= 58 %, Time= 60 minutes

Parameter	T_{CW}	T_{RCW}	$T_{R,a}$	T_{HWET}	T_{HWLT}	T_G	Q_E	Q_G	COP
Absolute uncertainty	0.02 °C	0.02 °C	0.02 °C	0.02 °C	0.02 °C	0.02 °C	0.03 kW	0.08 kW	0.04

7.1.6. Conclusions

In this study, a combined experimental and simulation analysis of a triple-hybrid grid-independent cooling system has been carried out to achieve the grid independent criterion and address various environmental concerns. The developed system incorporates absorption-based air-conditioning strategy with rated capacity of 4.06 kW that can be completely operated by thermal and electrical energy supplied by biomass and solar energy resources. Different concentrations of refrigerant-absorbent at distinct generator temperature are analysed. From this work, the conclusions are highlighted below,

- The values of attained cooling capacities for 58% concentration condition at generator temperature of 60 °C, 70 °C and 80 °C are 66.8 %, 71.1 % and 85.1 %, respectively. Increasing the solution concentration from 54 % to 58 %, improves the average COP by nearly 35.7 %, 23.5 % and 31.5 % against generator temperature of 60 °C, 70 °C and 80 °C, respectively.
- The average thermal energy to generator decreases with respect to the time because of the reduced thermal energy supplied by the gasifier. This is attributed to continuous decrement in the amount of biomass within the gasifier, which causes deterioration of the quality and the quantity of syngas with time, so, refilling is a solution towards this issue.
- The developed prototype can control the indoor air temperature up to 27.5 °C against 58% concentration solution and generator temperature of 80 °C. This configuration shows the system's maximum cooling ability and COP as 4.09 kW and 0.34, respectively.

The presented system and the results are concluded to offer a sustainable solution to the stubble burning problem and crop residue management for small and medium-scale applications. Further, it is also envisaged that simultaneous electricity generation and building air-conditioning towards the achievement grid independent status is possible through the present strategy.

7.2. Response surface and Inverse analysis of developed small-scale absorption system

7.2.1. System description and set-up details

The previous literature found that the estimation of *U* for all components of the absorption system using actual temperature and flowrate data values is not entirely reported. Further, a direct correlation for the evaporator load and evaporator temperature concerning the user-controlled parameters for an air-cooled single-effect absorption chiller based on the Box–Behnken design (BBD) is also not done earlier. In this study, a small-scale LiBr-water based absorption system is investigated (Figure 7.2.1a). The image of actual working prototype is also shown in Figure 7.2.1b. The notable aspects for this system include air-cooled condenser, water-cooled absorber, and helical-coiled heat exchanger setup for all heat exchanging devices. The fraction of water refrigerant is parted from the solution inside the generator by hot water. Using this heat, refrigerant and absorbent get heated up and steam is liberated and travels towards the condenser side. Thereafter, heat is rejected into the environment and liquid refrigerant reaches into the evaporator coils via capillary tube. There, outside water coming from the cooled space gives its heat to the refrigerant and consequently the refrigerant boils. This steam is attracted towards the absorber side, where it is engrossed by weaker solution (weak in refrigerant) and enriched solution (rich in refrigerant) is sent towards the generator side [J5].

The developed prototype involves a nominal cooling capacity of around 1.1 ton. Two vacuum gauges (at generator and at absorber) are installed in the system. In this study, the water-cooled absorber is preferred due to simplicity and performance enhancement of setup. In this study, temperature sensors (thermocouples of K-type) are used for measuring the temperatures, whereas, mass flow rates are manually measured.

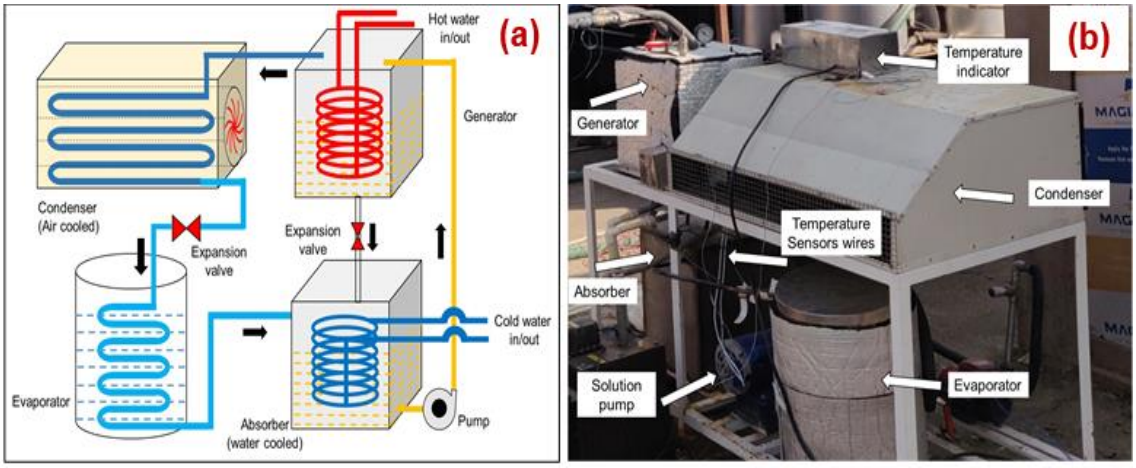

Figure 7.2.1: (a) Representation of absorption system, (b) actual absorption system setup

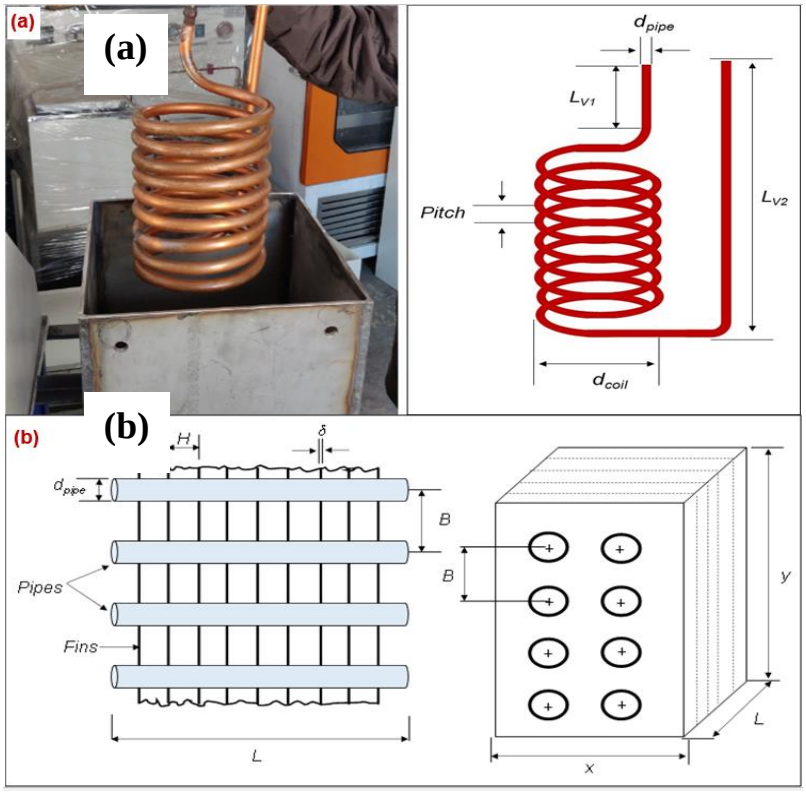

Figure 7.2.2: Details of heat exchangers (a) helical coil type (evaporator, absorber, generator), (b) condenser

7.2.2. Analysis of measured data

7.2.2.1. Heat transfer coefficient estimation

This study includes the estimation of overall heat transfer coefficient (U) for the different components of VA system (i.e., evaporator, absorber, generator and

condenser). In the calculation of U, the variable parameters are temperature of the generator (T_g) and the concentration of LiBr-water solution (c). Here, the T_g varies as 60 °C, 70 °C and 80 °C, whereas c varies from 54 % to 58 %. The literature [Pandya et al. 2017, and Iffa et al. 2017] shows that the optimum heat source temperature for single stage absorption systems is around 75ºC - 95ºC. Hence, the T_g limit (80 ºC) selection in the current study is based on the availability of heat source/hot water temperature at the working site. Further, the value of c with 54 % is selected according to the market availability and maximum enrichment up to 58 % is done due to the crystallization problem at higher concentrations. Here, absorber, generator, and evaporator comprise helical-coiled heat exchangers, as shown in Figure 7.2.2a. The air-cooled condenser of the system is shown in Figure 7.2.2b.

In the absorption system, the heat capacity rates of the cooling and heating streams are estimated using the following equations [Demesa et al. 2018],

$$Q_e = \dot{m}_{Ref}\left(h_{Ref,in} - h_{Ref,out}\right) = \dot{m}_{cw} c_p (\Delta T)_e \tag{7.2.1}$$

$$U_e = \frac{Q_e}{A_e \times (\Delta T_{lm})_e} \tag{7.2.2}$$

$$\text{where, } A_e = (\pi \times d_{pipe} \times L_{coil}) + \left[\pi \times d_{pipe} \times (L_{v1} + L_{v2})\right] \quad \text{and } L_{coil} = \text{No. of turns} \times \pi d_{coil} \tag{7.2.3}$$

Here, the pitch effect is neglected as it is very small as compared with the coil diameter. The values of the enthalpy for the water refrigerant and solution at different points are obtained using conventional charts [Arora 2000]. The logarithmic mean temperature difference (ΔT_{lm}) for evaporation process is a function of chilled water temperature and boiling point of water refrigerant [Demesa et al. 2018] that can be found using Eq. (7.2.4),

$$(\Delta T_{lm})_e = \frac{(T_{cw,in} - T_{Ref,s}) - (T_{cw,out} - T_{Ref,s})}{\ln \dfrac{(T_{cw,in} - T_{Ref,s})}{(T_{cw,out} - T_{Ref,s})}} \tag{7.2.4}$$

For the absorber, the heat transmission rates of cooling water and inside solution and U values can be estimated using the following equations [Demesa et al. 2018],

$$Q_{a,inside} = \dot{m}_{Ref}(h_{Ref,in}) + \dot{m}_{ws}(h_{ws,in}) - \dot{m}_{ss}(h_{ss,out}) \tag{7.2.5}$$

$$\text{where, } \dot{m}_{Ref} = \frac{Q_e}{(h_{Ref,in} - h_{Ref,out})} \tag{7.2.6}$$

$$Q_{tw} = \dot{m}_{tw}(h_{tw,in} - h_{tw,out}) \tag{7.2.7}$$

$$U_a = \frac{(Q_{a,inside} + Q_{tw})/2}{A_a \times (\Delta T_{lm})_a} = \frac{Q_a}{A_a \times (\Delta T_{lm})_a} \tag{7.2.8}$$

In the absorber, it is presumed that the heat transport occurs at the equilibrium temperature of the LiBr-water [Demesa et al. 2018]. So ΔT_{lm} for the absorber can be estimated by Eq. (7.2.9),

$$(\Delta T_{lm})_a = \frac{(T_{sol,equ} - T_{tw,out}) - (T_{sol,out} - T_{tw,in})}{\ln \frac{(T_{sol,equ} - T_{tw,out})}{(T_{sol,out} - T_{tw,in})}} \tag{7.2.9}$$

In the vapor absorption system, circulation ratio (λ). Using λ, mass flow rate of strong solution ($\dot{m}_{ss}$) and weak solution ($\dot{m}_{ws}$) can be estimated using the following equations [Pandya et al. 2017],

$$\lambda = \frac{\dot{m}_{ws}}{\dot{m}_{\text{Ref}}} = \frac{c_{ss}}{c_{ws} - c_{ss}} \tag{7.2.10}$$

$$\dot{m}_{ws} = \dot{m}_{\text{Ref}} \times \lambda$$
$$\dot{m}_{ss} = \dot{m}_{\text{Ref}} \times (\lambda + 1) \tag{7.2.11}$$

The generator heat capacity rates, heat transfer by hot water, and generator *U* value can be obtained using the following equations [Wang et al. 2017],

$$Q_{sol,g} = \dot{m}_{\text{Ref}}(h_{\text{Ref},Out}) + \dot{m}_{ws}(h_{ws,out}) - \dot{m}_{ss}(h_{ss,in}) \tag{7.2.12}$$

$$Q_{hw} = \dot{m}_{hw}(h_{hw,in} - h_{hw,out}) \tag{7.2.13}$$

$$U_g = \frac{(Q_{sol,g} + Q_{hw})/2}{A_g \times (\Delta T_{lm})_g} = \frac{Q_g}{A_g \times (\Delta T_{lm})_g} \tag{7.2.14}$$

$$\text{where, } (\Delta T_{lm})_g = \frac{(T_{hw,in} - T_{equ,g}) - (T_{hw,out} - T_{sol,in})}{\ln \frac{(T_{hw,in} - T_{equ,g})}{(T_{hw,out} - T_{sol,in})}} \tag{7.2.15}$$

The area of absorber (A_a) and generator (A_g) are same as that of the evaporator section. Next, for the condenser, the overall heat transport may be computed using the following set of equations. The net heat transmission area of the condenser is summation of tube and fins surface areas, which can be calculated as,

$$Q_{c,\text{Ref}} = \dot{m}_{\text{Ref}}(h_{\text{Ref},c,in} - h_{\text{Ref},c,out}) \tag{7.2.16}$$

$$U_c = \frac{Q_{c,\mathrm{Ref}}}{A_c \times (\Delta T_{lm})_c} \tag{7.2.17}$$

where, $A_c = A_{bare} + A_{fin}$

$$A_{bare} = N\left[\pi d_{pipe}(L_{row} - n\delta)\right] + N_{bend}(\pi d_{pipe} L_{bend})$$

$$A_{fin} = \left(2 \times \left[(xy) - N\frac{(\pi d_{pipe}^2)}{4}\right] \times n\right) + 2(\delta y) \times n \tag{7.2.18}$$

$$n = \frac{L_{row}}{H}$$

For the present analysis, fixed parameters related to the system can be found in reference [J5]. For the condenser, $(\Delta T_{lm})_c$ is obtained using the conventional method [Wang et al. 2017]. Other parameters used for obtaining the overall heat transfer coefficient are also provided in published work [J5]. Using the concept of mass conservation and considering the concentrations of the solutions entering (c_{ss}) and leaving (c_{ws}) the generator in the transient process, the conservation equation obtained is as follows [Wang et al. 2017],

$$\dot{m}_{ss} \cdot c_{ss} - m_{ws} \cdot c_{ws} - \dot{m}_{Ref,des} \cdot c_{Ref} = \frac{d(M_{sol,g} \cdot c_{ws})}{dt} \tag{7.2.19}$$

where, $\dot{m}_{Ref,des}$ is the mass flow rate of the water refrigerant desorbed from the solution and $M_{sol,g}$ is the total mass of the solution available inside the generator. The concentration of the water refrigerant will become zero. The mass conservation equation for the generated water vapor can be written as,

$$\dot{m}_{Ref,des} - \dot{m}_{Ref} = \frac{dM_{Ref,g}}{dt} \tag{7.2.20}$$

where, $M_{Ref,g}$ is the mass of water vapor refrigerant available in the generator. The properties of the solution available inside the generator housing is assumed similar to that of the solution leaving the generator [Wang et al. 2017]. The overall volume of the generator can be estimated using the following equation,

$$\frac{M_{sol,g}}{\rho_{ws}} + \frac{M_{Ref,g}}{\rho_{Ref,vapor}} = V_g \tag{7.2.21}$$

where, ρ_{ws} and $\rho_{Ref,vapor}$ are the density of the concentration-dependent weak solution (weak in refrigerant) leaving the generator, and water vapor leaving the generator, respectively. Further, V_g is the volume of generator. Here, in this study the volume of

absorber and evaporator are kept the same [Evola et al. 2013] and corresponds to its maximum value obtained after varying T_g and c.

7.2.2.2. Box-Behnken design (BBD) and analysis

Here, a response surface study has been performed for the developed prototype. For this purpose, 3-level BBD has been used to analyze various system-driving parameters' contribution to the parameters of interest. Here, two performance parameters are investigated, these are evaporator capacity (Q_e) and evaporator temperature (T_e). In this context, by performing screening analysis, 3 main operating parameters (namely: generator temperature (T_g), LiBr-water solution concentration (c), and hot water mass flow rate ($\dot{m}_{hw}$) are selected. At steady-state and for a given generator temperature (for example, T_g = 80^{o}C), the entering solution's concentration (for example, 58 %) and temperature (for example, T_{ss} = 38^{o}C), and leaving solution's concentration (say, 64 %) and temperature (for example, T_{ws} = 80 ^{o}C) remain almost fixed, so these parameters have not been considered in the correlation. In the present study, analysis has been focused for the fixed design specification. The role of key/major performance parameters like initial concentration, c, generator temperature, T_g and hot water mass flow rate, $\dot{m}_{hw}$ has been assessed.

The BBD is a generally used technique for experimental design [Rajeb et al. 2020]. BBD is established on a 3-level design: lower (-1), upper (+1) and middle points (0). The number of required runs for getting the predicted response can be estimated as, $2q(q\text{-}1) + p$, where p is the number of replicates at the center point for q number of driving factors. BBD obtains second degree polynomials between the response and operating parameters as follows [Rajeb et al. 2020],

$$Y = \alpha_0 + \sum_{q=1}^{3} \alpha_q X_q + \sum_{q=1}^{3} \alpha_{qq} X_q^{\,2} + \sum_{b=1}^{2} \sum_{q=b+1}^{3} \alpha_{qb} X_q X_b \qquad (7.2.22)$$

where, $X_1 \ldots\ldots X_3$ are the controlling/driving variables signifying T_g, c and $\dot{m}_{hw}$ for various response like Q_e and T_e as designated by Y. The value of coefficients are computed using Minitab and these are discussed later. Using the BBD for the set of driving parameters, only 15 experiments need to be done to obtain the correlation. Minitab is used for obtaining the orthogonal array of L15 type for the current work. After creating orthogonal array, 15 experiments are carried out on the experimental setup to get the response corresponding to the each set of experiment. The level

assignments are as follow: Level 1 (T_g = 60°C, c = 54 %, $\dot{m}_{hw}$ = 0.50 kg/s), Level 2 (T_g = 70°C, c = 56 %, $\dot{m}_{hw}$ = 0.67 kg/s) and Level 3 (T_g = 80°C, c = 58 %, $\dot{m}_{hw}$ = 0.84 kg/s).

Table 7.2.1: Uncertainty in parameters; ($T_g = 80 \pm 0.05$ °C, $c = 58 \pm 0.005$ %, $\dot{m}_{hw} = 0.667 \pm 0.0055$ kg/s)

Parameter	$T_{e,\,avg}$	$Q_{e,\,avg}$	$\dot{m}_{hw,avg}$	P_{avg}	c_{avg}
Absolute uncertainty	0.028 °C	0.0132 kW	0.0032 kg/s	0.76 kPa	0.0028

7.2.2.3. Error analysis

The absolute uncertainty (i.e., ψ_θ) for any parameter $\theta = f(K_1, K_2, K_3 ..... K_n)$, where, K is the number of independent quantities, is estimated using Eq. (7.2.23) [Moffat 1982],

$$\psi_\theta = \left[\left(\frac{\partial \theta}{\partial K_1} \times \psi_{K_1} \right)^2 + \left(\frac{\partial \theta}{\partial K_2} \times \psi_{K_2} \right)^2 + \left(\frac{\partial \theta}{\partial K_3} \times \psi_{K_3} \right)^2 + ... + \left(\frac{\partial \theta}{\partial K_n} \times \psi_{K_n} \right)^2 \right]^{0.5} \quad (7.2.23)$$

Using the above expression, uncertainty in the mean temperature with three replicates can be computed. The temperature data values are obtained from thermocouples with digital indicator. The least count of the indicator is 0.1 °C. So, the improbability in the measured temperature is taken as half of the least count (i.e., ψ_T = 0.05 °C). Here, the uncertainty in all replicates of temperatures is the same (i.e. $\psi_{T_1} = \psi_{T_2} = \psi_{T_3}$). The uncertainties values of various parameters are listed in Table 7.2.1

7.2.3. Results and analyses

The first portion deals with estimating and analyzing the overall heat transmission coefficient concerning different components of the developed absorption chiller. The second and third portions include the investigation of response surface design outcomes and inverse analysis.

7.2.3.1. Analysis of heat transport coefficient

The experiments on the developed setup were performed at different design conditions of c and T_g till the steady-state was achieved under the $\dot{m}_{hw}$ = 0.67 kg/s and other fixed

input parameters. All experiments were performed for the local weather conditions that are similar to the composite weather with environmental temperature varying in the range 35±1ºC. Using the temperature data, the values for enthalpy of water refrigerant can be estimated using steam table, and for LiBr-water solution, enthalpy is estimated using the available enthalpy-temperature-concentration chart.

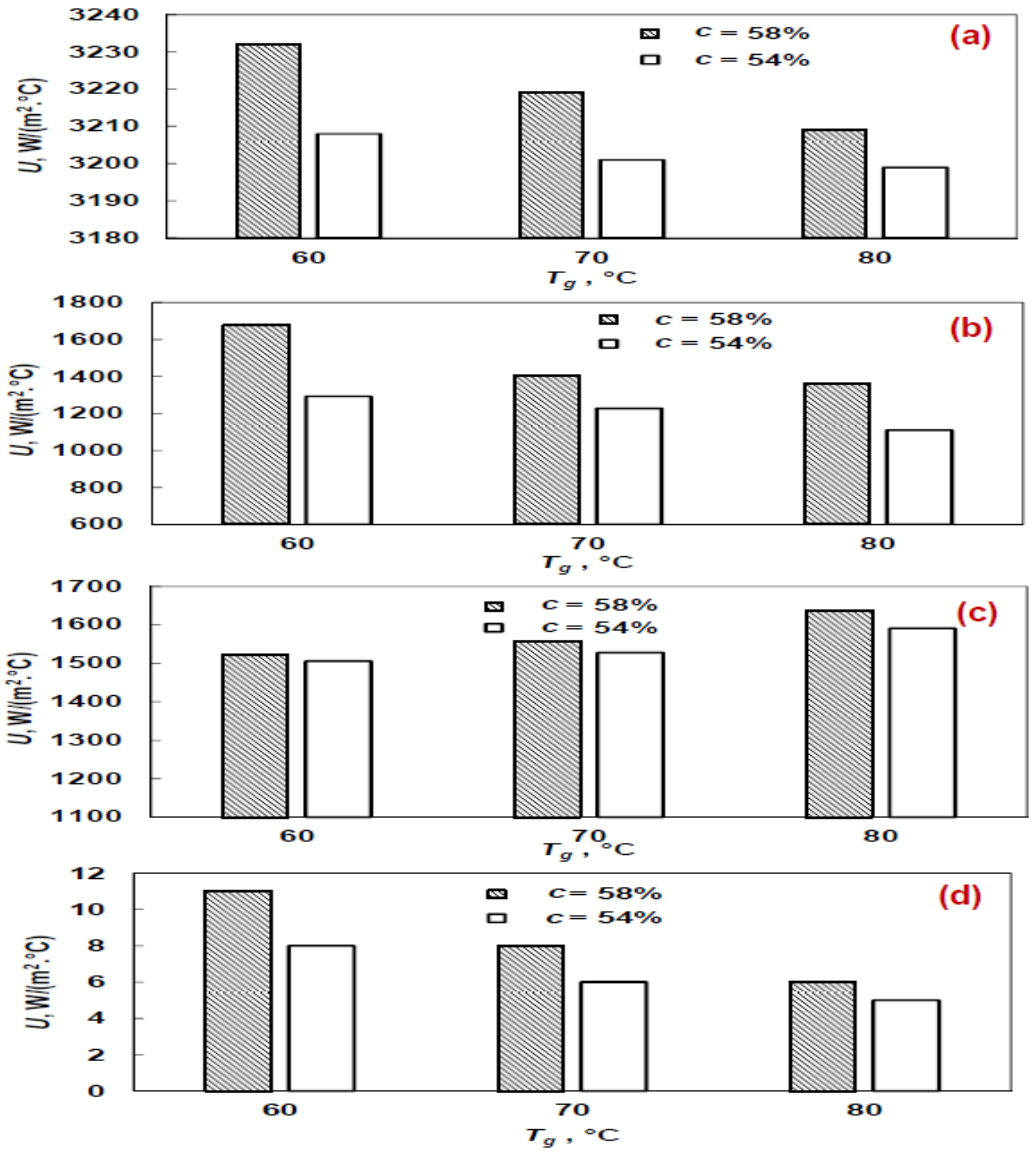

Figure 7.2.3: Variation in U at different T_g and c, (a) evaporator, (b) absorber, (c) generator and (d) condenser

Figure 7.2.3 shows the U values for the different components of the absorption system at different operational circumstances. For instance, the U value for the evaporator lies in the range of 3199-3232 W/(m^2.°C), whereas, the benchmark [Cengel 2014] value occurs in the range 1000-6000 W/(m^2.°C). Further, the values of U for the absorber,

generator and condenser respectively vary between (1110-1677) W/(m^2.°C), (1506-1637) W/(m^2.°C) and (5–11) W/(m^2.°C), whereas, the same for solution heat exchangers (like: absorber and generator) should lie within 850-1700 W/(m^2.°C) [33] and for condensers, it should be within 9-47 W/(m^2.°C) [Rouag et al. 2016].

From Figure 7.2.3, it is observed that the U values for any component of absorption system is lower in the case of c = 54 % as compared to that for c = 58 %. The reason is that Q values are lower for c = 54 % than those for c = 58 %, for any component. However, in case of ΔT_{lm}, the same is only true for evaporator and generator, whereas, the opposite is applicable for absorber and condenser [J5]. So, for evaporator and generator, the effect of increased ΔT_{lm} to cause decrement in U value is surpassed by increased Q values. In the published work [J5] it is further highlighted that capacity of the system, Q upsurges with both T_g and c, when any one is held at a constant value. For same T_g value, the reason for enhancement in cooling capacity is due to c value enrichment that increases affinity between the concentrated solution at absorber and the generated water/refrigerant vapor of evaporator. This affinity provides a driving force to transfer the vapor at a higher rate from evaporator to absorber section and due to this, capacity of the system improves. On the other hand, for a given value of c, at increased values of T_g, more refrigerant is liberated from the solution that causes the respective value of evaporator capacity Q_e to increase. Further, for a given value of c, with increase in T_g , U values for evaporator, absorber and condenser drop (Figure 7.2.3 a, b and d), while for generator (Figure 7.2.3c), it upsurges. This is essentially due to the ratio of Q and ΔT_{lm}, and it may be concluded that the increment of ΔT_{lm} is considerable than increment of Q, for evaporator, absorber and condenser section. But, the opposite is true for the generator [J5].

Theoretical pressure data values can be obtained by using the conventional methods (charts or equation) [Thomson 1946], whereas, the installed vacuum gauges measure the actual pressure data values. The saturation pressure corresponding to a particular condensing and evaporator temperature is estimated as [Thomson 1946],

$$\ln(P)_{sat} = Z_0 - \frac{Z_1}{(T + 273.15) + Z_2}; \text{ where, } Z_0 = 16.54, Z_1 = 3985 \text{ and } Z_2 = -39.0 \quad (7.2.24)$$

For the present study, the lowest average evaporator temperature (T_e) attained by the absorption chiller is 13.5 °C, and the condensing temperature (T_c) approximates around

38 °C for T_g = 80 °C, $\dot{m}_{hw}$ =0.67 kg/s, c = 58% and considering other input variables unchanged. Using Eq. (7.2.24), the saturation pressure obtained at the evaporator and condenser sections should be 1.56 kPa and 6.66 kPa, respectively. On the other hand, under the actual operating conditions, the values of pressures measured by the vacuum pressure gauge at the lower side and higher side of the absorption chiller are observed as 1.99 kPa and 7.33 kPa (absolute scale), respectively. The theoretical pressure drop $(\Delta P)_{Theoretical}$ from high pressure to low pressure side is nearly 5.10 kPa, while, the actual pressure drop $(\Delta P)_{Actual}$ is observed as 5.34 kPa. The percentage error between the actual and theoretical pressure drops is 4.71%.

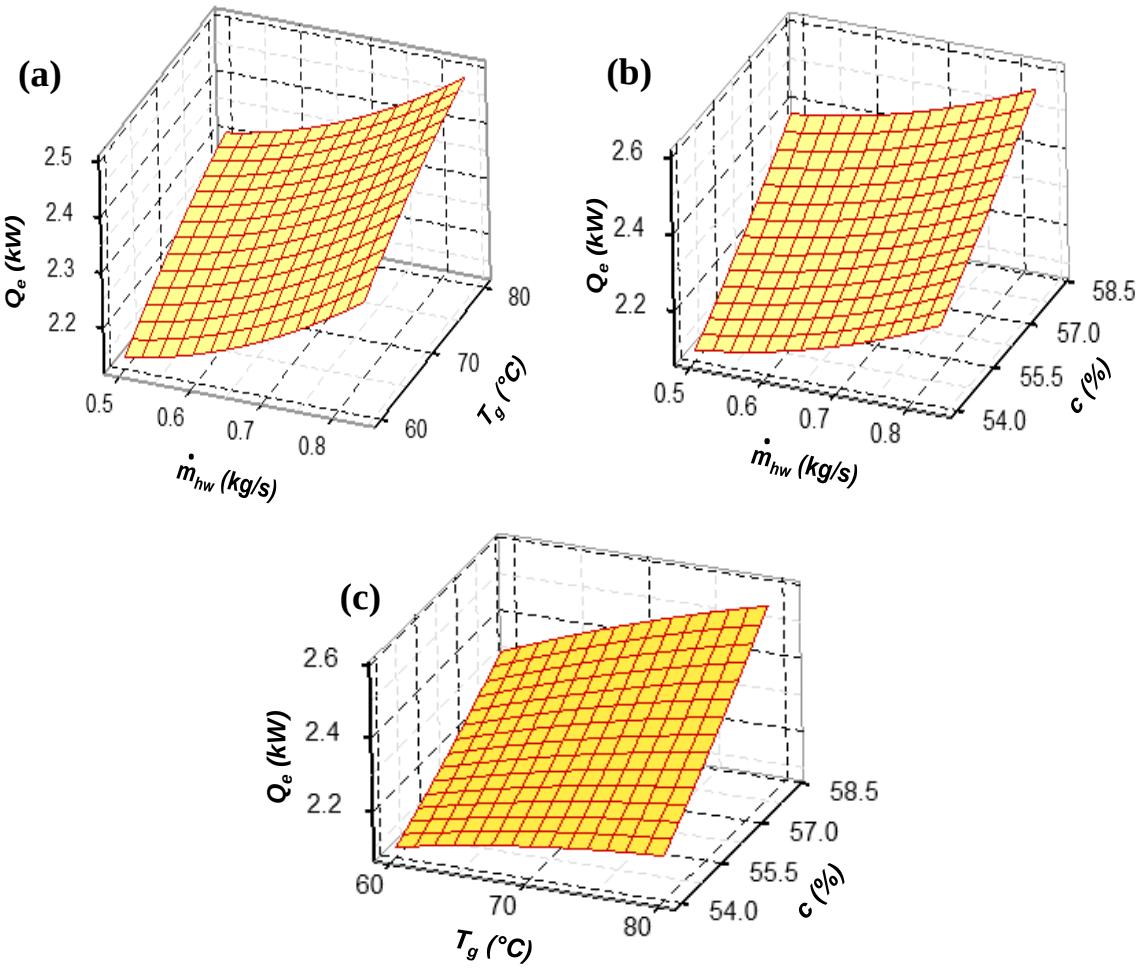

Figure 7.2.4: Effect of driving factors on Q_e at hold values, (a) c = 56%, (b) T_g = 70 °C and (c) $\dot{m}_{hw}$ = 0.67 kg/s

7.2.3.2. Analysis of response surface methodology

In this study, 3-level *BBD* has been implemented to evaluate the impact of system-driving factors (T_g, c, and $\dot{m}_{hw}$) the system-driven factors (Q_e and T_e). Table 7.2.2,

shows the orthogonal array comprising 15 experimental amalgamations of input/operating factors obtained using Minitab of *BBD*. The remaining input parameters (for instance, $\dot{m}_{cw}$ and $\dot{m}_{tw}$) other than these driving factors (T_g, c, and $\dot{m}_{hw}$) have been held constant. The corresponding experimental results against each combination are also shown in Table 7.2.2. As a final task, empirical correlations have been constructed for each system-driven factor in terms of the three system driving factors.

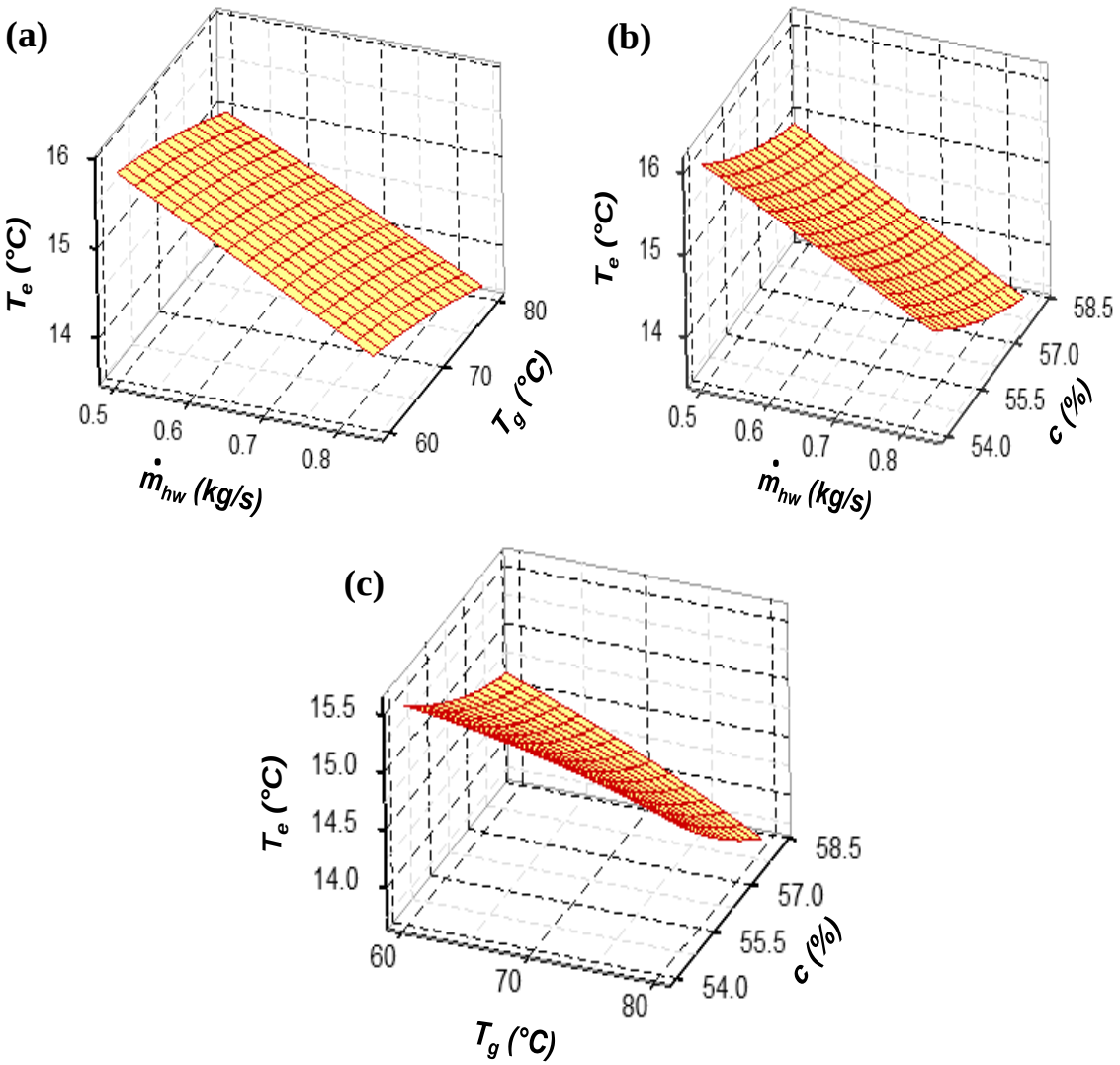

Figure 7.2.5: Effect of driving factors on T_e at hold values, (a) c = 56%, (b) T_g = 70 °C and (c) $\dot{m}_{hw}$ = 0.67 kg/s

In Figure 7.2.4 and Figure 7.2.5, the surface plots are drawn to show the combined effect of three independent operating/driving factors on the two performance/driven parameters by altering one, while keeping other constant. Figure 7.2.4 illustrates the effect of different combinations of operating factors on the evaporator capacity (Q_e) output. As T_g increases, the capacity of the absorption system, consequently it can be

said that $\dot{m}_{\text{Ref}}$ increases through condenser and evaporator. From Figure 7.2.4a, it is evident that Q_e increases as $\dot{m}_{hw}$ and T_g increase. The same effect can be observed in the case of LiBr concentration enrichment (Figure 7.2.4b), which causes the system to draw more refrigerant due to enhancement in absorber's affinity for water refrigerant. The combined effects of c and T_g on Q_e (Figure 7.2.4c) show that concentration enrichment is more important than the generator temperature.

Figure 7.2.5 deals with the impact of different combinations of driving factors on the obtained chilled water/evaporator temperature (T_e). This is actually the temperature of chilled water that is circulated around the coils of the evaporator. From Figure 7.2.5a, it is noticed that as T_g increases in the 60 °C to 80 °C, the minimum Te reduces due to high concentration of water refrigerant inside the solution. The same effect is noticed when the solution enrichment is done (Figure 7.2.5b, c). The minimum evaporator temperature obtained for the current prototype was around 13.4 °C with the operating conditions of generator temperature, concentration, and mass flow rate as 80 °C, 58 % and 0.84 kg/s, respectively. For T_e, the importance of all three factors (c, $\dot{m}_{hw}$ and T_g) are observed to be nearly equal.

After getting the various response surface plots for different combinations, *BBD* model provides the following second-order empirical correlations for the output performance parameters as shown below,

$$Q_e = 12.8 - 0.367\ c - 0.0774\ T_g - 0.79\ \dot{m}_{hw} + 2.81\times10^{-3}\ c^2 - 1.37\times10^{-4}\ T_g^2 + 0.995\dot{m}_{hw}^2 + 1.875\times10^{-3}\ c\cdot T_g - 1.0\times10^{-5}\ c\cdot\dot{m}_{hw} + 1.0\times10^{-6}\ T_g\cdot\dot{m}_{hw} \quad (7.2.25)$$

$$T_e = 80.8 - 2.46\ c + 0.378\ T_g - 0.98\ \dot{m}_{hw} + 0.0240\ c^2 - 5.42\times10^{-4} T_g^2 - 0.14\ \dot{m}_{hw}^2 - 6.25\times10^{-3}\ c\cdot T_g - 0.074\ c\cdot\dot{m}_{hw} + 0.0147\ T_g\cdot\dot{m}_{hw} \quad (7.2.26)$$

For the above correlations, values of correlation coefficient (R^2) for Q_e and T_e are 0.991 and 0.993, respectively, which show their accurateness.

Table 7.2.2: Experimental results for Q_e and T_e corresponding to the *BBD* combinations

	Combination for experiments			Experimental Results	
S. No.	c (%)	T_g (°C)	$\dot{m}_{hw}$ (kg/s)	Q_e (kW)	T_e (°C)
1	56	80	0.84	2.48	13.6
2	54	70	0.84	2.26	14.6
3	54	80	0.67	2.21	15.1
4	56	60	0.84	2.33	14.4
5	56	80	0.50	2.30	14.9
6	54	70	0.50	2.07	16.1
7	58	80	0.67	2.57	13.8
8	56	70	0.67	2.30	14.7
9	54	60	0.67	2.10	15.5
10	56	70	0.67	2.30	14.8
11	58	70	0.50	2.42	15.1
12	58	70	0.84	2.61	13.5
13	56	60	0.50	2.15	15.8
14	58	60	0.67	2.31	14.7
15	56	70	0.67	2.30	14.8

7.2.4. Conclusion

This study has experimentally studied a compact LiBr-water driven absorption chiller of 1 ton capacity. Using experimental results, new empirical correlations for its performance in terms of evaporator load and temperature against system driving factors such as concentration, hot water supply and temperature needed at the generator end have been developed. Box-Behnken design based response surface analysis has been done to analyze the variation of system driven parameters with respect to the factors driving the system. Thereafter, estimation of overall heat transfer coefficient (U) for each component is done. Other outcomes of the study are discussed below,

- By increasing the generator temperature, U values for evaporator, absorber and condenser decrease, whereas for generator this value increases. This is attributed to the mutual interplay between the system log mean temperature difference and heat load (Q).

- By increasing LiBr concentration, *U* and *Q* values for all components always increase. However, log mean temperature difference is found to increase in case of evaporator and generator, whereas, the same for absorber and condenser exhibit a reverse trend.
- With upsurge of the generator temperature, circulation ratio decreases that causes both mass flow rates of weak and strong solutions to decrease. But, at the same time, it increases the concentration of LiBr in the weak solution as well as increases the mass flow rate of refrigerant.

CHAPTER 8

* ASSESSMENT OF DIFFERENT AIR-CONDITIONING SYSTEMS FOR A COMMON BUILDING

This chapter examines the performance of all the above discussed air-conditioning systems on a single office building in terms of electrical energy. The ROIs of the different configurations are evaluated with respect to the conventional system. The effect of changing the value of overall heat transfer coefficient on the energy performance is also evaluated.

From the above discussion, it is observed that the performance of an air-conditioning system depends on the building structure, location, ambient conditions, input parameters, etc. Previously, in this thesis, the performance of various air-conditioning technologies has been assessed for a different place and building structure. Therefore in this chapter, an energy performance assessment of other air-conditioning systems has been done for a common building with the same location and input parameters. Further, the economic analysis has also been performed for all the configurations against the conventional VC-driven system.

8.1. System and building description

This study aims to analyze the energy consumption analysis of all the above-discussed configurations for a single common building structure with the same input variables. In this work, a medium office building of 5000 m^2 total floor area has been considered for evaluation purposes. The building layout is shown in Figure 8.1. The building consists of four floors with a total of 20 zones, each floor involving five zones. All the constructional parameters are taken as per the given reference standards [Khan et al. 2009 and Deru et al. 2011]. All the simulations have been done for the warm-humid climate. In this work, ten configurations are chosen for the energy analysis, shown in Figure 8.2. The details of varying building input parameters and obtained constructional properties are the same, as shown in Table 3.1.2. The description of different configurations is as follows.

Case 1 is conventional VC driven system, Case 2 is VA system in which solar and boiler are used for the thermal energy supply, Case 3 is radiant cooling system assisted by VC chiller with DOAS also assisted by VC system, Case 4 is VA coupled radiant cooling system with VC chiller based-DOAS. Next, Case 5 is a modified form of Case 3, where both desiccant and IEC have been coupled with VC based DOAS, while Case 6 is a modified form of Case 4, with desiccant and IEC being installed with VC-DOAS arrangement. Moving forward, Case 7 is the VRF based air-conditioning unit, and in Case 8, desiccant and IEC are also coupled in the DOAS with VRF based air-conditioning unit. Case 9 is a modified form of Case 1 where desiccant and IEC arrangements are coupled in the desiccant integrated DOAS with IEC installed to a VC system and lastly, Case 10 is the modified form of Case 9 in which an IEC is replaced with SHRW.

In Case 2 and Case 4, a loop of a solar collector with the natural gas boiler is installed to supply heat energy in hot water to the VA chiller. Along with this loop, an auxiliary heater is also installed to address any solar intermittency or system deficiency. The total seated solar collector area for supplying thermal energy to the VA chiller is around 650 m^2. In Case 6, another loop of a solar collector with an auxiliary heater, having a 500 m^2 collector area, is installed to feed the desiccant system; this 500 m^2 collector area loop is also used in Case 5, Case 8, Case 9, and Case 10.

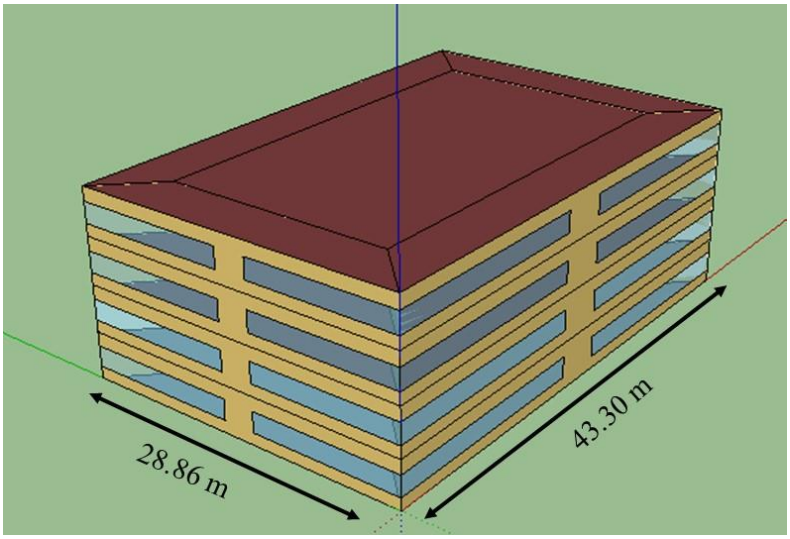

Figure 8.1: A medium scale office building considered for analyzing various air-conditioning strategies

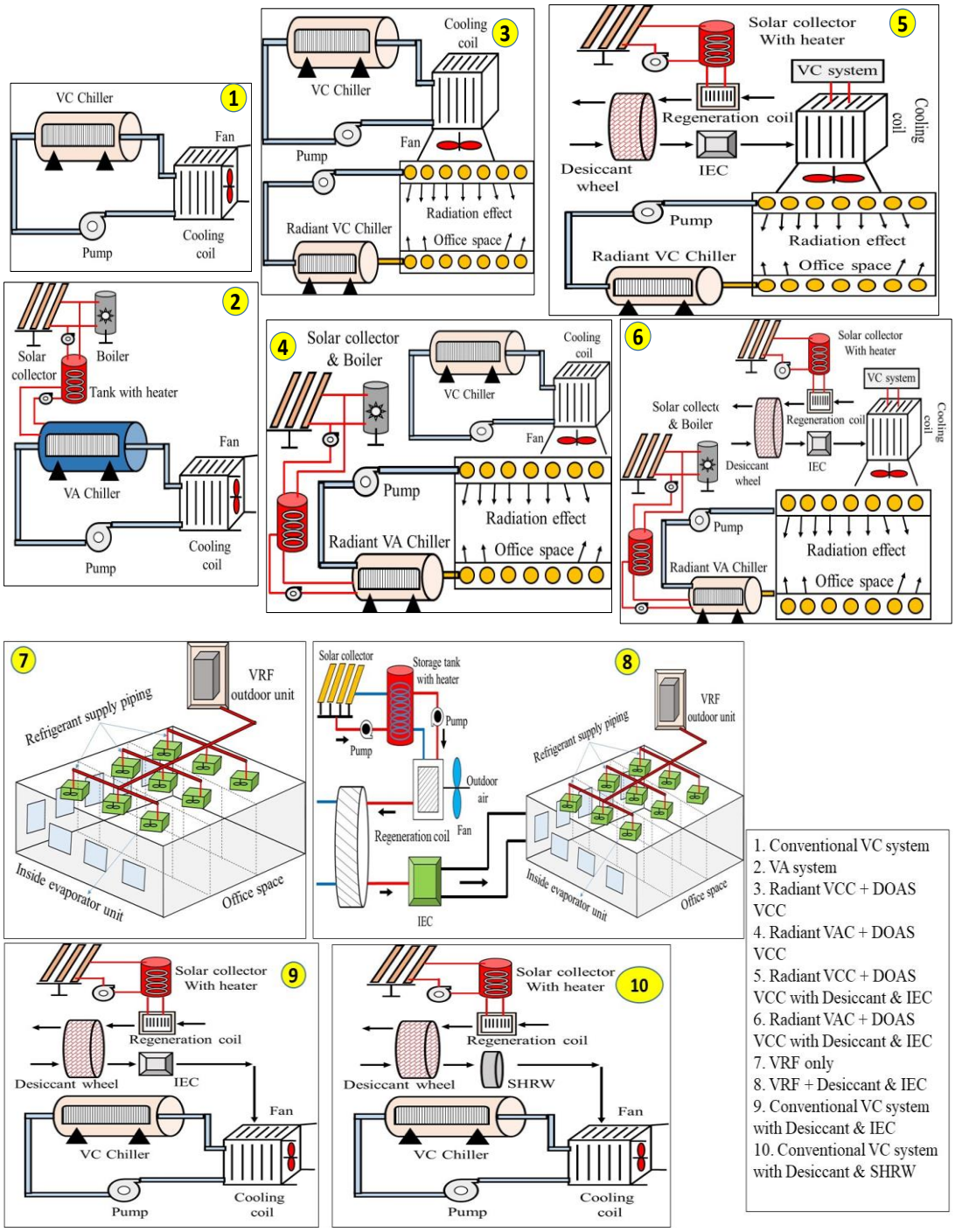

Figure 8.2: Schematic layout of different air-conditioning strategies

8.2. Energy consumption analysis and economic assessment

This study aims at evaluating the variational trends in the energy consumption for each configuration towards maintaining the required level of thermal comfort in the building. The annual electrical energy consumption analysis of different components installed in the air-conditioning system is shown in Figure 8.3. This analysis includes

the energy consumption of parts like the chiller, fan, pump, IEC, auxiliary heater, IEC, etc. From this figure, it is observed that the maximum energy consumption is in Case 2. In Case 2, the air-conditioning system depends entirely on the VA chiller only. The combined solar collector and boiler loop fulfill the VA chiller's thermal energy requirement. However, an auxiliary heater is also installed with this. From the simulation results, it is observed that in this particular case, according to the cooling demand of the building, the requirement of thermal energy is relatively high. In such conditions, the amount of solar energy delivered from the solar collector loop is not sufficient; therefore, the role of the auxiliary heater is very significant. The lowest energy consumption is observed in Case 6. The maximum energy savings of around 18.4% occurred in Case 6 against Case 1. The percentage of energy savings in Case 3, Case 4, Case 5, Case 6, Case 7, Case 8, Case 9, and Case 10 are 5.9%, 7.0%, 9.8%, 18.4%, 1.3%, 11.0%, 6.3%, and 13.0%, respectively.

Table 8.1: ROI assessment of different air-conditioning configurations

System	Total cost, in INR	Total annual electricity consumption, kWh	Excess cost with respect to case 1, INR	Cost of energy savings per year (INR/Year)	ROI, Years
Case 1	3610174	287861	NA (Base case)	NA (Base case)	NA (Base case)
Case 2	6628530	1071925	3018356	-784064 (Loss)	NA (Loss)
Case 3	8342750	270609	4732576	172520	27.43
Case 4	11050018	267433	7439844	204280	36.41
Case 5	10146665	259649	6536491	282120	23.16
Case 6	13319654	234729	9709480	531320	18.27
Case 7	3996260	284011	386086	38500	10.02
Case 8	6092974	255931	2482800	319300	7.77
Case 9	4688283	269634	1078109	182270	5.91
Case 10	4593729	250160	983555	377010	2.60

Here, the economic assessment has also been done to evaluate the ROI of the different systems (Cases 2-10) against the conventional VC-based system (Case 1). The cost of each component installed in the air-conditioning unit is considered according to the peak rated capacity of the element. The ROI of the different systems is evaluated by using the ratio of the access cost of the system to the cost of energy savings per year. Detailed procedure can be found in the published studies J1, J2, J3 and J7. By considering the price of 10 INR for each unit of electricity, the ROI of different configurations is evaluated in Table 8.1. It is found that minimum ROI is occurring for case 10 (i.e., VC system with desiccant and SHRW based DOAS), but, maximum energy saving potential occurs for case 6 (i.e., Radiant VAC with VC DOAS integrated with desiccant and IEC). This is because the installed components in Case 6 cost more than the revenue saved by reducing the electrical energy consumption. However, it is worth to mention here that the ROI is highly dependent upon the area of building and prevailing weather conditions.

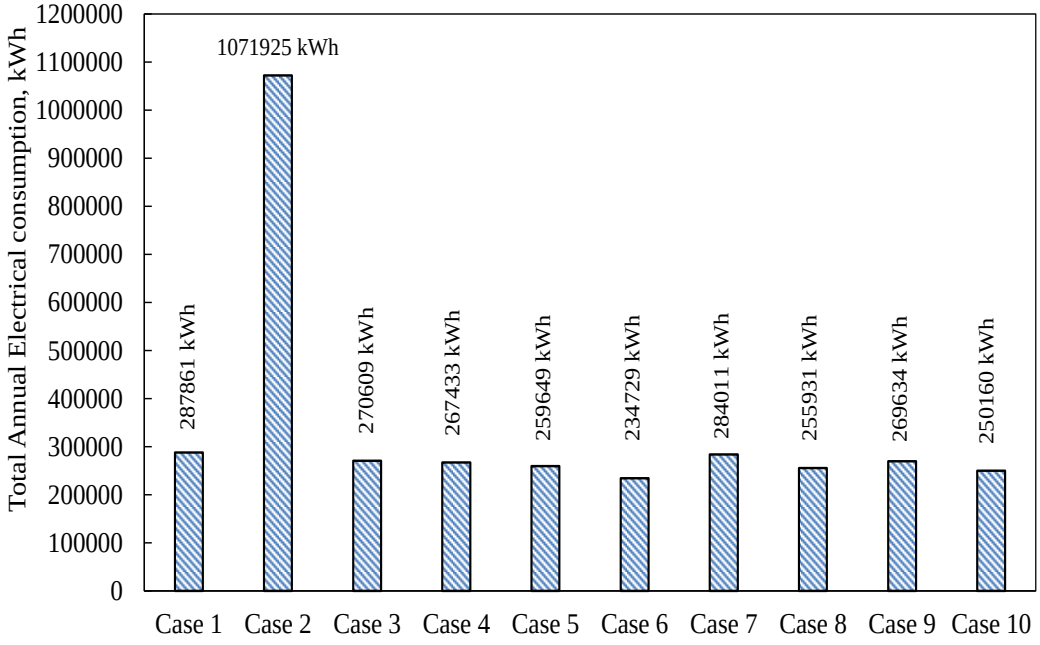

Figure 8.3: Total annual energy consumption for each air-conditioning configuration

8.3 Effect of *U* value on energy performance

This work also deliberates on estimating the effect of changing *U* value on the system energy performance. The variation in the *U* value of the building's opaque envelope, like roof and wall, is attained by changing the constructional property of the wall and

ceiling. For this purpose, only one property: the thermal conductivity of gypsum plaster is varied by the value of ±0.1 with the initial value of 0.16 W/(m.K). Then, simulations have been done on Case 1 with three values of gypsum plaster conductivity, namely, 0.15 W/(m.K), 0.16 W/(m.K), and 0.17 W/(m.K). These three thermal conductivity values provide three different *U* values for wall and roof, as shown in Figure 8.4. It can be observed that the increase in thermal conductivity augments the U value for the wall and roof. The effect of changing the *U* value on the annual electricity consumption is shown in Figure 8.4. It can be observed that the impact of the *U* value is not significant on the yearly electrical energy requirement. A minor increment in energy consumption is observed from this figure.

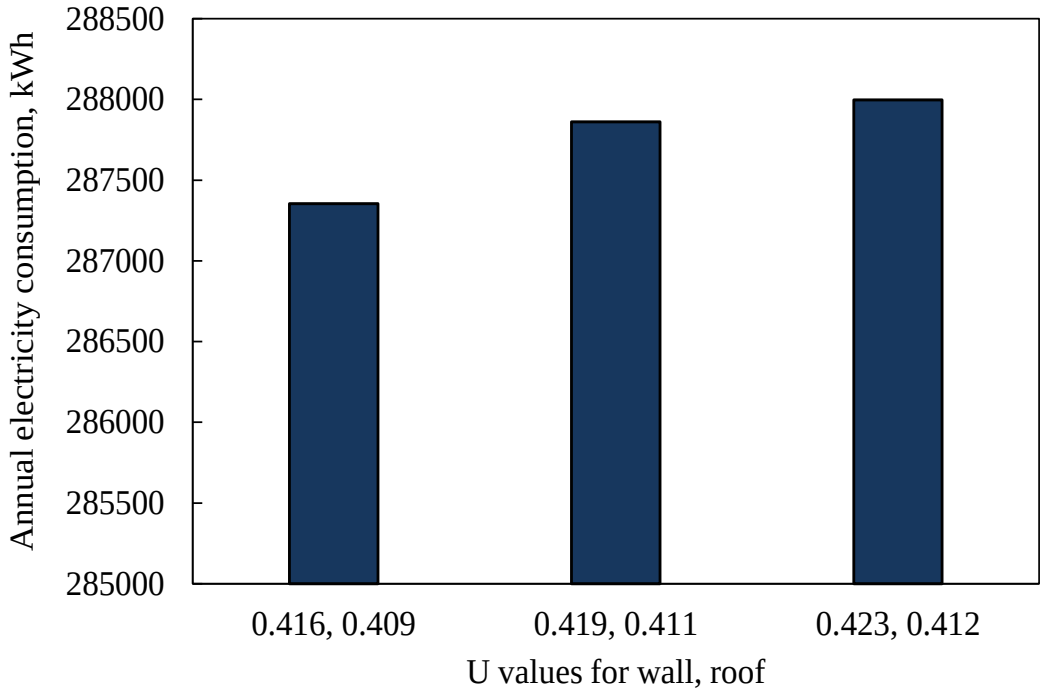

Figure 8.4: Annual energy consumption for different values of wall and roof heat transfer coefficients (for Case 1, i.e., conventional VC system)

8.4. Conclusion

In this study, the energy consumption evaluation for different air-conditioning system on a common office building has been done for warm-humid climatic conditions. Here, all the VA based chillers are operated with solar, boiler and auxiliary heater based systems. From, the energy consumption analysis, it was revealed that the maximum energy savings was attained with VA chiller based radiant cooling system with desiccant-IEC assisted DOAS against the conventional VC driven system. The energy

consumption of only VA chiller driven air-conditioning system is maximum due to limitation of thermal energy supply through solar collector. The auxiliary heater energy consumption is contributing a significant amount of energy due to which this case is showing maximum energy consumption. The economic assessment reveals that the minimum ROI is observed for Case 10 against the Case 1. It is an important observation that, the effect of changing the U value on the annual energy consumption is not significant.

CHAPTER 9

CONCLUSIONS, RECOMMENDATIONS AND FUTURE SCOPE

This thesis has presented various simulation and experimental studies on different configurations of air-conditioning systems to assess/evaluate the distinguish performance parameters such as: electrical, thermodynamic, etc. This thesis introduces the concept of integration of various renewable energy based resources such as: solar, biomass etc. with the commonly available air conditioning technology such as: vapor compression, vapor absorption, etc. to reduce or eliminate the grid dependency of building air-conditioning systems. From the above discussed studies following conclusions of practical interest can be drawn from this research work.

- Triple-hybridization is necessary with the VA based air-conditioning system to ensure continuous and satisfactory performance of the system throughout the year.
- By selecting a proper/discussed sized components such as: solar collector, pumps, heater etc., the solar, biomass and auxiliary electrical energy based triple-hybrid VACS saves up to 18.50 % of the annual electrical energy for warm and humid zone, and nearly 29.80 % of the annual electrical energy can be conserved in the composite environment With respect to a compression-based system.
- It is beneficial to Integrate IEC with the desiccant assisted DOAS as compared to the conventional DOAS.
- IEC and desiccant assisted DOAS coupled with absorption driven air-conditioning system provides surplus energy savings compared to the conventional VC driven system. This electrical energy savings can be attained up to 46% dependent on the climatic conditions.
- Energy savings attained by the absorption based air-conditioning system compared to the compression one is highly dependent on the installed solar collector area.

- Integration of the SHRW in place of IEC in the desiccant assisted DOAS will provide more energy savings. Under the composite climatic condition, SHRW driven DOAS provides around 5.04% of annual electrical energy savings.
- Double stage absorption system provides significant energy savings compared to the single-stage absorption (up to 83% savings) and compression driven system (up to 58% savings). However, the required heat source temperature in double-stage system is quite higher than single-stage one.
- Triple hybrid absorption chiller based radiant cooling system with desiccant dehumidification performs better than conventional design of radiant cooling system. It offers around 13.2% of electrical energy savings compared to the conventional radiant cooling design.
- The contribution of solar energy towards the total thermal energy requirement, i.e., solar fraction can be enhanced by adding either more advance solar collector system such as: point focused, line focused thermal collector can be used or increasing the area of solar collector.
- It is interestingly highlighted that, the absorption based radiant air-conditioning system offers better energy saving compared to the conventional compression driven radiant cooling systems. However, under the condition of solar energy as a resource medium only, the target of the grid independent energy building status can be achieved by compression driven radiant cooling systems. This is valid for composite and hot-dry climatic conditions. But it is also useful under warm-humid climates.
- With any configuration of air-conditioning, the possibility of attaining the grid independent energy building target is always minimum under warm-humid environmental condition.
- Energy savings are also possible in the air-conditioning setup by integrating solar energy with desiccant material in a VRF system.
- Solar energy-based desiccant-assisted VRF saves around 23.9 % and 9.5 % of electrical energy compared to the conventional all-air/VAV and VRF system, respectively under warm-humid climate. Under composite climate

these saving are 13.8 % and 9.4 %, respectively, whereas, these savings for hot-dry climate are 17.5 % and 11.6 %, respectively.

- A triple-hybrid grid-independent absorption cooling system has been developed to achieve the grid independent criterion and that system address various environmental concerns.
- The experimental results of the developed/fabricated system reveals the better performance of system under the condition of 58% salt solution concentration and high generator temperature (80 °C) condition.
- The developed prototype can control the indoor air temperature up to 27.5 ºC against 58% concentration solution and generator temperature of 80 ºC. This configuration shows the system's maximum cooling ability and COP as 4.09 kW and 0.34, respectively.
- Using experimental results, new empirical correlations for absorption system performance in terms of evaporator load and temperature against system driving factors such as concentration, hot water supply and temperature needed at the generator end have been reported with satisfactory performance.
- Other experimental analysis highlights that, by increasing the generator temperature, *U* values for evaporator, absorber and condenser decrease, whereas for generator this value increases. This is attributed to the mutual interplay between the system log mean temperature difference and heat load (*Q*).

At last, some of the recommendations and future scopes for the use and extension of present thesis work have been discussed in the succeeding section. In the future, the integration of some kind of thermal energy storage with the refrigeration unit can be explored to shuffle the peak load profile of electricity consumption pattern. Further, the performance of absorption system is highly dependent on the vacuum level of system. By some means, if we increase the vacuum level inside the absorption system that will improve the cooling capacity of the system by keeping the same other associated parameters.

Although the air-conditioning system have been comprehensively analyzed by researchers across the globe, nevertheless there is much scope for future research on

reducing the energy consumption, reducing peak load demand on grid, sustainable development etc. and effect of various system parameters that could prove useful. Some research gaps on this topic that should be addressed are mentioned below.

- Investigation of the radiant cooling system with integration of cooling tower for sensible load catering inside the building.
- Addressing/reducing the condensation problems on the radiant panels.
- Integration of highly efficient, high tempering operating range solar collector for the double stage absorption system.
- Excess available solar thermal energy can be used further for storing heat in thermal energy storage, process heating/drying, waste heat recovery devices etc.

REFERENCES

Abdulateef, J.M., Sopian, K., Alghoul, M.A. and Sulaiman, M.Y., 2009. Review on solar-driven ejector refrigeration technologies. Renewable and Sustainable Energy Reviews, 13(6-7), pp.1338-1349.

Agyenim, F., Knight, I. and Rhodes, M., 2010. Design and experimental testing of the performance of an outdoor LiBr/H_2O solar thermal absorption cooling system with a cold store. Solar Energy, 84(5), pp.735-744.

Ahlborn, B.K. and Gordon, J.M., 2000. The vortex tube as a classic thermodynamic refrigeration cycle. Journal of Applied Physics, 88(6), pp.3645-3653.

Alabdulkarem, A., Cristiano, M., Hwang, Y. and Radermacher, R., 2015. Design and testing of a separate sensible and latent cooling packaged terminal air conditioning unit. In Energy Sustainability American Society of Mechanical Engineers, Vol. 56840, pp. V001T01A001.

Al-Alili, A., Hwang, Y., Radermacher, R. and Kubo, I., 2012. A high efficiency solar air conditioner using concentrating photovoltaic/thermal collectors. Applied Energy, 93, pp.138-147.

Al-Farayedhi, A., Gandhidasan, P., Antar, M.A. and Gaffar, A., 2002. Experimental study of hybrid liquid desiccant based vapor compression cooling system. In The 6th Saudi Engineering Conference, KFUPM, Dhahran, December 2002.

Alhamid, M.I., Coronas, A., Lubis, A., Ayou, D.S., Saito, K. and Yabase, H., 2020. Operation strategy of a solar-gas fired single/double effect absorption chiller for space cooling in Indonesia. Applied Thermal Engineering, 178, pp.115524 1-14.

Ali, M., Habib, M.F., Sheikh, N.A. and Akhter, J., 2022. Experimental investigation of an integrated absorption-solid desiccant air conditioning system. Applied Thermal Engineering, 203, pp.117912 1-13.

Ali, M., Vukovic, V., Muhammad Ali, H. and Ahmed Sheikh, N., 2018. Performance analysis of solar-assisted desiccant cooling system cycles in world climate zones. Journal of Solar Energy Engineering, 140(4), pp. 041009 1-14.

Alobaid, M., Hughes, B., Calautit, J. K., O'Connor, D., and Andrew, H., 2017. A Review of solar driven absorption cooling with photovoltaic thermal systems, Renewable and Sustainable Energy Reviews, 76, pp. 728–742.

Al-Ugla, A.A., El-Shaarawi, M.A.I., Said, S.A.M. and Al-Qutub, A.M., 2016. Techno-economic analysis of solar-assisted air-conditioning systems for commercial buildings in Saudi Arabia. Renewable and Sustainable Energy Reviews, 54, pp.1301-1310.

Aman, J., Henshaw, P. and Ting, D.S., 2018. Bubble-pump-driven LiBr-H_2O and LiCl-H_2O absorption air-conditioning systems. Thermal Science and Engineering Progress, 6, pp.316-322.

Arora, C. P., 2000, Refrigeration and Air-Conditioning, Tata McGraw-Hill, New Delhi, India.

Arun, M.B., Maiya, M.P. and Murthy, S.S., 2001. Performance comparison of double-effect parallel-flow and series flow water–lithium bromide absorption systems. Applied Thermal Engineering, 21(12), pp.1273-1279.

Ashassi-Sorkhabi, H., Kazempour, A. and Salehi-Abar, P., 2018. A new insight into ionic liquid-water mixtures used as absorbent-refrigerant pairs: Theoretical and potentiometric aspects. Journal of Molecular Liquids, 251, pp.190-200.

Assilzadeh, F., Kalogirou, S.A., Ali, Y. and Sopian, K., 2005. Simulation and optimization of a LiBr solar absorption cooling system with evacuated tube collectors. Renewable Energy, 30(8), pp.1143-1159.

Avanessian, T. and Ameri, M., 2014. Energy, exergy, and economic analysis of single and double effect LiBr–H_2O absorption chillers. Energy and Buildings, 73, pp.26-36.

Aynur, T.N., 2010. Variable refrigerant flow systems: A review. Energy and Buildings, 42(7), pp.1106-1112.

Aynur, T.N., Hwang, Y., Radermacher, R., 2010. Integration of variable refrigerant flow and heat pump desiccant systems for the heating season. Energy and Buildings, 42 (4), pp.468–476.

Basu, D.N. and Ganguly, A., 2015. Conceptual design and performance analysis of a solar thermal-photovoltaic-powered absorption refrigeration system. Journal of Solar Energy Engineering, 137(3), pp. 031020 1-9.

Besagni, G., Mereu, R. and Inzoli, F., 2016. Ejector refrigeration: A comprehensive review. Renewable and Sustainable Energy Reviews, 53, pp.373-407.

Bi, Y., Qin, L., Guo, J., Li, H. and Zang, G., 2020. Performance analysis of solar air conditioning system based on the independent-developed solar parabolic trough collector. Energy, 196, pp.1170751-14.

Biogas Handbook, 2008, University of Southern Denmark Esbjerg, Denmark, http://www.lemvigbiogas.com/BiogasHandbook.pdf. Accessed: 04.02.2018.

Bohringer, C., 2003. The Kyoto protocol: a review and perspectives. Oxford Review of Economic Policy, 19(3), pp.451-466.

Buragohain, B., Mahanta, P. and Moholkar, V.S., 2010. Biomass gasification for decentralized power generation: The Indian perspective. Renewable and Sustainable Energy Reviews, 14(1), pp.73-92.

Cabrera, F.J., Fernández-García, A., Silva, R.M.P. and Pérez-García, M., 2013. Use of parabolic trough solar collectors for solar refrigeration and air-conditioning applications. Renewable and Sustainable Energy Reviews, 20, pp.103-118.

Cengel, Y., 2014, Heat and Mass Transfer: Fundamentals and Applications, McGraw-Hill, New York.

Chantrasrisalai, C., Ghatti, V., Fisher, D. E., and Scheatzle, D. G., 2003, "Experimental Validation of the EnergyPlus Low-Temperature Radiant Simulation," ASHRAE Transaction, Washington, DC, accessed July 6, 2018, https://simulationresearch.lbl.gov/dirpubs/fishe03.pdf.

Chen, J.F., Dai, Y.J. and Wang, R.Z., 2017. Experimental and analytical study on an air-cooled single effect LiBr-H_2O absorption chiller driven by evacuated glass tube solar collector for cooling application in residential buildings. Solar Energy, 151, pp.110-118.

Chen, J.F., Dai, Y.J., Wang, H.B. and Wang, R.Z., 2018. Experimental investigation on a novel air-cooled single effect LiBr-H_2O absorption chiller with adiabatic flash evaporator and adiabatic absorber for residential application. Solar Energy, 159, pp.579-587.

Chen, T. and Norford, L., 2020. Energy performance of next-generation dedicated outdoor air cooling systems in low-energy building operations. Energy and Buildings, 209, p.109677.

Chennai data, 2017. Weather data by location, https://energyplus.net/weather-location/asia_wmo_region_2/IND//IND_Chennai-Madras.432790_ISHRAE,
EnergyPlus weather file source. Accessed: 01.11.2017

Chiu, F., and Krarti, M., 2021. Impacts of Air-Conditioning Equipment Sizing on Energy Performance of US Office Buildings. Journal of Engineering for Sustainable Buildings and Cities, 2(2), pp. 021001.

Choudhury, B., Saha, B.B., Chatterjee, P.K. and Sarkar, J.P., 2013. An overview of developments in adsorption refrigeration systems towards a sustainable way of cooling. Applied Energy, 104, pp.554-567.

Colorado, D. and Rivera, W., 2015. Performance comparison between a conventional vapor compression and compression-absorption single-stage and double-stage systems used for refrigeration. Applied Thermal Engineering, 87, pp.273-285.

Crawley, D.B., Lawrie, L.K., Winkelmann, F.C., Buhl, W.F., Huang, Y.J., Pedersen, C.O., Strand, R.K., Liesen, R.J., Fisher, D.E., Witte, M.J. and Glazer, J., 2001. EnergyPlus: creating a new-generation building energy simulation program. Energy and Buildings, 33(4), pp.319-331.

Dai, Y.J., Wang, R.Z., Zhang, H.F. and Yu, J.D., 2001. Use of liquid desiccant cooling to improve the performance of vapor compression air conditioning. Applied Thermal Engineering, 21(12), pp.1185-1202.

Dalkilic, A.S. and Wongwises, S., 2010. A performance comparison of vapour-compression refrigeration system using various alternative refrigerants. International Communications in Heat and Mass Transfer, 37(9), pp.1340-1349.

Dang, C., Nakamura, Y. and Hihara, E., 2012. Study on ejector-vapor compression hybrid air conditioning system using solar energy, https://docs.lib.purdue.edu/iracc/1340/, 2541.

De Lucas, A., Donate, M., Molero, C., Villaseñor, J. and Rodrıiguez, J.F., 2004. Performance evaluation and simulation of a new absorbent for an absorption refrigeration system. International Journal of Refrigeration, 27(4), pp.324-330.

De Vega, M., Almendros-Ibañez, J.A. and Ruiz, G., 2006. Performance of a LiBr–water absorption chiller operating with plate heat exchangers. Energy Conversion and Management, 47(18-19), pp.3393-3407.

Demesa, N., Hernández, J. A., Siqueiros, J., and Huicochea, A., 2018, “Heat transfer coefficients for helical components inside an absorption heat transformer,” International Journal of Heat Mass and Transfer, 120, pp.342–349.

Deru, M., Field, K., Studer, D., Benne, K., Griffith, B., Torcellini, P., Liu, B., Halverson, M., Winiarski, D., Rosenberg, M., Yazdanian, M., Huang, J., and Crawley, D., 2011, “U.S. Department of Energy Commercial Reference Building Models of the National Building Stock,” National Renewable Energy Laboratory, Golden, CO, Report No. NREL/TP-5500-46861.

Dong, Z., Boyi, Q., Chunlong, W., 2019. Energy-saving evaluation and control optimization of an ASHP heating system based on indoor thermal comfort. Solar Energy 194, pp.913–922.

Elhelw, M., El-Maghlany, W.M. and Abdelaziz, A.H., 2022. Experimental and theoretical study of hybrid electric solar driven vapour compression system. Renewable Energy, 182, pp.452-466.

El-Shaarawi, M.A.I. and Al-Ugla, A.A., 2017. Unsteady analysis for solar-powered hybrid storage LiBr-water absorption air-conditioning. Solar Energy, 144, pp.556-568.

Eltawil, M.A. and Samuuel, D.V.K., 2007. Vapour compression cooling system powered by solar PV array for potato storage, International Commission of Agricultural Engineering, 9, pp.1-23.

Emani, M.S. and Mandal, B.K., 2018, June. The use of natural refrigerants in refrigeration and air conditioning systems: a review. In IOP Conference Series: Materials Science and Engineering IOP Publishing, 377, pp. 012064.

EnergyPlus, 2017, "EnergyPlusC 8.7 Open Source Software," U.S. Department of Energy, Washington, DC, accessed Nov. 1, 2017, https://energyplus.net/downloads.

Evola, G., Le Pierres, N., Boudehenn, F., and Papillon, P., 2013, "Proposal and validation of a model for the dynamic simulation of a solar-assisted single-stage LiBr/water absorption chiller," International Journal of Refrigeration, 36(3), pp. 1015–1028.

Fong, K.F. and Lee, C.K., 2014. Performance advancement of solar air-conditioning through integrated system design for building. Energy, 73, pp.987-996.

Fong, K.F., Chow, T.T., Lee, C.K., Lin, Z. and Chan, L.S., 2011. Solar hybrid cooling system for high-tech offices in subtropical climate–Radiant cooling by absorption refrigeration and desiccant dehumidification. Energy Conversion and Management, 52(8-9), pp.2883-2894.

Fong, K.F., Lee, C.K. and Lin, Z., 2019. Investigation on effect of indoor air distribution strategy on solar air-conditioning systems. Renewable Energy, 131, pp.413-421.

Gao, D.C., Sun, Y.J., Ma, Z. and Ren, H., 2021. A review on integration and design of desiccant air-conditioning systems for overall performance improvements. Renewable and Sustainable Energy Reviews, 141, pp.110809 1-25.

Ghaddar, N., Ghali, K. and Najm, A., 2003. Use of desiccant dehumidification to improve energy utilization in air-conditioning systems in Beirut. International Journal of Energy Research, 27(15), pp.1317-1338.

Goetzler, W., 2007. Variable refrigerant flow systems. ASHRAE Journal, 49(4), pp.24-31.

Goldsmid, H.J., 2010. Theory of thermoelectric refrigeration and generation. In Introduction to thermoelectricity, Springer, Berlin, Heidelberg, pp. 7-21.

Goldsworthy, M.J., 2017. Building thermal design for solar photovoltaic air-conditioning in Australian climates. Energy and Buildings, 135, pp.176-186.

Gomri, R. and Hakimi, R., 2008. Second law analysis of double effect vapour absorption cooler system. Energy Conversion and Management, 49(11), pp.3343-3348.

Gomri, R., 2010. Investigation of the potential of application of single effect and multiple effect absorption cooling systems. Energy Conversion and Management, 51(8), pp.1629-1636.

Gomri, R., 2013. Simulation study on the performance of solar/natural gas absorption cooling chillers. Energy Conversion and Management, 65, pp.675-681.

Gonzalez-Gil, A., Izquierdo, M., Marcos, J.D. and Palacios, E., 2011. Experimental evaluation of a direct air-cooled lithium bromide–water absorption prototype for solar air conditioning. Applied Thermal Engineering, 31(16), pp.3358-3368.

Guo, J. and Shen, H.G., 2009. Modeling solar-driven ejector refrigeration system offering air conditioning for office buildings. Energy and Buildings, 41(2), pp.175-181.

Hang, Y., Qu, M. and Ukkusuri, S., 2011. Optimizing the design of a solar cooling system using central composite design techniques. Energy and Buildings, 43(4), pp.988-994.

Horuz, I., 1998. A comparison between ammonia-water and water-lithium bromide solutions in vapor absorption refrigeration systems. International Communications in Heat and Mass Transfer, 25(5), pp.711-721.

Hossaini, N., Hewage, K. and Sadiq, R., 2015. Spatial life cycle sustainability assessment: a conceptual framework for net-zero buildings. Clean Technologies and Environmental Policy, 17(8), pp.2243-2253.

Hu, R. and Niu, J.L., 2012. A review of the application of radiant cooling & heating systems in Mainland China. Energy and Buildings, 52, pp.11-19.

Hu, T., Shen, Y., Kwan, T.H. and Pei, G., 2022. Absorption chiller waste heat utilization to the desiccant dehumidifier system for enhanced cooling–Energy and exergy analysis. Energy, 239, pp.121847 1-12.

Hu, Y., Xia, X. and Wang, J., 2022. Research on operation strategy of radiant cooling system based on intermittent operation characteristics. Journal of Building Engineering, 45, pp.103483 1-14.

Huang, B.J., Hou, T.F., Hsu, P.C., Lin, T.H., Chen, Y.T., Chen, C.W., Li, K. and Lee, K.Y., 2016. Design of direct solar PV driven air conditioner. Renewable Energy, 88, pp.95-101.

Hurdogan, E., Buyukalaca, O., Yılmaz, T., Hepbasli, A. and Uçkan, I., 2012. Investigation of solar energy utilization in a novel desiccant based air conditioning system. Energy and Buildings, 55, pp.757-764.

Ibrahim, G. and Ahmed, H.M., A theoretical analysis of hybrid liquid desiccant-vapor compression air conditioning systems, Proceedings of the 7th World Congress on Momentum, Heat and Mass Transfer (MHMT'22), pp. 1-12.

Iffa, R. B., Bouaziz, N., and Kairouani, L., 2017, "Optimization of absorption refrigeration systems by design of experiments method," Energy Procedia, 139, pp. 280–287.

Izquierdo, M., Venegas, M., García, N. and Palacios, E., 2005. Exergetic analysis of a double stage LiBr–H_2O thermal compressor cooled by air/water and driven by low grade heat. Energy Conversion and Management, 46(7-8), pp.1029-1042.

Jalili, M., Chitsaz, A. and Alhuyi Nazari, M., 2022. Investigating the fuel type influence on the thermo-economic performance of absorption refrigeration systems: a comparative study. Journal of Thermal Analysis and Calorimetry, 147(7), pp.4763-4780.

Jani, D.B., Mishra, M. and Sahoo, P.K., 2015. Performance studies of hybrid solid desiccant–vapor compression air-conditioning system for hot and humid climates. Energy and Buildings, 102, pp.284-292.

Jani, D.B., Mishra, M. and Sahoo, P.K., 2016. Experimental investigation on solid desiccant–vapor compression hybrid air-conditioning system in hot and humid weather. Applied Thermal Engineering, 104, pp.556-564.

Ji, Y., Duanmu, L., Liu, Y. and Dong, H., 2020. Air infiltration rate of typical zones of public buildings under natural conditions. Sustainable Cities and Society, 61, pp.102290 1-10.

Jia, C.X., Dai, Y.J., Wu, J.Y. and Wang, R.Z., 2006. Analysis on a hybrid desiccant air-conditioning system. Applied Thermal Engineering, 26(17-18), pp.2393-2400.

Jia, L., Wei, S. and Liu, J., 2021. A review of optimization approaches for controlling water-cooled central cooling systems. Building and Environment, 203, pp.108100 1-14.

Kaynakli, O., Saka, K. and Kaynakli, F., 2015. Energy and exergy analysis of a double effect absorption refrigeration system based on different heat sources. Energy Conversion and Management, 106, pp.21-30.

Kececiler, A., Acar, H.İ. and Dogan, A., 2000. Thermodynamic analysis of the absorption refrigeration system with geothermal energy: an experimental study. Energy Conversion and Management, 41(1), pp.37-48.

Ketfi, O., Merzouk, M., Merzouk, N.K. and Bourouis, M., 2017. Feasibility study and performance evaluation of low capacity water–LiBr absorption cooling systems functioning in different Algerian climate zones. International Journal of Refrigeration, 82, pp.36-50.

Ketfi, O., Merzouk, M., Merzouk, N.K. and El Metenani, S., 2015. Performance of a single effect solar absorption cooling system (Libr-H_2O). Energy procedia, 74, pp.130-138.

Khamis Mansour, M. and Hassab, M. 2012. Thermal design of cooling and dehumidifying coils, heat exchangers - Basics design applications, Dr. Jovan Mitrovic (Ed.), ISBN: 978-953-51-0278-6, InTech, Available from: http://www.intechopen.com/books/heat-exchangers-basics-design-applications/thermal-designof-cooling-anddehumidifying-coils (Accessed: July 15, 2021).

Khan, A., Bajpai, A., Rao, G. S., Mathur, J., Chamberlain, L., Thomas, P. C., Rawal, R., Kapoor, R., Tetali, S., Lathey, V., and Garg, V., 2009, Energy Conservation Building Code User Guide, 1st ed., Bureau of Energy Efficiency, New Delhi, India.

Khan, Y., Singh, G., Mathur, J., Bhandari, M. and Srivastava, P., 2017. Performance assessment of radiant cooling system integrated with desiccant assisted DOAS with solar regeneration. Applied Thermal Engineering, 124, pp.1075-1082.

Kim, D.S. and Ferreira, C.I., 2009. Air-cooled LiBr–water absorption chillers for solar air conditioning in extremely hot weathers. Energy Conversion and Management, 50(4), pp.1018-1025.

Kim, H.R., Jeon, J.U. and Kim, K.S., 2019, June. Performance measurements of an energy recovery ventilator (ERV) and effective ventilation strategy with ERV and hybrid desiccant system. In Building Simulation, Tsinghua University Press, Vol. 12, No. 3, pp. 489-504.

Kreider JF 2000. Handbook of Heating, Ventilation and Air Conditioning. Boca Raton, Florida: CRC press; 2000.

Kundu, B., Mondal, P.K., Datta, S.P. and Wongwises, S., 2010. Operating design conditions of a solar-powered vapor absorption cooling system with an absorber plate having different profiles: An analytical study. International Communications in Heat and Mass Transfer, 37(9), pp.1238-1245.

La, D., Dai, Y., Li, Y., Ge, T. and Wang, R., 2011. Case study and theoretical analysis of a solar driven two-stage rotary desiccant cooling system assisted by vapor compression air-conditioning. Solar Energy, 85(11), pp.2997-3009.

Li, N., Luo, C. and Su, Q., 2018. A working pair of $CaCl_2$–LiBr–$LiNO_3$/H_2O and its application in a single-stage solar-driven absorption refrigeration cycle. International Journal of Refrigeration, 86, pp.1-13.

Li, X., Kan, X., Sun, X., Zhao, Y., Ge, T., Dai, Y. and Wang, C.H., 2019. Performance analysis of a biomass gasification-based CCHP system integrated with variable-effect LiBr-H_2O absorption cooling and desiccant dehumidification. Energy, 176, pp.961-979.

Li, Y., Lu, L. and Yang, H., 2010. Energy and economic performance analysis of an open cycle solar desiccant dehumidification air-conditioning system for application in Hong Kong. Solar Energy, 84(12), pp.2085-2095.

Li, Z., Jing, Y. and Liu, J., 2016. Thermodynamic study of a novel solar LiBr/H_2O absorption chiller. Energy and Buildings, 133, pp.565-576.

Li, Z., Ye, X. and Liu, J., 2014. Performance analysis of solar air cooled double effect LiBr/H_2O absorption cooling system in subtropical city. Energy Conversion and Management, 85, pp.302-312.

Li, Z.F. and Sumathy, K., 2001. Experimental studies on a solar powered air conditioning system with partitioned hot water storage tank. Solar Energy, 71(5), pp.285-297.

Liao, X. and Radermacher, R., 2007. Absorption chiller crystallization control strategies for integrated cooling heating and power systems. International Journal of Refrigeration, 30(5), pp.904-911.

Lin, X., Lee, H., Hwang, Y. and Radermacher, R., 2015. A review of recent development in variable refrigerant flow systems. Science and Technology for the Built Environment, 21(7), pp.917-933.

Liu, Y., Chen, Y., Wang, D., Liu, J., Li, L., Luo, X., Wang, Y. and Liu, J., 2020. Performance evaluation of a hybrid solar powered rotary desiccant wheel air

conditioning system for low latitude isolated islands. Energy and Buildings, 224, pp.110208 1-13.

Liu, Y.L. and Wang, R.Z., 2004. Performance prediction of a solar/gas driving double effect LiBr–H_2O absorption system. Renewable Energy, 29(10), pp.1677-1695.

Lubis, A., Jeong, J., Saito, K., Giannetti, N., Yabase, H. and Alhamid, M.I., 2016. Solar-assisted single-double-effect absorption chiller for use in Asian tropical climates. Renewable Energy, 99, pp.825-835.

Ma, Q., Wang, R.Z., Dai, Y.J. and Zhai, X.Q., 2006. Performance analysis on a hybrid air-conditioning system of a green building. Energy and Buildings, 38(5), pp. 447-453.

Ma, X., Zhang, W., Omer, S.A. and Riffat, S.B., 2010. Experimental investigation of a novel steam ejector refrigerator suitable for solar energy applications. Applied Thermal Engineering, 30(11-12), pp.1320-1325.

Majdi, H.S., 2016. Performance evaluation of combined ejector LiBr/H_2O absorption cooling cycle. Case studies in Thermal Engineering, 7, pp.25-35.

Martínez, J.C., Martinez, P.J. and Bujedo, L.A., 2016. Development and experimental validation of a simulation model to reproduce the performance of a 17.6 kW LiBr–water absorption chiller. Renewable Energy, 86, pp.473-482.

Masson, S.V., Qu, M. and Archer, D.H., 2006. Performance modeling of a solar driven absorption cooling system for Carnegie Mellon University's intelligent workplace. https://oaktrust.library.tamu.edu/handle/1969.1/5448

Misra, D. and Ghosh, S., 2018. Evaporative cooling technologies for greenhouses: a comprehensive review. Agricultural Engineering International: CIGR Journal, 20(1), pp.1-15.

Misra, R.D., Sahoo, P.K., Sahoo, S. and Gupta, A., 2003. Thermoeconomic optimization of a single effect water/LiBr vapour absorption refrigeration system. International Journal of Refrigeration, 26(2), pp.158-169.

Mittal ML, Sharma C, Singh R. Estimates of emissions from coal fired thermal power plants in India, International Emission Inventory Conference; 2012; Tampa, FL, pp.13–16.

Moffat RJ (1982) Contributions to the theory of single-sample uncertainty analysis. Journal of Fluids Engineering, 104(2), pp. 250–258.

Mohammad, A.T., Mat, S.B., Sulaiman, M.Y., Sopian, K. and Al-Abidi, A.A., 2013. Survey of liquid desiccant dehumidification system based on integrated vapor compression technology for building applications. Energy and Buildings, 62, pp.1-14.

Mohammadi, K., Khaledi, M.S.E. and Powell, K., 2019. A novel hybrid dual-temperature absorption refrigeration system: Thermodynamic, economic, and environmental analysis. Journal of Cleaner Production, 233, pp.1075-1087.

Mohan, B.S., Tiwari, S. and Maiya, M.P., 2015. Experimental investigations on performance of liquid desiccant-vapor compression hybrid air conditioner. Applied Thermal Engineering, 77, pp.153-162.

Muneer, T. and Uppal, A.H., 1985. Modelling and simulation of a solar absorption cooling system. Applied Energy, 19(3), pp.209-229.

New Delhi data, 2017. Weather data by location, https://energyplus.net/weather-location/asia_wmo_region_2/IND//IND_New.Delhi.421820_ISHRAE, EnergyPlus weather file source Accessed: 01.11.2017

Nezhad, A.E., Rahimnejad, A. and Gadsden, S.A., 2021. Home energy management system for smart buildings with inverter-based air conditioning system. International Journal of Electrical Power & Energy Systems, 133, pp.107230.

Pandya, B., Patel, J., and Mudgal, A., 2017, "Thermodynamic Evaluation of Generator Temperature in LiBr-Water Absorption System for Optimal Performance," Energy Procedia, 109, pp.270–278.

Panja, P. and Ganguly, A., 2019. Modelling and analysis of a solar biomass hybrid vapour absorption refrigeration system for running a cold storage of potato in India. PREPARE@ u®| General Preprint Services.

Paolini, V., Petracchini, F., Segreto, M., Tomassetti, L., Naja, N. and Cecinato, A., 2018. Environmental impact of biogas: A short review of current knowledge. Journal of Environmental Science and Health, Part A, 53(10), pp.899-906.

Paurine, A., Maidment, G.G., Eames, I.W. and Missenden, J.F., 2012. Development of a thermo-gravity pumping mechanism for circulating the working fluids in a novel LiBr–H_2O vapour absorption refrigeration (VAR) system. Applied Thermal Engineering, 47, pp.25-33.

Perez-Lombard, L., Ortiz, J. and Pout, C., 2008. A review on buildings energy consumption information. Energy and Buildings, 40(3), pp.394-398.

Pongtornkulpanich, A., Thepa, S., Amornkitbamrung, M. and Butcher, C., 2008. Experience with fully operational solar-driven 10-ton LiBr/H_2O single-effect absorption cooling system in Thailand. Renewable Energy, 33(5), pp.943-949.

Porumb, R., Porumb, B. and Balan, M., 2017. Numerical investigation on solar absorption chiller with LiBr-H_2O operating conditions and performances. Energy Procedia, 112, pp.108-117.

Prasartkaew, B. and Kumar, S., 2013. Experimental study on the performance of a solar-biomass hybrid air-conditioning system. Renewable Energy, 57, pp. 86-93.

Prasartkaew, B., 2014. Performance test of a small size LiBr-H_2O absorption chiller. Energy Procedia, 56, pp. 487-497.

Pridasawas, W. and Lundqvist, P., 2004. An exergy analysis of a solar-driven ejector refrigeration system. Solar Energy, 76(4), pp.369-379.

PV cell efficiency, 2019, https://news.energysage.com/what-are-themost-efficient-solar-panels-on-the-market/ (Accessed on May 5, 2019).

Raghuvanshi, S.P., Chandra, A. and Raghav, A.K., 2006. Carbon dioxide emissions from coal based power generation in India. Energy Conversion and Management, 47(4), pp.427-441.

Rejeb, O., Shittu, S., Ghenai, C., Li, G., Zhao, X. and Bettayeb, M., 2020. Optimization and performance analysis of a solar concentrated photovoltaic-thermoelectric (CPV-TE) hybrid system. Renewable Energy, 152, pp.1342-1353.

Romero, R.J., Rivera, W., Gracia, J. and Best, R., 2001. Theoretical comparison of performance of an absorption heat pump system for cooling and heating operating with an aqueous ternary hydroxide and water/lithium bromide. Applied Thermal Engineering, 21(11), pp.1137-1147.

Rouag, A., Benchabane, A., Labed, A. and Boultif, N., 2016. Thermal design of air cooled condenser of a solar adsorption refrigerator. Journal of Applied Engineering Science & Technology, 2(1), pp.23-29.

Saleh, A. and Mosa, M., 2014. Optimization study of a single-effect water–lithium bromide absorption refrigeration system powered by flat-plate collector in hot regions. Energy Conversion and Management, 87, pp.29-36.

Scoccia, R., Toppi, T., Aprile, M. and Motta, M., 2018. Absorption and compression heat pump systems for space heating and DHW in European buildings: Energy, environmental and economic analysis. Journal of Building Engineering, 16, pp.94-105.

Seadi, T. A., Rutz, D., Prassl, H., Kottner, M., Finsterwalder, T., Volk, S., and Janssen, R., 2008, Biogas Handbook, University of Southern Denmark, Esbjerg, Denmark, accessed Feb. 4, 2018, http://www.lemvigbiogas.com/BiogasHandbook.pdf

Sokhansefat, T., Mohammadi, D., Kasaeian, A. and Mahmoudi, A.R., 2017. Simulation and parametric study of a 5-ton solar absorption cooling system in Tehran. Energy Conversion and Management, 148, pp.339-351.

Song, J. and Sobhani, B., 2020. Energy and exergy performance of an integrated desiccant cooling system with photovoltaic/thermal using phase change material and maisotsenko cooler. Journal of Energy Storage, 32, pp.101698 1-21.

Srikhirin, P., Aphornratana, S. and Chungpaibulpatana, S., 2001. A review of absorption refrigeration technologies. Renewable and Sustainable Energy Reviews, 5(4), pp.343-372.

Su, B., Han, W. and Jin, H., 2017. An innovative solar-powered absorption refrigeration system combined with liquid desiccant dehumidification for cooling and water. Energy Conversion and Management, 153, pp.515-525.

Su, W. and Zhang, X., 2017. Thermodynamic analysis of a compression-absorption refrigeration air-conditioning system coupled with liquid desiccant dehumidification. Applied Thermal Engineering, 115, pp.575-585.

Sun, D.W., 1997. Solar powered combined ejector-vapour compression cycle for air conditioning and refrigeration. Energy Conversion and Management, 38(5), pp.479-491.

Sun, J., Fu, L. and Zhang, S., 2012. A review of working fluids of absorption cycles. Renewable and Sustainable Energy Reviews, 16(4), pp.1899-1906.

Thomson, G.W., 1946. The Antoine equation for vapor-pressure data. Chemical Reviews, 38(1), pp.1-39.

Tierney, M., 2007. Options for solar-assisted refrigeration—Trough collectors and double-effect chillers. Renewable Energy, 32(2), pp.183-199.

Trane, 2010, "User Manual: The Trane Air-Conditioning Economics (TRACEVR 700)," TRANE, Dublin, Ireland, accessed June 10, 2018, http://software.trane.-com/CDS/TRACE%20700 %20-%20Users%20Manual.pdf.

Tsilingiris, P.T., 1993. Theoretical modelling of a solar air conditioning system for domestic applications. Energy Conversion and Management, 34(7), pp.523-531.

Unmet load hours troubleshooting guide, Integrated environmental solutions limited, virtual environment 2013, featured pack 1, (unmet load hours trouble shooter guide), https://www.iesve.com/support/faq/pdf/unmet-load-hours.pdf (Accessed on December 15, 2021).

Varvagiannis, E., Charalampidis, A., Zsembinszki, G., Karellas, S. and Cabeza, L.F., 2021. Energy assessment based on semi-dynamic modelling of a photovoltaic driven vapour compression chiller using phase change materials for cold energy storage. Renewable Energy, 163, pp.198-212.

Wang, H., Liu, L., Liu, L. and Cheng, Q., 2022. Performance analysis of different air conditioning systems in apartment buildings under different climates in China. International Journal of Refrigeration, 139, pp. 192-203.

Wang, J., Shang, S., Li, X., Wang, B., Wu, W. and Shi, W., 2017. Dynamic performance analysis for an absorption chiller under different working conditions. Applied Sciences, 7(8), p.797.

Wang, R., Wang, L. and Wu, J., 2014. Adsorption refrigeration technology: theory and application. John Wiley & Sons, New York.

Whitman, B., Johnson, B., Tomczyk, J. and Silberstein, E., 2012. Refrigeration and air conditioning technology. Cengage Learning.

Wojtkowiak, J., Amanowicz, L. and Mróz, T., 2019. A new type of cooling ceiling panel with corrugated surface—Experimental investigation. International Journal of Energy Research, 43(13), pp.7275-7286.

Wrobel, J., Walter, P. S., and Schmitz, G., 2013. Performance of a solar assisted air conditioning system at different locations, Solar Energy, 92, pp.69–83.

Wu, J.M., Huang, X. and Zhang, H., 2009. Theoretical analysis on heat and mass transfer in a direct evaporative cooler. Applied Thermal Engineering, 29(5-6), pp.980-984.

Xie, F., Liu, H., Gu, X., Li, P., Chen, W. and Ling, P., 2017. Matching suitability of solar-biomass hybrid absorption cooling system for ecological restaurants in different regions. Procedia Engineering, 205, pp.672-679.

Xie, G., Wu, Q., Fa, X., Zhang, L. and Bansal, P., 2012. A novel lithium bromide absorption chiller with enhanced absorption pressure. Applied Thermal Engineering, 38, pp.1-6.

Xu, Z.Y. and Wang, R.Z., 2017. Comparison of CPC driven solar absorption cooling systems with single, double and variable effect absorption chillers. Solar Energy, 158, pp.511-519.

Yadav, Y.K., 1995. Vapour-compression and liquid-desiccant hybrid solar space-conditioning system for energy conservation. Renewable Energy, 6(7), pp.719-723.

Yang, Y., Cui, G. and Lan, C.Q., 2019. Developments in evaporative cooling and enhanced evaporative cooling-A review. Renewable and Sustainable Energy Reviews, 113, pp.109230 1-10.

Yilmaz, M.E.H.M.E.T., Kaya, M.E.H.M.E.T., Karagoz, S. and Erdogan, S., 2009. A review on design criteria for vortex tubes. Heat and mass transfer, 45(5), pp.613-632.

Yin, Y.L., Song, Z.P., Li, Y., Wang, R.Z. and Zhai, X.Q., 2012. Experimental investigation of a mini-type solar absorption cooling system under different cooling modes. Energy and Buildings, 47, pp.131-138.

Yong, L., Sumathy, K., Dai, Y.J., Zhong, J.H. and Wang, R.Z., 2006. Experimental study on a hybrid desiccant dehumidification and air conditioning system, Journal of Solar Energy Engineering, 128(1), pp. 77-82.

Yoon, J.I., Choi, K.H., Moon, C.G., Kim, Y.J. and Kwon, O.K., 2003. A study on the advanced performance of an absorption heater/chiller with a solution preheater using waste gas. Applied Thermal Engineering, 23(6), pp.757-767.

Yu, F.W. and Chan, K.T., 2011. Improved energy performance of air-cooled chiller system with mist pre-cooling. Applied Thermal Engineering, 31(4), pp.537-544.

Yu, F.W., Chan, K.T., Sit, R.K. and Yang, J., 2013. Energy simulation of sustainable air-cooled chiller system for commercial buildings under climate change. Energy and Buildings, 64, pp.162-171.

Yu, F.W., Chan, K.T., Sit, R.K.Y. and Yang, J., 2014. Review of standards for energy performance of chiller systems serving commercial buildings. Energy Procedia, 61, pp.2778-2782.

Yutong, L. and Hongxing, Y., 2008. Investigation on solar desiccant dehumidification process for energy conservation of central air-conditioning systems. Applied Thermal Engineering, 28(10), pp.1118-1126.

Zhai, X., Li, Y., Cheng, X. and Wang, R., 2015. Experimental investigation on a solar-powered absorption radiant cooling system. Energy Procedia, 70, pp.552-559.

Zhang, G., Xiao, H., Zhang, P., Wang, B., Li, X., Shi, W. and Cao, Y., 2019. Review on recent developments of variable refrigerant flow systems since 2015. Energy and Buildings, 198, pp.444-466.

Zhou, X., Yan, D., An, J., Hong, T., Shi, X. and Jin, X., 2018. Comparative study of air-conditioning energy use of four office buildings in China and USA. Energy and Buildings, 169, pp.344-352.